
AD-674 981
This document has been approved
for public release and sale; its
distribution is unlimited.

SVM-2

Theory and Practice of Cushion Design

Gordon S. Mustin
Special Projects Consultants, Inc.

1968

The Shock and Vibration Information Center
United States Department of Defense

Contract No. [illegible]

Library of Congress Catalog Card No. [illegible]

FOREWORD

It has become apparent to us that there is a need for concise, critical, and comprehensive studies of the state of the art in specialized areas within the field of mechanical shock and vibration. Although we realize that there are a large number of subjects that could be treated, practical considerations force us to make what we hope is a judicious choice from the many excellent topics proposed. Also, to alleviate delay in publication, we have planned the overall to a series of monographs by authorities in the technology.

This book is intended primarily for those concerned with the design of cushioning systems for the protection of fragile items in shipment. It should be pointed out, however, that this is not a design handbook. It does not provide "cookbook" methods for the solution of package cushioning design problems. Instead, it guides the designer to the tools he needs to solve these problems.

The material contained here applies not only to package cushioning design, but also anywhere that shock and vibration are isolated by materials with distributed mass and elasticity. The contents should be helpful to those concerned with aerial delivery, space vehicle recovery and the isolation of underground structures from ground shock.

More than 300 references were used in writing this work. Some references are only mentioned in passing, while others are commented on critically and in detail.

The bulk of the monograph should not deter the reader. If he is interested in the theoretical analysis of the behavior of cushioning materials, he should consult Chapter 3. For basic design approaches with respect to shock isolation, Chapter 4 should be read. Chapter 5 discusses the methods available to analyze the response of the item being cushioned, and Chapter 6 is concerned with the special problem of vibration isolation. The author is careful to point out that vibration and shock isolation employ similar analytical techniques. The performance of cushioning materials under extreme environments is covered in Chapter 7, and Chapter 8 deals with drift and creep of these materials. For those not interested in the mathematical derivations, Chapter 9 provides a fairly comprehensive summary of the analysis of cushion behavior.

The Shock and Vibration Information Center hopes that this book and those to follow will be helpful to persons concerned with the technology. Suggestions for subjects of interest or for improved organization of future monographs are welcome.

Henry C. Pusey

Shock and Vibration Information Center
Washington, DC
1 May 1968

PREFACE

The assistance to prepare this monograph, and the necessary travel, was generously provided by the Office of Naval Research through Contract N00014-68-C0138 under the aegis of the Shock and Vibration Information Center.

Thanks are extended to the publishers of the following journals and the editorial boards herein for permission to reproduce the material identified below:

Source	Figure
Society of Plastics Engineers	3.3, 3.4, 4.74, 4.76, 7.4
Physics	3.19, 3.20, 3.30
J. of Polymer Science	3.19
J. of Applied Physics	3.21
J. of Applied Polymer Science	3.25, 3.27
British J. of Applied Physics	3.26
Package Engineering	4.3, 4.45, 4.47, 4.48, 4.49, 4.50, 4.51
The Bell System Technical J.	4.9, 4.10, 4.14, 4.17, 5.6, 5.9, 5.11
J. of the Acoustical Society of America	4.11, 4.12, 4.13, 4.16, 5.17, 6.4, 6.5, 6.6
Verpackungs Rundschau	4.31, 4.32, 4.33, 4.44, 4.56, 4.57, 4.58, 4.59, 6.4
McGraw-Hill Book Co.	4.36, 6.11, 6.12
Packaging (England)	4.61, 4.62, 4.63, 4.64, 6.3
John Wiley and Sons	5.10
J. of Applied Mechanics	5.7, 5.12, 5.16
Transactions ASME	5.13

The individual works from which each of the foregoing have been drawn are referenced in the pertinent figure captions. Each copyright owner graciously extended the license to the author and to the U.S. Government under the standard clauses governing rights in data furnished to the government under contract.

Particular thanks for constructive criticism of the manuscript in various stages of preparation are due R. H. Scholl of the Air Force Flight Dynamics Laboratory, Wright Patterson Air Force Base, R. Lazarevich and G. Zoll of the Plastics and Packaging Laboratory, Picatinny Arsenal, and W. W. Shock and H. C. Pusey of the Shock and Vibration Information Center. Credit for the high standard shown in all illustrations belongs to the Graphic Arts Section, Naval Research Laboratory. Special thanks to the Lanston Section at NRL for their preparation of the copy under very difficult conditions.

No book of this length can be prepared without the help of superior editing. I am indebted to Mr. Philip Barr, and to Mrs. Joan B. Goldbacher of the Shock and Vibration Information Center, for their real help to me.

I cannot close without acknowledging my indebtedness to the late Charles E. Crede and Irwin Vigness. Over many years, both made particular efforts to increase my understanding of the foundations of shock and vibration dynamics while continuing, to the day of their untimely deaths, to make enormous personal contributions to the field.

Finally, this book is primarily a compilation of the work of others. Their names are listed in the references. The credit for what is good belongs to them. For whatever else may be found herein, I take the blame.

Clarence S. Mesmer*

Washington, DC
15 January 1987

*At the time of the writing of this work the author was with Naval Program Communications Inc., 1629 Eye Street N.W., Washington, DC 20006. His current address is [illegible] Naval Ordnance Systems Command, Washington, DC 20360.

This monograph is available to qualified users from the Defense Documentation Center, Cameron Station, Alexandria, Virginia 22314. Others may purchase it from the Superintendent of Documents, U.S. Government Printing Office, Washington, D.C. 20402

The Shock and Vibration Information Center

William W. Mutch, Head

Henry C. Pusey

Rudolph H. Volin

Katherine G. Jahnel, Administrative Secretary

CONTENTS

Chapter 1

SCOPE

This monograph is a critical review of current art in selecting, designing, analyzing, and using cushions.

Cushions mitigate the effects of shock or vibration. They also prevent marring of highly finished surfaces, absorb spilled liquids, protect barriers from puncture from within or without, and even, fairly often simply fill void spaces so that irregular objects can be fitted into shaped containers.

The word "cushion," or the alternative "cushioning," has taken on several meanings over the years. It is appropriate, therefore, to begin with a description of what will and will not be covered in the following pages.

In the broadest sense, a cushion is anything interposed between one object and another to mitigate the effects of shock or vibration on the first object. The basic mechanism by which the cushion performs this function is through being deformed in response to the forces induced. This deformation occurs in accord with Newton's laws of mechanics. Since all materials will be deformed to a greater or lesser degree, we should restrict the area of inquiry.

This monograph is concerned with materials which will deform significantly under applied forces. The word "significantly" is not closely defined; quantitative limits can be set only by an individual designer with a specific problem to solve. However, this restriction has objective meaning. For example, those interested in ballistic impact, in body armor, in brittle fracture, or in basic strength of structural materials under impact conditions will not find their required answers here.

The main thrust of this monograph will be directed at materials rather than devices. Generally speaking, therefore, metal springs, shock struts (*e.g.*, airplane landing gear), and "shock mounts"—composite fabricated structures with a yielding element—will not be discussed. Such devices can receive the kind of mathematical treatment used throughout this monograph; one cannot draw a hard-and-fast line between such devices and cushions. It is frequently accepted that the mass of a cushioning device can be considered negligible in comparison with the mass of the cushioned object. As will be shown, this simplification is not possible with materials, except in very preliminary design considerations. Another difference: cushioning materials are not very often attached to the object cushioned, although many of the materials do have tensile and shear properties that permit such use. Actually, most of the effects under discussion are compressive effects.

Cushions used in contact with a specific object must be compatible with the object. Included are chemical compatibility, abrasion or marring characteristics, and absorbency. While these properties are important, they are

not mentioned in this monograph, which is limited to the mechanical properties exhibited by the material.

The basic objective of this monograph is to bring all persons concerned with cushions—theoretician, materials engineer, designer, specification writer, producer, and user—to the same point of reference. A secondary but important objective is to indicate cross-fertilization potentials between lines of work proceeding in widely separated localities and even to suggest possible new lines of endeavor which might produce fruitful results.

To the extent that either goal is achieved, the effort is worthwhile.

Chapter 2

BASIC QUALITATIVE CONSIDERATIONS

The function of a cushion is to mitigate the effects of shock or vibration on an object. Certain fundamental postulates and definitions are required so that this statement may have objective meaning.

Consider the generalized system shown in Fig. 2.1. The system consists of a substrate or support surface, a case, the cushion, and the item. The item contains one or more attached mechanical subassemblies, identified as element a and element b. The cushion is very much less rigid than the substrate, case, or item surface. In fact, it is usual to consider these three infinitely rigid—with little or no loss in accuracy, as will be shown. Elements a and b are most conveniently thought of as being less rigid than the case.

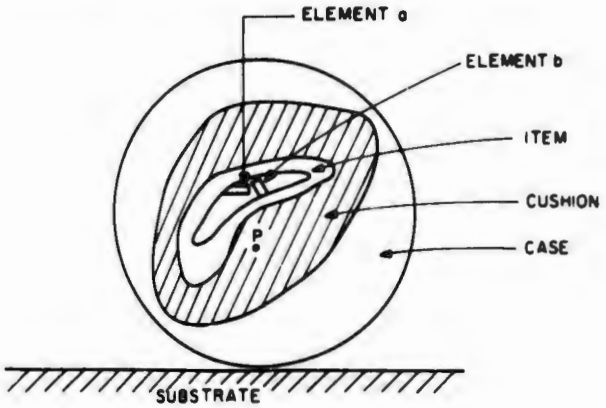

FIG. 2.1. Generalized cushion system.

Now let the case and its contents undergo a change in state of motion. Such a change might occur because of the case being stopped by collision with the substrate, or through one or more changes in the direction of displacement, or in the velocity of the substrate. In accord with Newton's laws, the item will tend to continue to move in the original direction, with this motion being resisted by the cushion.

If the item is an operating piece of equipment, such as a motor or similar mechanism, the motion may be induced from inside. In the majority of the cases discussed, however, the motion will be induced in some fashion from outside the system. The effort is then concentrated on finding the effects of

this motion at the item-cushion interface and as it proceeds further and further into the item.

The motion may be vibratory or it may constitute mechanical shock. Vibration is variation with time of the magnitude of a quantity. This quantity is descriptive of the motion or position of a mechanical system and its magnitude is alternately greater and smaller than some average value. Mechanical shock, on the other hand, is characterized by significant internal forces in a system resulting from sudden changes in excitation. Mechanical shock exists when a force, position, velocity, or acceleration is suddenly changed, exciting mechanical transients in a system.

The definitions of shock and vibration given in the preceding paragraph are both accurate and inclusive; they are made to cover all cases in which the two words can appear. For expository purposes, the thoughts of two authors are borrowed.

Morrow [1] has defined shock as a pulse, a transient, or a change of acceleration which stands out above the general vibration level and occurs in a relatively short period of time. This particular view permits one to consider a shock as a special case, warranting separate analysis, in the universe of motions to which an assembly may be exposed.

Fung [2] prefers to consider four separate types of shock problem. These depend largely on how the shock occurs and are:

1. Impact – This form of shock occurs in aircraft landings, in collisions, in package handling, and the like. It is frequently characterized by a change of velocity and was called velocity shock by Crede [3].
2. Imposed external loads – Typical examples are blast shock on buildings and near-miss explosions in general.
3. Ground acceleration – Here the base (or substrate) undergoes a sudden change in motion. Examples are buildings shaken by earthquakes, packages rattling in a vehicle, or instruments mounted on a larger structure which undergoes some form of shock.
4. Aeroelastic shock – Typical of this are gust loads on aircraft and ship slamming.

At least part of the difficulty in achieving satisfactory definitions which separate the meaning of "shock" from the meaning of "vibration" is that essentially the same equation is used in both types of problem. As an illustration, consider the simple systems shown in Fig. 2.2. In Fig. 2.2(a) a mass m is supported on a fixed foundation by a spring and a dashpot. The mass is then subjected to a force varying with time, $F_i(t)$. The equation of motion for this system is

$$m\ddot{x}_o + c\,\dot{x}_o + kx_o = F_i(t). \tag{2.1}$$

If the mass were simply displaced and then released and allowed to vibrate freely, $F_i(t) = 0$ and Eq. (2.1) would become the classical equation for damped free vibration.

Figure 2.2(b) is similar except that the excitation is the motion $x_i(t)$ of the foundation. The equation of motion for this system is

$$m\ddot{x}_o + c\dot{x}_o + kx_o = kx_i(t). \tag{2.2}$$

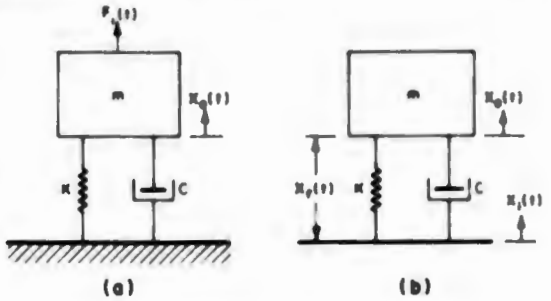

FIG. 2.2. Single-degree-of-freedom systems: (a) excited by force, and (b) excited by motion.

Equation (2.2) can be differentiated once with respect to time to yield

$$m\frac{d\ddot{x}_o}{dt} + c\ddot{x}_o + k\dot{x}_o = k\dot{x}_i(t). \tag{2.3}$$

This is the relation existing when the foundation disturbance is expressed in terms of velocity. Proceeding similarly, one finds that

$$m\frac{d^2\ddot{x}_o}{dt^2} + c\frac{d\ddot{x}_o}{dt} + k\ddot{x}_o = k\ddot{x}_i(t) \tag{2.4}$$

applies when the foundation disturbance is expressed in terms of acceleration. By introducing the term x_r as the relative motion between the foundation and the mass ($x_r = x_o - x_i$), Eq. (2.4) may also be written

$$m\ddot{x}_r + c\dot{x}_r + kx_r = -m\ddot{x}_i(t). \tag{2.5}$$

Since it is generally possible to differentiate Eq. (2.2) any number of times n, the following may also be written

$$m\frac{d^2}{dt^2}\left(\frac{d^n x_o}{dt^n}\right) + c\frac{d}{dt}\left(\frac{d^n x_o}{dt^n}\right) + k\frac{d^n x_o}{dt^n} = k\left[\frac{d^n x_i(t)}{dt^n}\right]. \tag{2.6}$$

Define the following quantities:

1. The square of the undamped natural frequency of the system as

$$\omega_n^2 = \frac{k}{m}; \tag{2.7}$$

2. The critical damping coefficient as

$$c_c = 2\sqrt{km}, \tag{2.8}$$

which is the smallest value of c for which the free vibration of mass m is not oscillatory;

3. The damping ratio as

$$\beta = \frac{c}{c_c} = \frac{c}{2\sqrt{km}}. \tag{2.9}$$

With appropriate substitution from Eqs. (2.7) through (2.9), Eqs. (2.1) through (2.6) can all be written as the same second-order differential equation

$$\ddot{\chi} + 2\beta\omega_n\dot{\chi} + \omega_n^2\chi = \omega_n^2 f_i(t), \tag{2.10}$$

where χ = generalized response variable, and

$f(t)$ = generalized, time-dependent, excitation variable

Table 2.1 summarizes alternate forms of response and excitation variables

TABLE 2.1 ALTERNATE FORMS OF EXCITATION AND RESPONSE

Excitation, $f(t)$		*Response*, χ	
Force applied to mass, base immobile	$\frac{F_1(t)}{k}$	Absolute displacement	x_0
Base displacement	$x_1(t)$	Absolute displacement	x_0
Base velocity	$\frac{\dot{x}_1(t)}{\omega_n^2}$	Absolute velocity	$\dot{x}_0$
Base acceleration	$\ddot{x}_1(t)$	Relative displacement	x_r
Base acceleration	$\ddot{x}_1(t)$	Absolute acceleration	$\ddot{x}_0$
nth derivative of base displacement	$\frac{d^n x_1(t)}{dt^n}$	nth derivative of absolute displacement	$\frac{d^n x_0}{dt^n}$

Practically all shock and vibration analyses stem from this relatively simple equation of motion although the solutions can, and do, become very complicated when $f(t)$ is not a simple function or when more than one degree of freedom is involved.

It can be shown from the theory of differential equations that the solution of Eq. (2.10) must take the form

$$\chi = \chi_1 + \chi_2, \tag{2.11}$$

where χ_2 is the particular integral and χ_1 is the complementary function. Values of χ_1 and χ_2 are determined by the initial and boundary conditions determined primarily by the nature of the excitation function.

At a given moment, the analyst may be more interested in one portion of the general solution than in the other. To illustrate this point a little more clearly, suppose that the simple system of Fig. 2.2(b) is exposed to a shock excitation of relatively simple form, and that this shock excitation is not repeated during the time being considered. A plot of response *versus* time would then appear somewhat as shown in Fig. 2.3. This figure illustrates that, after the initial large response, the mass continues to vibrate freely until the motion decays as a result of the system damping. If interest is concentrated on, say, the maximum value of the response, then only the portion of the motion between t_0 and t_1 will be of interest. In the analysis, the complementary function has major importance.

Suppose, however, that the same system is initially at rest and a relatively simple vibration excitation is applied to the base and continued for an indefinite period. Here there would be a starting transient – the shock – whose effects would gradually disappear, leaving the system vibrating only in response to the steady-state input vibration. By simply shifting the beginning

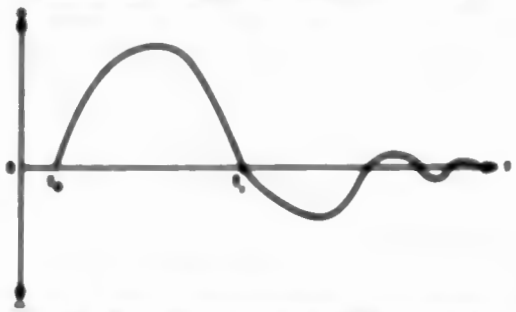

FIG. 2.3 Response time history of a simple system to a simple base shock

of the time of consideration from t_0 to t_1, the analyst discards the complementary function and concentrates on the particular integral. This intellectual operation is sketched in Fig. 2.4.

From the two figures it can be seen that shock can always be considered a special case of vibration. While mathematical elegance would normally dictate treating shock only as a special case of vibration, designers are not necessarily interested in viewing both aspects at the same time. Further, the bulk of the available literature deals with shock aspects alone. For these reasons, an artificial separation is maintained throughout this work, and the subject of shock is treated first.

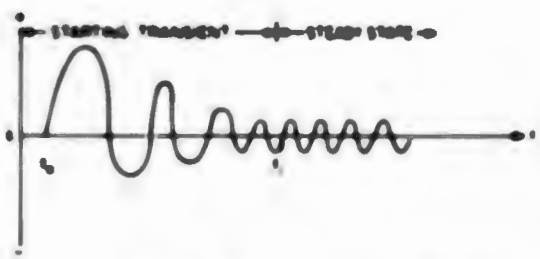

FIG. 2.4 Response time history of a simple system to steady-state forced vibration of the base, starting at time $t = t_0$

Shock or vibration may cause damage to an item in several ways [4,5]:

1. Ductile elements yield.
2. Brittle materials break.
3. Adjacent components collide, *e.g.*, between elements a and b in Fig. 2.1.
4. Friction bonds slip; and
5. Liquids spill.

These effects may occur either through exceeding the one-time failure stress limits of the structural materials or through fatigue phenomena leading to failure.

Failure may occur when the item is not operating, *e.g.*, during shipment or handling while packaged. If the item is turned on, the failure may also be a loss of efficiency through simple misalignment of components. Two of the

many possible examples are shaft bending and unacceptable noise in vacuum tubes.

Behavior of rubbers to complex. Complete understanding of all aspects of rubber behavior would probably require mastery of a number of technical disciplines, each of which is complicated. A large number of background texts exists in which basic concepts are more thoroughly explored than is possible in this monograph. The following writers in the broad fields indicated have proven particularly helpful to the author:

1. General historical background: Love [6], Timoshenko [7], Todhunter and Pearson [8], and Westergaard [9].
2. Elasticity: Bart [10], Fung [11], Landau and Lifshitz [12], Love [6], Sokolnikoff [13], Southwell [14], Timoshenko [7], and Westergaard [9].
3. Viscoelasticity: Alfrey [15], Bland [16], Davis [17], Eirich [18], Erdogan [19], Perry [20], and Fung [11].
4. Stress wave motion in solids: Bland [16], Brudnoy [21], and Kolsky [22].
5. Rheology: Alfrey [15], Eirich [18], and Hauwink [23].
6. Shock and vibration: Crandall [24], Crede [25], Den Hartog [26], Harris and Crede [26], McLachlan [27], Morrow [28], and Timoshenko [29].

Only enough of this tremendous volume of background material is extracted and repeated here to ensure that all readers start from the same base and to permit assessing the validity of statements concerning current state of the art.

Chapter 3

THEORETICAL APPROACH TO STRESSES IN A CUSHION

By Newton's third law, the force on a cushioned item is equal in magnitude to the force developed by the cushion. This chapter reviews some of the theoretical bases for analyzing the force developed by cushions.

In specific designs, the engineer is concerned with the absolute magnitudes of the forces developed and the motions generated in specific directions in cushions with specific shapes. The shapes are measured, for example, by surface area and thickness. It is more convenient, however, to express forces and deflections independently of their absolute magnitudes. The quantities used are defined as follows:

σ = stress – Consider a force, F, acting in a given direction on a cushion whose area exposed to this force is A. Stress is defined as the absolute magnitude of the force divided by the area upon which the force is acting. Note that, mathematically, one can take the area as large or as small as one pleases and that the latter option permits consideration of infinitesimally small forces on infinitesimally small areas.

ϵ = strain – Consider a vector whose scalar magnitude, in dimensions of length, is z. Consider a change in the magnitude of this vector, the magnitude of the change, in the same dimensions, being u. Strain is the dimensionless ratio between the magnitude of the change and the original magnitude. Again, both magnitudes may be taken as large or as small as one pleases, as long as consistency of units is maintained.

Mathematically, the definitions of these two quantities are

$$\sigma = \frac{F}{A_r} = \frac{dF}{dA_r} = \frac{\partial F}{\partial A_r},$$

and

$$\epsilon = \frac{u}{z} = \frac{du}{dz} = \frac{\partial u}{\partial z} \tag{3.1}$$

Both σ and ϵ are vector quantities and, therefore, both magnitude and direction require specification.

It should be understood that the definitions of Eq. (3.1) depend on an assumption of material continuity, *i.e.*, that the properties of a material remain unchanged no matter how small the sample might be. Real materials are never as homogeneous as that, and the assumption breaks down in the case of single-crystal behavior and, most notably, in molecular and atomic physics.

In work with cushions, however, one deals with macroscopic behavior and with properties macroscopically determined, the definitions of Eqs. (2.1) are to be regarded as convenient tools.

In the introduction it was stated that the cushion yields in response to the applied forces. This may be stated mathematically as

$$\sigma = f(\epsilon), \tag{2.2}$$

where $f(\epsilon)$ denotes some function, *i.e.*, a relationship between the quantity in parentheses and the quantity on the left side of the equation. Equation (2.2) states that *under identical conditions* the same stress (force) will produce the same strain (deflection) repeatedly.

In theory, if a functional relation exists, it can be expressed in explicit mathematical terms. From a practical standpoint, however, the final expressions may become so complicated as to be useless, at least for preliminary purposes. As will be shown, also, all of the functional relationship implied in Eq. 2.2 has not yet been exposed.

To set the stage for the practical expedients which have been adopted and to establish the limits of their applicability, the pertinent theory is reviewed.

2.1. Elastic Solids

The theoretical review is best begun with the simplest possible case: motion in a cushion which has linear characteristics in all directions, *i.e.*, obeys Hooke's law and is isotropic.

2.1.1. Motions in an Infinite Medium. Let the generalized system shown in Fig. 2.1 be subjected to a change in velocity. As a typical but nonexclusive example, let the system have a velocity, and let the motion be interrupted by contact with the substrate. Consider the motion of a point P somewhere within the cushion. For convenience, and for reasons that will be brought

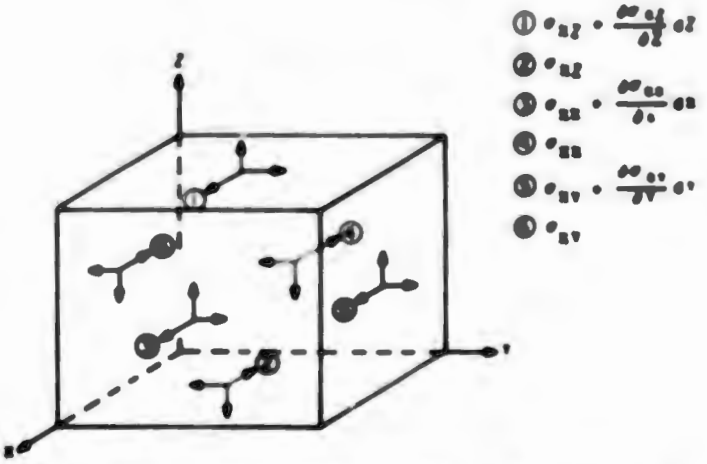

FIG. 2.1 Resultant stresses in the x-direction at the center of each face of the infinitesimal cube; similar expressions apply to each of the other axes.

out shortly, assume temporarily that point P is sufficiently far from the cone, from the rim, and from any free surface or interface, so that its motion can be completely described in terms of the stresses and strains in the cushion in the neighborhood of P. In the theoretical works, "sufficiently far" is undefined, and the treatment which follows assumes that all real cushion dimensions are so large that they may be regarded as practically infinite compared to the region being considered.

In this case, "neighborhood" denotes an infinitesimally small region around point P, but including some of the cushion. This region may be described geometrically in any convenient set of coordinates. Cartesian coordinates are used here, and Fig. 2.1 is a visualization of this region. In the figure, σ_{xx} denotes a stress in the x-direction acting in the yz-plane. Keisky [22], for one, has derived the equations of motion of P and has found that they can be written, ignoring body forces such as internal stresses and the acceleration of gravity, as

$$\rho \frac{\partial^2 u}{\partial t^2} = \frac{\partial \sigma_{xx}}{\partial x} + \frac{\partial \sigma_{xy}}{\partial y} + \frac{\partial \sigma_{xz}}{\partial z},$$

$$\rho \frac{\partial^2 v}{\partial t^2} = \frac{\partial \sigma_{yx}}{\partial x} + \frac{\partial \sigma_{yy}}{\partial y} + \frac{\partial \sigma_{yz}}{\partial z}, \qquad (2.3)$$

$$\rho \frac{\partial^2 w}{\partial t^2} = \frac{\partial \sigma_{zx}}{\partial x} + \frac{\partial \sigma_{zy}}{\partial y} + \frac{\partial \sigma_{zz}}{\partial z},$$

where ρ = density of the cushion,

u = deflection in the x-direction,

v = deflection in the y-direction,

w = deflection in the z-direction, and

t = time.

These equations of motion will hold, whatever the stress-strain relationships for the cushion may be. Their solution, however, requires substitution of the strains corresponding to the stresses, and this operation gives rise to formidable mathematical difficulties. In fact, a generalized solution to the configuration of Fig. 2.1 is not known to have been found, except for extended, isotropic solids with linear elasticity.

Hooke's law, when generalized to three dimensions, requires the use of 36 coefficients in the possible directions of motion, six for each component of strain in each of six possible stress modes.

It has been shown, by Love [6] for example, that these 36 coefficients can be reduced to 21 if the elastic energy is to be a single-valued function of strain, a key component of the hypothesis of linearity. For a linear isotropic solid, these 21 independent coefficients can be reduced to the two Lamé coefficients, λ and μ. This reduction can be accomplished on purely mechanical and geometric grounds but some investigators such as Landau and Lifshitz [12] prefer a reduction using thermodynamics, deriving λ and μ by considering a scalar expansion of the free energy of the body as a function of the strain tensor.

In measuring the properties of materials, it is more practical to consider four basic material constants instead of the two Lamé coefficients. These four constants and their symbols are defined as:

E = modulus of elasticity, the ratio between the applied stress and the fractional deflection when a cylindrical or prismatic specimen is subjected to a uniform stress over its plane ends and its lateral surfaces are free from constraint. In the immediate case, E is the same in all directions. As will be shown, E_x, E_y may be different for a given material, depending on the loading direction.

ν = Poisson's ratio, the ratio between lateral contraction (or extension) and the longitudinal extension (or contraction) of the specimen, with the lateral surfaces again free. As a result of its derivation, the range of ν is $0 \leq \nu \leq 0.50$.

K = bulk modulus, the ratio between the total pressure applied and the fractional change in volume when the solid is subjected to uniform hydrostatic compression on all its faces.

μ = rigidity modulus or shear modulus, the ratio between the shear stress and the shear strain. This modulus is identical with Lamé's second constant.

The moduli and Lamé's constants can be interrelated. Table 2.1 summarizes these interrelations. Which set is used is generally a matter of the individual author's preference.

In this treatise, the isothermally measured values are taken as if they were applicable. Landau and Lifshitz [12] note that any distortion of any solid involves a change in the internal energy level with a corresponding change in the heat content. The change in heat content in a specific region is usually so small, and the flux so slow that isothermal conditions may be assumed.

TABLE 2.1 RELATIONSHIP OF ELASTIC CONSTANTS

Constant	Elastic Constants Expressed in Terms of				
	λ, μ	K, μ	μ, ν	E, ν	E, μ
Lamé's constant, λ	λ	$K - \frac{2}{3}\mu$	$\frac{2\mu\nu}{1-2\nu}$	$\frac{E\nu}{(1+\nu)(1-2\nu)}$	$\frac{\mu(E-2\mu)}{3\mu-E}$
Lamé's constant, μ	μ	μ	μ	$\frac{E}{2(1+\nu)}$	μ
Elasticity modulus, E	$\frac{\mu(3\lambda+2\mu)}{\lambda+\mu}$	$\frac{9K\mu}{3K+\mu}$	$2\mu(1+\nu)$	E	E
Poisson's ratio, ν	$\frac{\lambda}{2(\lambda+\mu)}$	$\frac{3K-2\mu}{6K+2\mu}$	ν	ν	$\frac{E}{2\mu}-1$
Bulk modulus, K	$\lambda+\frac{2}{3}\mu$	K	$\frac{2\mu(1+\nu)}{3(1-2\nu)}$	$\frac{E}{3(1-2\nu)}$	$\frac{E\mu}{3(3\mu-E)}$
Rigidity or shear modulus, μ	μ	μ	μ	$\frac{E}{2(1+\nu)}$	μ

In truly precise work, or when designing for extreme temperature service, the adiabatic elastic constants should be used. The relationship between the isothermal, E_{ii}, and the adiabatic, E_{ad}, moduli of elasticity is, with good accuracy,

$$E_{ad} = E_{ii} + \frac{E_{ii}^2 T_o c_e^2}{9 c_p}. \tag{3.4}$$

where T_o = absolute temperature,

c_e = coefficient of thermal expansion, and

c_p = specific heat per unit volume.

Normally the second term on the right-hand side of Eq. (3.4) is quite small and is ignored.

But even our lack of the necessary tools does not excuse our ignoring heat development and the associated temperature rise in a cushion under prolonged cyclic stress.

Using Lamé's constants, the six stress-strain relationships are

$$\begin{gathered} \sigma_{xx} = \lambda\Delta + 2\mu\epsilon_{xx}, \quad \sigma_{yy} = \lambda\Delta + 2\mu\epsilon_{yy}, \quad \sigma_{zz} = \lambda\Delta + 2\mu\epsilon_{zz}, \\ \sigma_{yz} = \mu\epsilon_{yz}, \quad \sigma_{xz} = \mu\epsilon_{xz}, \quad \sigma_{xy} = \mu\epsilon_{xy}. \end{gathered} \tag{3.5}$$

where

$$\Delta = \epsilon_{xx} + \epsilon_{yy} + \epsilon_{zz}$$

is called the dilatation and represents the change in volume of a unit cube.

Substitute Eqs. (3.5) in Eqs. (3.3). The result is

$$\begin{aligned} \rho \frac{\partial^2 u}{\partial t^2} &= (\lambda + \mu) \frac{\partial \Delta}{\partial x} + \mu \nabla^2 u, \\ \rho \frac{\partial^2 v}{\partial t^2} &= (\lambda + \mu) \frac{\partial \Delta}{\partial y} + \mu \nabla^2 v, \\ \rho \frac{\partial^2 w}{\partial t^2} &= (\lambda + \mu) \frac{\partial \Delta}{\partial z} + \mu \nabla^2 w, \end{aligned} \tag{3.6}$$

where

$$\nabla^2 = \left(\frac{\partial^2}{\partial x^2} + \frac{\partial^2}{\partial y^2} + \frac{\partial^2}{\partial z^2} \right)$$

is the Laplacian operator.

It is a straightforward series of operations (see, for example, Kolsky's simple derivation [22]) to separate each of Eqs. (3.6) into two equations expressing the propagation of waves of dilatation and of rotation. If there is no rotation,

$$\rho \frac{\partial^2 u}{\partial t^2} = (\lambda + 2\mu) \nabla^2 u \tag{3.7}$$

holds for the motion in the x-direction. If there is no dilatation, then

$$\rho \frac{\partial^2 u}{\partial t^2} = \mu \nabla^2 u. \tag{3.8}$$

This separation may be regarded as the separation of a vector into its component parts.

The two waves travel with different velocities:

$$V_1 = \left(\frac{\lambda + 2\mu}{\rho}\right)^{1/2},$$
$$V_2 = \left(\frac{\mu}{\rho}\right)^{1/2}, \tag{3.9}$$

where V_1 is the velocity of the dilatational wave and V_2 is the velocity of the distortional wave.

Equations (3.7) and (3.8) are the classical wave equations written here only for u but with the understanding that corresponding relations exist for v and w.

The generalized solution for these equations is

$$u = f_1(x - V_{1,2}\,t) + f_2(x + V_{1,2}\,t), \tag{3.10}$$

where f_1 and f_2 are arbitrary functions depending on the initial and boundary conditions. The function f_1 corresponds to a wave traveling along the positive direction of the x-axis, while f_2 corresponds to a wave traveling in the negative direction along the same axis.

Once f_1 and f_2 are found, straightforward double differentiation with respect to time will produce a value for acceleration at any time at point P.

3.1.2. Effects of Boundaries. Suppose now that the yz-plane of Fig. 3.1 is a free surface and that an internal wave strikes this surface. The wave will be reflected back into the medium at an angle equal to the angle of incidence.

To complicate matters, however, each kind of wave (except at 0 or 90 degree incidence) will give rise to (at least) two waves, one of its own type and one of the other type. Thus, a dilatational wave will produce a dilatational wave at an angle of departure from the surface equal to the angle of incidence, and also a distortional wave at a different angle. Setting α_1, as the departure angle of the dilatational wave and β_1 as the departure angle of the distortional wave, it is found that

$$\frac{\sin \alpha_1}{\sin \beta_1} = \frac{V_1}{V_2}. \tag{3.11}$$

Note that the total energy content of the two waves must equal the energy content of the incident wave. On a simple single reflection, therefore, there would be two different types of wave, each with two different energy levels. It can be seen that finding the exact state of stress at any given instant can be difficult.

In addition, there are "Rayleigh surface waves." Their effect decreases rapidly with depth, and their propagation velocities are smaller than the two kinds of wave previously considered. Derivation of the equations of motion is complex (*e.g.*, Kolsky [22]) and will not be given here. The particle motion in Rayleigh waves is in a plane perpendicular to the surface along which the waves are traveling and parallel to the direction of propagation.

The velocity of Rayleigh waves is a fraction, κ_1, of the velocity of distortional waves, V_2. The value of κ_1 is obtained from

$$\kappa_1^6 - 8\kappa_1^4 + (2V_2 - 16\alpha_2^2)\kappa^2 + 16\alpha_2^2 - 16 = 0, \tag{3.12}$$

in which α_2 is an elastic constant of the material totally dependent on Poisson's ratio, such that

$$\alpha_2^2 = \frac{1 - 2\nu}{2 - 2\nu}. \tag{3.13}$$

Depth of penetration of the waves is of the order of a small fraction of the wavelength. With small cushions, Rayleigh waves may contribute a significant element to the overall stress state.

3.1.3. Plane Waves in Semi-Infinite Media and Rods. No restrictions have yet been placed on the direction of motion of the waves through the medium with respect to any particular set of coordinates; a designer can usually arrange coordinates to suit his convenience. We will now discuss the propagation of waves in specified directions.

Construct a set of three rectangular coordinates. Consider a wave propagated parallel to the x-axis in an infinite medium. In the body of the medium, construct two planes parallel to the yz-plane. A plane wave exists if there is one-to-one correspondence between the magnitudes and directions of motion of corresponding points in each plane. To obtain such correspondence, let there be uniform stress on the yz-surface of the infinitesimal cube shown in Fig. 3.1. In macroscopic real structures, the same restriction prevails; practically all available design information depends on this basic assumption.

Now let the velocity of propagation of this plane wave be V_3. Then the displacements, u, v, and w, will each be functions of a single parameter, $\psi = x - V_3 t$. We will then have the acceleration equations,

$$\frac{\partial^2 u}{\partial t^2} = V_3^2 \frac{\partial^2 u}{\partial \psi^2}, \frac{\partial^2 v}{\partial t^2} = V_3^2 \frac{\partial^2 v}{\partial \psi^2}, \frac{\partial^2 w}{\partial t^2} = V_3^2 \frac{\partial^2 w}{\partial t^2}, \tag{3.14}$$

and the acceleration equations,

$$\frac{\partial^2 u}{\partial x^2} = \frac{\partial^2 u}{\partial t^2}, \frac{\partial^2 v}{\partial x^2} = \frac{\partial^2 v}{\partial \psi^2}, \frac{\partial^2 w}{\partial x^2} = \frac{\partial^2 w}{\partial \psi^2}. \tag{3.15}$$

The differential coefficients of u, v, and w with respect to y and z will all be zero.

Substitute these six relations in Eqs. (3.3). The result is

$$\begin{aligned} \rho V_3^2 \frac{\partial^2 u}{\partial \psi^2} &= (\lambda + 2\mu) \frac{\partial^2 u}{\partial \psi^2}, \\ \rho V_3^2 \frac{\partial^2 v}{\partial \psi^2} &= \mu \frac{\partial^2 v}{\partial \psi^2}, \\ \rho V_3^2 \frac{\partial^2 w}{\partial \psi^2} &= \mu \frac{\partial^2 w}{\partial \psi^2}. \end{aligned} \tag{3.16}$$

Equations (3.16) can be satisfied in either of two mutually exclusive ways: Either

$$V_3^2 = (\lambda + 2\mu)/\rho$$

with both $\partial^2 v/\partial\psi^2$ and $\partial^2 w/\partial\psi^2$ equal to zero, or

$$V_3^2 = \mu/\rho$$

with $\partial^2 u/\partial\psi^2 = 0$.

In the former case, there are longitudinal waves traveling in the x-direction with the velocity of dilatational waves; in the latter, the motion is transverse and parallel to the wave front and moving with the speed of distortional waves. This does not mean that waves of the two types cannot coexist in the same solid, but it does mean that longitudinal motion is not affected by transverse motion, and *vice versa*; this permits emphasis on motion in any chosen direction.

Let us see how far this theory will go, when applied to cushions with finite dimensions. Consider a cushion such as that shown in Fig. 3.2; the shape of the upper surface being any closed curve whose area is A_c.

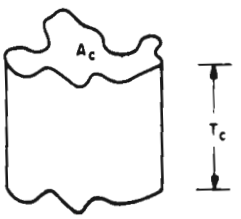

FIG. 3.2. A finite cushion.

When the stress is compressive, a plane wave obviously will no longer exist if the column buckles. The maximum allowable stress [30] for a column with unfixed ends is given by

$$\sigma = \frac{\pi^2 E I_n}{A_c T_c^2}, \tag{3.17}$$

where I_n is the area moment of inertia and T_c is the cushion thickness. In practice, stresses less than this should be used. Assuming reasonably large values of the dimensions in the y and z directions, Kerstner's [31] rule of thumb,

$$A_c \geq (1.33 T_c)^2, \tag{3.18}$$

proves satisfactory in practice.

Because of the boundary conditions imposed by the side walls, great theoretical difficulties are encountered in considering a cushion as a bar or uniformly stressed plate. The only complete theoretical treatments are concerned with uniform bars of circular cross section. These solutions involve the frequency and wavelength of the disturbance, the radius of the cylinder, the elastic constants λ and μ, and the density ρ. Even these are not exact for cylinders of finite length. When the length is very much larger than the radius, the residual stress becomes very small. In the exact theory, the waves move with the dilatational wave velocity. In the simplified solution (satisfactory only when the wavelength is approximately ten times the radius), the wave velocity is found to equal $(E/\rho)^{1/2}$. The Poisson effect is thereby ignored; actually it is very small, sometimes negligible, for many cushions. From the definition

of ν in terms of Lamé's constants (column 2 of Table 3.1) it can be seen that a necessary condition for $\nu = 0$ is that λ be zero also. With λ zero, dilatational velocity becomes $(2\mu/\rho)^{1/2}$, while E becomes equal to 2μ. Thus, V_3 must take on the value $(E/\rho)^{1/2}$, as indicated by the simplified theory. In other words, when Poisson's ratio is truly zero, the velocity given by the simplified theory will hold regardless of the dimensions of the top surface area, A_c, up to the buckling stress limit.

For plane waves passing through plates (dimensions of A_c are large compared with T_c as in Fig. 3.2), Bancroft [32] suggests a distinction between those cases where lateral motion is inhibited and those where it may occur without restriction. When lateral motion can occur freely, the operative elastic constant will be E; where it cannot, it will be $\lambda + 2\mu$.

Soper and Dove [33] examined the problem from the standpoint of an influence zone adjacent to the free edge of a cushion undergoing an impulsive loading. They considered a flat cushion confined top and bottom, as shown in Fig. 3.3. The stress laws of the cushion are linear and isotropic, and the system is infinite in the z-direction.

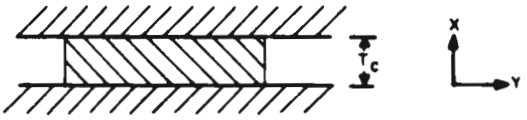

FIG. 3.3. Cushion system of Soper and Dove [33]; z-axis is normal to paper.

The stress laws applicable to the material in Fig. 3.3 are

$$E\epsilon_x = \sigma_x - \nu\sigma_y \quad \nu\sigma_z,$$
$$E\epsilon_y = \sigma_y - \nu\sigma_x - \nu\sigma_z, \tag{3.19}$$

and

$$E\epsilon_z = \sigma_z - \nu\sigma_x - \nu\sigma_y.$$

Material deformation begins with an instantaneous compression in the x-direction to a stress of σ_x. Immediately following compression, the state of strain in the material is everywhere constant, since there has been no time for waves to travel from the stress-free edges into the material. The conditions at this moment are

$$\epsilon_y = \epsilon_z = 0, \ \sigma_z = \sigma_y,$$

from which we obtain, by substitution in Eqs. (3.19),

$$\sigma_x = \sigma_y = \frac{\nu}{1-\nu}\sigma_z \tag{3.20}$$

and

$$\epsilon_x = \frac{1-2\nu}{(1-\nu)^2} \cdot \frac{\sigma_z}{E}. \tag{3.21}$$

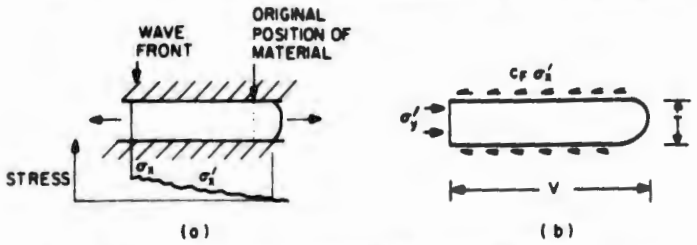

FIG. 3.4. Edge effects in a compressed cushion [33]: (a) visualization of wave front, and (b) free body diagram.

Following compression, a wave runs into the material from the free edge. Behind the wave the stresses are less, the y-strain is positive, and the material is slipping outward. The situation near an edge is shown in Fig. 3.4. Values behind the wave front are denoted by primes. Note that the shear stress exerted by the slipping portion is given by $c_f\sigma'_x$, where c_f is the coefficient of friction between the cushion and the confining surface.

The situation immediately after the start of relaxation wave motion can be described in terms of the following set of conditions

$$\sigma'_y = \epsilon'_y = 0, \quad \epsilon'_x = \epsilon_x, \quad \sigma'_x \geq \frac{1-2\nu}{(1-\nu)^2} \cdot \sigma_x .$$

From the definition of shear stress, these conditions give rise to the inequality

$$\sigma'_x \geq \frac{2vc_f}{T_c} \cdot \frac{1-2\nu}{(1-\nu)^2} \cdot \sigma_x , \tag{3.22}$$

where, as before, v is the motion in the y-direction. It can be seen that the value of σ'_x increases as v increases, since all other terms are constant for the system. When σ'_x attains its own maximum value σ_x, the wave must fail to exert significant influence on the x-direction state of strain. This limiting value of v is obtained by setting $\sigma'_x = \sigma_x$, from which the criterion

$$v = \frac{\nu T_c}{2c_f} \cdot \frac{1-\nu}{1-2\nu} \tag{3.23}$$

is achieved.

When c_f is zero, v is infinite, and relaxation waves alter the state of stress throughout the material. This fact is not troublesome, because frictional forces never vanish completely in real systems. Similarly, if $\nu = 0$, then $v = 0$; this is to be expected since the material does not tend to expand in the y-direction. This result was predicted by the other considerations summarized above.

For known real values of Poisson's ratio, the magnitude of the edge effect is clearly dependent on the value of this ratio and on the coefficient of friction. If, for example, both variables equal 0.3, then v equals about $0.9T_c$. On this basis, the edge-zone effect does not extend into the cushion by more than the order of magnitude of cushion thickness. Everywhere else, stress in the cushion is essentially uniform.

Thus, if the cushion surface is sufficiently large in comparison with the thickness, the relaxation-wave effects from the free edges can be ignored for practical purposes. If the Poisson effect is negligible, edge effects can be ignored regardless of cushion dimensions. Finally, edge effects can be ignored whenever the cushion can expand laterally with total freedom. Of course, when the stress is compressional, column stability is a factor.

What if the cushion is similar to that illustrated in Fig. 2.1, where there are no edges? Then, by specifying that the cushioned-item dimensions shall be large in comparison with cushion thickness, a semi-infinite continuum may be assumed.

3.1.4. Limitations of the Treatment. This monograph has so far given only a limited treatment to its subject. It has not done justice to the more fascinating problems of wave motion in extended solids. It is now time to review some key assumptions which have governed the treatment and discuss some of their practical implications.

1. An elastic material obeys Hooke's law; *i.e.*, stress and strain are linearly related. No materials obey this law exactly, although some metals almost do for small strains. In metallurgy and engineering, the point of departure from linearity is called the elastic limit, a well-recognized property of most materials. To be mathematically rigorous, we must say that the equations used here were derived and are valid only for infinitesimally small strains. Satisfactory theory for measurable strains seems lacking although Murnaghan [34] has made progress; also Green and Adkins [35] discuss the difficulties involved and show that considerable progress has been made. However, this theoretical limitation is true for almost every significant formula in the strength-of-materials field, and it has never prevented practical use of the findings.

2. All detailed derivations have proceeded on the assumption that the material is isotropic. It was pointed out that the original equations of motion, Eqs. (3.3), were independent not only of the form of the stress-strain relation in specified directions but also of the linearity or nonlinearity of the functions concerned. In an anisotropic solid, the 36 independent constants must be used. The problems are complicated, though responsive to the application of matrices in an electronic computer. However, by shifting to the concept of plane waves, we can—without significant loss in generality—concentrate on an elastic constant applicable to a given direction. The demands of rigor are not met in the determination of effects of edges on overall response, but the treatment used is acceptable in terms of orders of magnitude.

3. All derivations have assumed continuity of the material. How can conclusions based on this assumption be drawn when many of the materials dealt with are evidently macroscopically discontinuous? In Chapter 2, continuity is assumed almost as an article of faith. Smiley [36] investigated wave motion through rubberized curled hair, a cushion whose structure is obviously discontinuous. Working with strains on the linear portion of the stress-strain curve he computed wave-transit times, taking into account increased medium density with each increment of strain. Even though he ignored dissipative effects of internal friction in the medium, he found remarkably close correlation between the time of appearance of reflected pulses

in an accelerometer record taken from a drop test and the results to be expected from theory. In other words, there is some experimental evidence that the overall schema is adequate for supplying a description of the actual phenomena.

4. Hardest to justify is the assumption of linearity. Nonlinearity is the general rule for materials. Some aspects of this problem will be discussed in the next section.

3.2. Imperfectly Elastic Solids

Previous discussion has assumed that the stress-strain curve in a given direction, measured while the material is being loaded or unloaded, is as shown in Fig. 3.5. If this were the case, there would be no energy losses in the system; once disturbed, it would continue to oscillate with the same frequency and amplitude. Obviously this does not describe reality. Even an ideal pendulum, fabricated from a very thin wire with a weight at its end, will come to rest in time—whether the oscillation takes place in air or in a vacuum.

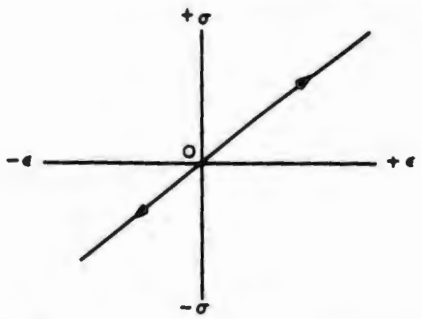

FIG. 3.5. Theoretical stress-strain curve for a linear undamped material under cyclic stress.

Imperfect elasticity exists whenever the material fails to conform to Hooke's law. A material may not obey Hooke's law because of inherent nonlinearity of its stress-strain relationship, or because it has been strained beyond the "proportional elastic limit" (where the stress-strain curve ceases to be linear) or beyond its "true elastic limit" (where deformation becomes permanent). Strains beyond this point are called plastic strains. Both types of imperfect elasticity occur in cushions. This overall discussion will begin with those deviations from perfect cushion elasticity due to internal causes classified as "damping" or "internal friction."

When a material is stressed, some energy is always lost as heat. The stress-strain relation, even for a material which appears linear when the stress is applied very slowly (usually called static or quasistatic loading), usually resembles the curve shown in Fig. 3.6. The area enclosed by the loop, called a hysteresis loop, is a measure of the energy loss. In vibration or shock work this energy loss is called "damping." Any material that tends to return to the zero point when stress is removed may be considered anelastic. This definition holds even when the time for return to zero is very long.

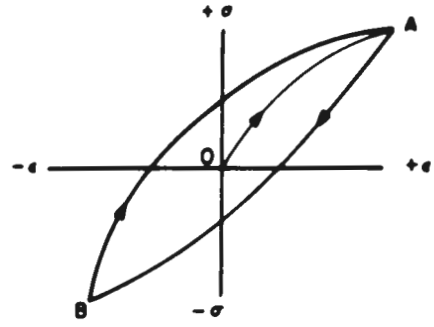

FIG. 3.6. Typical stress-strain diagram for an actual material under cyclic stress; OA represents initial loading, and ABBA is complete hysteresis loop.

A number of theories have been advanced to account for the phenomenon sketched in Fig. 3.6. For organic materials, the causes have been traced to the behavior of individual molecules; excellent discussions of these areas may be found in Alfrey [15], Ferry [20], Houwink [23], and Tobolsky, Powell, and Eyring [37]. In metals, a substantial cause appears to be the relative motion of individual crystals of the material; here, Zener's text [38] is considered classic. Lazan and Goodman [39] summarize by pointing out that damping may be associated with, but not limited to, plastic slip or flow, magnetomechanical effects, dislocation movements, and inhomogeneous strain. Kolsky [22] emphasizes the distinction between "static" hysteresis (where the damping is practically independent of frequency) and frequency-dependent energy losses (which may be considered viscous in character).

Regardless of root causes, the engineer must realize that the comfortable world of solids, liquids, and gases, with their well-defined laws of behavior, does not necessarily exist. Explanations of energy losses in cushions are forthcoming in the field of "viscoelasticity," a coined work which describes the fluid characteristics of deformed solids. Various aspects of viscoelasticity will be discussed in the following sections, in order to establish a frame of reference within which we may assess the current state of development of cushioning theory and practice.

3.2.1. Basic Concept of Viscoelasticity. Solid materials which possess certain fluid characteristics are called viscoelastic. They exhibit some qualities of rigidity characteristic of solid bodies but, at the same time, they flow and dissipate energy by frictional losses as do some fluids. Heat is generated by friction; therefore, thermal effects accompany mechanical deformation and flow.

Investigations of viscoelasticity are not new. However, possibly because of the demands of solid-propellant technology, what was once a quiet theoretical backwater has become one of the most active fields of research in theoretical mechanics. As an example of its activity, the files of the Defense Documentation Center produced about 300 abstracts of reports treating various aspects of viscoelasticity which had appeared between 1961 and 1966.

Complete review and assessment of such an active field is outside the scope of this monograph. For those interested in pursuing the subject further, Eringen and Grot [40] give a brief review of significant work in the field. Early work is summarized by Eirich [18], among others. The status of development of nonlinear theories through 1962 is discussed by Eringen [19]. An excellent review of progress in the entire field of continuum mechanics was prepared by Spencer [41].

Three pertinent facts about present theory may be stated:

1. Axiomatic, rigorous theories of viscoelasticity exists; see, for example, Refs. 19, 40 and 42.
2. There are adequate theories covering finite motions, such as those found in Refs. 43, 44, and 45.
3. Problems of wave motion in viscoelastic materials are being actively attacked by many investigators, notably M. E. Gurtin and his co-workers at Brown University.

This summary, though incomplete, indicates the existence of a broad body of rigorous theory upon which to base sound engineering practice.

Viscoelastic theory states that Eq. (3.2) does not fully describe the one-dimensional stress law applicable to a material. Instead, we must write

$$\begin{aligned} \sigma &= f_1(\epsilon, t, T_a) \\ Q_f &= f_2(\epsilon, t, T_a) \\ e_1 &= f_3(\epsilon, t, T_a) \\ e_2 &= f_4(\epsilon, t, T_a), \end{aligned} \tag{3.24}$$

where t = time,

T_a = absolute temperature,

Q_f = heat flux,

e_1 = internal energy density per unit mass, and

e_2 = entropy per unit mass,

thus forming a thermodynamic system in terms of observable values. When generalized for a three-dimensional volume, Eqs. (3.24) take a tensor form, and the functions, f_i, are "functionals" [46], *i.e.*, generalizations of ordinary functions. If a function is considered as a "mapping" of a set of numbers in the number space, then a functional is the operation of "mapping" a set of functions into another such set in the function space.

The arguments on the right-hand side of Eqs. (3.24) include not only present time but also time derivatives of strain and time derivatives of stress.

Engineering solutions to the general tensor equations, assuming that the appropriate material constants are available, are extremely complex; most practical work is done with as many simplifying assumptions as the problem allows.

In any case, however, it is clear that the stress in real materials is a function not only of strain but also of time (present time and rate) and of temperature. Studies of cushions are incomplete when they do not take these latter variables

into account. In determining specific properties of materials it is always important to stipulate measurement temperature and time.

The general theories of continuum mechanics of viscoelastic substances are extremely complex, as intimated above. The next several sections will extract from the body of general theory several important principles applicable to cushions. The equations will be written as though plane stresses were being applied, in order to avoid the difficulties of tensor notation. Further, unless otherwise indicated, these equations will assume a constant ambient temperature and no heat flux into or out of the cushion. The first of these conditions is easy to achieve experimentally. The second can be approximated by making stress application either so rapid that there is no time for heat transfer, or so slow that the heat generation rate is negligible.

3.2.2. The Memory Concept. Pretend that materials have a "memory." The purely elastic materials, which obey Hooke's law, have the simplest memory of all. When stress is removed, these materials invariably return to the "remembered" unstrained state. For most materials, however, memory is more complicated; the present state of the material cannot be determined unless its past history is known. Some of the consequences of this simple premise will now be developed, following the line taken by Fung [11].

Let the stress at time t be some time-dependent function, $\sigma(t)$. Also, let the total strain be a time-dependent function, $\epsilon(t)$. If $\sigma(t)$ is continuous and differentiable, then, in a small time interval, $d\tau$, the stress increment is $\dot{\sigma}(\tau)d\tau$. This increment will continue to act and contributes an element $d\,\epsilon(t)$ to the previous strain $\epsilon(t)$, depending on the time interval $(t-\tau)$ through a proportionality factor C. Hence,

$$d\,\epsilon(t) = C(t-\tau)\,\dot{\sigma}\,(\tau)\,d\tau. \tag{3.25}$$

Then, the entire history of the loading produces

$$\epsilon(t) = \int_0^t C(t-\tau)\,\dot{\sigma}\,(\tau)\,d\tau, \tag{3.26}$$

where $C(t-\tau)$, usually written $C(t)$ (since τ can have any arbitrarily small finite value) is called the creep function. Physically, $C(t)$ may be regarded as the deflection produced by sudden application at $t = 0$ of a constant force of unit magnitude, *i.e.*, of a unit step function, sometimes called the Heaviside Unit Function.

Since stress and strain are related through some functional arrangement, the following also holds:

$$\sigma(t) = \int_0^t r(t-\tau)\,\dot{\epsilon}\,(\tau)\,d\tau. \tag{3.27}$$

The group $r(t-\tau)$, or more simply, $r(t)$, is called the "relaxation function" and may be regarded as the force which must be applied at $t = 0$ to produce a normalized strain that changes from 0 to 1.0 and remains 1.0 thereafter. Materials behaving in accordance with Eqs. (3.26) and (3.27) are called Boltzmann solids.

In order to express non-retroactivity—*i.e.*, the requirement that the future shall not govern the present—it is customary to write the conditions

$$C(t) = 0, \; t < 0,$$
$$r(t) = 0, \; t < 0, \tag{3.28}$$

although non-retroactivity is implicit in setting t as the upper limit of integration in Eqs. (3.26) and (3.27).

Table 3.2 shows the creep and relaxation functions for a number of simple mathematical models made up of simple spring elements that are assumed linear and massless and of dashpots in which a piston is moving through a liquid that obeys Newton's law of viscosity (velocity is proportional to strain). Typical creep functions are shown in Fig. 3.7, while Fig. 3.8 shows relaxation behavior.

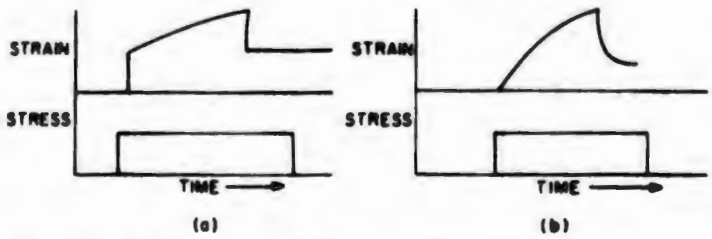

FIG. 3.7. Behavior of some simple creep functions: (a) Maxwell solid, and (b) Voigt solid.

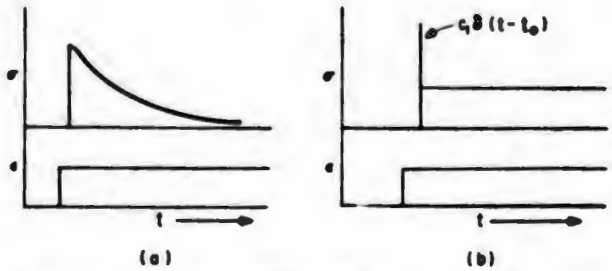

FIG. 3.8. Behavior of some simple relaxation functions: (a) Maxwell solid, and (b) Voigt solid.

In Table 3.2 the function $H(t)$ is the unit step function, defined as

$$H(t) = \begin{cases} 1.0, \; t > 0 \\ 0, \; t < 0 \end{cases}, \tag{3.29}$$

while $\delta(t)$ is the Dirac delta function. This latter function has the following characteristics:

$$\delta(t) = 0, \text{ when } t \neq 0,$$
$$\delta(t) = \infty, \text{ when } t = 0, \text{ and} \tag{3.30}$$
$$\int_{-\infty}^{\infty} \delta(t) \, dt = 1.0.$$

TABLE 3.2. SOME CREEP AND RELAXATION FUNCTIONS

Function	*Linear*	*Dashpot*	*Voigt Solid*	*Maxwell Solid*
Pictorial representation				
Stress law	$\sigma = E\epsilon$	$\sigma = c\frac{d\epsilon}{dt}$	$\sigma = E\epsilon + c\frac{d\epsilon}{dt}$	$\frac{\sigma}{c} + \frac{1}{E}\frac{d\sigma}{dt} = \frac{d\epsilon}{dt}$
Creep function	$\frac{1}{E} \cdot H(t)$	$\frac{t}{c} \cdot H(t)$	$\frac{1}{E}(1 - e^{-Et/c}) \cdot H(t)$	$\left(\frac{1}{E} + \frac{t}{c}\right) \cdot H(t)$
Relaxation function	$E \cdot H(t)$	$c \cdot \delta(t)$	$E \cdot H(t) + c\,\delta(t)$	$(Ee^{-Et/c}) \cdot H(t)$

The appearance of this latter function in the results indicates that the stress is infinite at the instant that strain occurs. A dashpot, unlike a spring, cannot give a finite instantaneous strain response to a finite instantaneous force change. Therefore, an infinite force is required to produce a finite instantaneous strain.

It is seen in Table 3.2 that the creep function for the Voigt solid contains the factor $e^{-Et/c}$, as does the relaxation function for the Maxwell solid. By setting $\tau' = c/E$, the descriptions can be simplified so that the creep function for the Voigt element can be written

$$C(t) = Y \cdot (1 - e^{-t/\tau'}) \cdot H(t), \tag{3.31}$$

where Y is the compliance, defined as $1/E$. Here, τ' is called the retardation time. Similarly, the relaxation function for the Maxwell solid can be written

$$r(t) = E \cdot e^{-t/\tau'} \cdot H(t), \tag{3.32}$$

where τ' is now called the relaxation time.

Consider, now, a number, n, of Maxwell units connected in parallel, as shown in Fig. 3.9. Two conditions prescribe the behavior of the model:

a. The total stress is the sum of the stresses in each element, or

$$\sigma(t) = \sum_{j=1}^{n} \sigma(t)_j, \; j = 1,2, \ldots, n. \tag{3.33}$$

b. The strain in each element is the same, or

$$\epsilon(t)_i = \epsilon(t)_j, \; i,j = 1,2, \ldots, n. \tag{3.34}$$

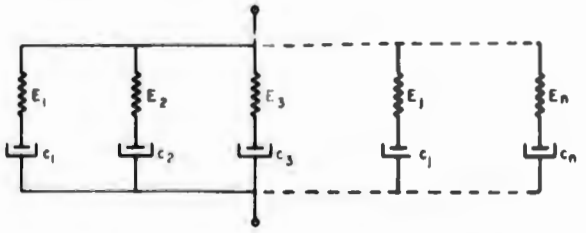

FIG. 3.9. A number (n) of Maxwell elements in parallel.

Using these principles, Bland [16] shows that any number of Maxwell elements may be added to arrive at a discrete relaxation spectrum for the solid

$$r(t) = \sum_{j=1}^{n} (E_j e^{-t/\tau_j}) \cdot H(t). \tag{3.35}$$

A particularly interesting special case arises when, in Fig. 3.9, $c_1 = 0$ (so that the first element is a linear spring) and $E_2 = 0$, (so that the second element is a dashpot only). Then, using the principles for combination – Eqs. (3.33) and (3.34) – Eq. (3.35) may be written

$$r(t) = E_1 \cdot H(t) + c_2 \cdot \delta(t) + \sum_{j=3}^{n} E_j \cdot e^{-t/\tau_j} \cdot H(t). \tag{3.36}$$

As $n \to \infty$, the summation term in Eq. (3.35) tends to an integral, so that

$$r(t) = H(t) \cdot \int_0^\infty r'(t) \cdot e^{-t/\tau} \cdot d\tau', \tag{3.37}$$

where $r'(t)$ is to be interpreted as the continuous relaxation spectrum.

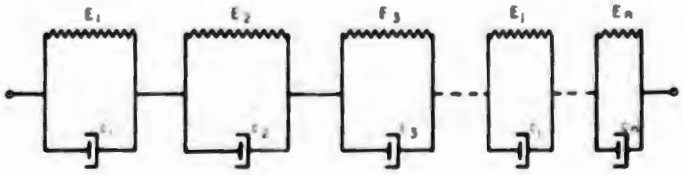

FIG. 3.10. A number (n) of Voigt elements in series.

Now, consider a number of Voigt elements connected in series, as in Fig. 3.10. The conditions on a series model of this nature are:

1. The external strain equals the sum of the strains on each element, or

$$\epsilon(t) = \sum_{j=1}^{n} \epsilon(t)_j, j = 1,2, \ldots, n. \tag{3.38}$$

2. The stress in each element is the same

$$\sigma(t)_i = \sigma(t)_j, i,j = 1,2, \ldots, n. \tag{3.39}$$

As before, the generalized creep function is

$$C(t) = H(t) \cdot \sum_{j=1}^{n} Y_j(1 - e^{-t/\tau_j}), \tag{3.40}$$

and, in the case of $c_1 = 0$ and $E_2 = 0$,

$$C(t) = H(t) \cdot \int_0^\infty C'(t) \cdot (1 - e^{-t/\tau'}) \cdot d\tau', \tag{3.41}$$

where $C'(t)$ is the generalized creep spectrum. The generalized Maxwell model and the generalized Voigt model take a particularly interesting simple

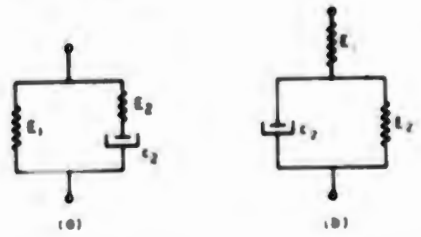

FIG. 3.11 Two equivalent mechanical models: (a) spring in parallel with a single Maxwell unit, and (b) spring in series with a single Voigt unit.

form when the number of elements is held to two, and either one damper or one spring is dropped. These forms are illustrated in Fig. 3.11. Evidently each is a special case of Figs. 3.9 or 3.10, with their relaxation and creep functions drawn directly from Eqs. (3.36) and (3.40).

The two models are mathematically and mechanically equivalent, provided that suitable adjustments are made in the spring and damping constants; thus it is purely a matter of convenience which model is used. Creep and relaxation behavior are identical and shown in Fig. 3.12. Note, in particular, the absence of the spike due to the Dirac delta function normally found in the relaxation function of a Voigt solid. Since the delta function is a mathematical abstraction, this feature suggests that either of these models gives perhaps the simplest possible description of a real viscoelastic material. Zener [38] has used the model with metals to such an extent that he calls it a standard linear solid. Neubert [47] shows quite clearly how the model can be generalized into a description of the macroscopic behavior of a number of real solids.

The mathematical similarity between Figs. 3.11(a) and 3.11(b) suggests that generalized Voigt and Maxwell solids may also be interchangeable, with suitable differences in elastic and damping constants. With some restrictions, this turns out to be true. Note, in this connection, that Bland's elegant approach [16] to the foundations of linear viscoelasticity is independent of the specific model assumed for engineering convenience, as is Eringen's more general axiomatic theory [42].

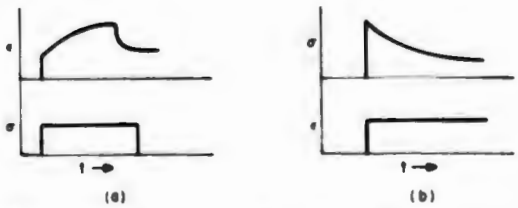

FIG. 3.12. Performance for the models of Fig. 3.11: (a) creep, and (b) relaxation.

As has been shown by Skudrzyk [48,49], the constant-temperature plane stress-strain equation for any linear viscoelastic material can be expressed as a linear partial differential equation of arbitrary order, or

$$\left[\sum_{0}^{n} A_n \frac{\partial^n}{\partial t^n}\right] \sigma = \left[\sum_{0}^{m} B_m \frac{\partial^m}{\partial t^m}\right] \epsilon, \tag{3.42}$$

where the arbitrary constants A_n and B_m may be zero or finite. Writing in tensor notation, Eringen [42] confirms an equivalent form as the general constitutive equation for three-dimensional linear viscoelasticity. Examples of applicability of Eq. (3.42) are

a. Linear spring only: A_0 and B_0 finite, all others zero;

b. Dashpot only: A_0 and B_1 finite, all others zero;

c. Voigt solid: A_0, B_0, and B_1 finite, all others zero;

d. Maxwell solid: A_0, A_1 and B_1 finite, all others zero;

e. Fig. 3.11(a): A_0, A_1, B_0, and B_1 finite, all others zero; and

f. Fig. 3.11(b): A_0, A_1, B_0, and B_1 finite, all others zero.

In Eq. (3.42), the low-order terms govern long-term behavior while the higher-order terms govern short-term behavior. If there is long-term viscous flow, B_0 is zero (*e.g.*, dashpot only or single Maxwell element); otherwise B_0 is positive and finite. If the material shows an instantaneous elastic response, $m = n$, but if the response is retarded, then $m = n + 1$.

On these or similar grounds, Alfrey [15] has shown topological similarities between specific models and shown some algebraic methods of transferring from one model to another. Gross [50] has classified the models in accordance with their topological similarities; see Table 3.3. Figure 3.13 illustrates equivalent models by response class. Shifts from one representation to another may only be made in a single class.

One can therefore decide at one's convenience to take a generalized Voigt or Maxwell solid as the model; if they are equivalent topologically, one can shift from one to another at will. Generally a Voigt model is used to present creep and complex compliance data, while a Maxwell model is used for relaxation and for complex modulus. Bland [16] demonstrates a procedure for curve-fitting for a number of simple models; Goldberg and Dean [51] give a semi-graphical method of considerable utility. Shifting from one model to another is a straightforward procedure, though laborious without an electronic computer. Elder [52] outlines the basic procedure and gives an example for a ten-element model of polyisobutylene at 25°C.

Thus, the concept of a material memory has led to laws covering creep and relaxation phenomena. However, this is not all that can be deduced from the idea of memory. The response of a single Maxwell model—using the stress law shown in Table 3.2—can be shown [17] to be

$$\sigma(t) = E_1 \cdot \epsilon(t) - \frac{E_1}{\tau'} \int_0^t e^{-t-\tau/\tau'} \cdot \epsilon(\tau) \cdot d\tau. \tag{3.43}$$

The first term on the right-hand side is the instantaneous response of the system; the second term represents the remembered response, assuming both E_1 and τ' to be finite. The term $(1/\tau')e^{-t-\tau/\tau'}$ is a weighting factor and is called the "memory function." Obviously, for a given E_1 and t, the relaxation time increases as τ becomes larger. The model thus has a decaying memory; this concept means that for engineering purposes we do not need to know the complete past history of the cushion.

TABLE 3.3. PROPERTIES OF LINEAR VISCOELASTIC MODELS BY CLASS

Class	*Elastic Response*	*Long-Term Viscous Flow*	*Form of Eq. 3.42*
I	Instantaneous	Absent	$i = j, \quad B_0 > 0$
II	Instantaneous	Present	$i = j, \quad B_0 = 0$
III	Retarded	Absent	$j = i + 1, B_0 > 0$
IV	Retarded	Present	$j = i + 1, B_1 = 0$

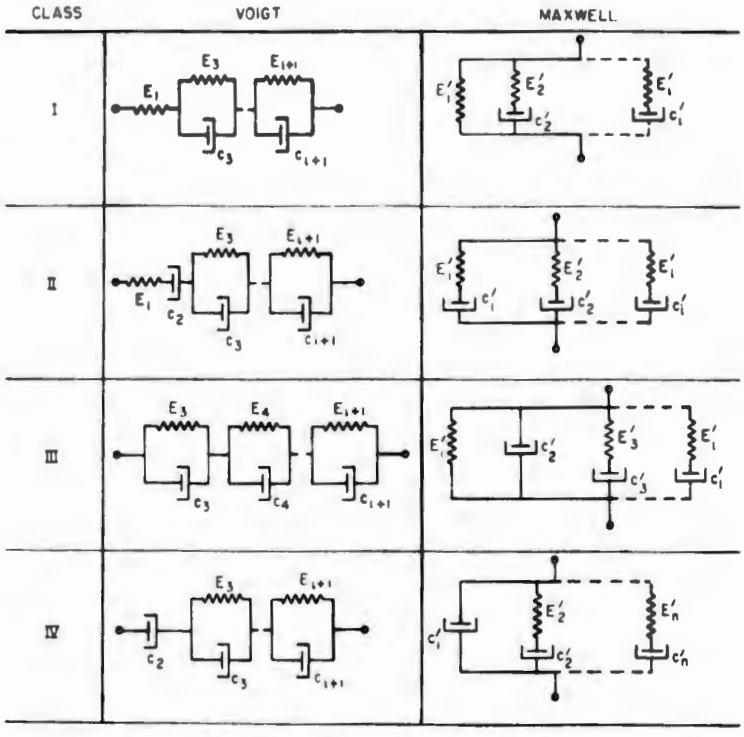

FIG. 3.13. Equivalent linear viscoelastic models; note that the standard linear solid is in class I. Elder [52].

Similarly, with Voigt models, it is found, for the single element, that [17]

$$\epsilon(t) = \frac{1}{c} \int_0^t \sigma(\tau)\, e^{-t-\tau/\tau'}\, d\tau. \tag{3.44}$$

Both Eqs. (3.43) and (3.44) can be expanded to Maxwell or Voigt models with any number of elements.

Hence, beginning with the concept of memory, expressions for the following properties of cushions have been derived:

1. Relaxation, or loss of stress under constant strain;

2. The concept of creep and relaxation spectra and means of deducing the elastic moduli of a continuum from these properties; and

3. The concept of a decaying memory wherein recent events are more important than those in a remote past.

All of the discussion in this section has been written on a plane-strain basis. From the previous section, however, it is easy to see that the results can be generalized (at the cost of mathematical complexity) to a three-dimensional continuum.

A real problem arises in generalizing these concepts to nonlinear stress laws—called "constitutive equations" in much of the theoretical literature—because:

1. The memory concept in a Boltzmann solid depends on the assumption that the effect of each deformation is independent of the others, and that the total effect is the result of super-position (a principle normally restricted to linear assemblages). Eringen [42], for one, overcomes this difficulty by stating that the memory function is smooth in the neighborhood of interest; he approximates the memory integral by a suitable functional and then proceeds successfully.

2. The examples given are all cases of functions that are linear in both elasticity and damping; the constitutive equations can be formed directly by using the principle of superposition, as shown in Eq. (3.42). For nonlinear materials, however, equations of this type are physically inadmissible. Nevertheless, it should be noted that any number of linear and nonlinear elements may be combined into either a generalized Maxwell solid where all strains are equal or a generalized Voigt solid where all stresses are equal.

Eringen [42], however, has developed an axiomatic theory for nonlinear materials satisfying the functional description of Eq. (3.24). The complete theory describes materials by lengthy constitutive relations; engineering solutions involve very complicated nonlinear boundary-value problems. Excluding some special simple problems (mostly one-dimensional), exact solution of the field equations is impossible. Approximate methods are available, and Eringen and Grot [40] list several promising schemes for obtaining solutions by computer.

For most cushioning work, at least for short-time vibration exposure and for shock problems, we can assume constant-temperature adiabatic conditions, as well as plane stress, thus avoiding tensor notation. Several methods of handling these simplified problems have been suggested. Some of the more useful ones are listed below.

1. Davis [17] suggests expanding the nonlinear elasticities as polynominals in strain (ϵ) and in strain rate ($\dot{\epsilon}$), thus taking advantage of Weierstrass' theorem that any continuous function can be so expanded to any degree of accuracy.

2. Snowdon [53,54] has calculated the response of tangent and arctangent elasticity with linear damping.

These two papers will be discussed somewhat later; they are cited here to lessen the discouragement that the complicated equations of Eringen and Grot [40] might produce.

3.2.3. Complex Modulus and Complex Compliance. This section examines the results of exposing a Boltzmann solid to a sinusoidal force. This is equivalent to defining the stress-time relation as the real part of

$$\sigma(t) = \sigma^* = \sigma_m e^{i\omega t}, \tag{3.45}$$

where σ_m is the peak value of stress reached in the steady state, ω is the frequency of force application in radians per unit time, and $i = \sqrt{-1}$.

For convenience, set the beginning of the motion at $t = -\infty$, and change the variable so that $\zeta = t - \tau$. When these changes are made, Eq. (3.26) becomes

$$\epsilon(t) = \int_0^\infty C(\zeta)\, \dot{\sigma}\, (t - \zeta)\, d\zeta. \tag{3.46}$$

Substituting Eq. (3.45) in Eq. (3.46) leads to

$$\epsilon(t) = i\omega\epsilon^* \int_0^\infty C(\zeta)\, e^{-i\omega\zeta}\, d\zeta, \tag{3.47}$$

where ϵ^* is a complex strain, defined below.

Now since $C(t)$ is zero when t is less that zero, the lower limit of integration in Eq. (3.47) can be set at $-\infty$ without loss of accuracy. Further, by definition, the Fourier transform of $C(t)$ is

$$C(\omega) = \int_{-\infty}^{\infty} C(\tau)\, e^{-i\omega t}\, d\tau, \tag{3.48}$$

from which, assuming the existence of the integral,

$$\epsilon(t) = i\omega t\sigma^*\, C(\omega). \tag{3.49}$$

Hence, $\epsilon(t)$ is a periodic function of strain. Let

$$\epsilon(t) = \epsilon^* = \epsilon_m e^{i(\omega t + \delta)}$$

and substitute in Eq. (3.49). The result is

$$\frac{\epsilon^*}{\sigma^*} = Y^* = i\omega\, C(\omega) = |\omega C(\omega)| e^{-i\delta}, \tag{3.50}$$

where Y^* is the "complex compliance" and δ is the phase angle (loss angle). The quantity $\tan\delta$ is a measure of internal friction, or damping, and is often called the "loss tangent."

A similar series of operations will produce the Fourier transform of the relaxation function

$$r(\omega) = \int_{-\infty}^{\infty} r(\tau)\, e^{-i\omega t}\, d\tau, \tag{3.51}$$

which leads to

$$\frac{\sigma^*}{\epsilon^*} = i\omega\, r(\omega) = E^* = |\omega r(\omega)|\, e^{i\delta}, \tag{3.52}$$

where E^* is the "complex modulus."

Combining Eqs. (3.50) and (3.52) produces a formal definition of the relation between the creep and relaxation functions:

$$-\omega^2 C(\omega) r(\omega) = 1, \tag{3.53}$$

which may also be written

$$E^* Y^* = 1. \tag{3.54}$$

Note that complex modulus is defined as a real term multiplied by $e^{i\delta}$. Using Euler's rule, and other conventions, E^* may take on any of several forms

$$E^* = Ee^{i\delta} = E(\cos \delta + i \sin \delta) = E_r (1 + i \tan \delta) = E_r + iE_i, \tag{3.55}$$

where

$$|E^*| = (E_r^2 + E_i^2)^{1/2},$$

and

$$\tan \delta = \frac{E_i}{E_r}.$$

E_r, the real part, is called the storage modulus while E_i, the coefficient of the imaginary part, is called the loss modulus.

The preceding approach to the concept of a complex modulus existing in the presence of sinusoidal excitation is adapted from Fung's text [11]. It was chosen for use here to show that a complex modulus can be thought of as existing for any material exhibiting creep or relaxation behavior.

For linear viscoelastic materials a more direct approach is possible using Skudrzyk's relation, Eq. (3.42). When stress varies sinusoidally as in Eq. (3.45), the partial derivatives in this relation can be expressed as

$$\begin{aligned} \frac{\partial^n \sigma}{\partial t^n} &= (i\omega)^n \sigma, \\ \frac{\partial^m \epsilon}{\partial t^m} &= (i\omega)^m \epsilon. \end{aligned} \tag{3.56}$$

Thus, Eq. (3.42) becomes

$$\sigma \cdot \sum_{n=0}^{n} A_n (i\omega)^n = \epsilon \cdot \sum_{m=0}^{m} B_m (i\omega)^m, \tag{3.57}$$

which may be written

$$E^* = \frac{\sigma}{\epsilon} = \frac{b'(\omega) + i\, b''(\omega)}{a'(\omega) + i\, a''(\omega)}, \tag{3.58}$$

where $a'(\omega)$, $a''(\omega)$, $b'(\omega)$, and $b''(\omega)$ are functions of the frequency. Since the ratio of two complex numbers is a single complex number, there is a single complex number for the complex modulus.

When a Voigt-solid model is used, complex compliance is the quantity usually found first, while with a Maxwell model, the complex modulus is the easier to find.

With the rules set forth in the previous section for establishing the response functions of generalized Maxwell or Voigt solids, Skudrzyk's scheme of presentation can be followed; then, after some manipulation of complex numbers, a specific expression for the complex modulus or complex compliance of any linear viscoelastic model can be derived. Some simple values

are shown in Table 3.4. Generalized expressions, using the notation defined in Fig. 3.13 are

$$E^* = E_1^* + \sum_{j=2}^{n} \left(\frac{1}{E_j} + \frac{1}{i\omega c'_j} \right)^{-1},$$
$$Y^* = Y_1^* + \sum_{j=3}^{n} (E_j + i\omega c_j)^{-1}, \tag{3.59}$$

where the complex compliance or complex modulus for the first unit are taken from the simple models in Table 3.4.

TABLE 3.4. COMPLEX MODULI AND COMPLIANCES OF SOME SIMPLE VISCOELASTIC MODELS

Type Solid	*Complex Modulus*		*Complex Compliance*	
	E_R	E_1/ω	Y_R	$Y_1\omega$
Elastic	E_1	0	$\frac{1}{E_1}$	0
Dashpot	0	c_1	0	$\frac{1}{c_1}$
Maxwell	$\frac{\omega c_1^2 E_1}{E_1^2 + \omega c_1^2}$	$\frac{c_1 E_1^2}{E_1^2 + \omega^2 c_1^2}$	$\frac{1}{E_1}$	$\frac{1}{c_1}$
Voigt	E	c_1	$\frac{E}{E^2 + \omega^2 c_1^2}$	$\frac{\omega^2 c_1}{E^2 + \omega^2 c_1^2}$

Consider the standard linear solid shown in Fig. 3.11(a). The stress law applicable to this unit is

$$E_2\sigma + c_2\dot{\sigma} = E_1E_2\,\epsilon + c_2\,(E_1 + E_2)\,\dot{\epsilon}. \tag{3.60}$$

From the sinusoidal stress input and strain response, the complex modulus is found [47] to be

$$E^* = E_1 \left(1 + \frac{E_2}{E_1} \cdot \frac{\omega\tau'}{\omega\tau' + \frac{1}{\omega\tau'}} + i\,\frac{E_2}{E_1} \cdot \frac{1}{\omega\tau' + \frac{1}{\omega\tau'}} \right), \tag{3.61}$$

where $\tau' = c_2/E_2$ and is the relaxation time of the system. From Eq. (3.55), the real part of the complex modulus is

$$E_r = E_1 + E_2 \frac{\omega\tau'}{\omega\tau' + \frac{1}{\omega\tau'}}, \tag{3.62}$$

and the loss tangent is

$$\tan\delta = \frac{1}{\omega\tau' \left(1 + \frac{E_1}{E_2} \right) + \frac{E_1}{E_2} \cdot \frac{1}{\omega\tau'}}. \tag{3.63}$$

This latter expression obviously has a maximum. Setting ω_0 as the frequency at which this maximum occurs, and differentiating Eq. (3.63) with respect to ω, leads to

$$\omega_0^2 = \left[\frac{c_2^2}{E_2}\left(\frac{1}{E_1}+\frac{1}{E_2}\right)\right]^{-1}. \tag{3.64}$$

Substitution of Eq. (3.64) in Eq. (3.63) produces

$$2\tan\delta_0 = \frac{c_2\omega_0}{E_1}, \tag{3.65}$$

and

$$\tan\delta = \frac{2\tan\delta_0}{\frac{\omega}{\omega_0}+\frac{\omega_0}{\omega}}. \tag{3.66}$$

When Eq. (3.65) is substituted in Eq. (3.64) there results a quadratic in $c_2\omega_0/E_2$, the solution of which, corresponding to the physics of the problem, is

$$\frac{c_2\omega_0}{E_2} = \sec\delta_0 - \tan\delta_0. \tag{3.67}$$

Equations (3.65) and (3.67) can be combined to give

$$\tan\delta_0 = \frac{E_2/E_1}{2\sqrt{1+E_2/E_1}} \tag{3.68}$$

and

$$\omega_0 = \frac{E_2}{c_2\sqrt{1+E_2/E_1}}. \tag{3.69}$$

Substitution of appropriate quantities in Eq. (3.62) leads to

$$\frac{E_1}{E_r} = 1 - \frac{2}{1+\frac{\omega_0^2}{\omega^2}}\cdot\frac{\sin\delta_0}{1+\sin\delta_0}, \tag{3.70}$$

where $\sin\delta_0 = (1+2E_1/E_2)^{-1}$.

These results are due to Kosten and Zwikker [55], who were among the early investigators of the properties of open-celled foam rubbers. Equations (3.66) and (3.70) are plotted in Fig. 3.14 with δ_0 assumed to be 20 degrees. It can be seen that, for $\omega >> \omega_0$, δ approaches zero while E_1/E_r approaches a finite asymptote

$$\left.\frac{E_1}{E_r}\right|_{\omega=\infty} = \frac{1-\sin\delta_0}{1+\sin\delta_0}, \tag{3.71}$$

One of the major advantages of the complex modulus is that for small excursions it corresponds mathematically to the linear elastic modulus. This correspondence permits solution of equations involving damping terms in simple form and then separation after a solution is found. Myklestad [56] was one of the earlier writers to urge use of the complex modulus in engineering problems. Snowdon [57-61] has used the complex modulus to solve

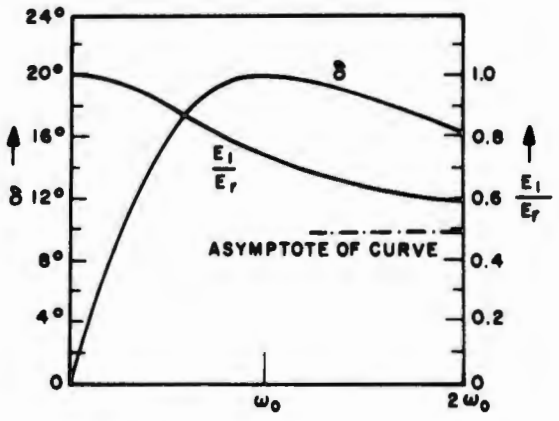

FIG. 3.14. Real portion of complex modulus and loss angle for a standard linear solid (δ_0 assumed to be 20%). Kosten and Zwikker [55].

problems of forced vibration of damped materials and there are a number of other solutions on record. Burgess [62] also urges use of the technique and discusses how impedance measurements can be used to obtain complex moduli.

In other words, the complex-modulus concept provides a powerful tool for predicting the behavior of cushions, provided that the pertinent materials data are available. Viscoelastic moduli of a number of materials are available in the literature. Lazan and Goodman [39] summarize in their Table 36.4a a large number of these moduli in shear (μ^*). Snowdon [57,60,61] also presents shear moduli for a number of elastomeric materials. Fletcher and Schofield [63] present useful data on a number of rubber compounds, while Cook, Lee, and Fitzgerald [64] have developed a large body of data evaluating the damping characteristics of several compounds.

Since most of the foregoing data involve solid materials, the shear values can also be used for small tensions and compressions on the assumption that Poisson's ratio (ν) is a true constant. The governing relation is

$$E^* = 2\mu^* (1 + \nu), \tag{3.72}$$

which is derivable directly from the interrelations summarized in the early part of section 3.1. Since Poisson's ratio, by definition, may only take on values between 0 and 1/2 and since for these limits,

$$2\mu^* \leq E^* \leq 3\mu^*, \tag{3.73}$$

the error in computing E^* from μ^* cannot exceed 50 percent. Thus, when ν is known to one significant figure, the error in shifting from shear moduli to tension or compression moduli will not exceed 5 percent [62].

A similar bank of data for most cushioning materials in compression does not appear to exist. Burgess [62] did, however, obtain the results shown in Table 3.5.

There are some restrictions on using E^* to solve dynamic problems. The limits propounded by Bland [16] are:

1. The elastic solution must be known or knowable;
2. The boundary conditions must remain the same; and
3. No operation in the elastic solution may have a corresponding operation in the viscoelastic solution that would involve separating the complex moduli into their real and imaginary parts, with the exception of the final-force determination.*

Strictly speaking, complex moduli are only exact when referring to sinusoidal disturbances of very small magnitude. However, there is no engineering

TABLE 3.5. ESTIMATED VALUES OF STORAGE MODULI AND LOSS TANGENTS FOR VARIOUS MEDIA IN THE FREQUENCY RANGE 10 TO 40 CYCLES PER SECOND

Material	E_R (psi)		E_l/E_R
	$f = 10$ cps	$f = 40$ cps	$f = 10$ to 40 cps
Microporous nitrile rubber	450	500	0.4 -0.6
Silastic homogeneous	350	400	0.25-0.35
Silastic w/solid inclusions	450	500	0.4 -0.5
Silastic w/holes	130	140	0.3 -0.4
Fibrous silicone rubber	5	5.2	0.15-0.20
BTR	1000	1000	0.15-0.3
Scottfoam (30 pores/inch)	5	6	0.1 -0.3
Scottfoam (20 pores/inch)	5	6	0.1 -0.4
Scottfoam (45 pores/inch)	5	6	0.2 -0.3
Scottfoam (60 pores/inch)	5	6	0.25-0.45
Neoprene latex foam	30	40	0.15-0.25

*There may be disagreement here. It is understood that, in the related discipline of mechanical impedance, real and imaginary parts are separated early in the computing program. Obviously much depends on how the separation is accomplished. We disclaim competence to judge validity at this time of writing.

objection to using the concept for nonsinusoidal disturbances, because Fourier's rules can always be used to represent an arbitrarily shaped disturbance as the sum of a series of sinusoids.

For large excursions, E_r and E_t can only be considered frequency-dependent constants over the linear range of the stress-strain curve. E_r and E^* may be regarded as the slope of the stress-strain curve which, if the function be differentiable, would become a continuous variable $d\sigma/d\epsilon$. There are relatively few data available on dynamic moduli at large deflections. An example of the variation in μ_r and μ_t for a proprietary low-temperature rubber compound is shown in Figs. 3.15 and 3.16 [65]. Painter has also obtained similar results on silicone rubber [66].

Is there a complex modulus at very large strains such as those which occur in shock loading on cushions? Even in the absence of definitive experimental evidence, we think we can say yes. For example, Soper and Dove (in a paper [67] to be discussed in greater detail in the next chapter) have shown that the shock response of a cushion system can be represented at constant temperature by

$$\frac{\sigma}{\int_0^{\epsilon} f(\epsilon,t)\, d\epsilon + \psi(t)} = f\left(\frac{\sigma_s V^2}{2 T_c}, \frac{V}{T_c}\right), \tag{3.74}$$

where $\psi(t)$ = an arbitrary function of time,

σ_s = static stress on the cushion,

T_c = cushion thickness, and

V = velocity of load application.

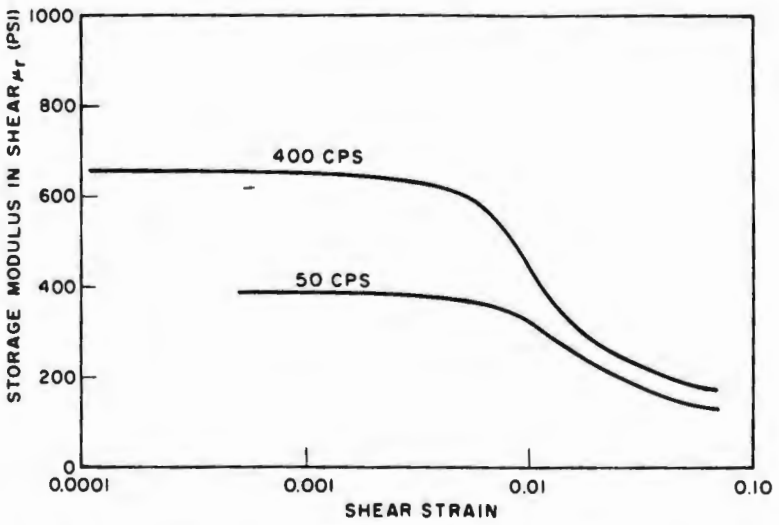

FIG. 3.15. Storage modulus as a function of strain for a silicone rubber. Painter [65].

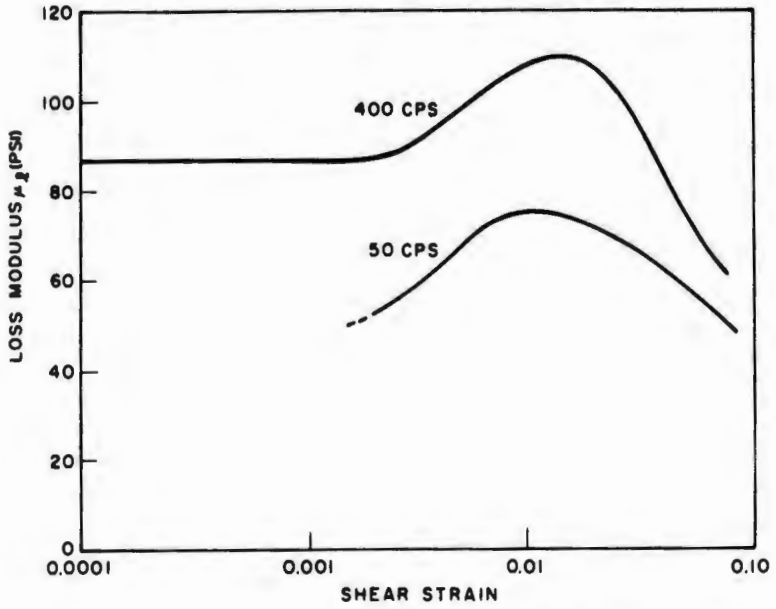

FIG. 3.16. Loss modulus as a function of strain for a silicone rubber. Painter [65].

By the principle of conservation of energy, and since V/T_c has the dimensions of reciprocal of time, Eq. (3.74) can be written

$$\sigma = f(\epsilon,t), \tag{3.75}$$

which could just as well be

$$E^* = \frac{\sigma}{\epsilon} = f(t). \tag{3.76}$$

When the viscoelastic system is nonlinear and these nonlinearities can be expressed as suitable functions, then powerful techniques exist for arriving at suitable solutions. It is not within the province of this monograph to make a complete review of the fast-moving field of nonlinear solid mechanics. Abramson [68] has written an excellent short review. More detailed methods may be found in Stoker [69], Minorsky [70], McLachlan [71], Levy and Baggott [72], Kryloff and Bogoliuboff [73], Andronow and Chaikin [74], Ku [75], and others. Automation, with its emphasis on feedback in servomechanisms, is responsible for much of the intense current interest in nonlinear oscillations.

Complex-modulus concepts provide powerful assistance for the existing methods of solving nonlinear differential equations, particularly where computers are available. One method, due to Davis [17], is summarized in what follows.

Define E_n as the nonlinear elastic coefficient and c_n as the nonlinear viscosity coefficient and E_0 and c_0 as the corresponding linear coefficients. Let ϵ_E and ϵ_c be the strains on the elastic and viscous elements, respectively.

Approximate (using Weierstrass' theorem) E_n and c_n by nth degree polynominals:

$$E_n = E_0 + \sum_{n=1}^{n} \gamma_E{}^n \, a_n \epsilon_E{}^n,$$
$$c_n = c_0 + \sum_{n=1}^{n} \gamma_c{}^n \, b_n \dot{\epsilon}_c, \tag{3.77}$$

where γ_E and γ_c are dimensionless constant parameters giving a measure of nonlinearity, and a_n and b_n are constants depending on E_0 and c_0. Restrict the foregoing equations to first-order nonlinearities so that all but the first power of γ_E and γ_c may be neglected. Then Eqs. (3.77) become

$$E_n = E_0 + \gamma_E \sum_{n=1}^{n} a_n \, \epsilon_E{}^n = E_0 + \gamma_E \, S_1,$$
$$c_n = c_0 + \gamma_c \sum_{n=1}^{n} b_n \, \dot{\epsilon}_c{}^n = c_0 + \gamma_c \, S_2. \tag{3.78}$$

For a single Voigt model the equation of motion can be shown to be

$$\ddot{\epsilon} + 2\beta_2 \, \dot{\epsilon} + \omega_1{}^2 \epsilon + \gamma_E \, S_1 + \gamma_c \, S_2 = \frac{1}{m_c} \, \sigma(t), \tag{3.79}$$

where $\omega_1{}^2 = E_0/m_c$,

$\beta_2 = c_0/2m_c$, and

m_c = mass of the Voigt element.

This is Duffing's equation, and methods of solution are clearly outlined in the literature [69,70].

For a Voigt solid, nonlinear complex compliances are found in the form

$$Y^* = Y_0{}^* + Y_1{}^* = Y_0{}^* + Y_{r1} + i \, Y_{t1}, \tag{3.80}$$

where $Y_0{}^*$ is the linear complex compliance and $Y_1{}^*$, is the first-order nonlinear contribution to Y^*. Davis found specific values for this contribution for quadratic and cubic nonlinearities. A cubic equation can be used quite often to simulate nonlinear stress-strain curves for cushions; "quadratic damping" (*i.e.*, damping force proportional to the square of the velocity) is sometimes found.

A similar approach to the Maxwell model yields nonlinear complex moduli in the form

$$E^* = E_0{}^* + \gamma_E \cdot [f(\epsilon)] - \gamma_c[f(\dot{\epsilon})] = E_r + i \, E_t, \tag{3.81}$$

and Davis found specific expressions for quadratic and cubic nonlinearities.

For coupled Voigt (and Maxwell) elements, the requirement that the strain (and stress) be constant in all elements leads to simple additive rules such that

$$Y^* = \sum_{n=1}^{n} Y_i{}^*$$
$$E^* = \sum_{n=1}^{n} E_i{}^*. \tag{3.82}$$

Superposition is therefore acceptable even for nonlinear complex compliances and moduli. Since Davis showed that linear complex moduli and compliances were special cases of the nonlinear; it follows that mixed models can be developed should the need arise. There is such a need—for materials exhibiting a collapsing-column effect in compression, *e.g.*, foamed elastomers.

Relationships between complex moduli and complex compliances have been derived. It has been shown that these derivations can be extended to nonlinear materials, and some examples have been given. The derivation of the formal expressions for complex modulus and compliance began with the concept of creep and relaxation functions which were shown to be interrelated in section 3.2.2. Thus, all four functions are interrelated through simple mathematical operations. Figure 3.17 summarizes these interrelations and makes a fit ending to this section.

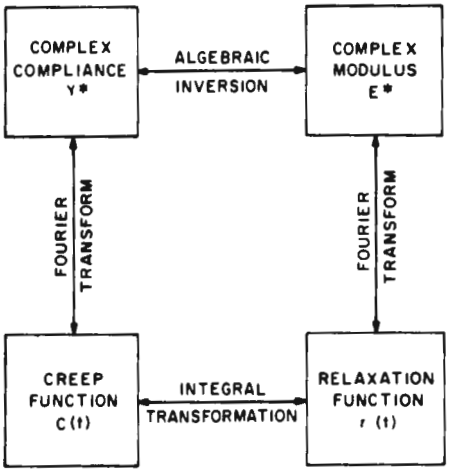

FIG. 3.17. Block diagram of interrelations among viscoelastic characteristics. DiTaranto [78].

3.2.4. Time and Temperature Superposition. Equations (3.24) state that stress is a function of strain, time, and temperature. In sections 3.2.2 and 3.2.3 the heat factor was ignored, although always with the tacit admission that any material constants developed would be affected by changes in temperature. This section considers the effects of temperature on the performance of viscoelastic materials.

Temperature changes affect the moduli of viscoelastic materials in very much the same manner as changes in frequency. Figure 3.18 summarizes this story and is typical of all materials with slight molecular cross-linking. Performance is divided into three zones:

1. The glassy zone where the storage modulus is large and the loss modulus is small, so that behavior resembles that of a stiff elastic material;
2. The rubbery zone, occurring at low frequencies or high temperatures, where the storage modulus and the loss modulus are both small and, therefore, energy dissipation is small; and
3. The transition zone, where the loss modulus peaks.

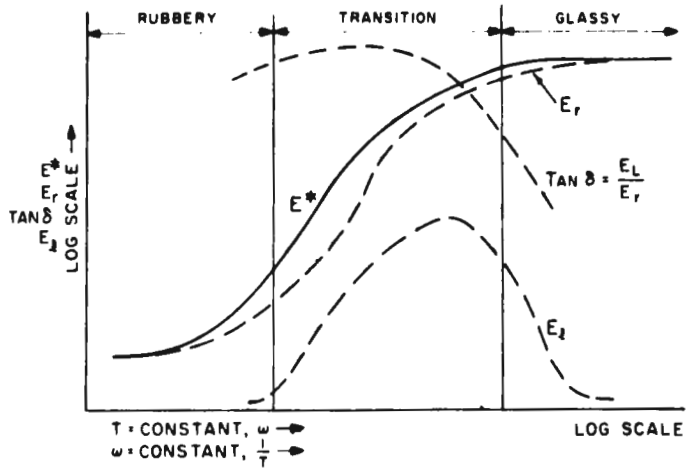

FIG. 3.18. Frequency and temperature effects on complex moduli.

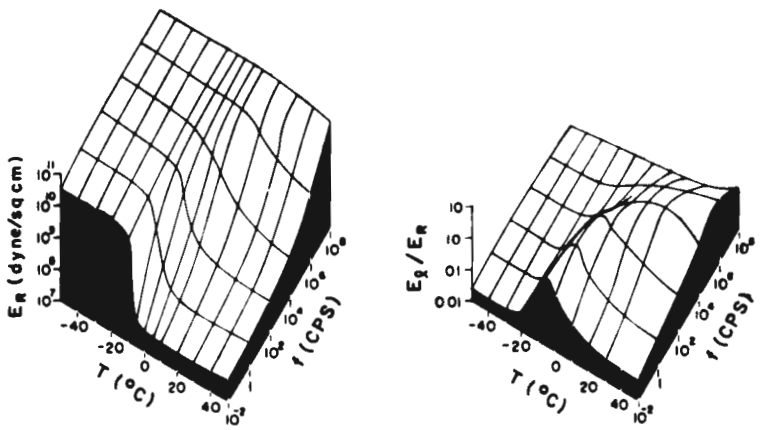

FIG. 3.19. Approximate behavior of E_r and loss tangent over a wide range of frequency and temperature; sketches are based on experimental data for a carbon-filled buna-N. Nolle [76].

Most practical shock and vibration problems are associated with the glassy and transition zones.

The effects noted occur simultaneously and demand a three-dimensional plot. Nolle's work in this area [76] is a classic. He derived data for natural rubber, buna-N, butyl, neoprene and GR-S; his results for carbon filled buna-N are shown in Fig. 3.19.

Prolonged vibration at a given frequency will produce heat which will often not dissipate as rapidly as formed. The result is an increase in the temperature of the material and, as Fig. 3.19 shows, a change in the mechanical properties. Fortunately, in most cases this particular problem can be ignored. Heat transfer and buildup is usually quite slow. However, in evaluating

the utility of specific materials, longer-term vibration behavior is of more than passing interest, whether it is expressed qualitatively or quantitatively.

There are a number of theories which account for the behavior of materials at varying temperatures, which seem to arise from the behavior of the molecule. The molecule may be visualized as a long curled elastic chain which may have more or less cross-linking with other molecular chains. Since molecular activity is a function of temperature, strain response – the summation of individual molecule responses – is also a function of temperature. On this basis, in the glassy zone (below T_g) molecular "curling and uncurling" cannot occur rapidly enough to follow the stress. In the rubbery zone, on the other hand, curling and uncurling are in phase with the stress; this is not conducive to energy dissipation.

In the light of the foregoing, it is logical to examine whether and how the time and temperature behaviors of a material are interrelated. These simplified considerations, plus many more of considerably greater depth, have led to the concept of time and temperature superposition, also called the method of reduced variables. The genesis of this concept is discussed by Tobolsky [77].

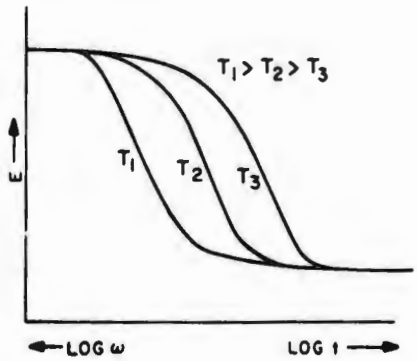

FIG. 3.20. Shift in elasticity characteristics as a function of time and temperature.

Let the elasticity of a material at a given temperature, T_1, be plotted against the natural logarithm of time. Suppose, now, that the curve shifts horizontally to the right as the temperature is lowered. This situation is illustrated in Fig. 3.20 for three temperatures. The behavior sketched in Fig. 3.20 is typical of many materials used as cushions. Materials which behave in this manner are called thermorheologically simple. Amorphous polymers behave in this manner while polymers with crystalline structures do not. Most cushioning materials may be considered amorphous. (Teflon and plasticized polyvinyl chloride are not amorphous, but they are rarely used as cushions.)

Consider the elastic modulus E, which is a function of time and temperature. When the material is thermorheologically simple, the following holds:

$$E(t,T_a) = E[(\log t) - f(T_a)]. \tag{3.83}$$

Function $f(T_a)$ is an unknown shift function which controls the manner in which the E *vs* log t curve shifts horizontally as the temperature is varied. By setting

$$f(T_a) = \log a_T, \tag{3.84}$$

Eq. (3.83) becomes

$$E(t,T_a) = E\left(\log \frac{t}{a_T}\right). \tag{3.85}$$

The term a_T is called the shift factor. The function $E(t,T_a)$ is called the master curve for the property of interest and determines the shape of all the curves of behavior of this particular property.

Since the shift is only horizontal along the log t axis, a given curve, $E(t,T_a)$, can be related to another curve, $E(t,T_0)$, for the same material through the shift function $f(T_a)$. This feature may be written

$$E(\log t,T_0) = E(\log t,T_a) + f(T_a - T_0). \tag{3.86}$$

Now, since $f(T_a - T_0)$ is a constant on the log t scale,

$$f(T_a - T_0) = -\log a_T. \tag{3.87}$$

Equation (3.86) thus becomes

$$E(\log t,T_a) = E(\log t,T_0) - \log a_T, \tag{3.88}$$

or

$$E_T(t) = E_{T_0}\left(\frac{t}{a_T}\right). \tag{3.89}$$

Since time and frequency are inversely related, Eq. (3.89) may also be written

$$E_T(\omega) = E_{T_0}(\omega a_T). \tag{3.90}$$

The foregoing simple summary of the principles of time and temperature interrelation is given by Di Taranto [78].

The above relations allow the construction of a master curve for any characteristic desired. The reduction in the quantity of data required is astonishing. Figure 3.21 shows typical reduction in the complexity of the data on the shear compliance Y_s of a given sample of polyisobutylene, taken from Ferry, Grandine, and Fitzgerald [79].

The master curve is usually obtained for the selected reference temperature (quite frequently 25°C) by proper shifting and joining of curves attained at different temperatures. The shift factor for each temperature is determined empirically from the amount of movement required to bring the curves into exact superposition. A plot of log a_T *vs* temperature can then be used in conjunction with the master curve to predict behavior over a wide range of temperatures or over a wide range of frequencies. A typical plot is shown in Fig. 3.22.

Williams, Landel, and Ferry [80] came to the conclusion that a single empirical equation could describe the behavior of the shift factor for all materials investigated. Their equation is

$$\log a_T = \frac{-8.86\ (T - T_0)}{101.6 + T - T_0}, \tag{3.91}$$

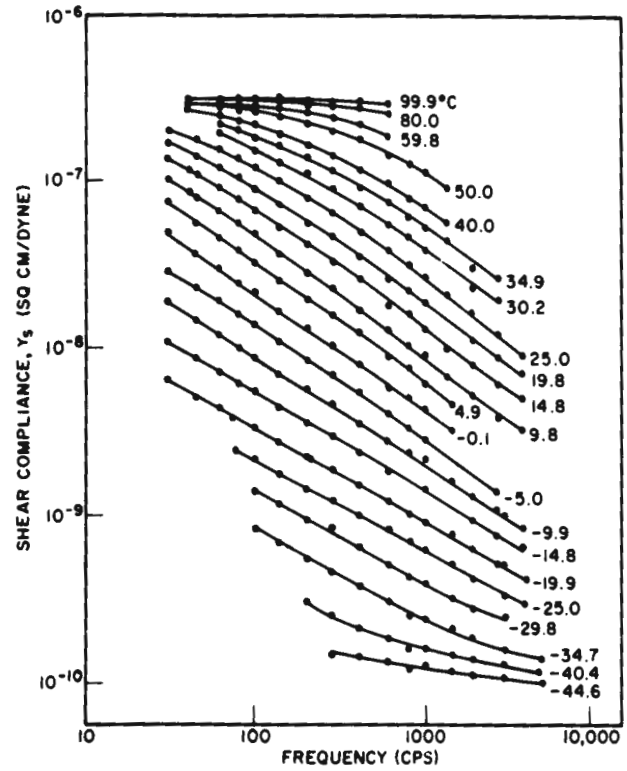

FIG. 3.21. Shear compliance of polyisobutylene: (a) original data at 22 temperatures, and (b) reduced curve at 25°C [79].

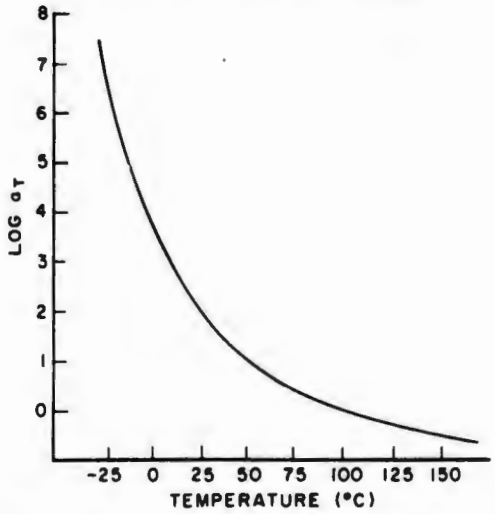

FIG. 3.22. Temperature shift factor for a material.

where T = test temperature (°K),

T_0 = arbitrarily chosen reference temperature, which for most systems is $T_g + 50°$ with a standard deviation of $\pm 5°$, and

T_g = glass temperature of the polymer.

The authors prefer this form because of difficulty in determining T_g accurately. The form of the equation forces coincidence at the reference temperature so that, if T_g is slightly in error, the entire curve will be in error. Nevertheless, using T_g as the reference temperature, they derived the relation

$$\log a_T = \frac{-17.44\ (T - T_g)}{51.6 + T - T_g}. \tag{3.92}$$

Tobolsky [81] has approached the problem from the standpoint of characteristic relaxation times and finds, using the foregoing empirical relation, that

$$\log \frac{K(T)}{K(T_g)} = \log a_T, \tag{3.93}$$

where $K(T)$ = characteristic relaxation time at temperature T, *i.e.*, the time for the tension relaxation modulus to attain a value of 10^9 dyne/cm^2,

$K(T_g)$ = characteristic relaxation time at the glass temperature.

Equations (3.91) and (3.92) are considered applicable only in the range $T_g \leq T \leq T_g + 100°$. Below T_g there will be deviations from the line. Above $T_g + 100°$ the material begins to behave as a liquid, and $\log a_T$ must be determined empirically. However, these equations at least provide a valuable practical prediction tool and a framework for a test program that verifies material performance.

Tobolsky [82] also states that the tension relaxation modulus could be expressed in terms of a distribution function $H(\log \tau)$, such that

$$E_R(t) = \int_{-\infty}^{\infty} H(\log \tau)\, e^{-t/\tau}\, d(\log \tau) \tag{3.94}$$

$H(\log \tau)$ can be estimated from experimental values of $E_R(t)$ [83,84,85]. Values of $H(\log \tau)$ at 298°K as a function of $\log \tau$ have been tabulated by Tobolsky and Catsiff [84]. Tobolsky and Eyring [85] showed that storage and loss moduli of polymers could be computed from $H(\log \tau)$ through

$$\begin{aligned} E_r &= \int_{-\infty}^{\infty} \frac{\omega^2\tau^2}{1+\omega^2\tau^2} H(\log \tau)\, d(\log \tau), \\ E_l &= \int_{-\infty}^{\infty} \frac{\omega\tau}{1+\omega^2\tau^2} H(\log \tau)\, d(\log \tau), \end{aligned} \tag{3.95}$$

and results are given by Tobolsky and Catsiff [84,86].

In plotting master curves [87], it is customary to plot the factor of interest as a group function against the reduced time factor in order to express the variable in a fashion consistent with the material's thermodynamics. Thus, for compliance one would plot

$$\begin{aligned} \log \frac{Y_r T_0 \rho_0}{T_a \rho} &= f(\log \omega a_T), \\ \log \frac{Y_l T_0 \rho_0}{T_a \rho} &= f(\log \omega a_T). \end{aligned} \tag{3.96}$$

For complex modulus the following relations are pertinent:

$$\begin{aligned} \log \frac{E_r T_a \rho}{T_0 \rho_0} &= f(\log \omega a_T) \\ \log \frac{E_l T_a \rho}{T_0 \rho_0} &= f(\log \omega a_T) \end{aligned} \tag{3.97}$$

In Eqs. (3.96) and (3.97), ρ and ρ_0 are the material densities at T and T_0. The factor ρ/ρ_0 is often taken as 1.0 within the limits of experimental error. T_0 is often taken as any convenient reference temperature, such as 25°C.

The shift factor must be the same, whatever mechanical property is being measured. Hence, a master stress-strain curve would be plotted as

$$\log \frac{\sigma T_0 \rho_0}{T \rho} = f\left(\log \frac{\epsilon}{\dot{\epsilon}\, a_T}\right). \tag{3.98}$$

Static drift (or creep) is defined as the percentage loss in thickness as a function of time and static stress. Hence, a master drift curve would be plotted as

$$\log \frac{T\rho}{T_0 \rho_0} (1 - \epsilon) = f\left(\log \frac{t}{a_T}\right). \tag{3.99}$$

The simplification that time and temperature superposition offers to the experimenter is obvious. Most rigs capable of vibrating a specimen through some regime will, sooner or later, develop characteristic resonances. These resonances will prevent further valid data from being obtained. It is, however, relatively simple to vary the temperature surrounding the test apparatus in a controllable and reproducible manner. Thus, if the experiment is repeated through a limited frequency range with varying temperature, the data may be safely extrapolated to a wide range of frequencies. Snowdon [60], as an example, used time and temperature superposition and the shift factor of Eq. (3.91) to plot the storage and loss moduli of a number of polymers over the frequency range of 1 to 10,000 cps at 25°C.

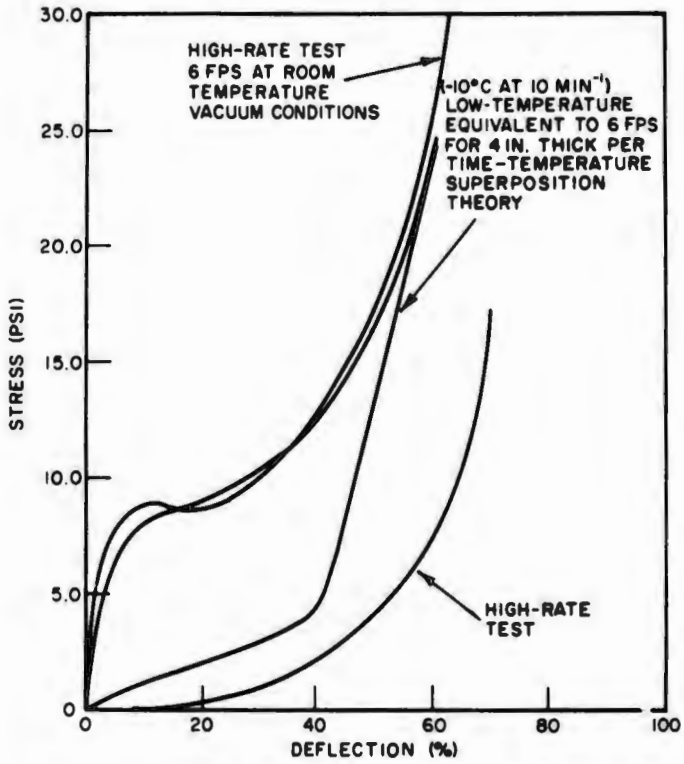

FIG. 3.23. Predicted and measured stress-strain curves in vacuo for a polyurethane foam, impact velocity 6 fps. Volz [89].

The only work known to be in progress using time and temperature superposition on foam cushions is that recently briefed by Volz [88,89]. Low-speed compression tests (at 0.1, 1.0, and 10.0 inches of thickness) were run at three temperatures: 2°, −10°, and −20°C. Figure 3.23 shows experimental *versus* calculated results for a 6-ft/sec impact. Note that the impact test was conducted in a vacuum to eliminate trapped air effects. Complete analysis of the behavior of a foam requires estimation of these effects and will be discussed in the next section.

3.3. Behavior of Some Models of Real Cushions

The majority of resilient cushioning materials for which extensive data are available are open- or closed-cell elastomeric foams. This section will discuss some of the inner structural details that govern the behavior of such materials and will then discuss existing, relevant, mechanical, and mathematical models.

Gent and Thomas [90] summarize the mechanisms peculiar to the behavior of foam. The paragraphs which follow concerning the static tension and compression behavior of open- and closed-cell foams are based directly on their analysis.

A simplified model of an open-celled foam is shown in Fig. 3.24. The foam consists of thin threads whose unstrained length is l_0 and whose cross-sectional area is D_1^2. The threads are joined together to form a cubical lattice. The intersections are cubical regions whose volume is D_1^3; these intersections are assumed rigid, or substantially undeformable.

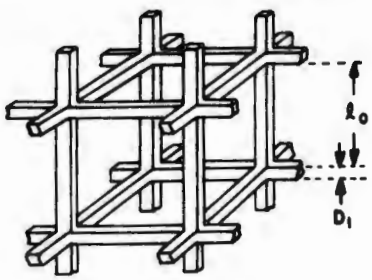

FIG. 3.24. Structural model of a foam material. Gent and Thomas [90].

Apply a small stress in tension parallel to the axis of one set of threads. The strain ϵ taken by the overall foam lattice is associated with a strain ϵ' in the thread, such that

$$\epsilon' = (1 + Q_1)\,\epsilon, \tag{3.100}$$

where $Q_1 = D_1^2/l_0$.

The threads occupy a fraction of the area for any cross section perpendicular to one set of threads. This fraction is $Q_1^2/(1 + Q_1)^2$.

The tension modulus of elasticity for the foam model, E_f, is given by

$$E_f = E_m \cdot \frac{Q_1^2}{1 + Q_1}, \tag{3.101}$$

where E_m is the tension modulus for the unfoamed material.

The density of the model is determined by considering a cube whose side is $D_1 + l_0$, centered on one intersection. The ratio of the volume of solid material to the total volume of the model is given by

$$V_R = \frac{V_m}{V_f} = \frac{3\,Q_1^2 + Q_1^3}{(1 + Q_1)^3}. \tag{3.102}$$

At low densities V_R is approximately equal to $3Q_1^2$.

The parameter Q_1 is thus a direct measure of foam density. The relation between model density and Q_1 is shown in Fig. 3.25.

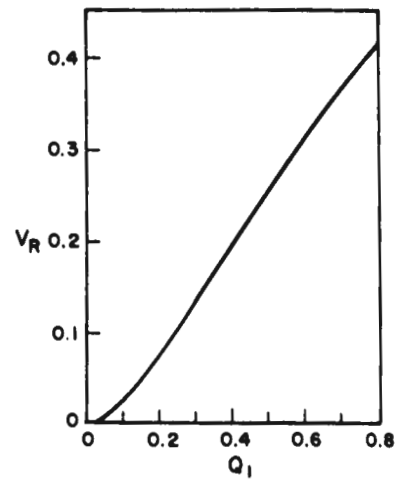

FIG. 3.25. Relation between model density and parameter Q_1 [90].

These relations are reported as keeping the same general form even for more complex foam lattice shapes. For example, when n randomly dispersed threads enter each intersection and the intersection is approximated by a sphere of surface area nD^2, the density of the foam is still given by Eq. (3.102).

When a random structure is stressed in tension, Young's modulus is

$$E_f = E_m \cdot \frac{Q_1^2}{2(1 + Q_1)}, \tag{3.103}$$

which differs from the previous value by a factor of 1/2.

Equations (3.102) and (3.103) indicate a relation between density and foam modulus through the factor Q_1. Figure 3.26 plots the experimentally measured relationship and the theoretical relationship.

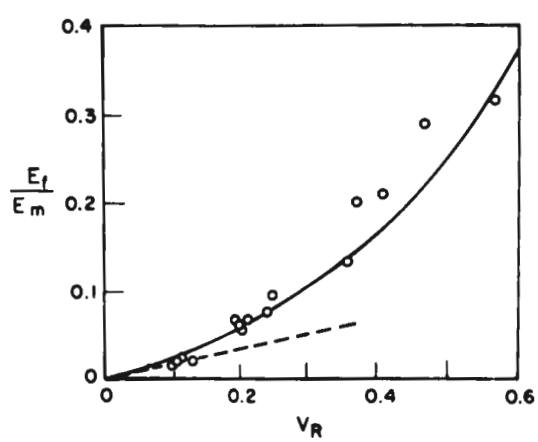

FIG. 3.26. Experimental relation between the ratio of the Young's moduli of foam and solid rubbers, E_f/E_m, and the volume fraction V_R of rubber in the foam; full curve is the theoretical relation, and dashed curve represents the limiting form of the theoretical relation for low-density foams [90].

Gent and Thomas further record that Poisson's ratio for the simple model is zero, since transverse threads are not deformed. For randomly disposed threads, Poisson's ratio is 1/4, independent of density.

Apply a compression stress parallel to one set of threads and assume that compression takes place as a result of thread buckling. It can be shown that the average compressive stress will be given by

$$\sigma = E_m \cdot \frac{Q_1^4}{(1 + Q_1)^2} \cdot f(\epsilon'), \tag{3.104}$$

where $f(\epsilon')$ is an unknown function of the strain assumed by the thread ends. A contribution to the total deformation will be made by simple compression of the threads in the amount σ/E_m, but the main deformation will result from thread buckling, particularly with low-density foams.

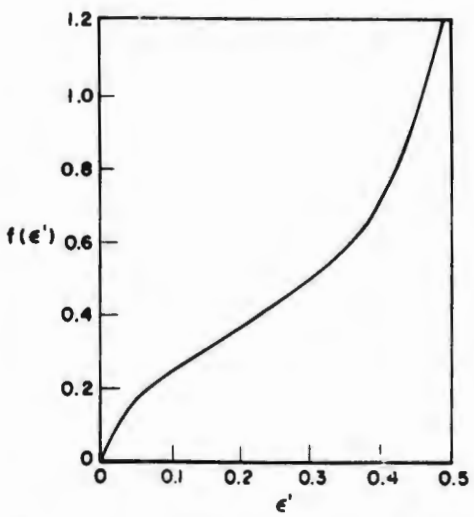

FIG. 3.27. Experimental relation between $f(\epsilon')$ and ϵ' obtained from the stress-strain relations for six low-density natural-rubber foams [90].

Compression tests were run on six natural rubber foams of low density (V_R less than 0.2). The average results are shown in Fig. 3.27 which shows the familiar "knee effect" expected of collapsing columns. The knee is not as abrupt as would be expected with a simple strut, presumably (partly, at least) because of wide variation in individual thread dimensions. For more regular foams a more marked plateau effect is to be expected and is found to exist with low-density polyurethane foams.

Resistance to compression is strongly dependent on foam density. Figure 3.28 shows the compressive stress at 25 percent compression plotted against the volume fraction. It can be seen that theory and experimental results closely agree.

A closed-cell foam is a three-phase system: the material matrix, the enclosed gas, and the ambient atmosphere. Assuming that matrix behavior is the

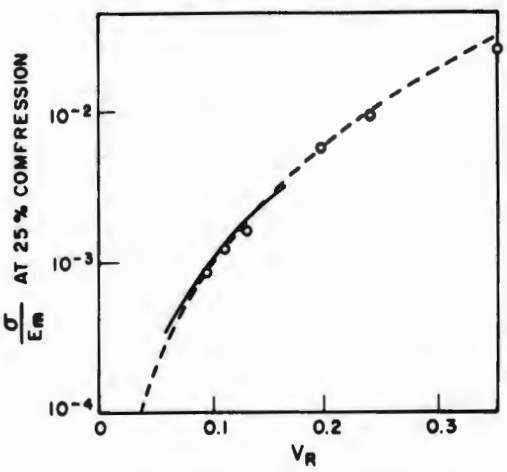

FIG. 3.28. Experimental and theoretical compression test values of stress at 25 percent compression and volume fraction; circles and solid line represent experimental results, and dashed curve indicates calculated results [90].

same for an open-celled foam, the problem reduces to determining the effects of the trapped gas. For small compressions, Gent and Thomas show that the compression modulus is given by

$$E_f = \frac{2\left[5K_c + (p_a - p_i) + \dfrac{3p_i}{2\,(1 - V_R)}\right]\,[4K_c - (p_a - p_i)]}{\left[8K_c + (p_a - p_i) + \dfrac{2p_0}{1 - V_R}\right]}, \tag{3.105}$$

where $5K_c$ is the value of the compression modulus for the corresponding open-celled foam, defined in Eq. (3.103), and p_a and p_i are the ambient and internal pressures, the latter being measured when the foam is unstrained. Poisson's ratio is

$$\nu = \frac{\left[2K_c + (p_a - p_i) + \dfrac{p_0}{(1 - V_R)}\right]}{\left[8K_c + (p_a - p_i) + \dfrac{p_0}{(1 - V_R)}\right]}. \tag{3.106}$$

If the internal and external pressures are equal, *i.e.*, $p_a = p_i = p$, the last two equations become

$$E_f = \frac{2K_c\,[10K_c\,(1 - V_R) + 3p]}{4K_c\,(1 - V_R) + p}, \tag{3.107}$$

$$\nu = \frac{2K_c\,(1 - V_R) + p}{2[4K_c\,(1 - V_R) + p]}. \tag{3.108}$$

When the foam modulus $5K_c$ is much greater than p, then E_f and ν have the same values as the corresponding open-celled foams. When p is much greater

than the foam modulus, the two values become equal to $6K_c$ and 1/2, respectively. In the latter case, closed-cell structure does not have much effect on static mechanical properties. For a soft closed-cell foam, the compression modulus cannot be more than 20 percent higher than that of equivalent open-celled foam.

Under deformations varying with time, foam materials will exhibit viscoelastic behavior. Energy is dissipated in the material, as expected. In addition, in open-celled foams energy is dissipated as air flows through the pores. In closed-cell foams, the contained gas is compressed and expands rapidly as stress is removed. Damping constants in gases are very small, and (with some exceptions—one will be discussed in the section on quasi-resilient foams) energy dissipation is small in closed-cell foams. Another drawback has been found with some soft closed-cell foams: under prolonged static load, contained gas under pressure apparently migrates through the cell wall to the ambient atmosphere, causing excessive creep in the material.

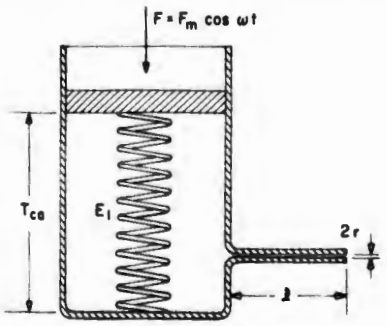

FIG. 3.29. Kosten and Zwikker's analogy to fine-pored open-celled plastic or rubber foams [55].

Among the earliest investigators of the dynamic characteristics of open-celled foams were Kosten and Zwikker in 1937 [55]. They postulated that the behavior of an open-celled foam was similar to the mechanical model shown in Fig. 3.29. A frictionless, massless piston moves inside a cylinder which communicates with ambient air (pressure p_a) through a capillary of length l and radius r. As the air behind the piston is compressed, some pressure is relieved by flow through the capillary, which thus has the effect of a damper. This analogy is, therefore, exactly similar to the standard linear solid shown in Fig. 3.11a and analyzed in section 3.2.2; E_1 being the static modulus for the foam in compression; E_2, the resistance to compression of the air; and c, the damping coefficient (a function of capillary resistance to the flow of air).

E_2 and c, per unit surface area of foam, can be estimated from the relations

$$E_2 = \frac{n_a p_a}{T_{ca}}, \tag{3.109}$$

and

$$c = \frac{8c_v\, l A_c}{\pi r^4}, \tag{3.110}$$

where T_{ca} = average thickness of the air in the foam sample,

n_a = ratio of the specific heats of air at constant volume and at constant pressure (1.0 for isothermal processes and 1.4 for adiabatic compression),

A_c = area of the piston, and

c_v = viscosity coefficient of air.

Strictly speaking, Eq. (3.109) is only applicable to very small compressions of air. Equation (3.110) is directly derivable from Poiseuille's law on the assumption of laminar flow.

Using the previous expressions, the peak loss angle can be approximated by

$$\tan \delta_0 = \frac{n_a p_a / E_1 T_{ca}}{2\sqrt{1 + \frac{n_a p_a}{E_1 T_a}}}, \tag{3.111}$$

and the associated frequency by

$$\omega_0 = \frac{n_a \pi r^4 p_a}{8 c_v \ell A_c T_{ca} \sqrt{1 + \frac{n_a p_a}{E_1 T_{ca}}}}. \tag{3.112}$$

Although the peak loss tangent is independent of area, it is not independent of T_{ca} which is a function not only of cushion thickness but also of porosity. The characteristic frequency depends not only on foam area but also on the average length of the pores and on the thickness parameter T_{ca}. Thus, there is definitely a shape factor in the behavior of foam materials; predictions that ignore this factor are probably inaccurate. However, these dimensional constants enter as the first power, while the capillary radius enters as the fourth power and, when different foams are compared, has a much stronger influence.

Figure 3.30 shows some results Kosten and Zwikker found experimentally for a specific foam. Volume fraction was around 30 percent. For this foam they computed a peak loss angle of 20.9 degrees on the assumption of isothermal compression. Compare also the curves of Fig. 3.30 with the theoretical curves of Fig. 3.14, taken from the same paper. Note that the measured loss-angle curve does not pass through the origin as predicted by theory; thus, there must be some damping in the rubber matrix. For this particular foam, however, the material contribution was not large.

The foregoing discussion clearly establishes the important influence of air on the damping capacity of open-celled foams. It also shows how easy it is to learn something about the performance of individual foams in a vibratory environment.

More recently, Venning [91] has been investigating the viscoelastic properties of polyurethane foams. He has found that behavior (before the collapsing-column effect) can be simulated by the models shown in Figs. 3.31 and 3.32. Measured values of the complex modulus from which these models are derived are shown in Fig. 3.33. Figure 3.31 is obviously very similar to the standard linear-solid concept investigated by Kosten and Zwikker but with

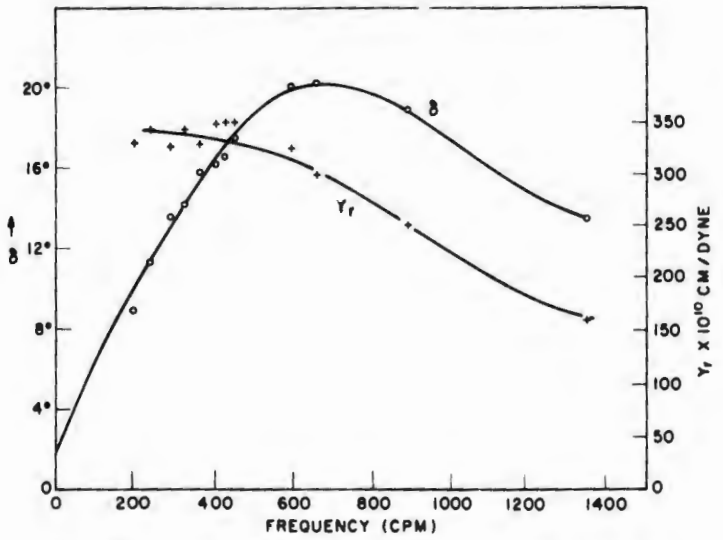

FIG. 3.30. Kosten and Zwikker's results on a rubber foam [55].

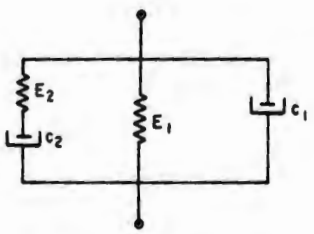

FIG. 3.31. Model for 1.8-pcf polyurethane foam at small compressions in the frequency range 20 to 100 cps; E_1 is 12.81 lb/in./sq in., E_2 is 5.22 lb/in./sq in., c_1 is 0.00425 lb-sec/in./sq in., c_2 is 0.025 lb-sec/in./sq in. Venning [91].

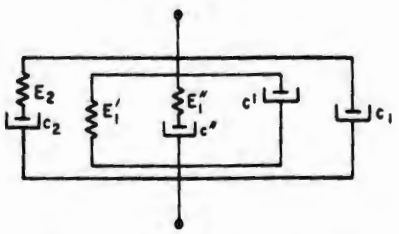

FIG. 3.32. Model for 1.8-pcf polyurethane foam at small compressions in the frequency range 0.5 to 100 cps; E_2, c_1, and c_2 are as before, E'_1 is 6.56 lb/in./sq in., E''_1 is 2.75 lb/in./sq in., c' is 0.125 lb-sec/in./sq in., c'' is 0.83 lb-sec/in./sq in. [91].

the addition of a damper, c_1, to account for material damping. However, at low frequencies the springlike behavior of the material is more complicated and E_1 must be broken up into several spring and damping components (Fig. 3.32). Nevertheless, the principle still holds that foams can be represented by mechanical models of their viscoelastic behavior, at least within the range of quasi-linear response.

The genesis of the work summarized in the preceding paragraph is worth discussing. Venning and Guttridge [92,93] first proposed an analog-computer approach to package-cushioning problems. But because of the difficulty of predicting dynamic performance they shifted to a hybrid system in which the cushion itself generated the dynamic stress data directly. A block diagram of the experimental rig is shown in Fig. 3.34. Some preliminary results are shown in Table 3.6.

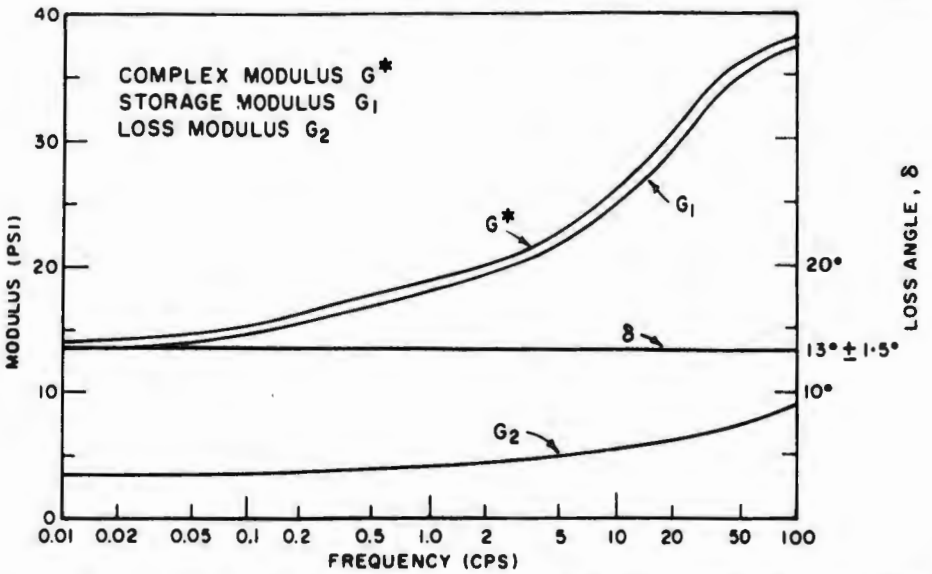

FIG. 3.33. Complex modulus for 1.8-pcf polyurethane foam; note constant loss angle over this frequency range indicating that air is not sole damping mechanism [91].

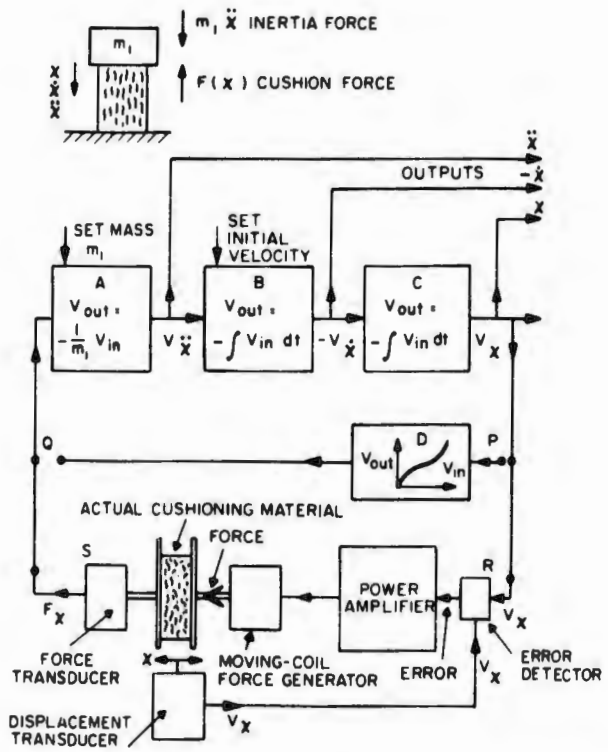

FIG. 3.34. Venning and Guttridge's analog cushion computer [93]; unit P is an electrical analog of the stress law, while the units between R and S generate the stress law directly.

TABLE 3.6. SOME RESULTS BY VENNING AND GUTTERIDGE

Material	*Pulse Length* (msec)	*Peak Stress* (psi)	*Peak Strain*
4-pcf rubberized hair	125	0.58	0.23
4-pcf rubberized hair	214	1.03	0.38
2-pcf polyester urethane	136	1.92	0.49
12-pcf open-celled polyvinyl chloride	145	2.43	0.83
Cellulose wadding	152	1.42	0.92

The device used to obtain the results of Table 3.6 was a standard vibration generator modified to provide a 2-inch stroke. A later modification, currently being checked for performance, includes the use of air bearings to reduce spurious chatter. The largest velocity which can be achieved with the existing experimental rig is determined by the ratio of the peak force available to the total moving mass. On the currently available machine, peak velocity is limited to about 20 inches per second, about one-fifth the velocity attained in an 18-inch drop test.

Further, Venning's device starts with the compression platen in contact with the cushion, applying a measured static stress. It is obviously impossible to create a true-velocity step at the start of a compression stroke; this would require infinite force. Figure 3.35 shows a comparison between analog-computer results and test results at large strains. Venning attributes the discrepancy to one or more of the following possible causes:

1. Low-frequency stiffness of the model being higher than that of the actual sample;
2. Use of viscous damping elements in the model leading to higher frictional forces than necessary; and
3. Compression velocity in the experimental measurements being too low during the initial part of the compression stroke.

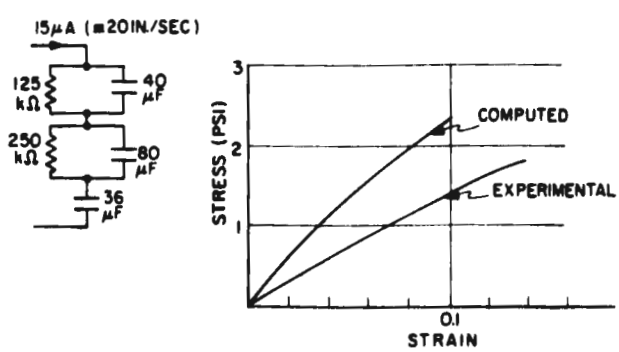

FIG. 3.35. Venning's comparison [91] between computed and measured results at finite strains of a polyurethane foam.

TABLE 3.7. SCALING FACTORS FOR ELECTRICAL ANALOGS

Mechanical Quantity		*Electrical Quantity*		*Relationship*[a]
Name	*Symbol*	*Name*	*Symbol*	
Mass	m	Inductance	L	$m = S_1 L$
Displacement	x	Charge	Q	$x = S_2 Q$
Time	t_m	Time	t_e	$t_m = S_3 t_e$
Velocity	V	Current	I	$V = S_4 I$
Force	F	Voltage	E	$F = S_5 E$
Damping constant	c	Resistance	R	$c = S_6 R$
Spring compliance	$1/k$	Capacitance	c	$1/k = S_7 C$
Frequency	f_m	Frequency	fe	$f_m = S_8 fe$

[a] $S_4 = S_2/S_3$, $S_5 = S_1 S_2/S_3^2$, $S_6 = S_1/S_3$, $S_7 = S_3^2/S_1$, $S_8 = 1/S_3$.

Using an analog-computer representation requires selection of the correct dynamic model. Soroka [94] shows many such analogies. The basic shift from mechanical to electrical systems is attained by using the analogies summarized in Table 3.7. Although eight scaling constants are shown, the last five (as noted in the footnote to the table) are functions of the first three. Note, further, that it is possible to slow down the time scale (S_3) so that a transient occupying a millisecond in real time can take a full second on the computer, thus permitting the use of relatively inexpensive recording devices.

Osborn and his associates at Wilmot Packaging, Ltd. [95] are working on a larger version of Venning's initial concept. This device will accelerate the moving head before it comes in contact with the cushion surface, so that higher initial velocities will be possible. Because of the general compactness—as compared with a conventional drop tester or a pendulum impact rig—accurate measures of deflection under dynamic load should be possible. After making the necessary checks, we should obtain some interesting results more closely approaching the velocity-shock situation.

Volz' model [89] is shown in Fig. 3.36. This is more complicated than Kosten and Zwikker's model [55] (though less complicated than Venning's [91]).

The element K_s represents the nonlinear static load deflection characteristics of the foam. The changes in the Maxwell element are due to changes in strain rate. These two elements, added together, produce the dynamic stress-strain curve independent of any effects due to trapped air.

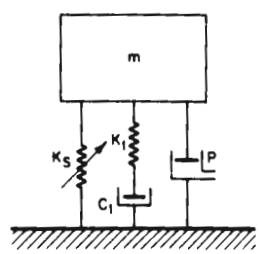

FIG. 3.36. Volz' model of a polyurethane foam [89].

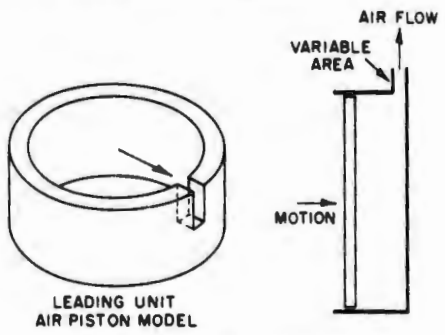

FIG. 3.37. Volz' cushion problem [89].

The third element in the model is a piston with an orifice. This orifice has a variable diameter to simulate the reduction in cushion thickness during compression. A simplified version of the reality considered is shown in Fig. 3.37. The value for the area of the orifice, A_0, at any instant was found to be

$$\left(\frac{A_0}{A_i}\right)^2 = \frac{4d_c}{c'_f \ell} \cdot \frac{V_{rt}^3}{1 - V_{rt}}, \tag{3.113}$$

where A_i = initial area of free edge of the element of the cushion being considered,

d_c = average foam cell diameter,

c'_f = air friction coefficient factor, or drag,

ℓ = a characteristic length of the cushion (in Fig. 3.37, $\ell = L/2$), and,

V_{rt} = instantaneous value of porosity, or volume fraction.

For a stipulated foam, pore diameter is readily estimated from the number of pores per inch. The quantity ℓ is dictated by the geometry of the cushion and is readily estimated. The instantaneous porosity, V_{rt}, is a function of the strain at a given instant, while initial porosity is the ratio of free-air volume to total volume.

The drag coefficient, c'_f, can be obtained by measuring the pressure drop across a sample and then using the relation

$$\frac{\partial P}{\partial \ell} = -\frac{c'_f}{d_c} \cdot \frac{\rho V^2}{2} \left(\frac{1 - V_{rt}}{V_{rt}^3}\right), \tag{3.114}$$

where $\frac{\partial P}{\partial \ell}$ = rate of change of pressure with distance,

ρ = air mass density, and

V = air velocity.

The forces from the individual single-piston models were then summed around the ring, as were the elastomer forces, to make mathematical model of behavior during an impact test; these predictions were compared with test results, Fig. 3.38.

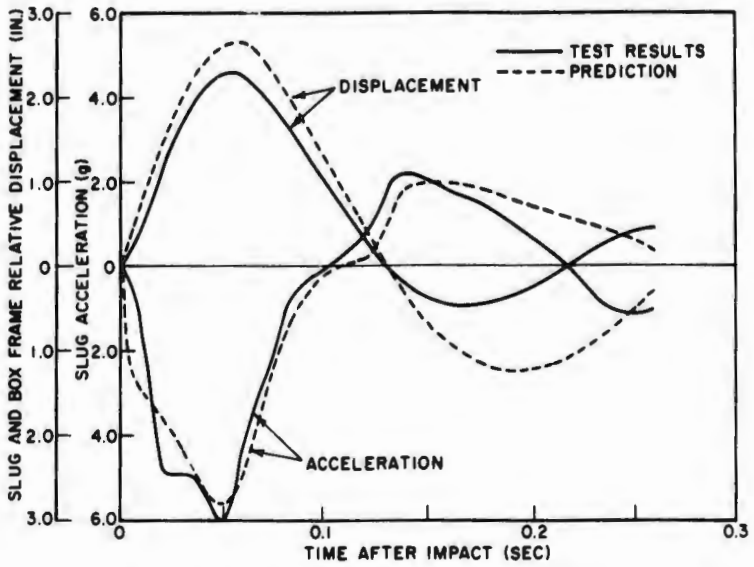

FIG. 3.38. Predicted and measured results on an air-cushion ring. Volz [89].

Note the anomalous behavior of the measured acceleration curve between 0 and 0.2 seconds. This anomaly was later traced to a tight-fitting Teflon liner between the cushion and the tube liner which adhered to the liner long enough to cause the foam opposite the impact face to be loaded in tension and to develop an effective vacuum. It is difficult to foretell every event; nevertheless, it can be seen that good predictions of cushion performance can be made from calculations.

Chapter 4

PEAK SHOCK TRANSMITTED BY A CUSHION

A designer must nearly always begin by evaluating the peak acceleration at the interface between the cushion and the object he is trying to protect. This chapter deals with this topic on the assumption that the system is undergoing velocity shock, *i.e.*, that the state of motion of the system has been suddenly changed, say by contact with a rigid surface after a free drop or, if the system is at rest on the substrate (Fig. 2.1), by a sudden velocity change by this substrate.

In practical terms, the condition to be analyzed is typical of those encountered by designers working in the following fields:

1. Package cushioning;
2. Aerial delivery, whether by free fall or parachute;
3. Near-miss shock absorbers;
4. Recoil pads; and

many others. Controlling the peak shock is often the limit of the designer's responsibility.

Most of the available data is concentrated in this particular area of interest, thus providing an additional reason for devoting an entire chapter to this single topic.

It is assumed that the designer has a realistic limiting value for allowable peak acceleration. It has often been stated that this quantity is a prerequisite for completely rational design; no matter how obtained, it is assumed to be an input constraint.

For the sake of consistency, all equations have been written on the assumption that the problem is to reduce the shock produced by falling from a height h. In any equation where found, h may be replaced by $V^2/2g$, where g is the acceleration of gravity. In equations where g is given as a numerical constant, the value 32.2 ft/sec^2 or 386.4 in./sec^2 has been used.

Occasionally the designer will be given the input shock as a peak acceleration of so many g. Conversion to the equations used here is a reasonably straightforward operation, provided that the input shock waveform is also specified. Jacobsen [96] has recently published a slide rule and associated instruction book which make conversion a routine exercise.

4.1. Historical Note

The beginning of a scientific approach to cushions is generally credited to Mindlin's classic paper of 1945 [97]. There is, however, evidence [98,99,100]

TABLE 4.1. SOME PAPERS BASED ON USING SIMPLE ELASTICITY RELATIONS AS A BASIS FOR DESIGN

Reference	*Author*	*Date*
102	H.H. Berk	1946
103	R.A.L. Cole	1946
104	R.F. Ettinger	1953
105	D.J. Gasch	1953
106	R.E. Jones	1953
107	R.E. Jones and D. L. Hunzicker	1954
108	K.Q. Kellicutt	1946
109,110	E.O. Lisberg	1953
111	M. Masel	1953
112	I. McNamee	1954
113,114	G.S. Mustin	1953
115	S.J. Ruffini	1959
116	F. Stowell, H.C. Pusey, and K.N. Carr	1954
117,118	A.M. Underhill	1946, 1950

that others were considering the problem; the long, fruitful Forest Products Laboratory work in this area had already begun [101]. Mindlin's paper mentions a procedure adopted by the Committee on Packing and Handling of Radio Valves of the British Radio Board.

Mindlin's paper was followed by a number of discussions by authors who adopted his procedures practically unchanged. Some of these, not elsewhere mentioned, are listed in Table 4.1.

The next major step forward was the concept of cushion efficiency as developed by Gretz [119,120,121] and the more sophisticated development of optimum efficiency design points by Janssen [122,123,124]. Both these pioneers, like Mindlin, stayed with material properties determined by quasi-static means, *i.e.*, stress-strain curves determined on a conventional compression tester with the speed of compression quite slow, *i.e.*, not more than about 2 inches per minute. The Janssen approach produced design data in more usable form than did Gretz's and soon became the standard for practically all approaches. Many papers were written around this theme; a number of them are mentioned in Table 4.2.

Mustin [135] pointed out that Yurenka and Giacobine [136] had proved a clear connection between Janssen and Mindlin.

TABLE 4.2. SOME PAPERS EXPANDING ON JANSSEN'S CONCEPT

Reference	*Author*	*Date*
125	H. Himelblau	1954
126	J.A. Hoffman	1959
127,128,129	R.E. Jones and W.L. James	1955, 1956
130,131,132	R.B. Orensteen	1953, 1954
133	R.E. Slaughter	undated
134	J.C. Snowdon	1959

An interesting variation of the Janssen approach was that of Hardigg [137], who found that the stress-strain functions for several different types of cushioning materials could be reduced to a single function by dividing actual stress for a given material by Janssen's optimum stress for that material and plotting this reduced variable against actual strain divided by the material's optimum strain. This concept was also discussed in the open literature [138,139,140], and the master curve is shown in Fig. 4.1. This curve seems to hold for materials whose stress-strain curves appear essentially smooth. It is not necessarily valid, however, for materials strongly exhibiting collapsing-column behavior, like some of the polyurethane foams.

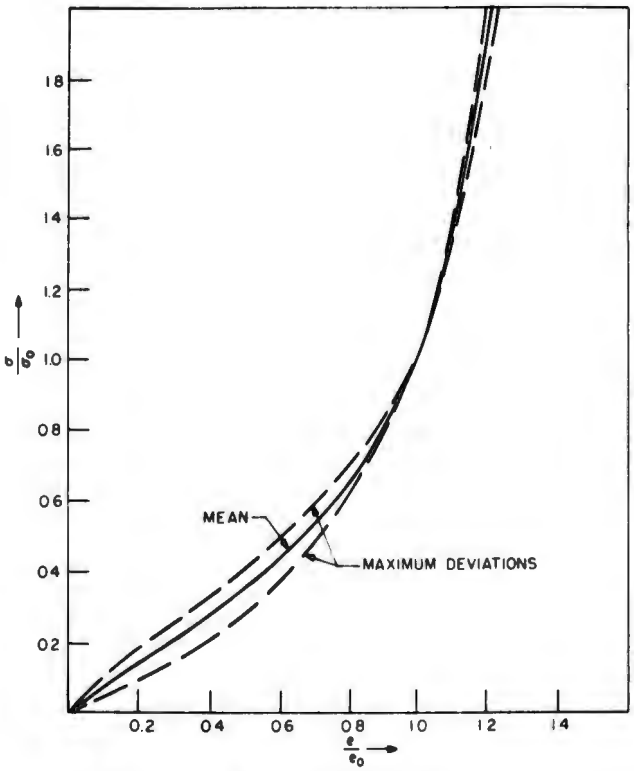

FIG. 4.1. Hardigg's master function [137].

Hermansen, Evans, and Mustin [141] extended Hardigg's concept to the whole family of rubberized hairs and attempted to develop a correlation between performance characteristics and density (Fig. 4.2).

However, it soon became apparent that single curves based on the static stress-strain of a material would not describe the dynamic behavior. Several methods of presentation, all involving families of curves, were tried. Gradually Kerstner's suggestion [31] became the most popular. In this approach, a family of curves is drawn for each material thickness at each drop height, plotting peak dynamic stress (or acceleration) against the original static stress. A typical set of such curves, taken from Humbert and Hanlon [142],

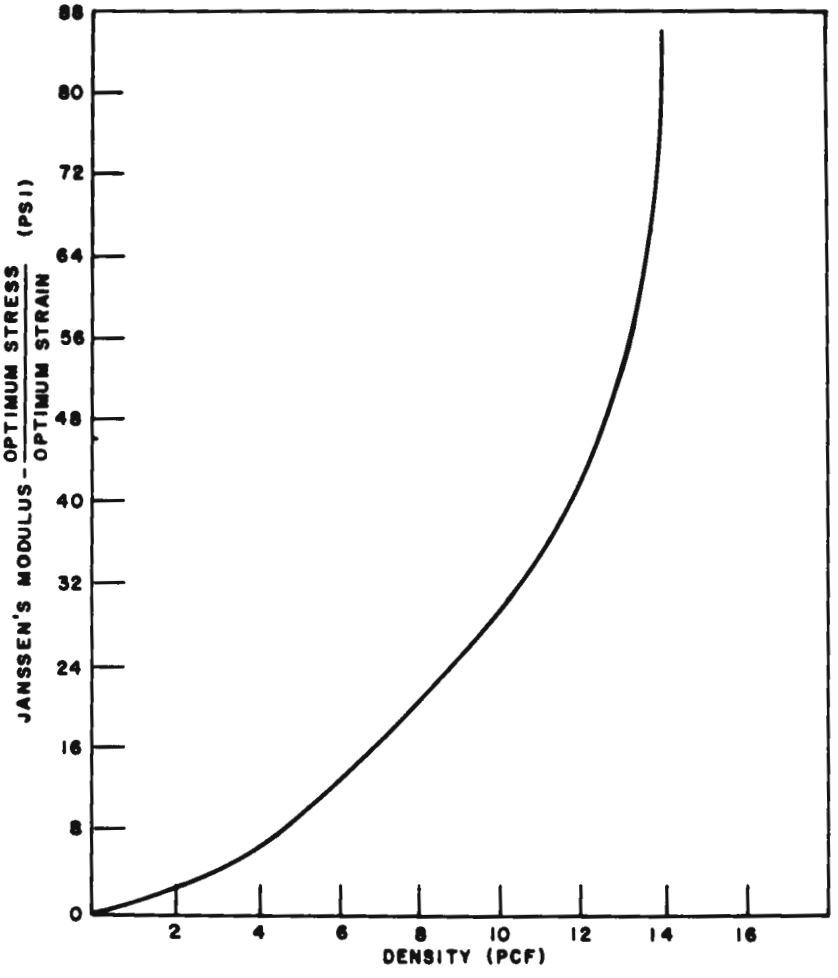

FIG. 4.2. Janssen's modulus *versus* apparent density of rubberized hair. Hermansen, *et al.* [141].

is shown in Fig. 4.3. Many of the principal papers containing such families of curves are listed in Table 4.3.

In 1961 and 1962, Soper and Dove [33,67] showed that peak acceleration should be plotted as a function of energy per unit volume and of a parameter equalling velocity at impact divided by thickness of the pad. Their plots thus took care of the material damping factor more compactly than the Kerstner suggestion, which necessitates a multiplicity of curves. More recently it has been shown by Mustin [171] that the two variables can be separated, and, at least for optimum design points, two simple empirical functions describe the behavior of 16 cushioning materials undergoing velocity shock.

4.2. The Fundamental Equations of Velocity Shock Isolation

Consider the system shown in Fig. 4.4. At first ignore the mass of the cushion so that the isothermal stress law is a continuous function

$$\sigma = f(\epsilon,t),\ 0 \leqslant \epsilon \leqslant 1.0,\ t \geqslant 0. \tag{4.1}$$

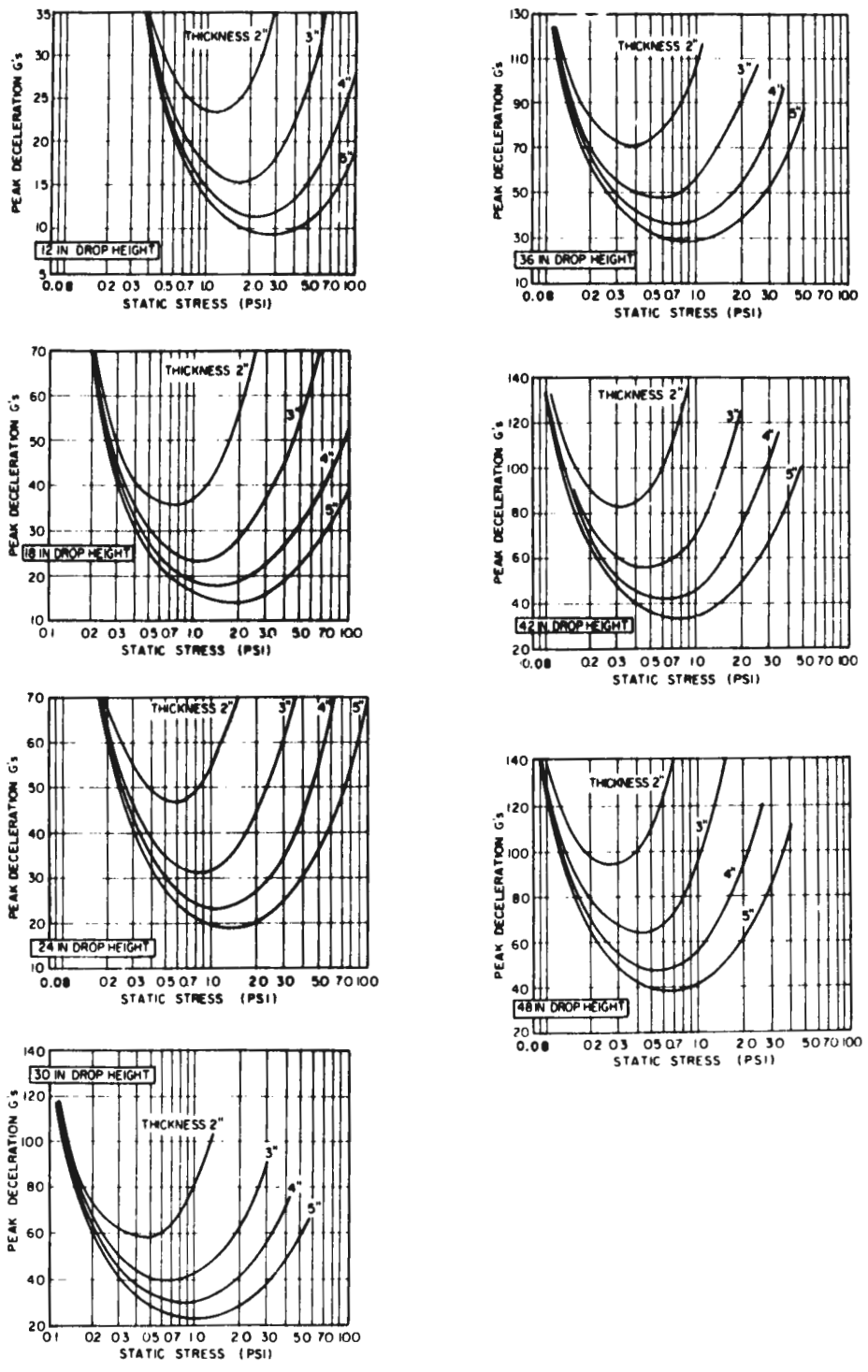

FIG. 4.3. Peak-acceleration *versus* static-stress curves for polyethylene foam. Humbert and Hanlon [142].

TABLE 4.3. SOME PAPERS CONTAINING DYNAMIC PERFORMANCE CURVE FAMILIES

Reference	*Author*	*Date*
143	C.H. Abner	1958
144,145,146,147	H.C. Blake	1962, 1964
148	Department of Defense	1964
149	E.A. Falkner	1962
150	General Electric Co.	1959
151,152	M.E. Gigliotti	1960, 1961
153,154	T.J. Grabowski	1960, 1962
155	G.A. Gordon	1960
156	G.A. Gordon and E.E. Wheeler	1961
157	R.G. Hanlon	1962
158	J.S. Hardigg and G.C. Thomas	1959
159	J.S. Hardigg	1961
160	M.T. Hatae and P.E. Franklin	1957
161	P.E. Franklin and M.T. Hatae	1961
162	P.E. Jockle, Jr. and L.T. Wilson	1958
163	S.M. Krakover and A. Olevitch	1958
164	North American Aviation	1957
165,166,167,168	R.K. Stern	1958, 1959, 1960, 1962
169,170	L.T. Wilson	1957, 1959

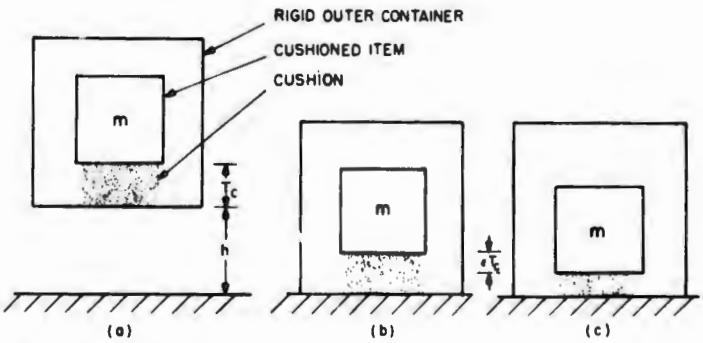

FIG. 4.4. Basic cushioning problem: (a) at instant of release, (b) at instant of contact with the floor, and (c) at time of maximum stress.

Following the line taken by Mindlin [97], it is easy to show that the acceleration of mass m is given by

$$\frac{1}{2} m V^2 + A_c T_c \left[\int_0^{\epsilon} f(\epsilon,t)\, d\epsilon + \psi(t) \right] = mg\,(h + T_c\epsilon), \tag{4.2}$$

where $t = 0$ is taken as the instant of contact with the floor. In Eq. (4.2), A_c is cushion area, T_c is cushion thickness, and the value of arbitrary function $\psi(t)$ is determined by the initial and boundary conditions. Equation (4.2) expresses the law of conservation of energy, since $(1/2)m\ V^2$ is the instantaneous kinetic energy of m, the term containing the integral is the energy

stored in the cushion at any instant, and the right-hand member is the potential energy of the mass at its initial height above the instantaneous position.

It is evident that ϵ is at its maximum ϵ_m when the velocity becomes zero, so that, for maximum stress σ_m,

$$\int_0^{\epsilon_m} f(\epsilon,t)d\epsilon + \psi(t) = \frac{mg}{A_c T_c}(h + T_c\epsilon_m), \tag{4.3}$$

which is more conveniently handled when written in operator notation as

$$D^{-1}\,\sigma_m = \sigma_s\left(\frac{h}{T_c} + \epsilon_m\right), \tag{4.4}$$

where σ_s is the static stress on the cushion and $D^{-1}\,\sigma_m$ is the complete integral defined in Eq. (4.3). $D^{-1}\,\sigma_m$ is the energy absorbed per unit volume of the cushion.

From energy considerations alone it is apparent that the peak force on the item equals its inertial force plus its own weight. This relation may be written

$$\sigma_m = \sigma_s(G_m + 1), \tag{4.5}$$

where G_m is the peak acceleration divided by the acceleration of gravity. With the aid of Eq. (4.5), σ_m can be substituted for σ_s in Eq. (4.4) which can then be solved for peak acceleration ratio. The result is

$$G_m = \frac{\sigma_m}{D^{-1}\,\sigma_m}\left(\frac{h}{T_c} + \epsilon_m\right) - 1 = J\left(\frac{h}{T_c} + \epsilon_m\right) - 1. \tag{4.6}$$

Peak acceleration and cushion thickness, two quantities of prime importance in any design problem, are thus directly related through the parameter J which is the ratio of peak stress developed in the cushion to the energy stored per unit volume of the cushion. J is called the cushion factor by some writers, and denoted by C, but its significance for cushion design was first derived by Janssen [122] who assigned the symbol J.

In normal situations, h is very much larger than T_c and ϵ_m is less than 1.0 by definition. In actual practice, maximum possible compressive strain is on the order of 0.8 or 0.9, since the cushion consists of a real material which becomes incompressible for all practical purposes. The numerical contribution of actual strain to peak acceleration can nearly always be ignored, since h/T_c greatly exceeds ϵ_m.

The subtrahend, -1, in Eq. (4.6) can also be dropped in most cases without significant loss of numerical accuracy, since peak acceleration ratios are generally much larger than 1.0. At $G_m = 10.0$, the error is 10 percent.

On the basis of the two preceding paragraphs we can write with good accuracy:

$$G_m = J\frac{h}{T_c}. \tag{4.7}$$

Note that errors resulting from these simplifications tend to offset one another.

Equation (4.4) can also be solved for static stress. To the same degree of accuracy as in Eq. (4.7), the result is

$$\sigma_s = \frac{T_c}{h} \cdot D^{-1}\,\sigma_m = \frac{J}{G_m} \cdot D^{-1}\,\sigma_m. \tag{4.8}$$

With G_m and h given, T_c is found from Eq. (4.7), and required static stress from Eq. (4.8). A straightforward division of the weight of the cushioned object by the required static stress gives the required cushion area.

Obviously T_c is minimized as J is minimized. Most real materials show minimal values of J and it is convenient to show the conditions under which J_0, the minimum value of J, exists.

Since the function defining J is continuous, it is integrable. Assume that it is differentiable (which is reasonable since it is a continuous function of real variables). It is clearly evident from its definition, Eq. (4.6), that J is some function of ϵ and of t, since $D^{-1}\,\sigma_m$ contains these variables as does σ_m (Eq. (4.1)). For J to reach a single minimum value, it is necessary that

$$\begin{aligned} \frac{\partial J}{\partial \epsilon} &= 0, \\ \frac{\partial J}{\partial t} &= 0, \end{aligned} \tag{4.9}$$

simultaneously. Working only with the partial derivative with respect to strain, we obtain a locus of points in the J surface, each one of which is optimum for a given value of the arbitrary function, $\psi(t)$.

For all practical purposes, then, J_0 must be accepted as a time-dependent variable. If a real material shows a steady value for J_0 it must be regarded as an exceptional case. Of course, the way in which time enters the relation may, for some materials, have an effect that cannot be determined experimentally so that constancy of J_0 may be a practical engineering approximate assumption.

Nevertheless, it is useful to consider the consequences of the first of Eqs. (4.9). Differentiating gives

$$D_\epsilon\, J_0 = D_\epsilon \left[\frac{\sigma_0}{D^{-1}\,\sigma_0}\right] = D_\epsilon \left\{\frac{f(\epsilon_0, t)}{D^{-1}[f(\epsilon_0, t)]}\right\}, \tag{4.10}$$

where σ_0 and ϵ_0 are the dynamic stress and strain producing J_0. Setting Eq. (4.10) equal to zero and simplifying leads to

$$D^{-1}\,\sigma_0 = \frac{{\sigma_0}^2}{D_\epsilon\,\sigma_0} \tag{4.11}$$

as a condition for the existence of J_0.

Specific values for J_0 can be found by solving Eq. (4.11) for corresponding ϵ_0 and then substituting in the original elasticity statement and its integral.

Without an electronic computer and a large quantity of data, it would be tedious work to apply the criteria just given, in all possible cases. Nevertheless, certain important conclusions can be drawn by considering various classes of elasticity which are not time-dependent in their mathematical statements; this is done in the next section.

4.3. Some Computed Values of J_0 and the Consequences

The information contained in this section is an expansion of the work of Yurenka and Giacobine [136] who considered tangent, algebraic, and logarithmic elasticities. Mindlin [97] used a different approach for tangent elasticity but the results are the same, thus buttressing confidence in the results reported here.

Assume that the cushion consists of a real material with a strain that cannot be exceeded, and call this strain the bottoming strain ϵ_b. Bottoming strain is defined as the strain that would require an infinite stress to increase it With this concept, rewrite the general stress law (Eq. (4.1)) to read

$$\sigma = f(\epsilon/\epsilon_b, t),\ 0 \leq \epsilon/\epsilon_b \leq 1.0,\ t \geq 0. \tag{4.12}$$

But only non-time-dependent systems are to be considered, so, for purposes of this section, write

$$\sigma = f(\epsilon/\epsilon_b),\ 0 \leq \epsilon/\epsilon_b \leq 1.0, \tag{4.13}$$

where the function is continuous and differentiable.

By the Weierstrass theorem, any nonperiodic function which is continuous between limits can be represented to any degree of accuracy by a polynomial of suitable degree. It is always tempting to try matching experimentally determined stress-strain curves to a polynomial, especially when so many electronic computers have "canned" routines for accomplishing the work in minimal time. Accordingly, we start with an examination of the implications of using polynomial elasticity statements to describe the behavior of cushions.

The generalized polynomial may be written

$$\sigma = A_0 + \sum_{n=1}^{n} A_n\,(\epsilon/\epsilon_b)^n, \tag{4.14}$$

where the A_n are independent of ϵ/ϵ_b and may have any finite value on the real-number line.

The integral, considering ϵ/ϵ_b as the variable, is

$$D^{-1}\,\sigma = A_0(\epsilon/\epsilon_b) + \sum_{n=1}^{n} \frac{A_n}{n+1}\,(\epsilon/\epsilon_b)^{n+1}. \tag{4.15}$$

Dividing Eq. (4.14) by Eq. (4.15) and separating into partial fractions produces

$$J = \frac{1}{(\epsilon/\epsilon_b)} + \frac{n \sum_{n=1}^{n} A_n\,(\epsilon/\epsilon_b)^{n-1}}{a_0(n+1) + \sum_{n=1}^{n} A_n\,(\epsilon/\epsilon_b)^n} \tag{4.16}$$

It is clear by inspection that, so long as J is a monotonic function, it reaches its minimum when ϵ/ϵ_b reaches its maximum of 1.0.

Values of J for a few classes of elasticity of interest are shown in Table 4.4.

The linear function is the most thoroughly analyzed and the least useful in an immediate sense. Nevertheless, it forms a basis for the analysis of systems that are intrinsically nonlinear or have dissipative mechanisms that

TABLE 4.4. J FOR CERTAIN POLYNOMIALS

Function	*Function Symbol* σ	J
Linear, zero slope	a_0	$\dfrac{1}{\epsilon/\epsilon_b}$
Linear	$a_1\left(\dfrac{\epsilon}{\epsilon_b}\right)$	$\dfrac{2}{\epsilon/\epsilon_b}$
Linear with preload	$a_0 + a_1\left(\dfrac{\epsilon}{\epsilon_b}\right)$	$\dfrac{1}{\epsilon/\epsilon_b} + \dfrac{1}{2\dfrac{a_0}{a_1} + \dfrac{\epsilon}{\epsilon_b}}$
Cubic	$a_1\left(\dfrac{\epsilon}{\epsilon_b}\right) + a_3\left(\dfrac{\epsilon}{\epsilon_b}\right)^3$	$\dfrac{2}{\epsilon/\epsilon_b} + \dfrac{\epsilon/\epsilon_b}{\dfrac{a_1}{a_3} + \dfrac{1}{2}\left(\dfrac{\epsilon}{\epsilon_b}\right)^3}$
Cubic with preload	$a_0 + a_1\left(\dfrac{\epsilon}{\epsilon_b}\right) + a_3\left(\dfrac{\epsilon}{\epsilon_b}\right)^3$	$\dfrac{1}{\epsilon/\epsilon_b} + \dfrac{2a_1 + 3a_3\,(\epsilon/\epsilon_b)^2}{4a_0 + 2a_1\left(\dfrac{\epsilon}{\epsilon_b}\right) + a_3\left(\dfrac{\epsilon}{\epsilon_b}\right)^3}$

produce nonlinear dynamic behavior. The linear function with zero slope was shown by Mindlin [97] to be the limiting case for hyperbolic tangent elasticity; he extensively analyzed the cubic function as a design tool for devices (like springs) that are essentially linear but have nonlinear geometries.

In general, most cushioning materials for which data have been examined indicate an ϵ_0 less than ϵ_b, characterized by a relatively smooth arrival and departure from J_0. It is believed, therefore, that polynomial characterization is not a valid general approach to material properties. However, for specific design problems, using polynomials can sometimes lead to quick engineering answers.

Before leaving polynomial elasticity, note that 1.0 is a reasonable assumption for the least possible value of J_0. Theoretically, the value could be less if one or another of the summation terms were negative, but this appears unlikely in practice with monotonic (single-valued) functions.

There are at least four stress functions satisfying the criterion $\epsilon_0/\epsilon_b < 1.0$. These four are defined in Table 4.5 and are plotted in Fig. 4.5.

In the first five functions, the term a_0 is to be construed as the initial slope of the stress-strain curve (with the dimensions of stress). It is, in effect, the initial "stiffness" parameter of the material.

In the sixth equation, p_i is the reference pressure in the container, or in the individual cells in a closed-cell material usually considered atmospheric. It may be regarded as directly equivalent to the term a_0 in the first five equations. While there exists a theoretical bottoming strain (resulting from packing all the air molecules into a "solid"), the practical limit occurs before this is reached and is set by the bursting strength of the walls of the container. This design problem is outside the scope of this monograph.

Hence, the air equation may be considered exactly equivalent to the first five equations, except that $\epsilon_b = 1.0$ for all practical purposes. All equations,

TABLE 4.5. SOME NONLINEAR ELASTICITY FUNCTIONS[a]

Function	*Function Symbol* σ
Tangent	$\frac{2}{\pi} a_0 \epsilon_b \tan \frac{\pi}{2} \cdot \frac{\epsilon}{\epsilon_b}$
Inverse tangent	$\frac{a_0}{a_1} \epsilon_b \tan^{-1} a_1 \frac{\epsilon}{\epsilon_b}$
Hyperbolic tangent	$\sigma_0 \epsilon_b \tanh \frac{a_0}{\sigma_0} \cdot \frac{\epsilon}{\epsilon_b}$
Algebraic	$a_o \epsilon \left(1 - \frac{\epsilon}{\epsilon_b}\right)^{-1}$
Logarithmic	$-a_0 \epsilon_b \left[\log \left(1 - \frac{\epsilon}{\epsilon_b}\right)\right]$
Air[b]	$p_i (1 - \epsilon)^{-n}$

[a]All angles in radians. All logarithms are natural logarithms.

[b]p_i is reference pressure in cushion; usually taken as atmospheric. Exponent, n, is 1.0 for isothermal compression and 1.4 for adiabatic compression.

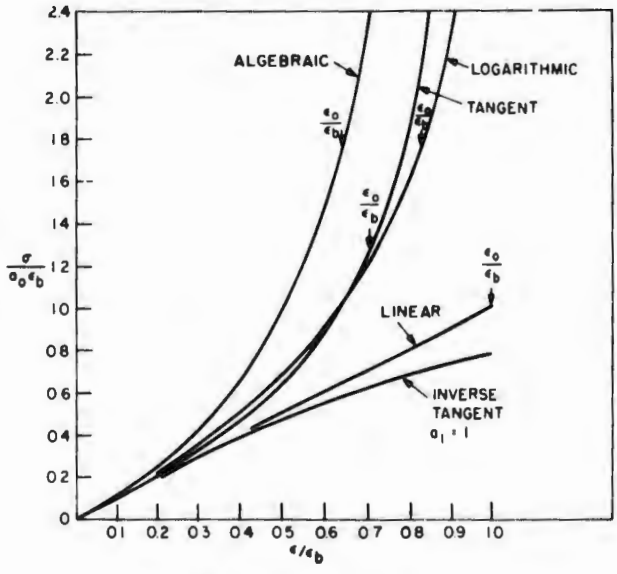

FIG. 4.5. Some elasticity functions.

therefore, contain a characteristic multiplier, $a_0\epsilon_b$, so that it is convenient to rewrite Eq. (4.12) in the form

$$\sigma = a_0\epsilon_b\,[f_1(\epsilon/\epsilon_b)] = a_0\epsilon_b\,\sigma'. \tag{4.17}$$

Differentiating with respect to ϵ gives

$$D\sigma = a_0\,D\sigma'. \tag{4.18}$$

Integrating gives

$$D^{-1}\,\sigma = a_0\epsilon_b^2\,D^{-1}\sigma'. \tag{4.19}$$

σ' may be regarded as a reduced stress variable.

These relations can be substituted in Eq. (4.11) to find ϵ_0. Some values of ϵ_0 and J_0 are shown in Table 4.6.

TABLE 4.6. SOME VALUES FOR ϵ_0 AND J_0

Function	ϵ_0	J_0	
Tangent	$0.707\ \epsilon_b$	$3.9/\epsilon_b$	$2.8/\epsilon_0$
Algebraic	$0.686\ \epsilon_b$	$4.6/\epsilon_b$	$3.2/\epsilon_0$
Logarithmic	$0.835\ \epsilon_b$	$3.4/\epsilon_b$	$2.8/\epsilon_0$
Air, adiabatic	0.569	3.25	3.25

Note that ϵ_b is difficult to determine experimentally. Thus least-squares fits of empirically derived stress-strain curves (more particularly those derived by relatively slow compression-testing machines) could be difficult. On the other hand, a_0 can be estimated fairly readily from a rough plot of the data, while ϵ_0 can be computed rather closely through numerical integration of the data. Hence, the estimating equations of Table 4.7 are recommended for curve-matching purposes. In each of these equations, when $\epsilon = \epsilon_0$, optimum dynamic stress becomes a function of a_0 and ϵ_0 only.

TABLE 4.7. ESTIMATING EQUATIONS

Function	*Stress-Strain* σ	*Optimum Stress of Material*[a] σ_0
Tangent	$0.91\ a_0\ \epsilon_0 \tan 1.11\ \epsilon/\epsilon_0$	$1.7\ a'_0\ \epsilon_0$
Algebraic	$1.46\ a_0\ \epsilon_0 \dfrac{\epsilon/\epsilon_0}{1.46 - \epsilon/\epsilon_0}$	$3.2\ a'_0\ \epsilon_0$
Logarithmic	$-1.2\ a_0\ \epsilon_0 \log (1 - 0.835\ \epsilon/\epsilon_0)$	$2.2\ a'_0\ \epsilon_0$

[a] a'_0 = optimum initial slope of stress-strain curve.

The author regrets not having test-matched the rubberized hair curves [141] to each of the three possible functions and selected the best overall fit. Perhaps the final results would then have been more useful. Since the operation is relatively easy with an electronic computer, it is hoped that such matching will be tried in the future.

Combining Eqs. (4.4) and (4.19), the reduced integral is

$$D^{-1}\sigma' = \frac{\sigma_s h}{a_0 \epsilon_b^2 T_c}, \tag{4.20}$$

ignoring the contribution of ϵ to the right-hand side. Solving with ϵ_0 to produce σ'_0 leads to expressions for optimum initial slope, a'_0. The results are shown in Table 4.8.

TABLE 4.8. OPTIMUM INITIAL STIFFNESSES

Function	*Value of Reduced Integral,* $D^{-1}\sigma'_0$	*Optimum Initial Stiffness*	
		$a'_0 \cdot \frac{\epsilon_b^2 T_c}{\sigma_s h}$	$a'_0 \cdot \frac{\epsilon_0^2 T_c}{\sigma_s h}$
Tangent	0.32	3.1	1.55
Algebraic	0.47	2.1	1.0
Logarithmic	0.54	1.9	1.33

Postulate, now, a linear material with the same initial stiffness a_0 as the nonlinear material but without a bottoming strain. The applicable stress law is

$$\sigma_l = a_0 \epsilon_1, \tag{4.21}$$

where ϵ_1 is a fictitious strain that the material would assume. Keep static stress, thickness, and drop height the same as before. Integrating over the strain produces

$$D^{-1}\sigma_l = \frac{1}{2} a_0 \epsilon_1^2 = \frac{\sigma_s h}{T_c}. \tag{4.22}$$

Substituting Eq. (4.22) in Eq. (4.20) produces

$$D^{-1}\sigma = D^{-1}\sigma_l = \frac{1}{2}\left(\frac{\epsilon_1}{\epsilon_b}\right)^2. \tag{4.23}$$

Dividing Eq. (4.17) by Eq. (4.21) results in

$$\frac{G}{G_1} = \frac{\sigma}{\sigma_l} = \frac{J}{J_l} = \frac{\sigma'}{\epsilon_1/\epsilon_b}. \tag{4.24}$$

Plots of the acceleration ratio as a function of ϵ_b/ϵ_1 for several elasticities are given in Fig. 4.6. For tangent elasticity, Mindlin [97] found that

$$\frac{G}{G_1} = \frac{2\epsilon_b}{\pi\epsilon_1}\sqrt{e^{-\pi^2\epsilon_1^2/4\epsilon_b^2} - 1}. \tag{4.25}$$

Simple expressions of this type are not compatible with the transcendental integrals obtained from logarithmic and algebraic elasticities.

Now let the a_0 of the hypothetical linear material differ from the optimum value of initial stiffness, a'_0. Combining Eqs. (4.20) and (4.22) gives

$$\frac{a_0}{a'_0} = 2\left(\frac{\epsilon_b}{\epsilon_1}\right)^2 D^{-1}\sigma'_0. \tag{4.26}$$

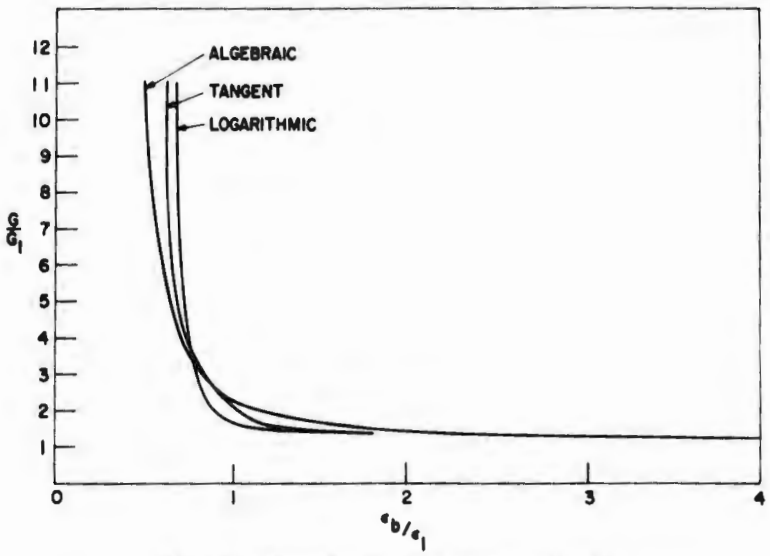

FIG. 4.6. Acceleration *versus* space available.

J for the hypothetical linear cushion is J_t and is found directly from Eqs. (4.21) and (4.22) to be $2/\epsilon_1$. From this one obtains, using Eq. (4.24),

$$\epsilon_1 = \frac{2\,G_0}{J_0\,G_1}, \tag{4.27}$$

where G_0 is the acceleration produced at J_0. Equation (4.26) thus becomes

$$\frac{a_0}{a'_0} = \frac{J_0\sigma'_0}{2}\left(\frac{G_1}{G_0}\right)^2. \tag{4.28}$$

Recall that a_0 was originally defined as the initial stiffness of a nonlinear material. Using the limits of G/G_1, suggested by Fig. 4.6 permits setting limits on the initial stiffness ratio of Eq. (4.28). From this figure it is apparent that the acceleration ratio begins to rise rapidly after ϵ_b/ϵ_1 becomes less than 1.0. Setting this as the minimum safe value for ϵ_b/ϵ_1 and taking the corresponding value of G/G_1 produces one set of limits. The other set of limits is evidently established for stiffening materials when $G_0 = G_1$. Results of the pertinent calculations are shown in Table 4.9.

TABLE 4.9. VARIATIONS IN INITIAL STIFFNESSES FOR CONSTANT THICKNESS

Class of Elasticity	*Minimum*		*Optimum*		*Maximum*	
	G/G_1	a_0/a'_0	G/G_1	a_0/a'_0	G/G_1	a_0/a'_0
Tangent	2.00	0.61	1.56	1.0	1.0	2.45
Algebraic	3.36	0.94	–	1.0	1.0	5.04
Logarithmic	1.73	1.0	1.73	1.0	1.0	3.04

The foregoing discussion of the effect of varying the initial material stiffness for nonlinear materials while holding area and thickness constant is a generalization of the results for tangent elasticity obtained by Mustin [135].

The foregoing indicates primarily that a wide variety of materials may be usable at a given thickness. There are two other potential benefits from the range of usable values shown in Table 4.9. These other benefits are:

1. Stiffness of most materials is affected by temperature changes. The surprisingly good performance of some materials at low temperatures may be directly related to the range of usable values. Further discussion of this point will be found in Chapter 7.
2. Most of the materials used in package cushioning vary in their published properties because of manufacturing tolerances. The usable value range permits use of the published values with more confidence that the maximum G will not be exceeded.

The effect of varying the area of a given cushioning material with a fixed supported weight can be estimated by looking at the effects of varying static stress. Each class of elasticity examined so far has a J_0 corresponding to an optimum static stress σ'_s for the conditions of drop. Dividing each side of Eq. 4.6 by these optimum values for each class of elasticity gives a relation of the form [171]

$$\frac{J}{J_0} = \frac{G}{G_0} = f\left(\frac{\sigma_s}{\sigma'_s}\right), \quad \frac{h}{T_c} = \text{a constant.} \tag{4.29}$$

The results are plotted in Fig. 4.7. It is particularly noteworthy that the curves practically coincide where $\sigma_s/\sigma'_s \leq 1.6$ and are flat where $0.6 \leq \sigma_s/\sigma'_s \leq 1.6$.

Figure 4.7 indicates that the designer has considerable latitude in selecting a conveniently dimensioned actual area in order to achieve desired shock levels within engineering limits of accuracy.

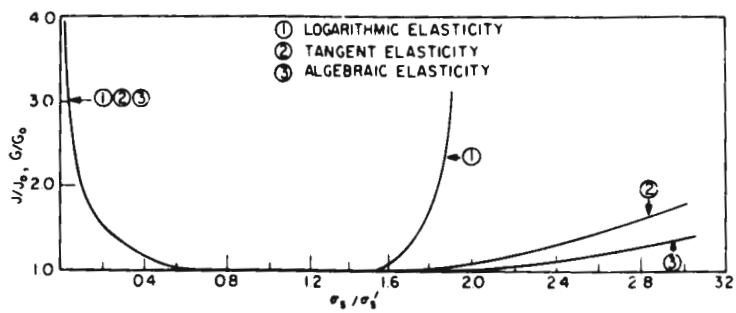

FIG. 4.7. Effect of varying surface area.

4.4. Effects of Damping

In the previous section, material damping was not considered in deriving the equations for J and J_0. Since it has previously been shown that damping has a significant effect on the behavior of materials, let us see what we can

learn about the behavior of real cushions from the rather limited literature on damping effects in velocity shock.

For simplicity, begin with the familiar Voigt solid sketched in Fig. 4.8. It is simple to show [97] that the equation of motion for such a cushion is given by

$$\ddot{\epsilon} + 2\beta_c\, \omega_n\, \dot{\epsilon} + \omega_n^2\, \epsilon = 0, \tag{4.30}$$

where

$$\omega_n = \sqrt{\frac{EA_c}{mT_c}} = \sqrt{\frac{Eg}{\sigma_s T_c}},$$

$$\beta_c = \frac{cA_c}{2m\,\omega_n} = \frac{cg}{2\sigma_s\,\omega_n}.$$

Equation (4.30) is analogous to Eq. (2.10).

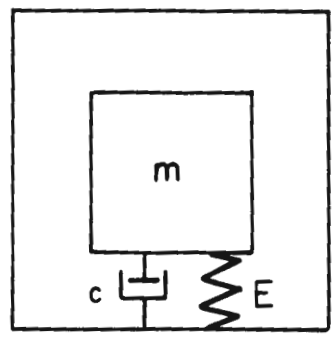

FIG. 4.8. Linear massless cushioning with viscous damping (Voigt solid).

Proceeding as outlined in section 4.2, we find that peak acceleration is given by

$$\ddot{\epsilon} = -\frac{\omega_n\sqrt{2gh}}{\sqrt{1-\beta_c^2}}\, e^{-\beta_c\omega_n t} \cos\left(\omega_n t\,\sqrt{1-\beta_c^2} + \gamma\right), \tag{4.31}$$

where

$$\tan\gamma = \frac{2\beta_c^2 - 1}{2\beta_c\sqrt{1-\beta_c^2}}.$$

Mindlin's results for various values of the critical damping ratio (β_c) are shown in Fig. 4.9.

With the hypothetical undamped linear cushion defined in Eq. (4.21), consider the effect of damping on peak acceleration. When $t = 0$,

$$\frac{G_m}{G_1} = 2\beta_c, \tag{4.32}$$

and, after $t = 0$,

$$\frac{G_m}{G_1} = e^{-\beta_c\omega_n t_m}, \tag{4.33}$$

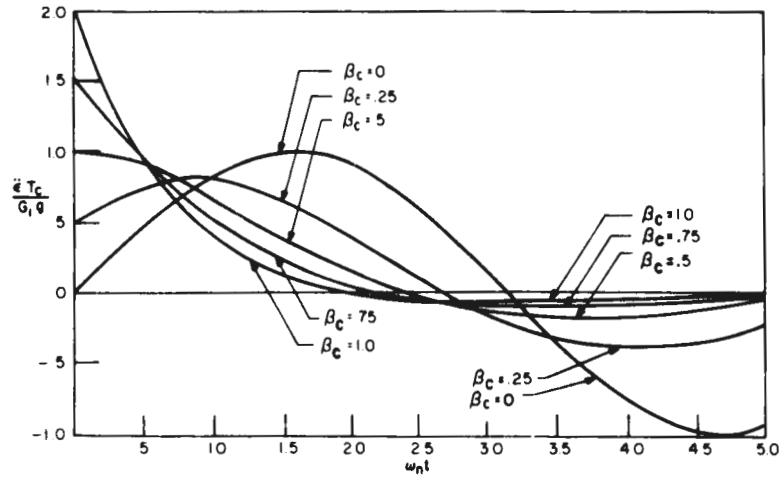

FIG. 4.9. Effect of cushion damping on acceleration. Mindlin [97].

where the time of maximum acceleration t_m is given by

$$\tan \omega_n t_m = \frac{1 - 4\beta_c^2}{\beta_c\,(3 - 4\beta_c^2)}. \tag{4.34}$$

The larger of the two values obtained from Eqs. (4.32) and (4.33) is plotted against β_c in Fig. 4.10. Note that this figure is also a plot of J_0 *versus* damping fraction, since there is a direct relation between J and G at equivalent drop heights and thicknesses.

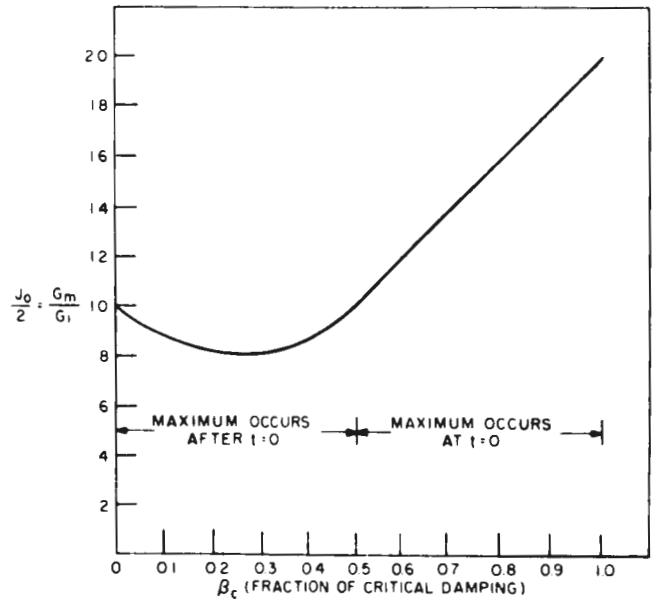

FIG. 4.10. Effect of cushion damping on peak acceleration. Mindlin [97].

Nobody, apparently, explicitly treats damped nonlinear elasticities in the same manner as Mindlin. Snowdon [53,54] considers the response of damped tangent and inverse-tangent elasticities to base disturbance caused by a "rounded step" function defined as

$$x_0(t) = 0 \text{ when } t < 0$$

$$x_0(t) = x_{max} \cdot (e^2/4)\,(\lambda_1\omega_n t)^2\, e^{-\lambda_1\omega_n t}, \tag{4.35}$$

where x_{max} is a constant, and ω_n is the natural frequency of the equivalent linear system. The parameter λ_1 determines the duration of the displacement pulse. Equation (4.35) is plotted for several values of λ_1 in Fig. 4.11.

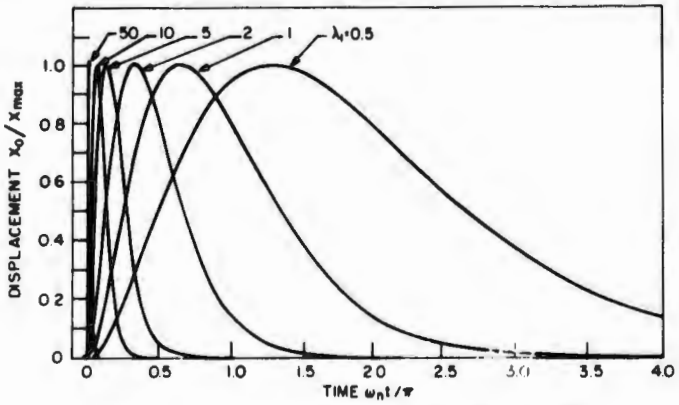

FIG. 4.11. Rounded-step velocity change function used by Snowdon [54].

This disturbance function is similar to, though not identical with the rigid-base concept in Mindlin's analysis. In fact, it may be thought of as what would actually occur if the impact floor were not infinitely rigid, or if there were a stiff body, such as a box, between the floor and the cushion. Thus the results shown here are more conservative than they would be if the Mindlin approach were followed literally. They may also be considered closer to reality, since all impacted surfaces exhibit their own elasticities.

Figure 4.12 shows the response of a tangent mounting at about $\epsilon'/\epsilon_b = 0.95$ and $\beta_c = 0.10$; Fig. 4.13 shows the same with $\beta_c = 0.05$. Note that, in both cases for $\lambda_1 = 50$ (the nearest approach to the Mindlin case), peak acceleration ratio is close to 9, as compared with the maximum of 2 for the damped linear case. For inverse-tangent elasticity, the effect is not so drastic, but Fig. 4.14 shows wide variation with respect to acceleration rise time.

It is evident, then, that variation in damping can produce wide variation in response. More particularly, it can produce wide variation in the value of J_0 for a specific material. Hence, one is forced to the conclusion that J_0 can never, except by coincidence, be a single-valued function for all values of drop height and static stress.

We must say again that, as a minimum, the isothermal stress-strain relation in real cushions is as given in Eq. (4.12), *i.e.*,

$$\sigma = f(\epsilon/\epsilon_b,\, t),\ 0 \leq \epsilon/\epsilon_b \leq 1.0,\ t \geq 0.$$

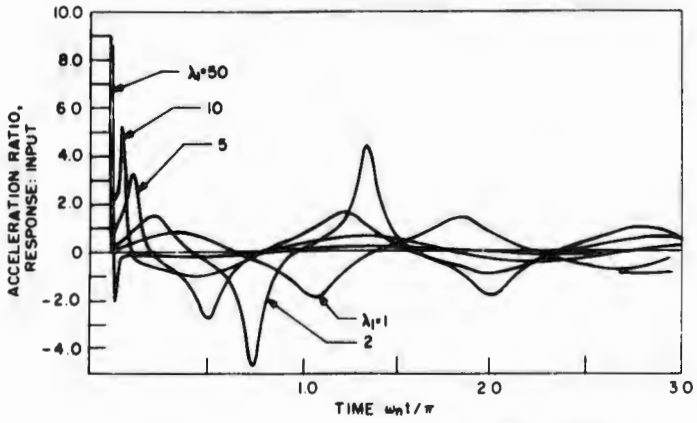

FIG. 4.12. Acceleration response of a tangent mounting with 10 percent critical damping [54].

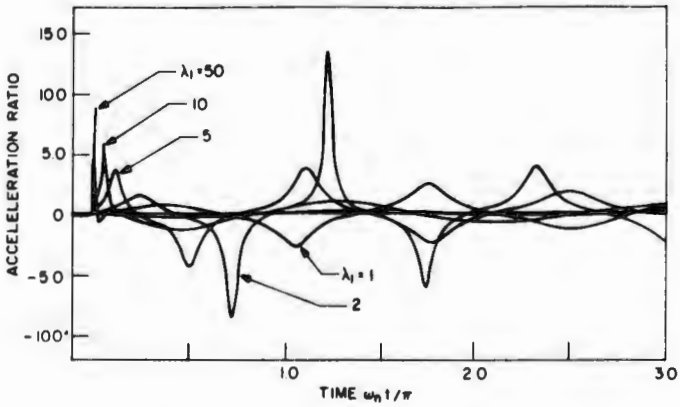

FIG. 4.13. Acceleration response of a tangent mounting with 5 percent critical damping [54].

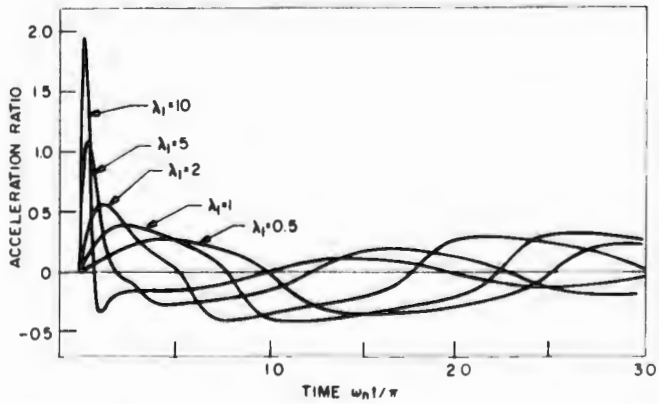

FIG. 4.14. Response for inverse-tangent elasticity at $\epsilon_1/\epsilon_h = 0.95$ and 10 percent critical damping [54].

4.5. Effects of the Mass of the Cushion

Explicit formulations of the effects of cushion mass on the acceleration response to velocity shock seem to have been explored only for linear elasticity [97].

Consider the system shown in Fig. 4.15. Assume that the conditions for one-dimensional waves are met (see section 3.1.3), so that

$$\frac{\partial^2 u}{\partial t^2} = V_3^2 \frac{\partial^2 u}{\partial x^2}, \tag{4.36}$$

where

$$V_3^2 = \frac{E}{\rho}.$$

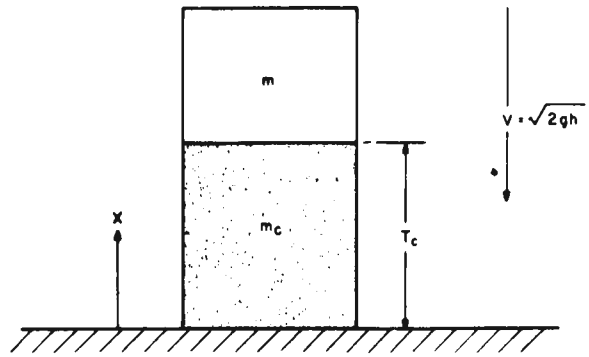

FIG. 4.15. Undamped linear cushioning with distributed mass.

The initial and boundary conditions are

$$[u]_{t=0} = 0, \left[\frac{\partial u}{\partial t}\right]_{t=0} = -V = -\sqrt{2gh},$$

$$EA_c \left[\frac{\partial u}{\partial x}\right]_{x=T_c} = -m \left[\frac{\partial^2 u}{\partial t^2}\right]_{x=T_c}, \quad [u]_{x=0} = 0,$$

from which the complete solution is found to be

$$u = -\sum_{i=1}^{\infty} \frac{2V_3 \sin \frac{\omega_i x}{V_3} \sin \omega_i t}{\omega_i \left(\frac{\omega_i T_c}{V_3} + \frac{1}{2} \sin \frac{2\omega_i T_c}{V_3}\right)}, \tag{4.37}$$

where ω_i is the ith root of the transcendental equation

$$\frac{\omega_i T_c}{V_3} \tan \frac{\omega_i T_c}{V_3} = -\frac{m_c}{m}. \tag{4.38}$$

The acceleration at $x = T_c$, *i.e.*, the acceleration of mass m, is then obtained by double differentiation of Eq. (4.37) and is

$$\left[\frac{\partial^2 u}{\partial t^2}\right]_{x=T_c} = V_3\omega_n \sum_{i=1}^{\infty} B_i \sin \omega_i t, \tag{4.39}$$

where

$$B_i = \frac{2\sqrt{\dfrac{m_c}{m}\left(\dfrac{m_c^2}{m^2} + \dfrac{\omega_i^2 T_c^2}{V_3^2}\right)}}{\dfrac{m_c}{m} + \dfrac{m_c^2}{m^2} + \dfrac{\omega_i^2 T_c^2}{V_3^2}} \tag{4.40}$$

and

$$\omega_n^2 = \frac{EA_c}{T_c m}, \tag{4.41}$$

which is the natural frequency of the massless linear spring.

The peak acceleration of mass m, therefore, is a sum of sinusoids of frequency ω_i and amplitude $V_3\omega_n B_i$. Now, $V_3\omega_n$ is G_1, the acceleration that the mass would obtain if the cushion were effectively massless. Calling G_{im} the maximum acceleration corresponding to ω_i, we have

$$\frac{G_{im}}{G_1} = B_i. \tag{4.42}$$

Equations (4.42) and (4.38) are plotted in Figs. 4.16 and 4.17.

It can be seen that the mass of the cushioning generally tends to reduce peak acceleration in the basic mode. If, however, the packaged article has an element whose natural frequency corresponds to one of the higher values

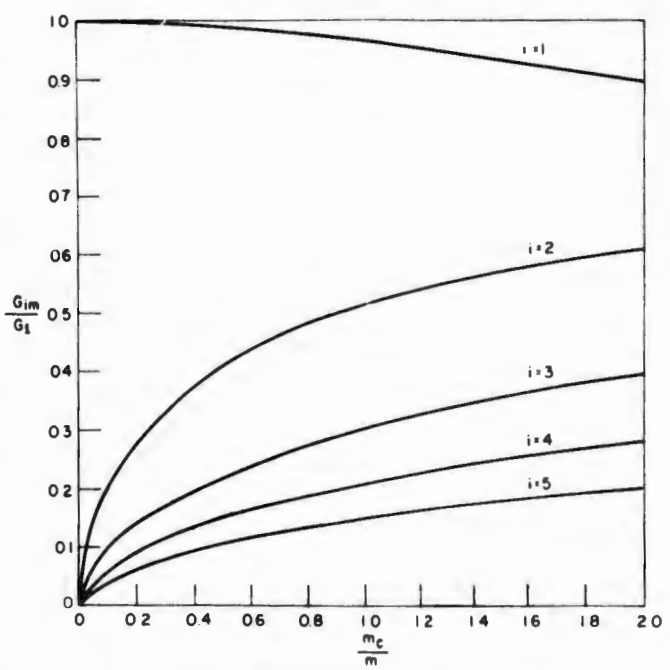

FIG. 4.16. Influence of mass on peak acceleration. Mindlin [97].

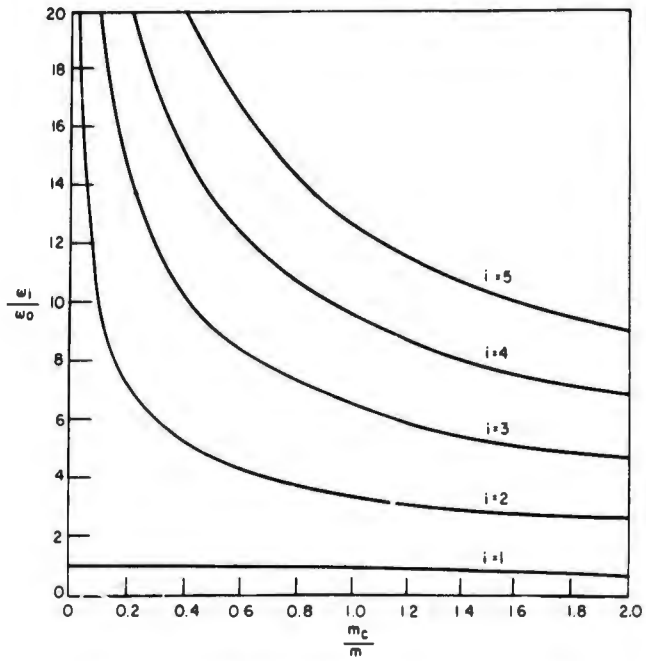

FIG. 4.17. Influence of mass on natural frequency [97].

of ω_i, then this element could be damaged even though fundamental mode acceleration is quite low.

In any case, sections 4.4 and 4.5 demonstrate that damping and cushion mass modify the amplitude and shape of the acceleration pulse transmitted to the cushioned object and this change affects the response of elements of this object. Hence, the considerable interest in shock spectra, to be discussed in the next chapter.

4.6. Room-Temperature Behavior of Real Materials

Sections 4.4 and 4.5 demonstrate that formulating correct elasticity statements, and solutions of the equations of motion involving such statements, can become a very difficult exercise—so laborious as to forbid its use in preliminary design. This is especially true in package cushioning where, quite often, the design is one of a kind and must be prepared under the pressure of short deadlines. In any case, computer solutions are rarely worth the effort unless a preliminary selection has been made; in preliminary design, simplified solutions are the best.

Hence, most data on real materials are empirical although, with new techniques recently made available, we can generalize somewhat more now than in the past.

Real materials used for the isolation of velocity shock can be divided into three broad groupings:

1. Resilient materials, such as lightweight open-celled plastic foams, rubberized hair, and the like, designed to absorb relatively small amounts of energy and, within reasonable time, absorb a similar amount again.

2. Quasi-resilient materials that remain substantially resilient under small excursions but, when large distortions are applied, do not recover completely.

3. Non-resilient materials used for one-time absorption of very large amounts of energy. Distortion under loading is invariably intended to be in the plastic range, and the designer is content if the material performs its function once. Prize examples of usage here are aerial delivery of cargo, astronaut recovery, pilot's escape pods, and the like.

The line between groups 1 and 2 is difficult to draw on purely mechanical grounds, because materials usually classed under group 1 show some permanent set under repeated loads. Hence, we draw the line as dictated by the designer's intent.

For convenience, not in order of importance, these three groupings will be discussed in this order.

4.6.1. Resilient Materials. The literature on resilient materials is very large. As an example, van der Toorn's comprehensive bibliography [172], prepared in 1961, runs to more than 250 pages with abstracts. Gigliotti's study [152] contains some 70 pertinent references; the Package Cushioning Design Handbook [148], though drastically limiting its scope, has 59 citations. Pendered's [173] excellent recent review contains 83 detailed references and cites six pertinent bibliographies.

The most common current practice is to present the data concerning specific materials as curves of peak acceleration *versus* static stress, in line with the suggestion by Kerstner [31]. See Fig. 4.3. This manner of presentation, based on data obtained with flat cushions, has certain drawbacks primarily in terms of the number of curves a designer must consult to obtain the best design for a specific problem. Soper and Dove [33,67] analyzed the problem of presenting data for cushioning materials. Starting with the assumption of an adiabatic process (justified by the short duration of response to an impulsive load), and using the principle of similitude for an arbitrary package as in Fig. 2.1, they arrived at a generalized scaling law for the response of the cushion system:

$$\frac{a_p}{V^2/2\ell_c} = f\left(\frac{mV^2}{2\ell_c^3}, \frac{V}{\ell_c}, c_f\right), \tag{4.43}$$

where a_p = peak acceleration (in./sec^2),

V = velocity change of the package (in./sec) without rebound,

ℓ_c = any characteristic length of the cushion (in.), and

c_f = coefficient of friction between the cushion and the cushioned item (dimensionless).

In deriving the foregoing relation, Soper and Dove made the further assumption that the stress laws applicable to the cushion involve only time derivatives and integrals of the component functions, *e.g.*, Skudrzyk's relation Eq. (3.57). Mass of the cushioning is not included (a slightly conservative assumption, as shown in the previous section), nor the acceleration of gravity (a minor factor when peak acceleration is more than ten times as great).

From this general scaling law they derived a specialized scaling law, valid for a broad number of practical problems:

$$\frac{a_p}{V^2/2T_c} = f\left(\frac{mV^2}{2A_cT_c}, \frac{V}{T_c}, c_f\right). \tag{4.44}$$

Note that, in this law, area of the cushion may be varied independently of the thickness, thus providing design flexibility. In order to be valid, the configuration must be such that the local stress state in the cushion depends only on the angle at which the stress is applied, the coefficient of friction, time, strain, and the constants of the material's stress-strain function. Configurations for which the specialized law is valid (not necessarily exhaustive) include:

1. Material thickness everywhere very small relative to dimensions of the cushioned article, and no slippage at one or both interfaces;
2. Flat, uniform cushion, laterally confined or possessing negligible Poisson effect; and
3. Flat uniform cushion and lubricated surfaces.

Cases 2 and 3 obviously do not involve a friction component. Hence, for a plane cushion, where most of the data gathering has occurred,

$$\frac{a_p}{V^2/2T_c} = f\left(\frac{mV^2}{2A_cT_c}, \frac{V}{T_c}\right). \tag{4.45}$$

By definition,

$$a_p = \frac{\sigma_m A_c}{m}, \tag{4.46}$$

so that Eq. (4.45) becomes

$$\frac{\sigma_m}{mV^2/2A_cT_c} = J = f\left(\frac{mV^2}{2A_cT_c}, \frac{V}{T_c}\right), \tag{4.47}$$

which may be written

$$J = f\left(\frac{\sigma_s h}{T_c}, \frac{h}{T_c}\right). \tag{4.48}$$

If the material is undamped, then the term h/T vanishes and

$$J = f\left(\frac{\sigma_s h}{T_c}\right), \tag{4.49}$$

which is the expression for J originally found by Janssen [122] and derived in general terms in section 4.2.

Soper and Dove have shown that the peak response of an impulsively loaded cushion system is a function of only two variables: energy per unit volume and an initial-strain rate. Their results require, for complete accuracy, that the systems be geometrically similar and that the effects of gravity and cushion mass be practically negligible. Under certain circumstances, fortunately the most common, the requirement for geometric similarity may be relaxed to permit varying cushion thickness independently of other dimensions.

Based on these findings, Soper and Dove recommend that a single family of curves (one for each value of V/T_c) could suffice if the ordinate were J or GT_c/h and the abcissa $\sigma_s\ h/T_c$. The compactness inherent in this schema, as compared with Fig. 4.3 is obvious. For the designer, however, the advantage is ephemeral since his unknowns are T_c and σ_s while acceleration and velocity change (or height of drop) are the knowns. Working from such curves, with T_c appearing in the ordinate, the abcissa, and the individual curves, the only possible design technique is successive approximation.

The possibility of simplifying the relationship for preliminary design purposes has been investigated recently [171]. The treatment is largely limited to simplification with respect to the minimum point on the J curve which, by definition, is the optimum point of the design. The treatment is far from rigorous, but the attainment of useful results justifies the line followed.

As was made clear in Eq. (4.47), energy per unit volume appears on both sides of the functional relation. Hence, it seems logical to write

$$\sigma_0 = \sigma'_s\ G_0 = f\left(\frac{\sigma'_s\ h}{T_c}, \frac{h}{T_c}\right). \tag{4.50}$$

Dividing through by σ'_s leads to

$$G_0 = f\left(\frac{h}{T_c}\right). \tag{4.51}$$

Substitute for J_0 its equivalent from Eq. 4.7. Dividing both sides by energy per unit volume gives

$$\frac{G_0\ T^2}{\sigma'_s\ h^2} = f\left(\frac{h}{T_c}\right), \tag{4.52}$$

which may be further simplified and written as

$$\sigma'_s = f\left(G_0\ \frac{h}{T_c}\right). \tag{4.53}$$

By means of least squares, the 16 materials identified in Table 4.10 have been fitted to straight lines

$$G_0 = a\left(\frac{h}{T_c}\right) + b. \tag{4.54}$$

Values of the constants a and b are shown in Table 4.11 along with a standard deviation for each regression line and various statistical operations (such as Chi squared test, correlation coefficient and Students t test) designed to test the goodness of fit. Note that 19 materials are listed in Table 4.11. Materials 15, 16, and 17 are three different densities of polystyrene foam. The Forest Products Laboratory [148] combined data concerning the same materials into a single set, identified as material 4. Data concerning materials 15, 16, and 17 are combined into 18; then all of 18 and 4 are combined into 19.

Working primarily with high-energy absorptive materials, Soper and Dove [33] found that J_0 tended to become constant and postulated this tendency as

TABLE 4.10. IDENTIFICATION OF MATERIALS ANALYZED BY MUSTIN [171]

Material No.	*Description*
1	Polyester polyurethane foam, 4.0 pcf
2	Rubberized hair, 1.4 pcf
3	Rubberized hair, 1.5 pcf
4	Polystyrene foam, 0.4 to 1.5 pcf
5	Polyester polyurethane foam, 2.0 pcf
6	Polyether polyurethane foam, 1.5 pcf
7	Wood fiber felt, 1.8 pcf
8	Wood fiber felt, 2.4 pcf
9	Rubberized hair, 2.0 pcf
10	Polyethylene foam, 2.0 pcf
11	Wood fiber felt, 1.5 pcf
12	Cellulose wadding, asphalt-treated, plain or embossed
13	Polyester polyurethane foam, large-celled, 4.0 pcf
14	Bound fiberglass, 1.1 pcf
15	Resilo-Pak 200
16	Resilo Pak 300
17	Resilo Pak 400

a characteristic of many cushioning materials. If we divide both sides of Eq. (4.54) by h/T_c we obtain

$$J_0 = a + \frac{b}{h/T_c}. \tag{4.55}$$

Where b is small, J_0 can be considered a constant for all practical purposes, even at the relatively low strain rates used here. In any case, for these materials, the larger h/T_c becomes, the lesser the influence of the constant b on the value of J_0 to be used. Sabbagh [174], working with many of the same types of materials as those covered in Table 4.10, but at h/T_c ratios on the order of 80, found single stress-strain curves to be sufficient material descriptors. Thus, the empirical equation derived agrees with observed data. Further, if the material is assumed to be viscoelastic, such as represented by the "standard linear" solid or the more generalized Maxwell and Voigt solids, then it is evident that observation agrees with theory. In effect, at very high rates of initial strain, the dashpot element does not have time to respond to the stress pulse; thus, movement in the dashpot does not affect stress response.

From Eq. (4.53), it has been found that the same 16 materials provide a satisfactory least-squares fit to the explicit equation

$$\sigma'_s = c\left(G_0 \frac{h}{T_c}\right)^d \tag{4.56}$$

Values of the constants c and d are shown in Table 4.12, which also contains the standard deviation and the χ^2 statistic. Previous remarks concerning materials 4 and 15 through 19 apply.

TABLE 4.11. SOLUTIONS TO THE ACCELERATION EQUATION

Material No.	*No. of Data Points*	*a*	*b*	*Standard Deviation*	*Computed* χ^2	*Maximum* χ^2 $P = 0.99$[a]	*Correction Coefficient*	*Computed t*	*Minimum t* $P = 0.99$[b]
1	16	3.65	−2.53	2.50	3.620	5.229	0.9953	22.912	2.977
2	19	2.73	2.91	2.14	4.440	7.012	0.9512	14.318	2.898
3	27	2.85	2.71	2.75	7.321	12.198	0.9650	20.025	2.787
4	22	3.98	3.46	1.50	1.424	8.897	0.9983	76.646	2.845
5	26	3.13	−4.61	2.32	10.069	11.524	0.9923	40.745	2.797
6	16	4.67	−9.43	2.58	2.551	5.229	0.9904	28.105	2.977
7	16	2.79	3.74	1.67	1.464	5.229	0.9887	25.941	2.977
8	16	3.72	6.83	1.18	0.600	5.229	0.9968	47.781	2.977
9	28	3.64	0.44	3.50	9.267	12.879	0.9726	22.910	2.779
10	28	3.95	0.25	0.87	0.826	12.879	0.9992	126.823	2.779
11	16	2.37	4.31	2.18	0.310	5.229	0.9813	19.077	2.977
12	8	3.10	13.14	2.96	2.006	2.167[c]	0.9456	8.475	3.707
13	12	3.25	−4.02	2.70	2.220	3.053	0.9788	16.434	3.169
14	7	3.12	6.26	1.78	1.279	1.635[c]	0.9880	15.477	4.032
15	15	4.88	−0.35	1.31	1.123	4.660	0.9965	44.131	3.012
16	21	4.51	1.20	3.52	5.719	8.260	0.9916	34.673	2.861
17	20	4.52	0.68	2.00	2.080	7.633	0.9956	46.067	2.878
18	56	4.54	1.03	2.62	9.536	27.012	0.9934	65.221	2.67
19	78	4.26	2.47	3.11	16.909	43.054	0.9915	68.036	2.64

[a] From R. A. Fisher's "Statistical Methods for Research Workers."

[b] From G. W. Snedecor "Calculation and Interpretation of Analysis of Variance and Co-Variance," Collegiate Press, Ames, Iowa, 1934.

[c] This value of χ^2 is for $P = 0.95$.

TABLE 4.12. SOLUTIONS TO THE STATIC-STRESS EQUATION

Material No.	*No. of Data Points*	*c*	*d*	*Standard Deviation*	*Computed* χ^2	*Maximum* χ^2 $P = 0.99^a$
1	16	0.80	−0.23	0.025	0.035	5.229
2	19	0.35	−0.41	0.016	0.065	7.012
3	27	0.21	−0.26	0.017	0.106	12.198
4	22	6.81	−0.40	0.070	0.134	8.897
5	26	0.37	−0.13	0.052	0.297	11.524
6	16	0.41	−0.12	0.038	0.097	5.229
7	16	0.11	−0.18	0.009	0.028	5.229
8	16	0.20	−0.23	0.017	0.072	5.229
9	28	0.72	−0.43	0.011	0.032	12.879
10	28	11.86	−0.48	0.190	0.754	12.879
11	16	0.091	−0.15	0.009	0.030	5.229
12	8	0.069	−0.18	0.004	0.005	1.239
13	12	1.00	−0.23	0.022	0.019	3.053
14	7	0.31	−0.36	0.016	0.023	0.872
15	15	3.54	−0.31	0.101	0.157	4.660
16	21	4.76	−0.32	0.196	1.088	8.260
17	20	3.72	−0.29	0.137	0.417	7.633
18	56	3.68	−0.29	0.164	1.843	27.012
19	78	4.36	−0.32	0.156	2.240	43.054

[a] From Fisher's tables.

It is evident from Tables 4.11 and 4.12 that reasonably acceptable fits to the data have been obtained. No one, however, should leap to the conclusion that the empirical fits are the true measure of the variation in J_0 and σ'_x. All that has been proved is a strong probability that these variations can be expressed as continuous functions and that two sets of functions have been found that are reasonably satisfactory for engineering purposes.

Equations (4.54) and (4.56) are plotted for a single material in Fig. 4.18. It is evident that, with these two curves, the designer can operate near optimum no matter what the drop height.

It must be noted that Birnbaum [175] mentioned some possible straight-line relationships in 1950. Apparently the wrong variables were sought, with unfruitful results, and the effort was abandoned.

The same 16 materials were also examined in the light of Eq. (4.29). The envelope of results is plotted in Fig. 4.19. Most of the materials developed what appeared to be a single curve independent of the parameter h/T_r but the rubberized hairs did not. Though an interesting topic for investigation, this area was not explored; in the face of the finding it was found that all curves practically coincide in the stress ratio region where $0.4 \leq \sigma_x/\sigma'_x \leq 1.5$ and are flat where $0.7 \leq \sigma_x/\sigma'_x \leq 1.3$.

Figure 4.19 demonstrates that wide static-stress variation from optimum can occur without significant effect on peak acceleration. This and the

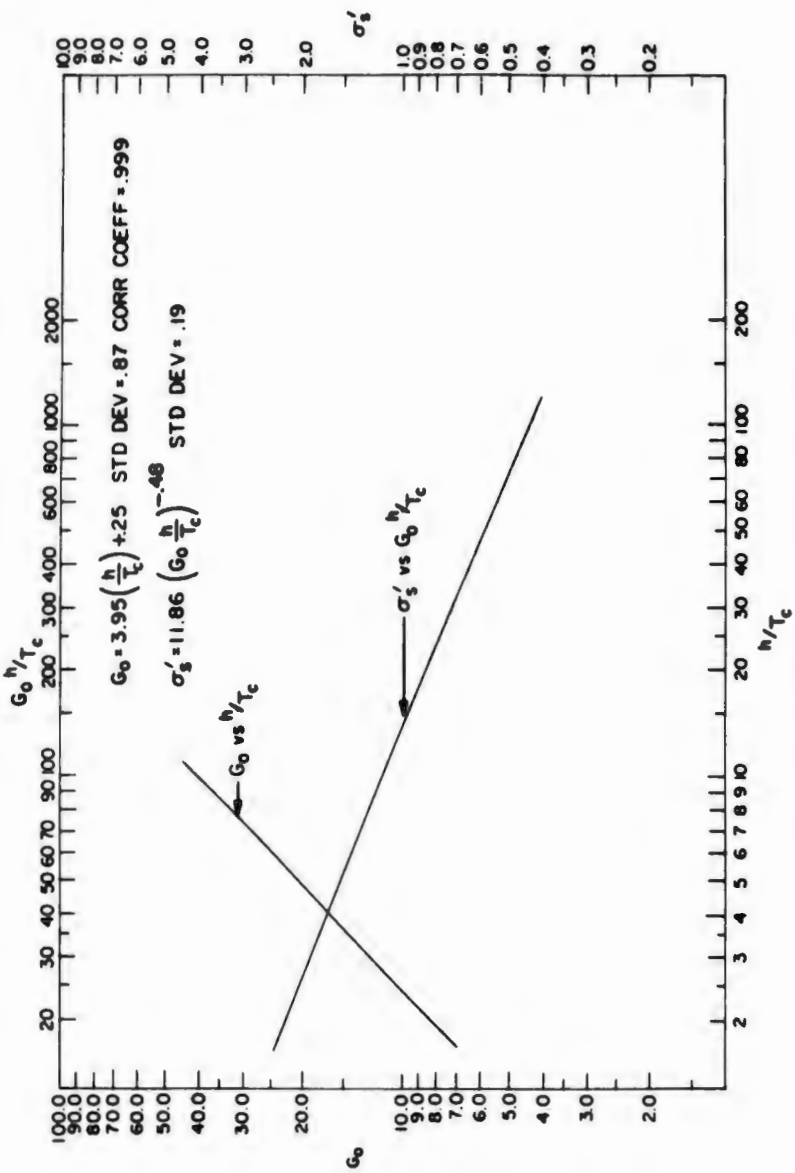

FIG. 4.18. Design curves for material No. 10. Mustin [171].

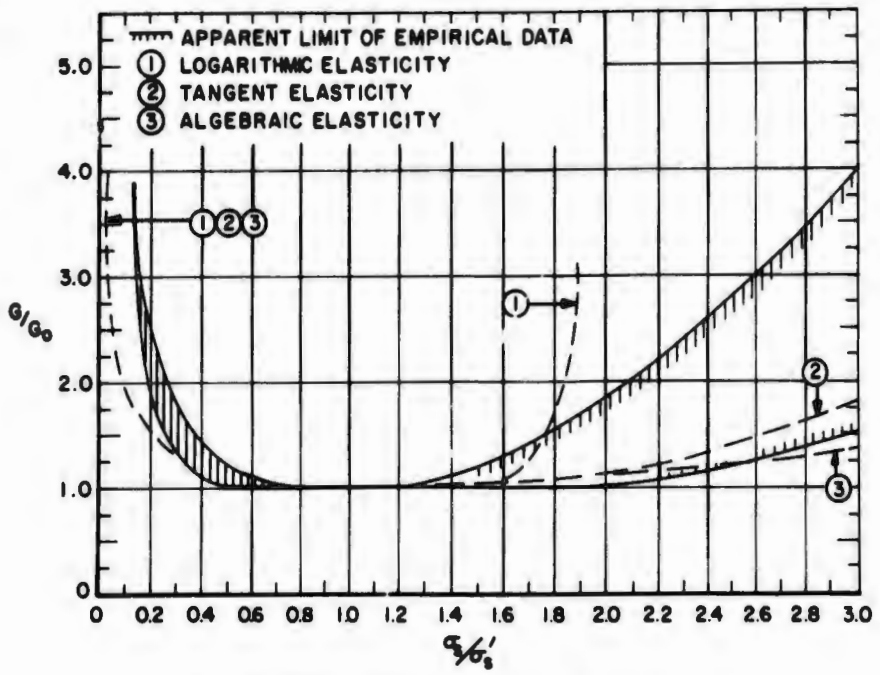

FIG. 4.19. Acceleration *versus* static stress ratios [171].

theoretical findings summarized in Table 4.9 indicate that the designer has wide latitude both in selecting materials and in detailing the design. But in any case, Fig. 4.19 establishes reasonably wide limits on the accuracy with which G_0 and σ'_s must be determined for any given material.

Normally, the designer starts with the projected area of the object to be cushioned as a determinant of the static-stress range in which he must work. Figure 4.20 can be used as a guide in narrowing choice. A more elegant form of Fig. 4.20 has been published by the Ministry of Aviation [176], and is shown in Fig. 4.21 for use with materials available in the United Kingdom, identified in Table 4.13. The effect with either type of presentation is essentially the same. Blake [177] also recommends starting the design on the basis of surface area although his curves are still limited to the 30-inch drop test.

There are some definite limitations on the validity of Mustin's approach. These limitations are amplifications of those stated in the original paper [171] and are:

1. Secondary data, processed for publication, were used for the curve matches found. The most important source of error is the investigator's reading of semilogarithmic plots without intermediate grid lines. Numerous checks have been made, however, and these curves predict as well as the original curves, to slide-rule accuracy. The second possible source of error is the method of gathering data [178]. Three specimens are used and five drops at each velocity and static stress are made. Results of the first drop are discarded and the remaining four are averaged; then the results of the

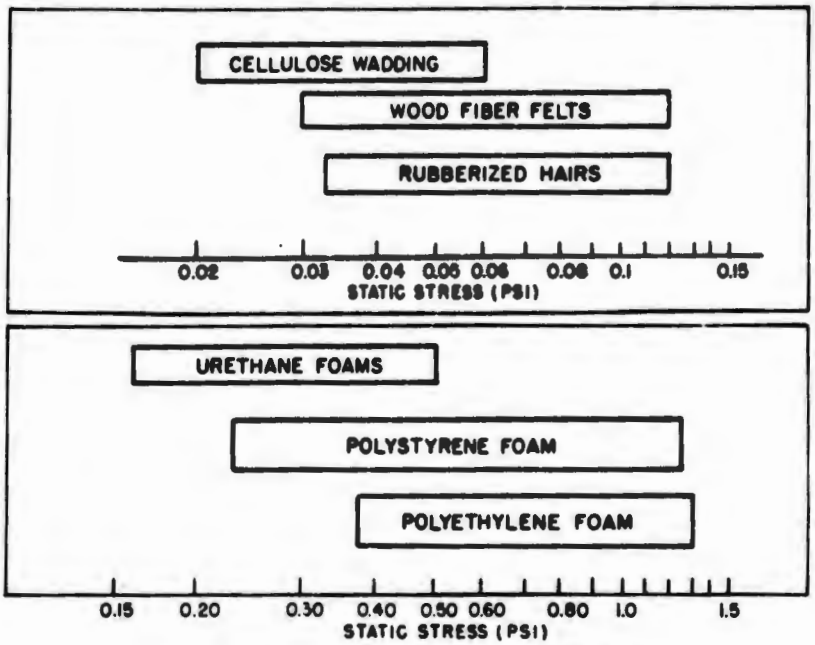

FIG. 4.20. Range of recorded optimum static stresses.

three replicates are averaged to obtain a single data point. When dynamic compression set (measured three minutes after the last drop) exceeds 10 percent, a new set of samples is used. The reason for the procedure is that many if not all of the materials exhibit some degree of dynamic "permanent" set after impacting. Typical behavior, taken from Zell [179], is shown in Fig. 4.22. As can be seen, statistical operations are being piled on statistical operations; obviously it would be better to use the original readings to obtain the least-squares fit.

2. Most of the data were obtained using constant-surface-area cushions in which the thickness was varied. Since in most cases samples are $8 \times 8 \times T_c$ (inches), it can be seen that a six-inch thickness is not sufficiently negligible to satisfy the criterion of Soper and Dove. Further, there is definite evidence (see section 3.5) that the behavior of some package-cushioning materials is influenced by the length of the path that escaping air must travel, *i.e.*, by shape. While it is true that acceptable curve matches were found even with six-inch samples, there is no guarantee that the slope of the curve would not have changed, supposing, for example, that the ratio of surface area to side area had been kept reasonably constant. In connection with shape effects in general, note that Poisson effects in the material must be reasonably small if the technique is to be valid. Thus, a design using solid rubber slabs must still use the classical technique, summarized very well by Burns [180], and also appearing in Crede [3], Payne and Davey [181], and Harris and Crede [26]. As a general rule, most solid elastomers are far too incompressible to be used as a solid slab under a substantial portion of the applied load. Thus they fall into the category of "point" isolators and are outside the scope of this monograph.

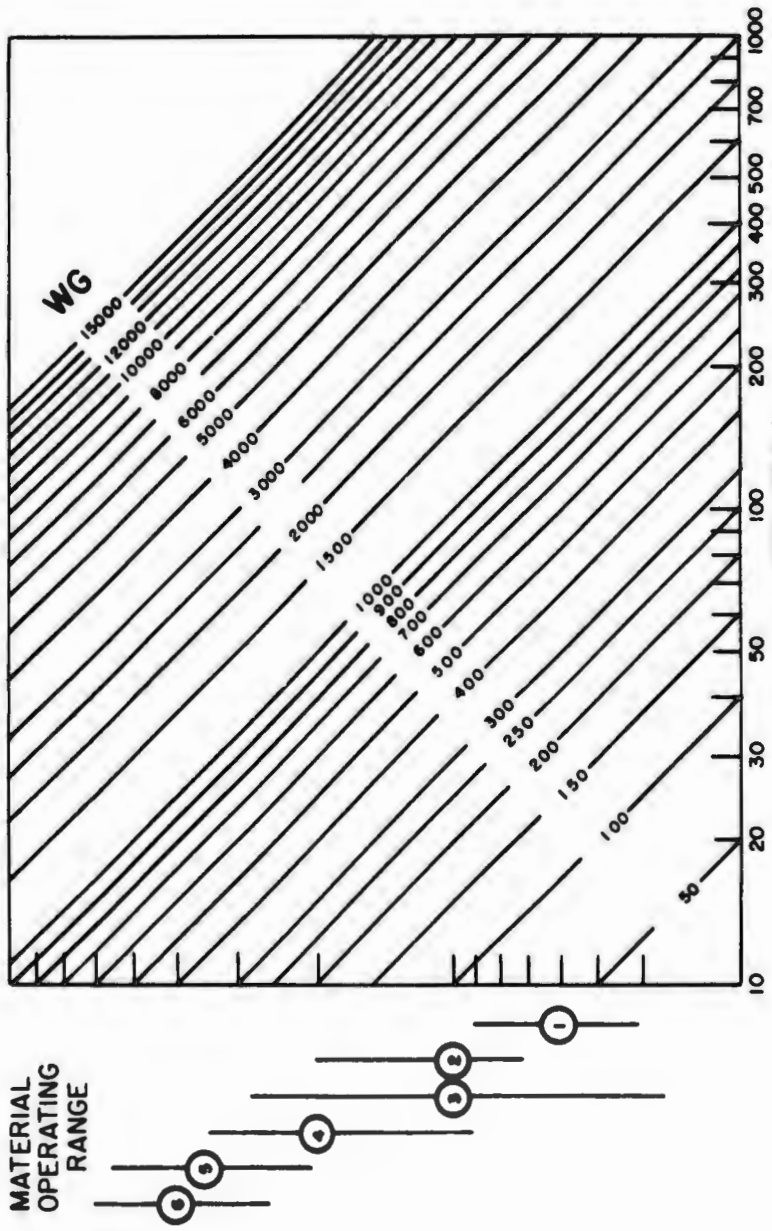

FIG. 4.21. Ministry of Aviation cushion-selection chart.

TABLE 4.13. MATERIALS IN MINISTRY OF AVIATION CHART

No.	*Material Description*	*Density (pcf)*	*Specification*
1	Rubberized hair	4	UK/AID/919
2	Rubberized hair	6	UK/AID/919
3	Latex foam	10	C.S. 3067
4	Expanded rubber (light)	10	C.S. 2808
5	Expanded rubber (medium)	16	C.S. 2808
6	Expanded rubber (heavy)	33	C.S. 3092

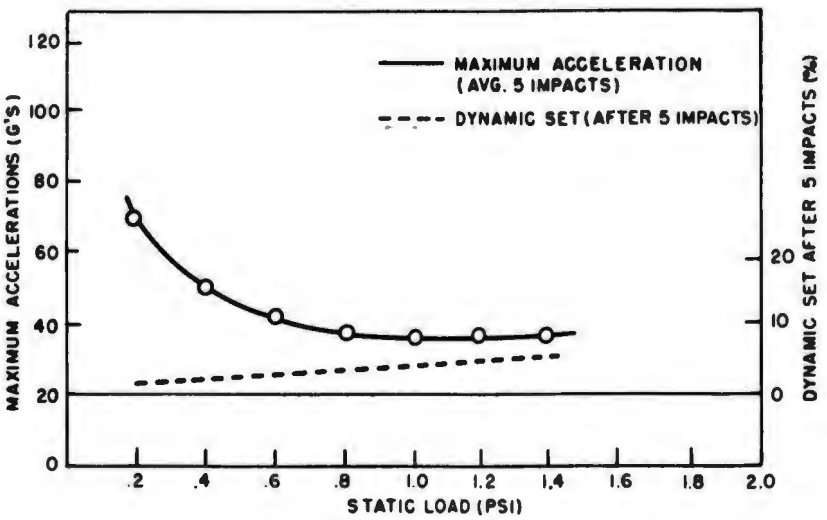

FIG. 4.22. Peak accelerations and dynamic set for 5-in., 1.5-pcf polystyrene foam. Zell [179].

3. Many of the materials are open-celled plastics. Hence, ability of air to escape might affect the results obtained with a specific design. Also it is doubtful what would happen if the sides of the cushion were partially or totally sealed. Some aspects of this problem have been explored by Gigliotti [151] and Blake [182]. The mathematical models developed by Volz [89], Venning [91], and Kosten and Zwikker [55] also include an air-escape constraint.

4. These data apply only to room-temperature conditions. Available information on extreme temperature performance will be summarized in a later section.

5. The optimum static-stress values developed here are valid only for the shock condition. They may be too high for satisfactory control of drift under prolonged storage. There is some evidence [179] also, that in some cases they may be so high that unacceptable drift will occur under prolonged vibration; this factor will be discussed in a later section.

6. One major disadvantage in plotting *J versus* energy per unit volume or G *vs* σ'_p, and in Mustin's simplified approach, is that alteration in the stress-strain behavior of the material by dynamic conditions is masked in the data reduction.

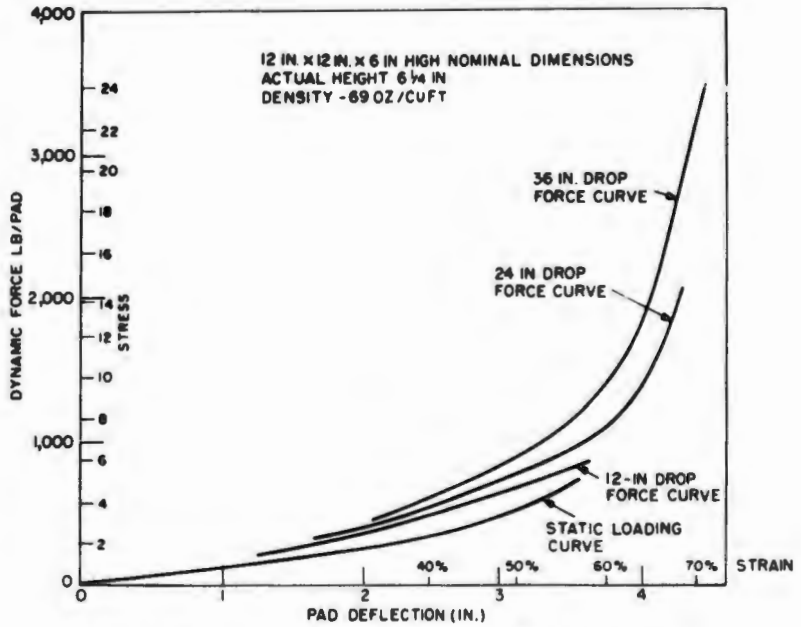

FIG. 4.23. Dynamic stress-strain curves for rubberized hair. After Schuler [183].

For many materials the shape of the stress-strain curve is not significantly altered by strain-rate considerations. Figure 4.23, taken from Schuler [183], illustrates the change in stress-strain curves for various drop heights with rubberized hair. On the other hand, with materials that are heavily dependent upon trapped air for their composite dynamic properties, a complete change in the shape of the material's stress-strain curve may result when the loading is dynamic. Figure 4.24, plotted from two separate curves in Keast and Baruch [184], illustrates the problem. A change in properties for the whole material indicates that trapped air and its release from the edge of the cushion can be a strong enough influence to mask the collapsing-column effect of the cushion matrix. The point at which the knee effect disappears is not clearly established. Figure 4.25, taken from Venning [91], shows a distinct knee at compression rates up to 12 in./sec.

Dynamic stress-strain curves can be plotted from the original data used to derive the curves previously discussed. It may often be informative to make these plots when specific mathematical models of behavior are to be selected.

In sum then, there is much information available concerning the dynamic shock behavior of resilient cushions, most of it collected for use in package cushioning. The suggestions of Soper and Dove [33,67] give a logical basis for plotting the behavior of the materials in a fashion that explicitly recognizes damping in the material. Mustin's analysis [171] gives a short method,

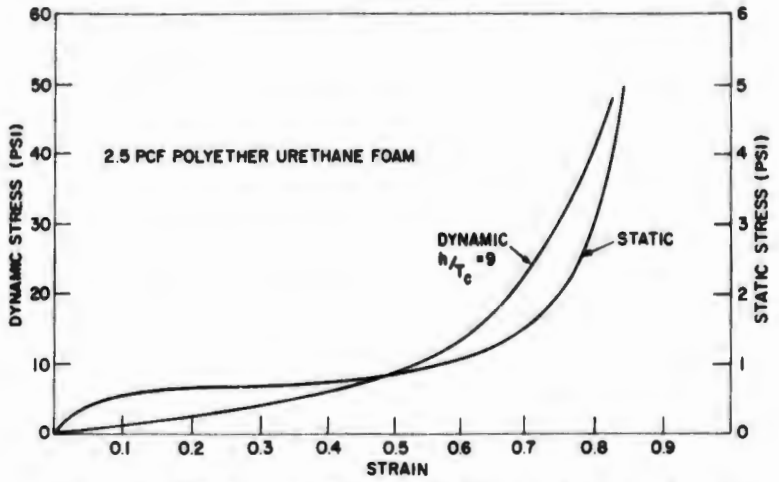

FIG. 4.24. Typical static and dynamic stress-strain curves for a polyether urethane foam. Keast and Baruch [184].

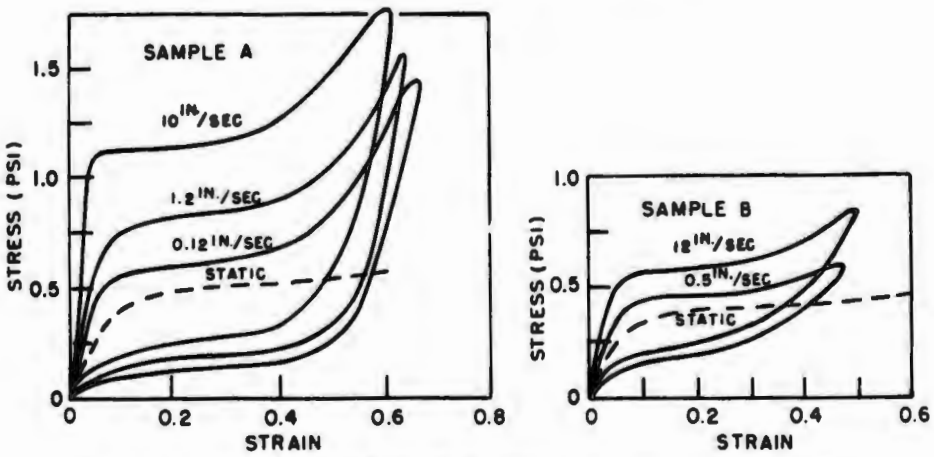

FIG. 4.25. Some stress-strain curves for polyurethane foams. Venning [91].

usable at least for preliminary design, for achieving near-optimum shock-isolation designs with available materials.

In other words, we have come a long way toward rationalizing design with cushions, but we are no closer to reducing the design process to a "cook book" operation. We are possibly even farther from a complete theoretical explanation of observed behavior.

4.6.1.1. *Some Methods of Modifying Material Performance.* The data summarized in the immediately preceding section were concerned exclusively with pads shaped as rectangular parallelepipeds. In addition, most measurements were taken on the material in the as-produced state and orientation and thus would be valid for all conditions only if the material were isotropic. This section will discuss some of the design variations for which data or reasonable inferences are available.

Shape of Cushioned Object. If the cushioned object is hemispherical, Soper and Dove [33] show that, at least for one material, J curves are directly usable if the effective area is taken as 0.81 of the projected area of the cushioned object. If, as a drawing board exercise, one plots the position of a cylindrical object at maximum deflection, one will find that the remaining area is of the same order of magnitude. Hence, the shape factor of 0.81 appears a useful figure for preliminary design purposes.

Edge Loading. Rubberized hair blankets in commercial production, and probably most molded shapes, are definitely anisotropic. In general, there is a tendency for the hair lengths to be oriented somewhat more parallel than normal to the surface of the blanket. Edge-loaded pads can be made by slitting the material to the desired thickness and then gluing the strips into blocks which are loaded edgewise. Figure 4.26 shows a typical example of the modification in performance so obtainable.

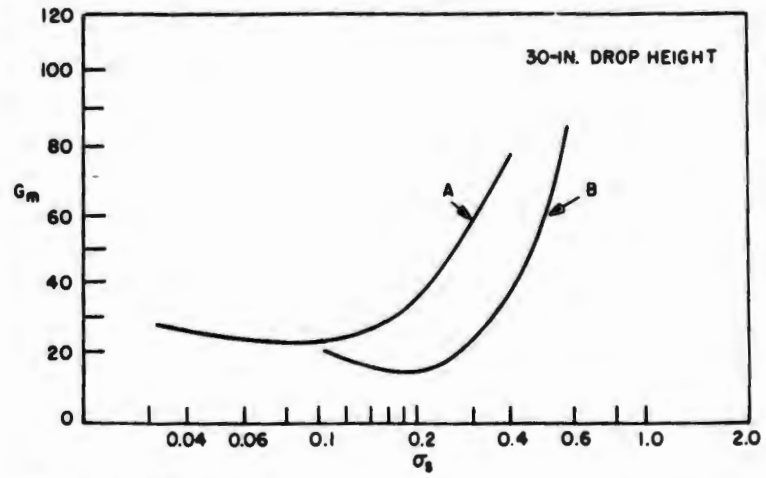

FIG. 4.26. Effect of edge loading 5-in. thick rubberized hair; curve A is 2 pcf loaded flat, and curve B is 1.8 pcf loaded on edge [148].

There are some signs that polyurethane foam may not be isotropic [185]. Figure 4.27 shows the effects of laminating this material in different directions. The work is still in progress and it is too early to draw definitive conclusions. Note, however, that horizontal lamination produced the largest reduction in peak acceleration. It would seem plausible that the interface causes internal reflections of the stress wave (as expected by theory), thus reducing the final peak acceleration ratio achieved. It is interesting to speculate on the effect of carrying the laminating technique to the limit of an infinity of layers.

Convoluted Surfaces. A convoluted surface can be produced in a foam material by techniques well recognized in the industry. Typical effects are shown in Fig. 4.28. Here, apparently, the total area being compressed increases as the load deflects, thus increasing the effective spring rate of the material [185]. Note, however, that drastic decrease in optimum static stress

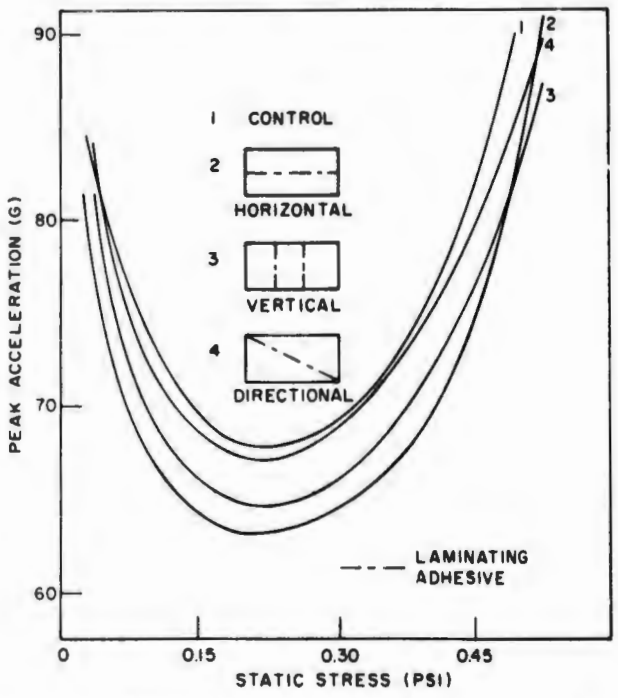

FIG. 4.27. Effect of laminating a 2.4-pcf polyurethane foam; h/T_r is 15. Goldberg [186].

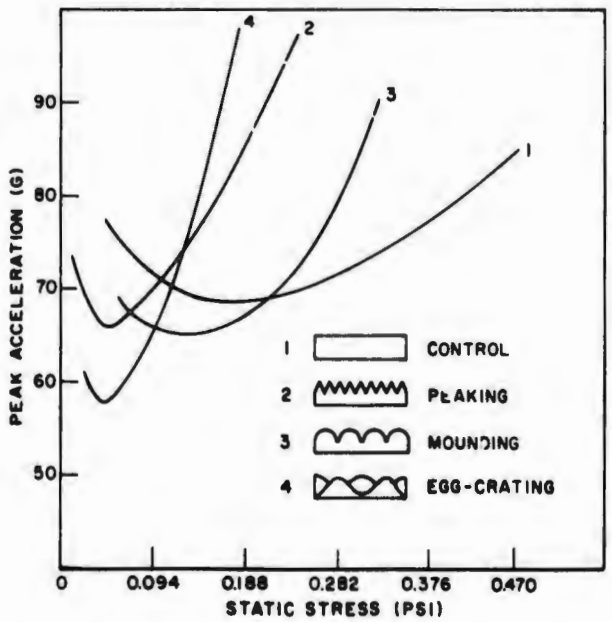

FIG. 4.28. Effect of convoluting a 2.4-pcf polyurethane foam; h/T_r is 15 [186].

also occurs and must be allowed for in design. Drift potential under prolonged static load also needs evaluation.

Hole Cutting. Effects of die-cutting 1-inch diameter holes in the surface of a polyurethane pad are illustrated in Fig. 4.29. Here the reduction in peak acceleration is a function not only of the reduction in overall stiffness of the material but also of the change of shape, reducing the path required for air to escape.

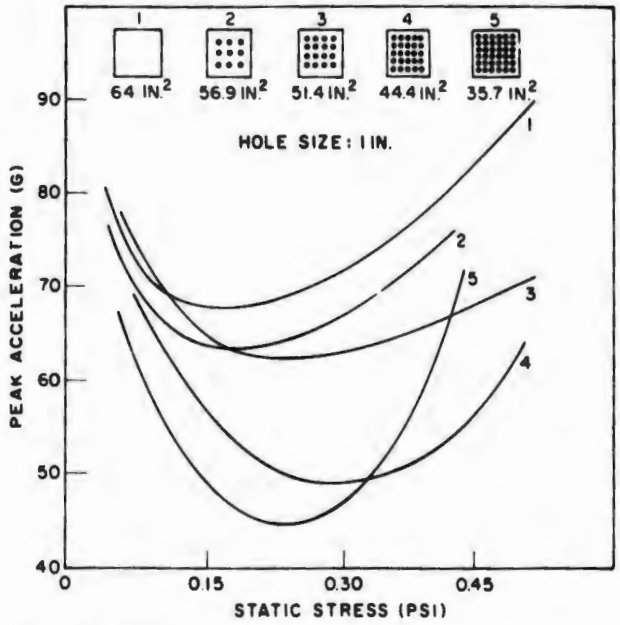

FIG. 4.29. Effect of die-cutting a 2.6-pcf polyurethane foam; h/T is 15 [186].

Table 4.14 summarizes the effects of varying the size of the hole while keeping surface area constant. These results of Goldberg [185, 186] form one more piece of evidence that polyurethane foam is heavily air-damped. Mouri [187] has continued this study with the tentative conclusion that shock absorption increases as hole size decreases. On an 8- by 8-inch sample, 16 holes 1/4-inch in diameter in 1.6-inch centers, produced a 54 percent reduction in peak acceleration, as compared with the unmodified pad.

Mouri [187] also compared the effects of horizontal and vertical holes. Four 1/4-inch horizontal holes in 2.2-pcf polyester urethane on 2-inch centers showed 24 percent reduction in peak acceleration, as compared with the 16-vertical-hole configuration. Apparently, easing passage of air completely out of the sample has beneficial results.

The logical end product of the various hole-cutting techniques is a composite mount with the foam elements in the form of columns. In limited tests, Mouri had anomalous results; he did not recommend further study of this configuration.

TABLE 4.14. EFFECTS OF VARYING HOLE AREA

No. of Holes	*Diameter of Hole* (in.)	*Cushion Area Reduction* (sq in.)	*Total Hole Area* (sq in.)	*Minimum Peak Acceleration* (g)	*Percent Reduction*
0	–	0	0	64.5	–
1	4	12-1/2	25.2	64.0	0.8
3	2-1/4	12-1/2	42.2	63.0	2.3
16	1	12-1/2	100.8	58.0	10.0

Rupture and Dissolution. Goldberg [186] also notes that the cellular structure of polyurethane is a thick ribbed polyhedron forming the lattice structure with thin membranes stretched between the ribs, with more or fewer holes in the membranes. These membranes can be ruptured by passing the foam between rollers. Between 7 and 15 percent reduction of peak acceleration at optimum static stress is reported, without significant change in this optimum.

Material can also be dissolved out of the matrix chemically. Figure 4.30 is indicative of the effects. For short dissolution periods, reduction in peak

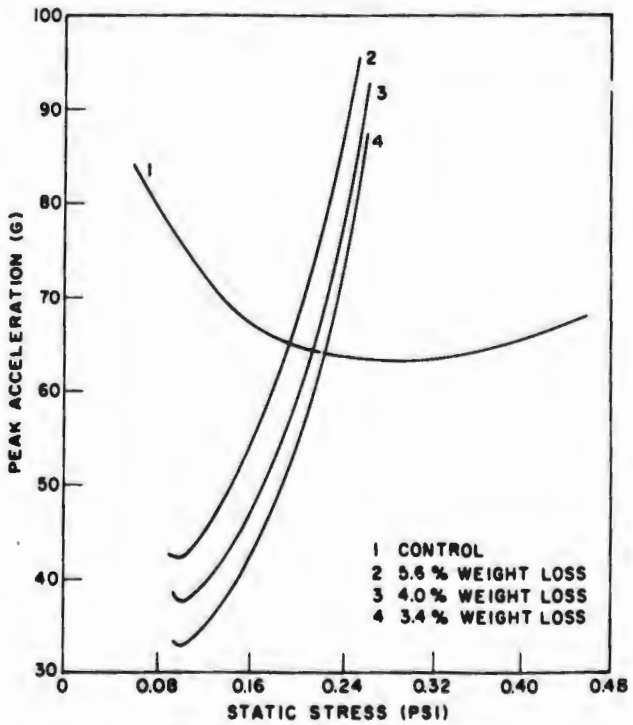

FIG. 4.30. Effect of dissolving membrane on a 2.6-pcf polyurethane foam; h/T is 15 [186].

acceleration on the order of 10 percent is achieved without significant reduction in optimum static stress. This result suggests that the main loss is in membranous structure.

Schmidt and Hoffmann [188], however, attribute dynamic drift under successive impacts not only to the number of impacts but also to the progressive breakdown of thin membranes between structural ribs. This breakdown is apparently caused by compressed air. Figure 4.31 shows stabilization of properties after a number of drops for three different polyurethane foams. Decrease of the specific air resistance Z with increased number of drops is shown in Fig. 4.32.

These factors suggest that the properties of some foams can be stabilized before use, by controlling the specific air resistance.

Most of the foregoing techniques are documented for polyurethane foam but the literature says little about similar treatment of other materials.

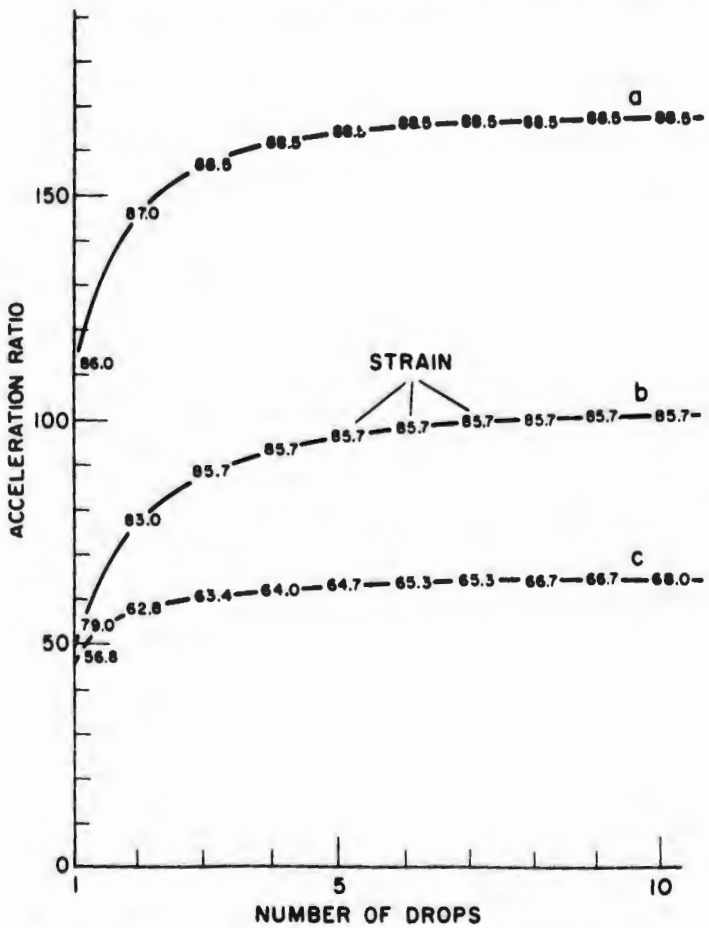

FIG. 4.31. Relation of acceleration to number of impacts for three polyurethane foams: (a) polyether, 40.6 kp/m³, initial $Z = 5.0$ Rayl/cm; (b) polyether, 23.0 kp/m³, initial $Z = 5.0$ Rayl/cm; and (c) polyester 36.7 kp/m³, initial $Z = 6.5$ Rayl/cm (static stress on all was 10.5 p/cm² and h/T was 20). Schmidt and Hoffmann [188].

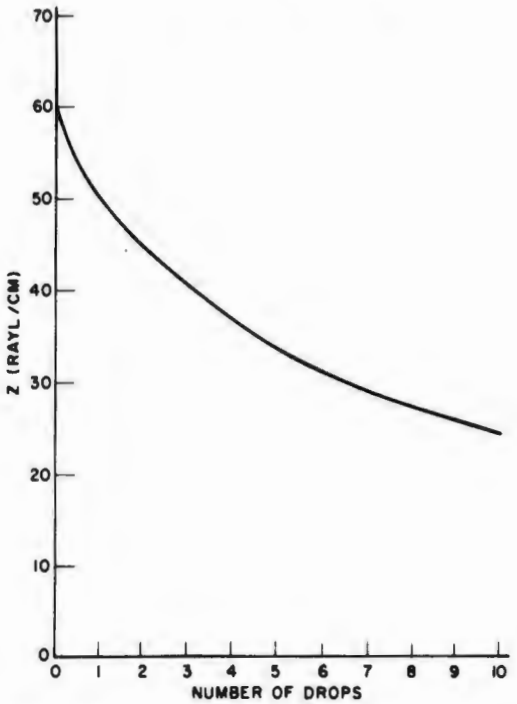

FIG. 4.32. Relation of specific air resistance Z to number of drops for a soft polyurethane foam; static stress was 10 p/cm², h/T was 18.2 and strain was 90 percent on each drop [188].

In any case, it is clear that the designer need not confine himself to the properties of the material in its as-produced form. Whether he exercises any of the suggested options will depend on availability and cost considerations.

Effects of Pre-Compression. In all of the previous discussions of design techniques, it has been assumed that the material becomes unstressed during the course of the free drop. In most packages, however, there is a pad above the cushioned object; the top and bottom pads, at least at the time of packing, are under some preload.

There are indications, at least in theory based on static considerations, that this preload is beneficial to overall performance of the package. Yurenka and Giacobine [136] considered a single pad of an unspecified material and found that 20 percent precompression was optimum. Masel [111], on the other hand, considered an arbitrary material with the same material pressing down from above and found that 10 percent precompression of the lower cushion was optimum. These two findings are not inconsistent.

However, there must remain some doubt concerning the real benefits of precompression, in view of the well known tendency of materials to creep under prolonged static load. In actual design one usually makes some allowance for creep and then closes the container with some convenient amount of preload (largely dictated by the strength of the closure or of the

closer) to assure a snug pack. While our present state of ignorance exists, this practical expedient must be tolerated.

Effect of Side Cushions. When the cushioning surrounds the object, say on all six sides of a cubical container, then the side pads are in shear or are applying frictional constraints, or both. Hohmann, Penzkofer and Heiss [189] packed a wooden block in various cushioning materials inside a corrugated fiberboard box. Comparison of the drop test results in packages with the drop test results on flat pads is shown in Fig. 4.33.

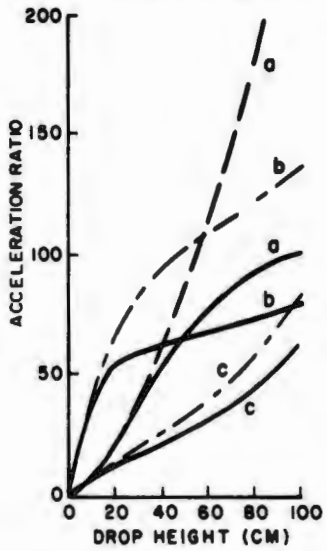

FIG. 4.33. Relation between peak acceleration and drop height for a packaged item and for pads unstressed at instant of impact; dashed lines are for the material itself, and solid lines represent performance in a package: (a) rubberized cocoa fiber, (b) polystyrene foam, and (c) polyurethane foam. Hohmann, *et al.* [189].

Allen [190] compared measured accelerations with predicted values based on flat-pad design data. His results were

Package No.	*Design g*	*Measured g*
1	5	13
2	20	30
3	30	39

Note that as the design acceleration rises, the frictional component remains reasonably constant.

But in any case the method of packaging is shown to have significant effects on actual behavior. This is another way of emphasizing the necessity of testing.

Composite Structures. Five particular developments are noteworthy:

1. Pearsons and Ungar [191] propose a cushion assembly (that can be produced at will and to any desired configuration) consisting of buckling levers and collapsing columns of foam-cushioning material. This structure approximates a constant restoring force.
2. Jacobsen [192] proposes pads, or mounts, with Teflon rods imbedded in a silicone rubber matrix. The rods enhance the damping characteristics of the material.

3. Hardigg [159] increases the static-load-bearing capacity of conventional polyurethane foam by imbedding hollow rubber tubing in the material matrix. When the stress exceeds some predetermined value, the tube column buckles; the foam then takes over as the primary cushioning material.

4. Payne [193] shows a corrugated rubber mat with J_0 as low as 2.1.

5. Bache [194] describes the design of a torsion bar unit which has become popular in the United Kingdom.

4.6.1.2. *Effects of Outer Container.* We would expect that a cushion will behave one way in an actual container and another way when tested as a flat pad. Actually, there have been very few direct comparisons in this area, the assumption being that flat-pad data result in conservative designs.

TABLE 4.15. TYPICAL EFFECT OF OUTER CONTAINER ON PEAK ACCELERATION

	Static Stress (psi)	*Thickness* (in.)	*D-1596 g's* (avg)[a]	*Package g's* (avg)[a]
Corrugated board containers				
48-in. drop height	0.76	4	56	45
30-in. drop height	0.19	1-3/4	90	72
	0.19	2-3/4	66	61
	0.19	5-1/4	40	36
	0.18	1-1/2	108	84
	0.18	2-1/2	70	61
	0.18	5	42	41
Wood crate + corrugated-board container (30-in. drop height only)				
At room temperature	0.64	4-3/4	32	29
	0.64	5	30	27
	0.64	5	30	24
	0.64	5-1/2	28	25
	0.64	5-3/4	27	23
	0.64	7-1/8	21	21
	0.64	7-7/8	20	22
At +150°F	0.64	5-1/2	28	23
At −40°F	0.64	4-3/4	32	30
	0.64	5-1/8	30	26
	0.64	7-1/8	22	21
	0.64	7-1/4	22	21
Small steel cylindrical container (30-in. drop height only)				
	0.72	3	49	47
	0.52	3	50	55
	0.72	4	36	33
	0.52	4	38	45
	0.72	5	31	29
	0.52	5	33	41
	0.72	6	26	24
	0.52	6	29	31

[a]Rounded to the nearest whole g.

Grabowski [154], using foamed polystyrene and flat drops, developed the data shown in Table 4.15. In obtaining these data, Grabowski did not fill the bottom of the container with the material. Stern [167] has shown the effects of various containers on the performance of a rubberized hair and a polyurethane foam, Figs. 4.34 and 4.35. In this case, it was not clear from the reference whether the cushion abutted against the side walls of the container.

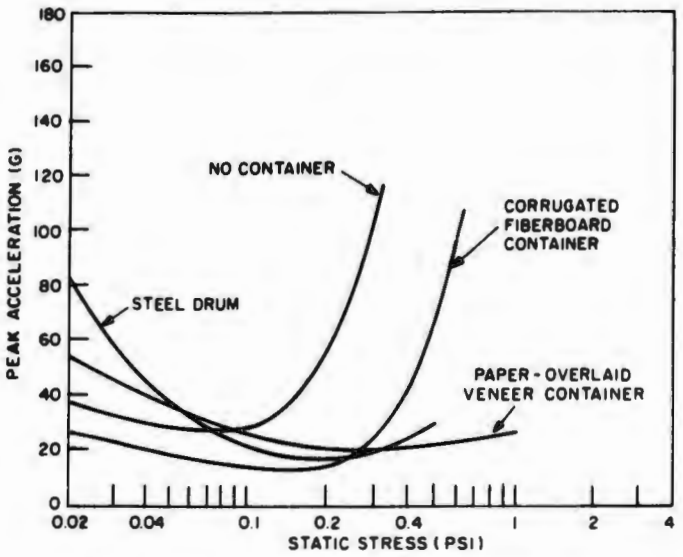

FIG. 4.34. Effects of various kinds of containers on rubberized hair performance [167].

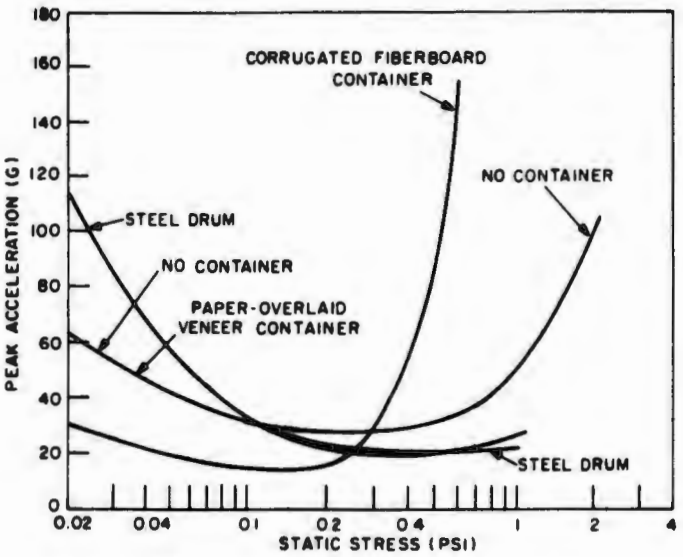

FIG. 4.35. Effects of various kinds of containers on urethane foam performance [167].

Blake [182] tested a variety of materials contained in corrugated fiberboard boxes. In all cases the cushion was on the bottom only of the test load, supported by the double thickness of corrugated board representing the flaps of a square based container. When the 8- by 8-inch pads were placed in 8- by 8-inch boxes, peak accelerations averaged 50 percent above design expectancy. When the same cushions were placed in similar boxes but with inside dimensions 8-1/4 by 8-1/4 inches, accelerations at about 80 to 90 percent of expectancy were measured. Thus, for air-damped materials, even the presence of a fairly flexible fiberboard box can affect the results.

4.6.1.3. *Non-Flat Drops.* The data discussed so far were all obtained in simulated flat-drop conditions. Apart from the fact that a true flat drop is not easy to arrange, container tests are more frequently run as corner or edge drops, or rotational drops.

Gammell and Gretz [195] compared the effects of corner and edge drops to flat drops in a report that has not apparently been added to. They dropped a box containing a wood block surrounded by a cushion system and measured the accelerations in three mutually perpendicular axes, recording the resultant peak acceleration.

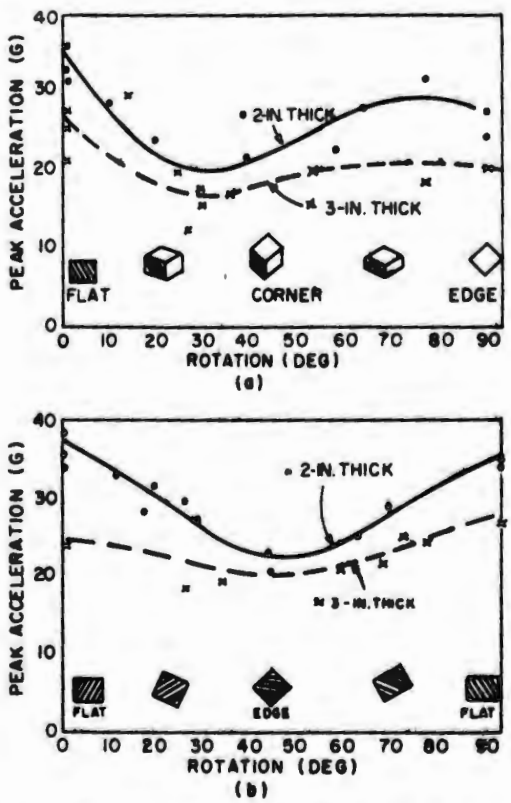

FIG. 4.36. Effect of container orientation on peak acceleration: (a) sequence is flat to corner to edge, and (b) sequence is flat to edge to flat. Gammell and Gretz [195].

The first series of tests began with a flat drop. Subsequent drops were made with varying orientation until a true corner drop was reached. The angle of impact was then varied until an edge drop was attained. A second series began with a flat drop, continued to an edge, and concluded with a flat drop on a side normal to the original side. The results are summarized in Fig. 4.36.

Based on the somewhat limited results obtained, the Cushioning Handbook [148] recommends considering corner-drop cushioning the same as flat cushioning except when working with the projected area of the cushioned object suspended in its dropping position. For a rectangular parallelepiped-shaped object, the projected area is

$$A_p = \frac{3(LWD)}{\sqrt{L^2 + W^2 + D^2}}. \tag{4.57}$$

Writing an analytical solution to the problem of a corner or edge drop can be very complicated. In fact, as far as is known, a complete set of equations of motion for the corner drop has never been attempted. Chase and Vigness [196], however, did consider an edge drop of a system symmetrical about the xy-plane. The essential geometry is shown in Fig. 4.37. They have shown that the equations of motion prevailing while the edge is in contact with the floor can be written as

$$\begin{aligned}
&\ddot{\theta}_2 + \ddot{\theta}_1 + \frac{1}{I_1}\frac{\partial U}{\partial \theta} = 0,\\
&\ddot{a}' + b_1\ddot{\theta}_1 - 2\dot{\theta}_1\dot{\theta}_2 - a_1\dot{\theta}_2^2 + g\sin\theta_1 + \frac{1}{m_1}\frac{\partial U}{\partial a'} = 0,\\
&\ddot{b}' + a_1\ddot{\theta}_1 + 2\dot{\theta}_1\dot{\theta}_2 - b_1\theta_2^2 + g\cos\theta_1 + \frac{1}{m_1}\frac{\partial U}{\partial b'} = 0,\\
&C_1\ddot{\theta}_1 + a_1\ddot{b}' - b_1\ddot{a}' + 2(a_1\dot{a}' + b_1\dot{b}')\dot{\theta}_1 + g\left(\frac{m_2}{m_1}a_2 + a_1\right)\cos\theta_1\\
&\qquad - g\left(\frac{m_2}{m_1}b_2 + b_1\right)\sin\theta_1 = 0,
\end{aligned} \tag{4.58}$$

where m_1 = mass of object,

m_2 = mass of container,

U = energy stored in the springs due to deflection from equilibrium position,

$$C_1 = \frac{m_2}{m_1}\left(\frac{I_2}{m_2} + a_1^2 + b_1^2\right) + \frac{I_1}{m_1} + a_1^2 + b_1^2,$$

I_1 = moment of inertia of mass m_1 about its center of gravity (c.g.) in the xy plane, and

I_2 = moment of inertia of mass m_2 about its center of gravity (c.g.) in the xy-plane.

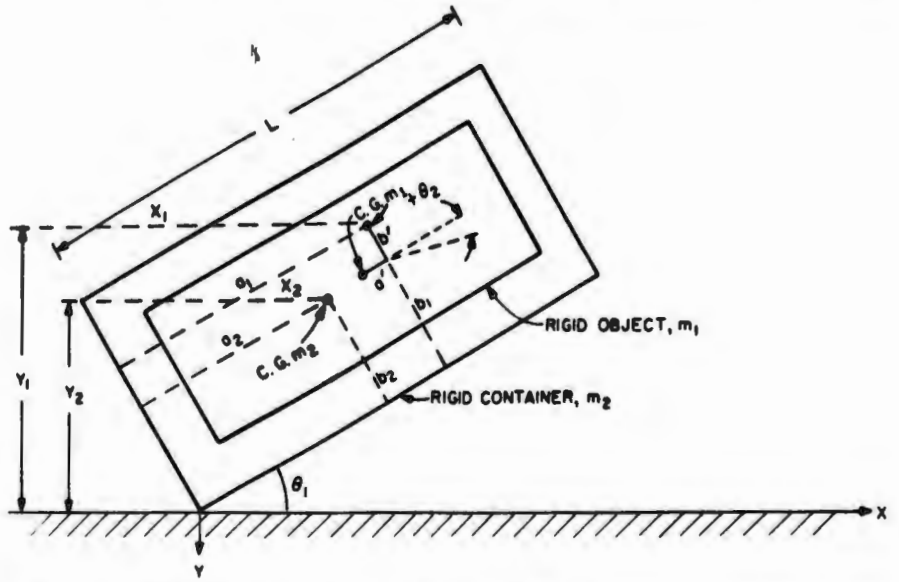

FIG. 4.37. Edgewise drop test, after impact with floor; initial position of c.g. of m_1 is displaced downward by distance b' and to left by distance a'.

The initial boundary conditions depend on the translational and rotational velocity of the package at impact. Assume that the item is at its equilibrium position in the container and that their relative motions are zero. Then, just before the impact,

$$a' = b' = \theta_2 = \dot{a}' = \dot{b}' = \dot{\theta}_2 = 0. \tag{4.59}$$

If the drop is arranged in such a fashion that the system c.g. is directly above the impact edge at the time of striking (as normally attempted in this kind of test), then, at the instant of impact,

$$\theta_2 = \dot{x} = 0. \tag{4.60}$$

If minor differences between heights of the item c.g., container c.g. and system c.g. are ignored, the velocities of the item c.g. are given by

$$\begin{aligned} \dot{\theta}_1 &= \dot{\theta}_2 \\ \dot{a}' &= \sqrt{2gh}\sin\theta_1 + b_1\dot{\theta}_1. \end{aligned} \tag{4.61}$$

Chase and Vigness then proceeded to trace the behavior of the package through direct rebound, toppling over onto the flat side, and combinations of the two motions. Because of dissipative forces in the system, the second impact will usually be less severe, in terms of peak acceleration, than the first; therefore, the analysis is stopped with the first impact. As for toppling over, the equations of motion are similar (with different initial conditions) to those used in the rotational drop test. Since this test will be discussed next, the analysis is not given here.

Though equations (4.58) are complicated, they can be solved provided that suitable expressions for U can be substituted. Such substitution requires knowledge of the dynamic-load-deflection characteristics of the isolating medium and knowledge of the geometry of placement of the mounts or cushion pads. Note that the force-deflection curve need not be expressed as a mathematical function but can be fed into the computer by any curve-following device, together with the other factors involved in the equations, and solved by analog or digital methods. Evidently, however, a concept of the design should exist before the solutions are begun.

Another common form of test involves a rotational drop, usually used on longer containers (say 5 feet long, or more). The essential geometry of this test is shown in Fig. 4.38. One end of the container is supported on a block of height h_2 (usually a nominal 6 by 6 inches, so that h_2 is approximately 5 inches). The other end of the container is raised to a height h_1 and then allowed to fall freely. The problem is to limit the acceleration at some point on the packaged item away from the pivot point, O. This point is identified in the figure as having the coordinates $a_1 b_1$.

Upon impact the container will cease its motion (at least for a brief instant) but the cushioned item will tend to continue its motion, resisted by whatever elastic medium may be placed between the item and the container. In the xy-plane this motion will consist of a rotation, θ_2, of the entire unit in the cushion, a displacement in the x-direction, and a displacement in the y-direction. Similar displacements in the yz-plane give a minimum of six degrees of freedom.

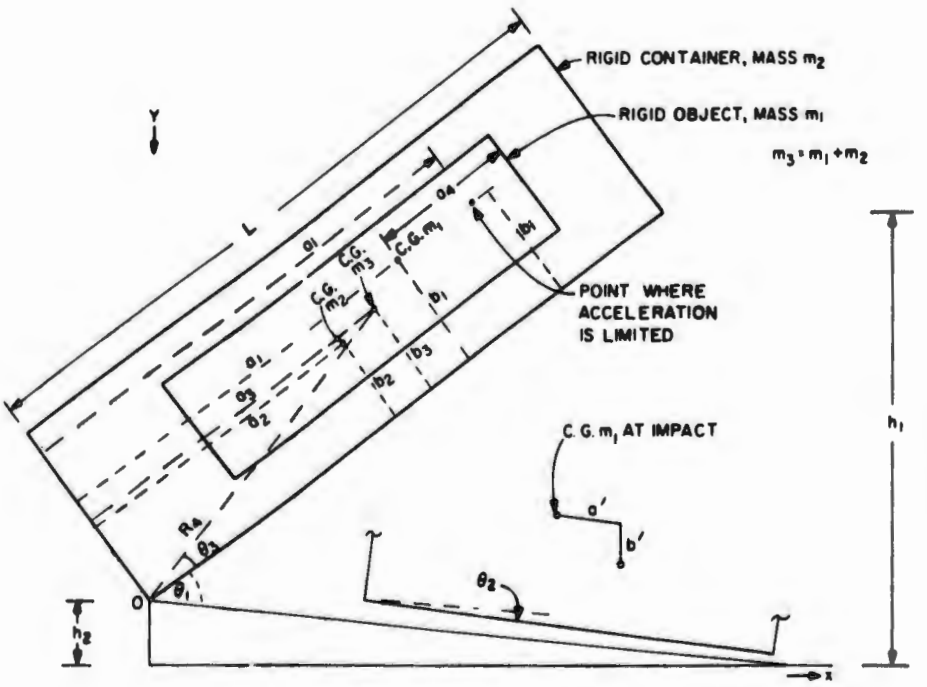

FIG. 4.38. Rotational drop test.

In most practical cases, the designer is concerned only with motions in the xy-plane, and the analysis is somewhat simplified. Such analysis is permissible provided that the complete system is symmetrical about the xy-plane passing through the center of gravity of the item, the center of gravity of the container, and (as a result) through the center of gravity of the combined system. This is the two-dimensional problem shown in Fig. 4.38.

The system response is a function of the angular velocity attained at the moment of impact after passing through angle θ_1. Equating the kinetic energy of the motion with the potential energy of the position prior to drop (and ignoring pre-impact motion in the cushioning medium as in the flat drop), gives

$$\dot{\theta}_1 = \sqrt{\frac{2W_3h}{I_0}} = \sqrt{\frac{2gh}{R_3^2 + R_4^2}}, \tag{4.62}$$

where I_0 = moment of inertia of the complete system about the pivot point, O,

h = height of drop of the center of gravity of combined mass m_3,

W_3 = weight of the combined mass = m_3g

$R_3 = \sqrt{\frac{I_3g}{W_3}}$, the radius of gyration about system center of gravity,

$R_4 = \sqrt{a_3^2 + b_3^2}$, the radius of gyration about point O, and

I_3 = moment of inertia of the complete system about its center of gravity.

Solution of Eq. (4.62) requires knowledge of a_3, b_3, and W_3, none of which the designer has at the beginning of the work. It is therefore usual to add allowances for these quantities as a preliminary estimate (allowances based on experience). Although the design must be approached by successive approximations, experience has shown that errors of several inches in b_3 have little effect on the result. The value of a_3 can be approximated by considering the end-impact condition first. It takes a fairly large error in W_3 to affect significantly the value of R_3^2 which, in any case, is usually considerably smaller than R_4^2. Hence, although successive approximations are required, their number is not great.

The value of the height of drop h of the center of gravity of the combined mass is determined by the geometry of the container system and the drop conditions. Using the inverse trigonometric identities involved we obtain, for the general case,

$$h = b_3\left[\frac{h_1a_3}{L_1b_3} + \sqrt{1 - \left(\frac{h_1 - h_2}{L_1}\right)^2} - \sqrt{1 \quad \left(\frac{h_2}{L_1}\right)^2}\right]. \tag{4.63}$$

In the special case where h_2 is zero,

$$h = b_3\left[\frac{h_1a_3}{L_1b_3} + \sqrt{1 - \left(\frac{h_1}{L_1}\right)} - 1\right]. \tag{4.64}$$

Where h_1/L_1 is small (*e.g.*, 0.3 or less) the approximate formula

$$h = a_3 \frac{h_1}{L_1} \tag{4.65}$$

is satisfactory for preliminary design. In the further special case where the center of gravity is vertically above the pivot point, O, as in a tip-over test of a tall container, then

$$h = R_4 - b_3 \tag{4.66}$$

applies.

Assume that during the course of rotational motion the container remains constantly in contact with the pivot point O, and that it lands onto a perfectly rough surface—so that there is no sliding in the x or z direction—and consider the period when the container is in contact with the floor, *i.e.*, when $\theta_1 = 0$. Chase and Vigness [196] have shown that the general equations of motion during this interval, provided that the packaged object is in its equilibrium position at the instant of impact, are

$$\begin{aligned} \ddot{\theta}_2 + \frac{1}{I_1}\frac{\partial U}{\partial \theta_2} &= 0, \\ \ddot{a}' + \frac{1}{m_1}\frac{\partial U}{\partial a'} &= 0, \\ \ddot{b}' + \frac{1}{m_1}\frac{\partial U}{\partial b'} &= 0. \end{aligned} \tag{4.67}$$

The initial conditions are

$$\begin{aligned} a' = b' = \theta_2 &= 0, \\ \dot{a}' &= b_1 \dot{\theta}_1, \\ \dot{b}' &= a_1 \dot{\theta}_1, \end{aligned} \tag{4.68}$$

and $\dot{\theta}_1$ is given by one of Eqs. (4.63) through (4.66). Equations (4.68) will no longer hold if the reaction of m_1 causes the container to bounce backwards, rotating around pivot point O, or to rotate about the impact edge. The former event occurs when

$$m_1 \left(a_1 \ddot{b}' + \frac{I_1}{m_1} \ddot{\theta}_2 - b_1 \ddot{a}' \right) + (m_1 a_1 + m_2 a_2) g < 0; \tag{4.69}$$

the latter event occurs when

$$m_1 \left[(a_1 - L_1) \ddot{b}' + \frac{I_1}{m_1} \ddot{\theta}_2 - b_1 \ddot{a}' \right] + [m_1(a_1 - L_1) + m_2 (a_2 - L_1)] g > 0.$$

When h_2 is zero, the container may land flat and the reaction of m_1 may cause a simple bounce without noticeable rotation around either edge. This will occur when

$$m_1 \ddot{b}' + (m_1 + m_2) g < 0. \tag{4.70}$$

Equations (4.69) and (4.70) thus make a suitable end to analysis.

When appropriate substitutions are made for U—even for linear springs—it is found that the three equations are not independent but, rather, are coupled and require simultaneous solution. The linear spring case has been extensively analyzed by Ayre and Abrams [197]. The analysis has been repeated by Blake [198] in his excellent review of basic vibration theory. The complete analysis will not be given here. For clarity, however, it is worthwhile considering a particular system of linear springs as shown in Fig. 4.39. These linear springs operate in tension and compression. The equations of motion for this system are

$$\begin{aligned} m_1\,\ddot{x} + K_x x - K_x R_y \theta_2 &= 0, \\ m_1\,\ddot{y} + K_y y + K_y R_x \theta_2 &= m_1 g \\ I_1 \ddot{\theta}_2 + K_\theta \theta_2 - K_x R_y x + K_y R_x y &= 0, \end{aligned} \tag{4.71}$$

where the spring and coupling constants are defined in Table 4.16. In determining the moments, $k_i s_i$, it is simple to keep the signs straight by assigning positive and negative directions to the x- and y-axes with respect to the center of gravity of m_1 and then following this sign convention.

It can be seen that Eqs. (4.71) are mutually dependent because of the coupling constants R_x and R_y. Partial decoupling occurs when either coupling constant can be made zero, and complete decoupling occurs when both constants are zero. The condition for a zero coupling constant is obviously that the algebraic sum of the pertinent moments be zero. The easiest way to reach this goal, if the configuration of the item permits, is to make the pertinent spring rates equal and to space them equidistantly about the pertinent axes through the center of gravity. Other techniques are possible, but normal design practice should start with this arrangement.

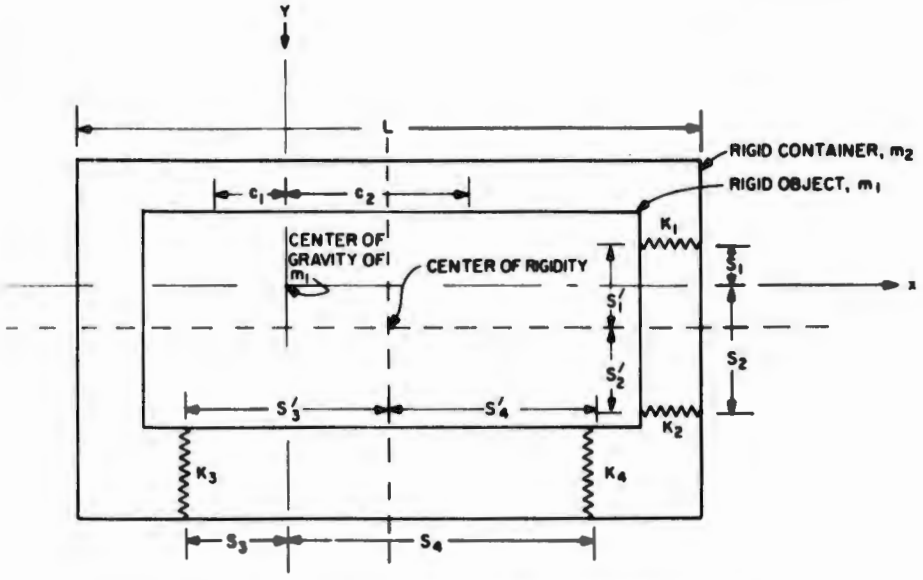

FIG. 4.39. A particular container with linear springs.

TABLE 4.16. SPRING AND COUPLING CONSTANTS FOR EQUATIONS (4.71), (4.76), AND (4.77)

Constant	*General Value*	*Particular Value for Fig. 4.39*
K_x	$\Sigma_x k_i$	$k_1 + k_2$
K_y	$\Sigma_y k_i$	$k_3 + k_4$
R_x	$\dfrac{\Sigma_y k_i s_i}{K_y}$	
R_y	$\dfrac{\Sigma_x k_i s_i}{K_x}$	
$\Sigma_y k_i s_i$		$k_3 s_3 - k_4 s_4$
$\Sigma_x k_i s_i$		$k_2 s_2 - k_1 s_1$
K_θ	$\Sigma k_i s_i^2$	$k_1 s_1^2 + k_2 s_2^2 + k_3 s_3^2 + k_4 s_4^2$

The basic schema used in deriving K_x, K_y, and K_θ can be generalized to a very large number of individual springs. Going to the limit would produce a continuous linear cushion. For analytical purposes all springs could be lumped into a single spring whose line of action would be at the centroid of the springs located on either side of the pertinent axis. If the cushion is, for example, continuous under the object, then the centroid will be found at half the distance from the pertinent axis to the end of the object. Referring to Fig. 4.39, we would have $s_3 = c_1$, and $s_4 = c_2$.

However, the designer still has the problem of deciding what spring rates and spacings to select in order to achieve a given design goal. One of the first to publish a designer's solution was Goodill [199]. Unfortunately, his method requires an arbitrary assumption concerning deflections (or accelerations) due to translational and rotational motion of the item while the container is in contact with the ground. It has been shown [135] that such an arbitrary division is unnecessary, and the reasoning—which can be fairly general—is worth repeating.

Referring to Fig. 4.38, suppose that it is desired to limit peak acceleration normal to the base of the container to some value, G_m, at the impact end of the cushioned object so that $a_i = a_1 + a_4$. The stopping distance at this point must be controlled, thus determining the total deflection d_T required. With neglibible error (even by conservative estimation) this stopping distance is given [135] by

$$d_T = \frac{2h}{G_m} \cdot \frac{a_i^2}{R_4^2}, \tag{4.72}$$

where R_4 = radius of gyration of total mass about pivot point, O. As before, useful preliminary approximations can be made.

Consider the ratio, M, of total deflection d_T to deflection due to translation alone, d_t. This ratio [135] is

$$M = 1 + \frac{d_\theta}{d_T} = 1 + a_4 \sec \theta_1 \sqrt{\frac{N_\theta K_y}{N_t K_\theta}} = 1 + \frac{a_4 R_1}{a_1} \sqrt{\frac{K_y}{K_\theta}}, \tag{4.73}$$

where d_θ = deflection due to rotation,

N_θ = rotational energy, and

N_t = translational energy.

In the very special case where threefold symmetry is achieved by using shear mounts equally spaced along the x-axis, Eq. (4.73) becomes

$$M = 1 + \frac{a_4 R_1}{a_1 s_3}. \tag{4.74}$$

This special case teaches that there are certain practical limits to the value of M. Thus s_3 will rarely exceed a_4 because excessive container volume would ensue. Similarly, experience indicates that rotational natural frequency becomes very low when $s_3 < R_1/3$. Hence, the practical designer's limits on the value of M for a specific object are

$$1 + \frac{r_1}{a_1} \leqslant M \leqslant 1 + 3\frac{a_4}{a_1}. \tag{4.75}$$

These limits may be expected to remain reasonably valid regardless of the types of symmetry prevailing in the final design. An even rougher approximation of the value of M is to state that its most probable value lies between 1+ and 4.0. Note that the limits of M in Eq. (4.75) are independent of drop height, spring rate, or allowable acceleration.

Mustin [135] further extended the work to isolators exhibiting tangent elasticity, but the technique obviously will fail to predict with accuracy the response of strain-rate-sensitive cushions since strain rate varies continuously with distance from pivot point O.

By ringing appropriate changes on Eq. (4.73), it is possible to select from currently available mounts and to fix the spacing for useful results. Then, solution of Eq. (4.71) for final check of the design is straightforward.

The specific design techniques suggested by Ayre and Abrams [197] and Mustin [135] both assume linear mounts which are undamped or in which damping is so small as to be negligible. Ayre and Abrams did extend their work to undamped cubic elasticity [200]. Tsui and Stern [201], however, show how the approach can be expanded to cover damping and nonlinearities. The equations of motion, analogous to Eqs. (4.71) are

$$\begin{aligned}
&m_1 \ddot{x} + C_x \dot{x} + K_x x - C_x R'_y \dot{\theta}_2 - K_x R_y \theta_2 = 0 \\
&m_1 \ddot{y} + C_y \dot{y} + K_y y + C_y R'_x \dot{\theta}_2 + K_y R_x \theta_2 = m_1 g \\
&I_1 \ddot{\theta}_2 + C_\theta \dot{\theta}_2 + C_y R'_x \dot{y} + C_x R'_y \dot{x} + K_\theta \theta - K_x R_y x + K_y R_x y = 0,
\end{aligned} \tag{4.76}$$

where c_i = coefficient of viscous damping in the ith mount,

$C_x = \Sigma_x c_i$,

$C_y = \Sigma_y c_i$,

$C_\theta = \Sigma c_i s_i^2$,

$$R'_y = \frac{\Sigma_x C_i s_i}{C_x},$$

$$R'_x = \frac{\Sigma_y C_i s_i}{C_y},$$

and the other constants are defined in Table 4.16.

In deriving Eqs. (4.76) it was assumed that each mount had its own damping, *i.e.* was a Voigt solid. The equations could be generalized to a continuous series of Voigt elements without inherent difficulty. Where the spring is nonlinear, the equations are not so straightforward but may be written in the form

$$\begin{aligned} &m_1 \ddot{x} + C_x \dot{x} - C_x R'_y \dot{\theta}_2 + \Sigma F_i(x_i) = 0, \\ &m_1 \ddot{y} + C_y \dot{y} + C_y R'_x \dot{\theta}_2 + \Sigma F_i(y_i) = m_1 g, \\ &I_1 \ddot{\theta}_2 + C_\theta \dot{\theta}_2 + C_y R'_x \dot{y} + C_x R'_y \dot{x} - \Sigma F'_i(x_i) + \Sigma F'_i(y_i) = 0, \end{aligned} \tag{4.77}$$

where $F_i(x_i)$ = force in the ith mount due to displacement x_i,

$F_i(y_i)$ = force in the ith mount due to displacement y_i,

$\Sigma F'_i(x_i)$ = algebraic sum of each force in each mount resisting rotation by displacement x_i, and

$\Sigma F'_i(y_i)$ = algebraic sum of each force in each mount resisting rotation by displacement y_i.

Tsui and Stern stated that there seems to be no acceptable approach to the analytical solution of the general problem except when the vertical mount spring spacing equals the object's own radius of gyration and the horizontal mounts are along the x-axis.

However, computer solutions are perfectly feasible, either digital (using finite differences) or analog. The authors showed a useful analog computer and give results for a particular example.

If Eqs. (4.77) are going to be solved by a computer, they can be further generalized to account for nonlinear damping terms or to use any mathematical model of behavior desired, including a generalized Maxwell or Voigt solid as a diffuse cushion. Such procedures would be possible should suitable models of specific cushioning materials become available, but the designer would still have to narrow his field of choice to specific materials.

Mustin's [171] simplified approach to the flat-drop problem can be adapted to this preliminary-choice dilemma by rewriting Eq. (4.62) in terms of the equivalent height of drop h_i of any point a_i along the item, *i.e.*,

$$h_i = \frac{a_i^2}{2g} \dot{\theta}_1 = \frac{a_i^2 h}{R_4^2}. \tag{4.78}$$

The appropriate material design curves can now be entered for material choice. This will probably be dictated by thickness and the static stress likely to occur. This gives the designer a concrete concept for further analysis or testing.

4.6.1.4. *Air Bags.* Performance of large air bags of U.S. and U.K. design is discussed by Thompson and Ripperger [202]. These bags inflate themselves during descent and compress themselves during impact. Special blow-off patches are provided so that, when air reaches a predetermined pressure, escape is allowed; this reduces rebound energy. A straightforward design procedure is given by Browning [203].

The two designs discussed in the previous paragraph are made from rubber or synthetic rubber. Matlock and Thompson [204] report some preliminary results on an air bag, fabricated from paper with plywood facing plates, developed by Hardigg. A weak spring opens the bag during fall. During impact, small openings permit escape of air at varying velocities as the shape of the opening varies with distortion of the bags. These were not as efficient as the rubber air bags. It was suggested that light-weight blow-off patches might improve their performance but further test data are not available.

Den Hartog, Newland, and Flory [205] investigated problems of shock, isolating a very large structure; large corrugated metal bellows gave promising results. Some design procedures using such bellows were suggested.

4.6.2. Quasi-Resilient Materials. Quasi-resilient materials were defined in the introduction of section 4.6 as materials that remain substantially resilient under small distortions but do not completely recover under large distortions. Materials are classified as quasi-resilient or nonresilient according to the designer's intended use of them.

Two broad classes of material are classified as quasi-resilient in this monograph: corrugated fiberboard structures and plastic foams, usually of higher density than those foams discussed in section 4.6.1. They have nonresilient as well as resilient properties; both will be discussed in this sub-section.

There are many other quasi-resilient materials but we lack data on most of them. Popcorn was investigated by Stern but found unsuitable for military packaging [206].

4.6.2.1. *Corrugated Fiberboard.* Corrugated fiberboard is far and away the most used of cushion materials. It is also the most misunderstood by engineers. They seem to dismiss it, believing that it is only good for one shock, or on the grounds that anything so familiar must be beneath contempt.

This paradox of utility *versus* engineering interest has been exhibited many times; it is something that positively cries out for further investigation. It suggests, also, that most items are much stronger than we care to admit; our general ignorance, added to our particular ignorance about corrugated fiberboard, makes us overly protective. In this monograph, we can but show what information is available.

One possible reason that we know so little about corrugated fiberboard as a cushion is its versatility. It can readily be creased and folded into many shapes. Figure 4.40 shows 59 reasonably common configurations for corrugated inner packing pieces. Most box designers select a configuration and a material on the basis of experience; sometimes this is assisted by performance tests of the complete package. The examples in the figure show that the material can be loaded not only in compression normal to the respective faces, but also as plates, columns, and beams. The available data are mostly limited to use of the material as plain pads (singly and in stacks) and as partitions.

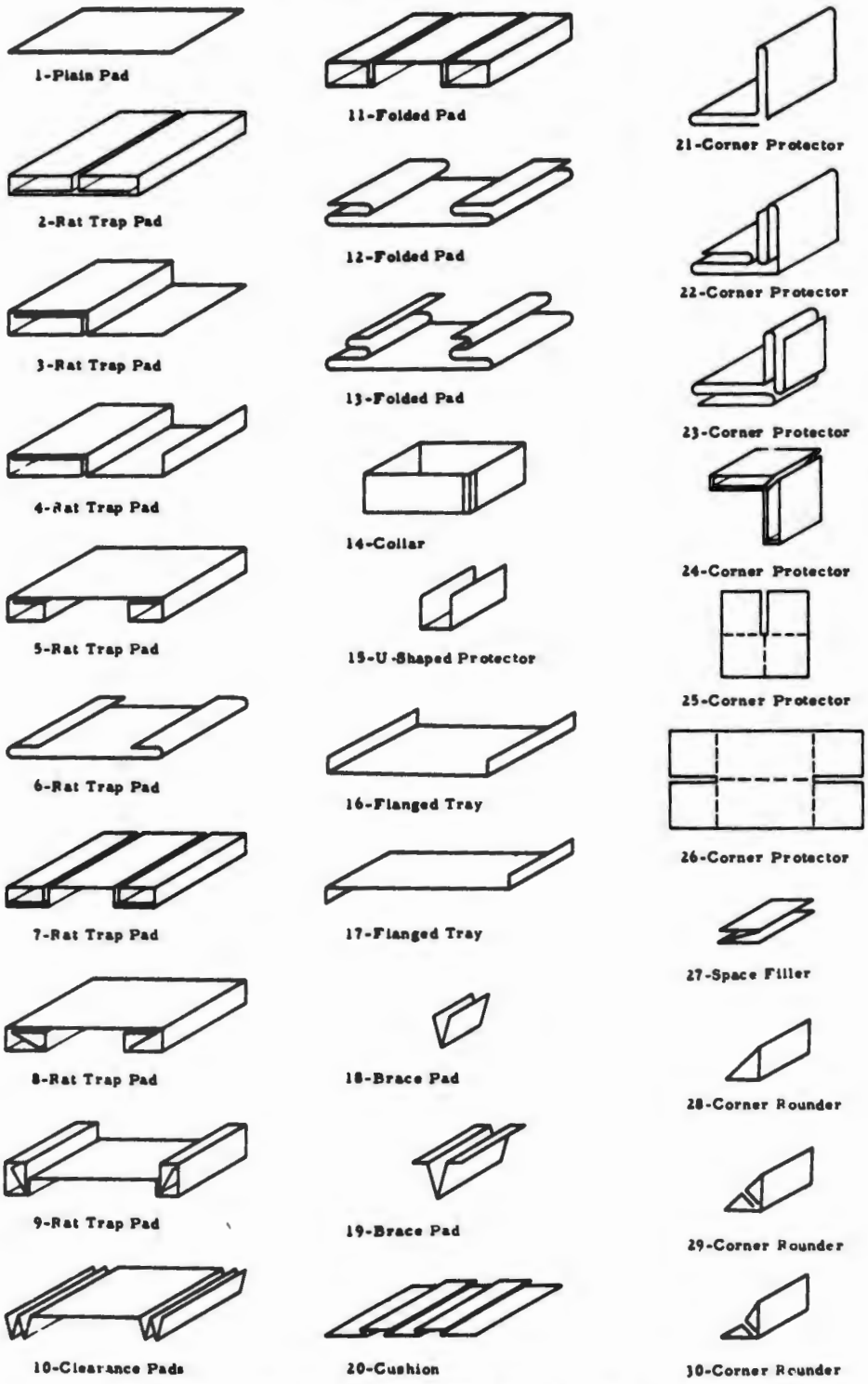

FIG. 4.40. Some interior packing pieces.

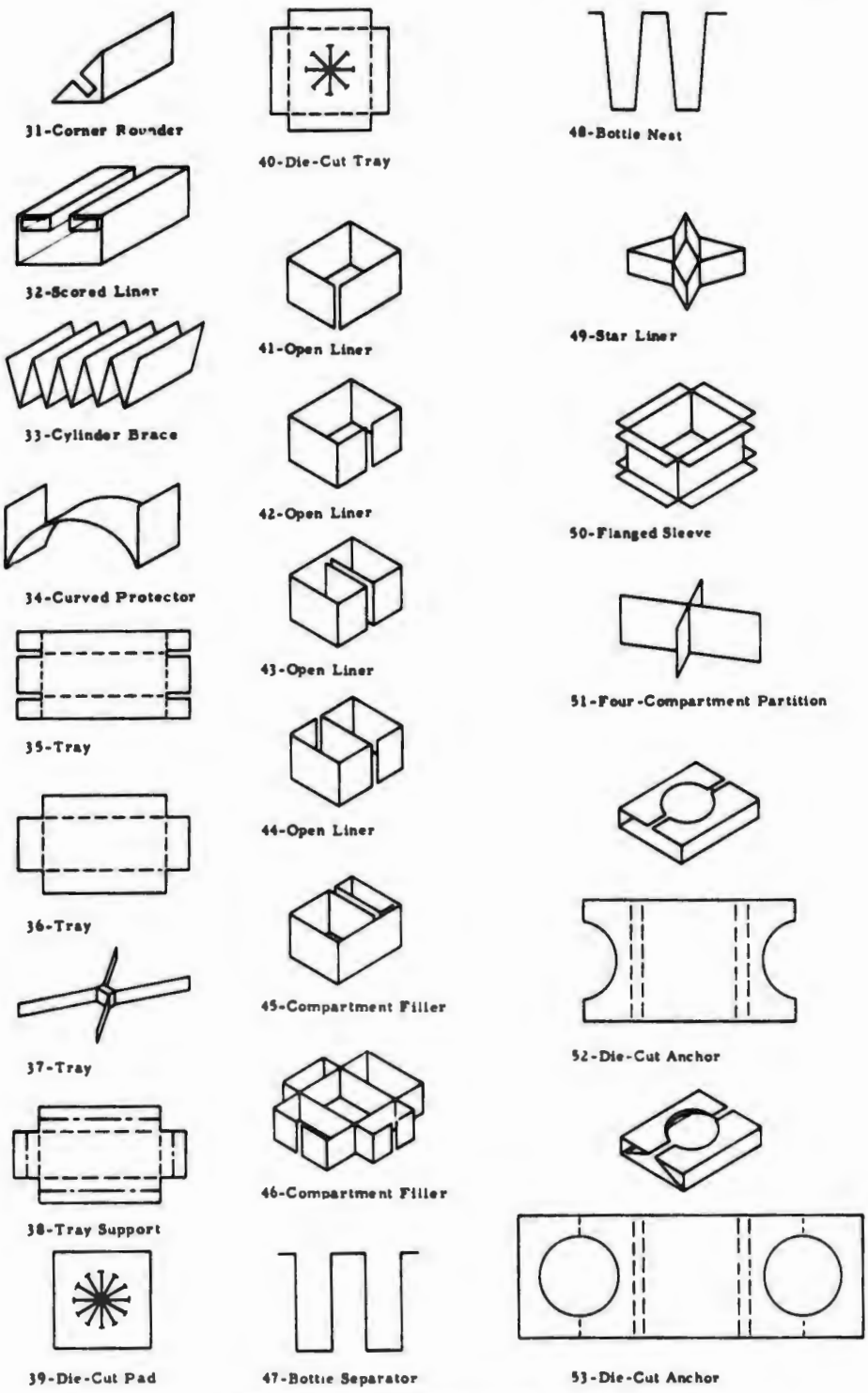

FIG. 4.40 (*Continued*). Some interior packing pieces.

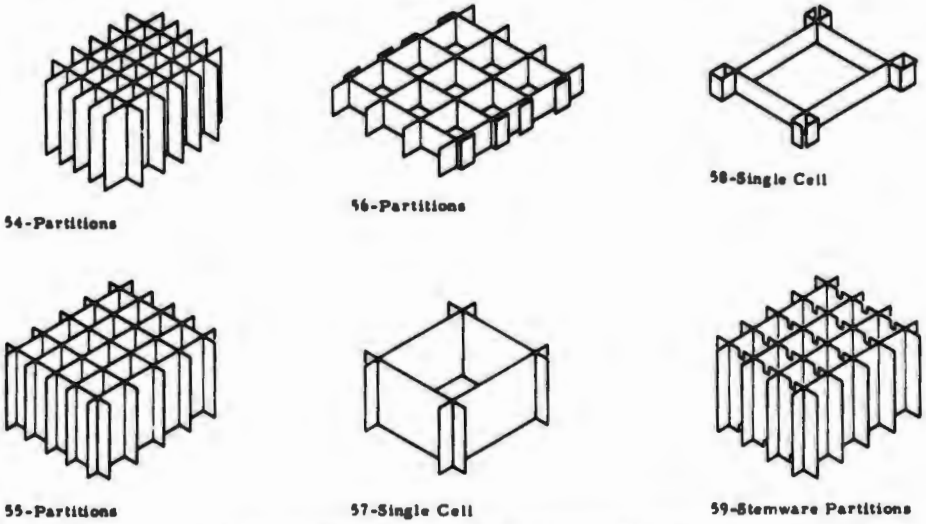

FIG. 4.40 (*Continued*). Some interior packing pieces.

The material itself is regularly available in many configurations and strengths. General configurations available are summarized in Fig. 4.41. The corrugations themselves can be made in four different styles, three of which (A-, B-, and C-flute) are shown in Fig. 4.42 with the dimensions conforming to United States practice. The fourth style, E-flute is relatively recent and there do not appear to be any published data concerning its use as a cushion.

The corrugating medium can be fabricated from several different kinds of paper, with or without resin additives for wet strength. In most commercial corrugated boards in the United States the medium must be at least 0.009 inch thick (9-point board), while the medium for V- and W-Board used by the services is stipulated as being 10-point. There are some commercially available boards with even thicker corrugating media, but the usual practical upper limit is about 12-point material.

In addition, when the material is required to act as a column or a plate supported at the edges, the many variations possible in facing materials and strengths add more complications; they will not be reviewed here.

A compressive load normal to the faces of a single sheet of double-faced corrugated fiberboard will evidently cause deformation of the arches; then, at some point, these arches will collapse as the result of elastic instability. A typical stress-strain curve for corrugated fiberboard is shown in Fig. 4.43. Almost always the materials show a primary peak; also a secondary peak which characterizes an arch beginning to assume a new shape and then collapsing again. Below 35 percent strain, the curve is very nearly linear. The apex of the first peak is called the flat-crush value. The flat-crush test is frequently run in the corrugated box trade as a measure of the quality with which arches are formed and with which liners are glued to the corrugating medium. Values will vary with the character of the corrugating medium, but certain minimum expectancies from a well-made piece of board

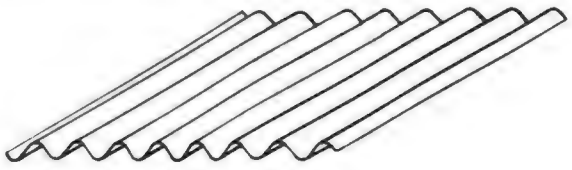

UNLINED

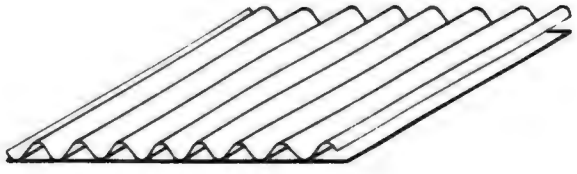

SINGLE-FACED

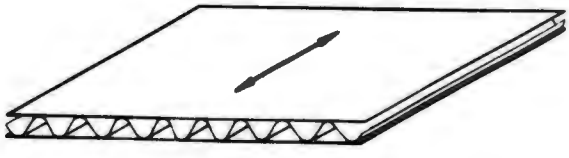

DOUBLE-FACED (SINGLE WALL)

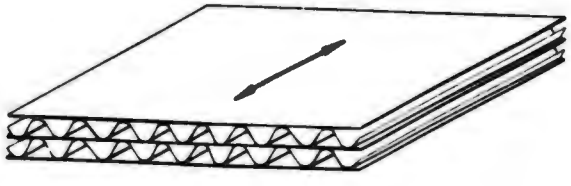

DOUBLE WALL

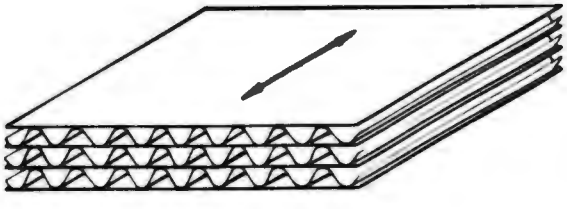

TRIPLE WALL

FIG. 4.41. Types of corrugated fiberboard.

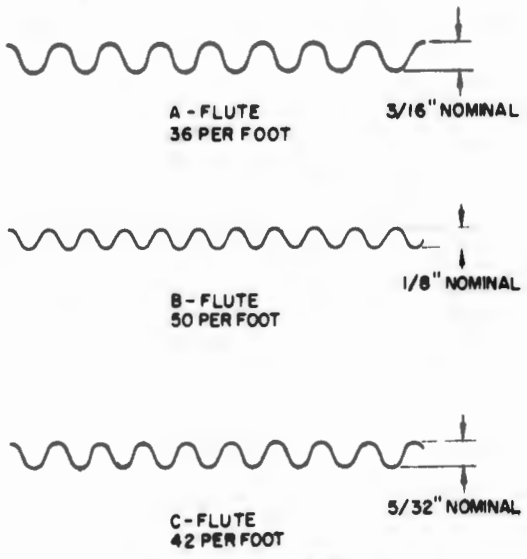

FIG. 4.42. Flutes.

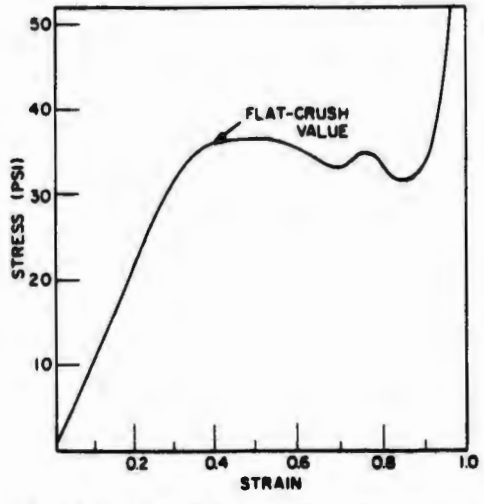

FIG. 4.43. Typical static stress-strain curve for corrugated fiberboard.

TABLE 4.17. FLAT-CRUSH EXPECTANCIES FOR CORRUGATED FIBERBOARD

Flute	*Flat Crush* (psi)	
	Single Wall	*Double Wall, per Layer*
A	25	21
B	35	31
C	30	26

have come to be considered normal. These expectancies are summarized in Table 4.17.

Dagel [207] has considered the nature of the stress-strain curve as a problem in elastic instability. After setting up a force diagram, Fig. 4.44, he derives the stress-strain equation for compression as

$$\sigma = \frac{4\pi^2 E_c I_a n \sin^2\alpha_3}{T_c^2}\left[C_2\epsilon - \frac{3}{4}C_2^2\epsilon^2 + \frac{5}{8}C_2^3\epsilon^3 - \ldots\right], \tag{4.79}$$

where E_c = Young's modulus of the corrugating medium,

I_a = area moment of inertia of the corrugating medium,

n = number of flutes per unit length, and

$$C_2 = \frac{T_c^2}{36\sin^2\alpha}.$$

This equation is valid up to the point of collapse of the arches. A linear first approximation is obviously satisfactory for most purposes and can be written

$$\sigma = \left[\frac{\pi^2}{9}E_c I_a n \sin\alpha_3\right]\epsilon. \tag{4.80}$$

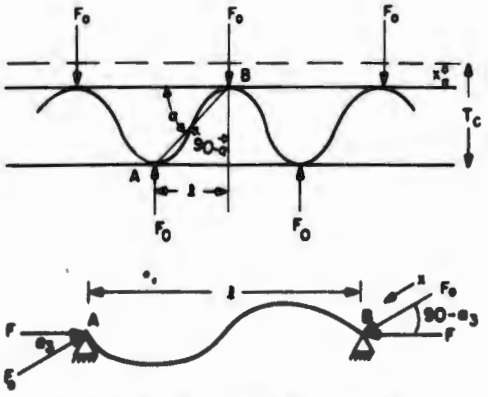

FIG. 4.44. Corrugated fiberboard in compression. Dagel [207].

Complete viscoelastic solutions in analogous form have not been obtained. Anderson [208] discusses buckling of shallow viscoelastic arches, but the shapes considered are not directly applicable. Goff [209], however, did investigate the damping characteristics of corrugated board. Using A-flute semichemical medium with 42-pound kraft liners, he found that the loss angle varied between 1.2 and 1.8 degrees in the range 0.125 to 7.5 cps. Actual values appeared to depend on stress amplitude and to be inversely proportional to static stress. All static stresses tested were well below the flat-crush point for the material.

Since strains were small in Goff's work, one would not expect that air trapped in the rather large corrugated structure would exert significant

influence. At very high strain rates, coupled with collapse of the arches, one would normally expect air to play an additional role.

Figure 4.45, taken from Ali [210], illustrates the type of effect although the citation did not identify the material being tested.

A limited number of dynamic tests, using a crude but reasonably effective test rig, were run by Marvin and Page [211]. Figure 4.46 shows changes in cushioning values for single thicknesses with repeated impacts at two

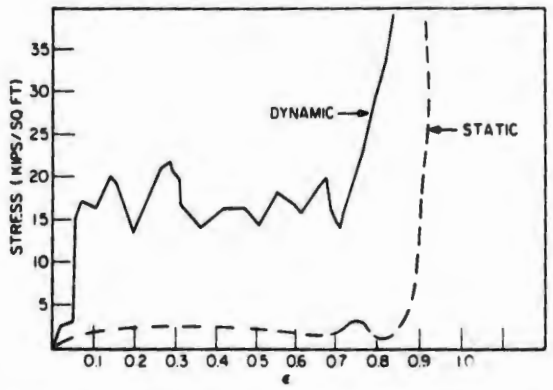

FIG. 4.45. Static and dynamic compression curves for 2-1/2-in.-thick corrugated fiberboard; impact velocity 24.8 fps. Ali [210].

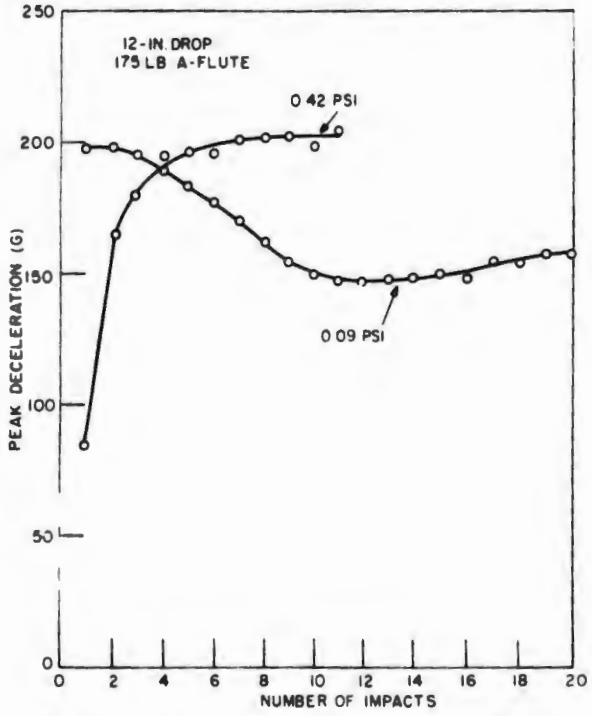

FIG. 4.46. Cushioning properties of 175-lb A-flute. Marvin and Page [211].

different static stresses. These results indicate that recovery after each impact is definitely less than 100 percent. Figure 4.47 plots peak deceleration *versus* static stress for A-flute and B-flute, showing that choice between the flutes will depend on the static stress.

There was some evidence (Fig. 4.48) that the area and the number of flutes affect performance. Doubling the thickness causes improvement (Fig. 4.49); facing basis weight also has an effect (Figs. 4.50 and 4.51). Why, we do not know. Perhaps different thicknesses of facing paper passing through the corrugator rolls or the double backer may produce very slight changes in arch shape that could significantly affect the stress-strain relation, Eq. (4.79).

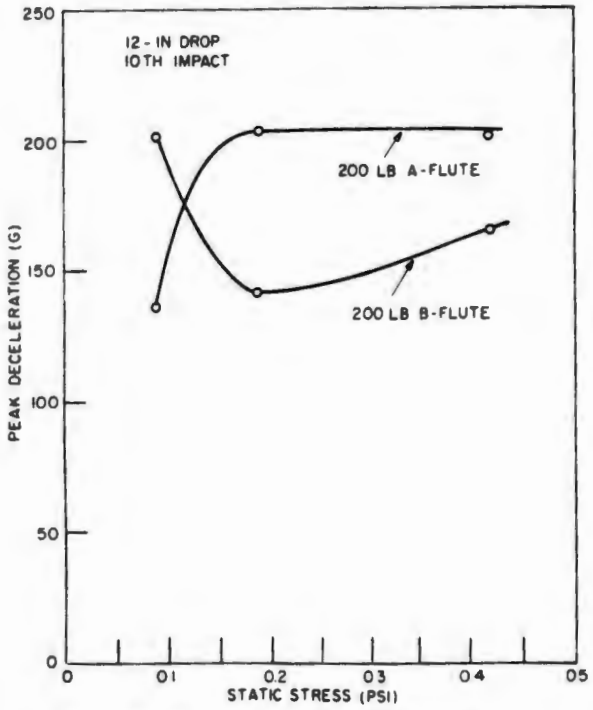

FIG. 4.47. Cushioning properties of A-flute and B-flute [211].

Because of the progressive nature of the breakdown of corrugated fiberboard, practical tests have concentrated on evaluating this form of behavior. A system is tested to failure and the number of drops at various heights is summed and recorded as foot-falls to failure (1 foot-fall equals one drop from a height of 1 foot). Toulouse and Berens [212] reasoned that, for glass bottles, failure occurred as a result of glass-to-glass contact. Accordingly, a logical failure point is when the bottle has completely crushed the flutes between two adjacent bottles. The bearing area of the bottle at the halfway point was computed by simple geometry. Figure 4.52 shows their results. The equations for the regression lines are

$$\begin{aligned} \log y &= 1.21 - 1.17 \log x \\ \log y &= 1.372 - 2.988 \log x \end{aligned} \tag{4.81}$$

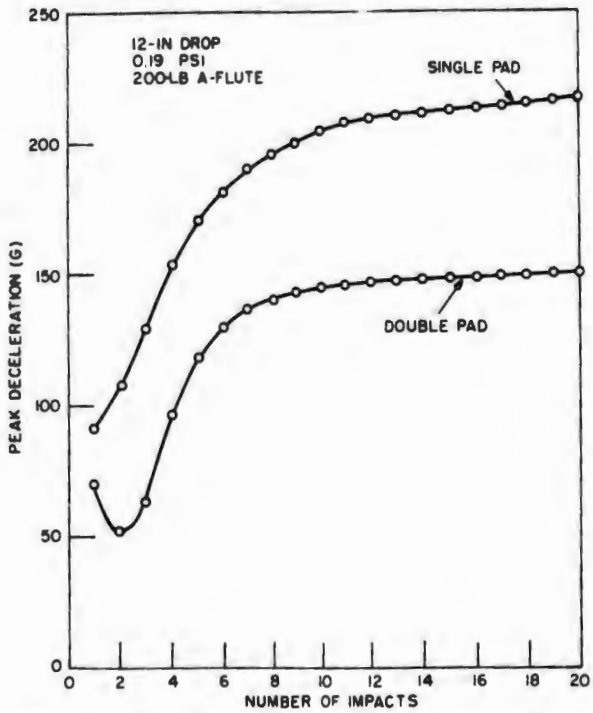

FIG. 4.48. Effect of different areas of same material [211].

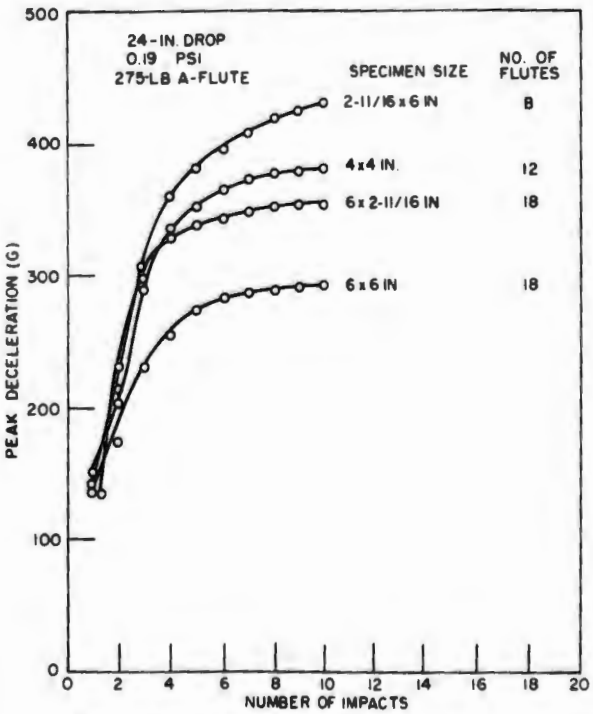

FIG. 4.49. Effect of doubling thickness [211].

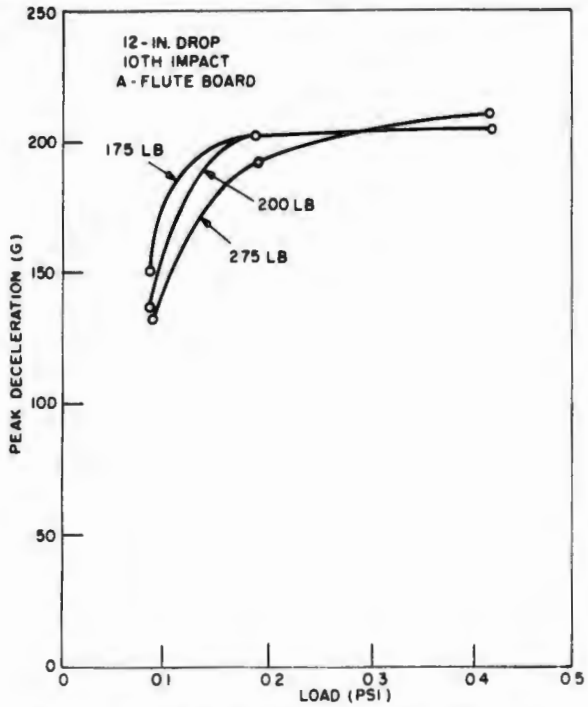

FIG. 4.50. Effect of facing weight for different loads [211].

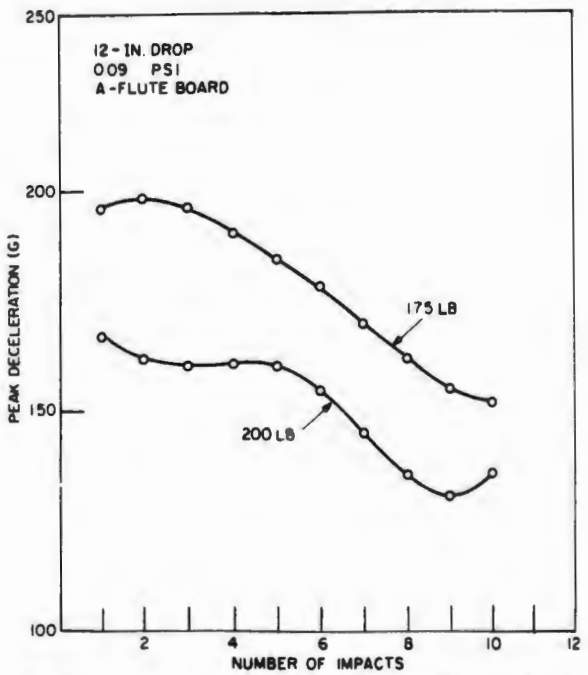

FIG. 4.51. Effect of facing weight for different numbers of impacts [211].

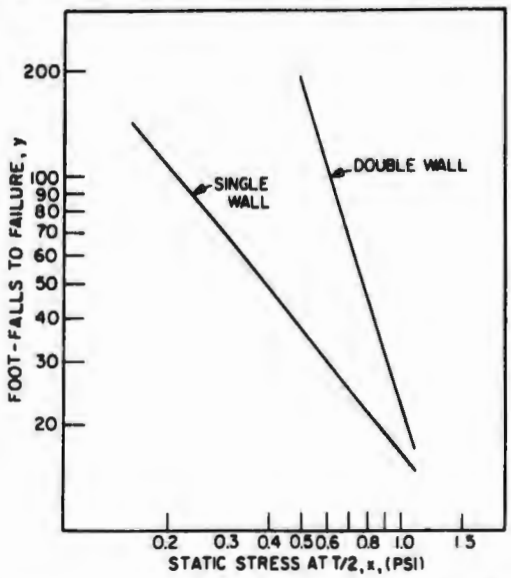

FIG. 4.52. Foot-falls to total compression of corrugated fiberboard. Toulouse and Berens [212].

where the first equation applies to single wall and the second to double wall. y is foot-falls to failure and x is the static stress at the failure point, *i.e.*, bottle halfway through the board.

Matching in this fashion did not reveal significant differences between constructions. Later, however, Beardsell and Kipnees [213] investigated whiskey-bottle packaging extensively, using a failure criterion of foot-falls to breakage or foot-falls to 500 g acceleration, whichever occurred first. Significant differences were found between board constructions; they selected

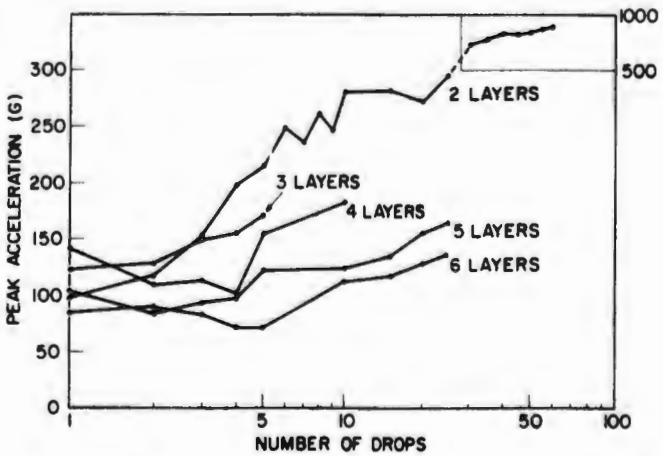

FIG. 4.53. Performance of multiple layers of 200-lb test A-flute corrugated fiberboard. Static stress 0.182 psi. Blake [214,215].

their final pack (which has largely become an industry standard) upon what would now be called cost-effectiveness grounds. Note that the two criteria of a test endpoint differ.

The School of Packaging at Michigan State University has been conducting a cooperatively sponsored research program on control of damage in shipment for the past several years. During the course of their work, some evaluations of the performance of corrugated fiberboard under multiple-impact conditions have been conducted [214,215,216]. Figure 4.53 illustrates the performance capability of layers of 200-lb test A-flute corrugated board when repeatedly dropped from a height of 24 inches. The two-layer configuration is the same as the number of board thicknesses encountered at the top and bottom of a regular slotted container with a square or nearly square opening. Thus, the curve for two layers also indicates the shock reduction to be expected

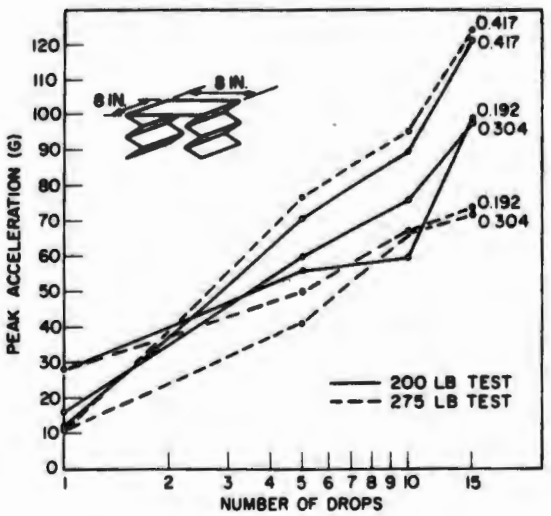

FIG. 4.54. Performance of A-flute spring pads at various static stresses. Blake [216].

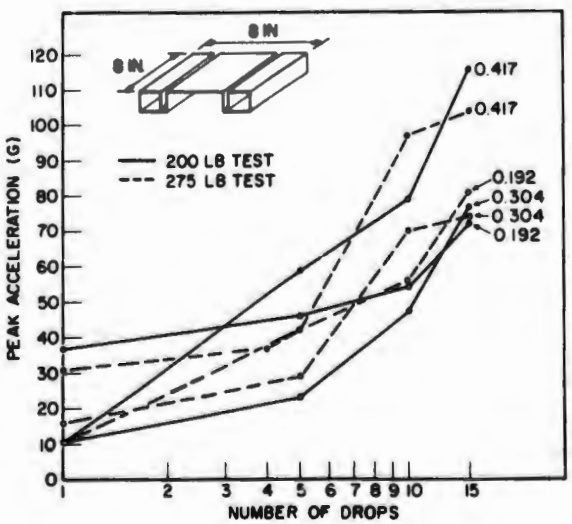

FIG. 4.55. Performance of A-flute rat trap pads at various static stresses [216].

from a corrugated container without inner cushions or pads. Note that, from the 25th drop onward, performance is greatly degraded.

Figures 4.54 and 4.55 illustrate the protection attainable from two different styles of formed inner pads. While performance for a small number of drops is quite good, the pads tend to collapse rather soon and, by the 15th drop, are of marginal utility.

4.6.2.2. *Quasi-Resilient Plastic Foams.* Many elastomeric materials can be produced as foams: rubbers (natural or synthetic), polyurethane, polystyrene, polyethylene, vinyl, phenolic, silicone, cellulose acetate, urea formaldehyde, and epoxy. Of these, the first four are the ones most commonly used as cushions, although all are candidates. Most of the data available on quasi-resilient behavior is limited to polystyrene and polyurethane foams, the majority of which are classified as semi-rigid or rigid.

The utility of any foamed plastic material as a cushion depends on the specific characteristics of the foam (size of cells, porosity, and volume fraction of material) and on the specific thermorheological properties of the plastic substance. These latter, in turn, will vary depending upon the characteristics of the individual molecules. Useful cushions are usually required to have good properties in the transition and glassy regions (see Fig. 3.18). Thus the temperature at which glassy behavior starts is a useful classifying scale for materials.

Schmidt and Hoffmann [188] have plotted the rigidity modulus for a number of polyurethane foams, Fig. 4.56. The rigid foams are almost always used in the glassy state, and mechanical properties are nearly temperature-independent down to −50°C. Soft and semi-rigid foams, by contrast, are

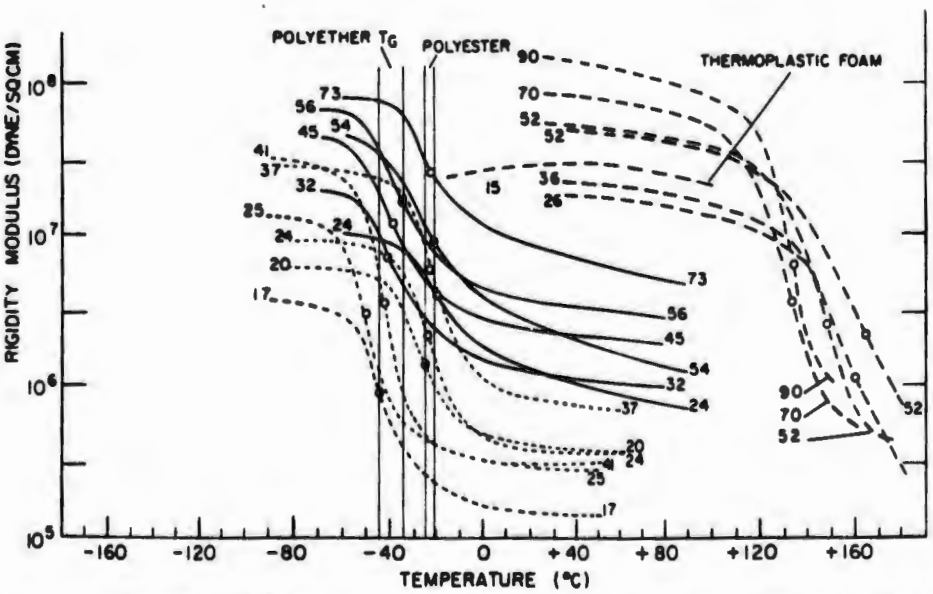

FIG. 4.56. Rigidity modulus for a number of polyurethane foams; dotted lines are for soft foams, dashed lines for rigid foams, and solid lines for semi-rigid foams; the small numbers opposite each line represent the apparent density of the foam. Schmidt and Hoffmann [188].

generally used in transition-zone temperatures. Note that the glass temperature T_g is considerably lower for polyether foams than for polyester foams. However, polyether foams tend to hydrolyze in the presence of water and this limits their use in practical design. Temperature-dependence of all usable polyurethane foams is clearly demonstrated in Fig. 4.56.

Damping characteristics for semi-rigid foams are far less air-dependent than for soft foams because of cross-linking in the molecules. For semi-rigid foams the static stress-strain curves lie from 50 to 70 percent below the dynamic curves. The plateau area remains prominent, as shown in Fig. 4.57. For rigid materials, the dynamic curves are only about 20 to 30 percent higher than the static (Fig. 4.58).

For both semi-rigid and rigid foams, recovery from stresses below the knee is quite good though not rapid. Stresses above the knee are probably irreversible. This irreversibility may not necessarily result in higher accelerations under impact shock, even though, in a package, the contents may become loose with time. Figure 4.59 shows that the plateau area contributes to continued good shock-isolation performance through a number of impacts.

The figure shows a progressive dynamic drift of the strains actually encountered (with zero strain being measured before the test syllabus). For low static stresses, the cushion was still working its way over the knee. For intermediate stresses, strains were in the plateau region and, for high stresses, strains were on the second sharply increasing portion of the curve.

Basically, Fig. 4.59 shows that if the design can be so arranged that dynamic strain is less than some critical value (about 30 percent in the figure), repeated impacts of the same magnitude will not result in higher peak accelerations,

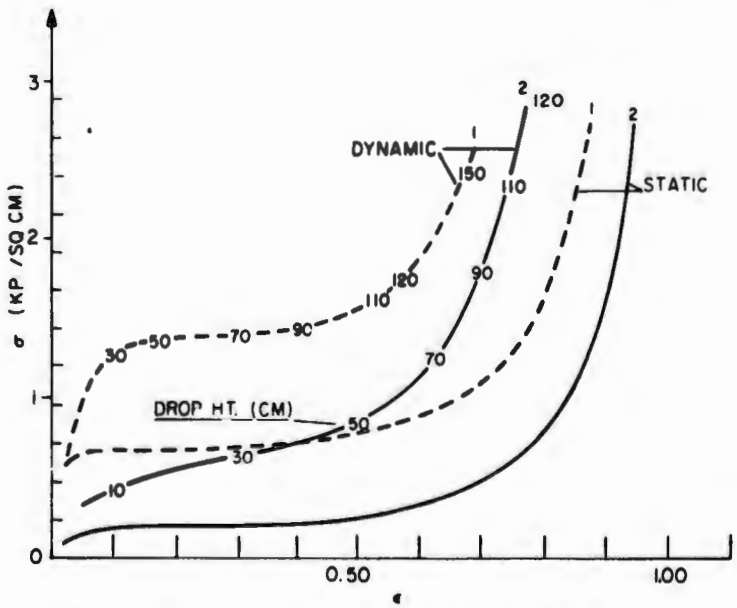

FIG. 4.57. Static and dynamic stress-strain curves for semi-rigid polyester urethane foams; thickness 3 cm, static stress curve 1—density 54.0 kp/m³, curve 2—density 75.0 kp/m³ [188].

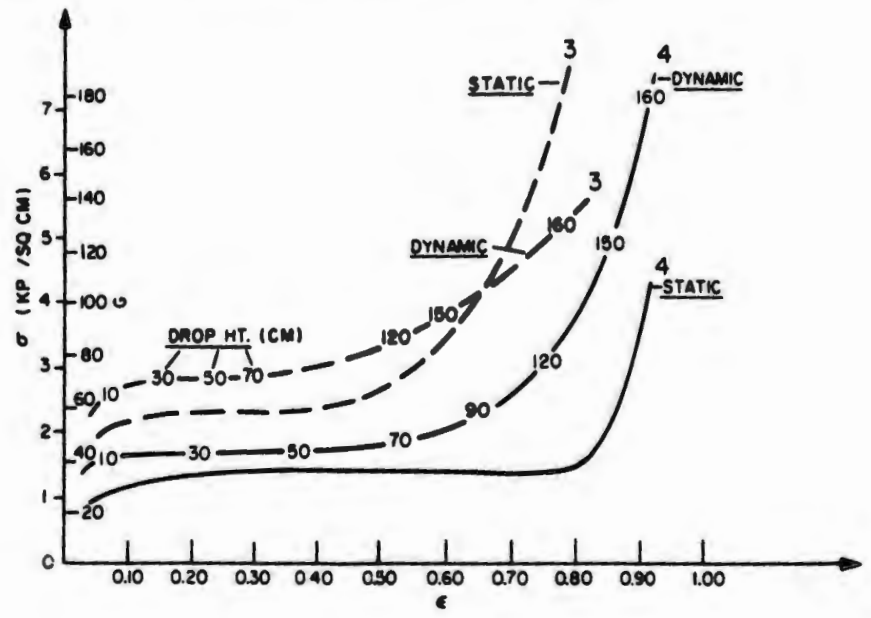

(a)

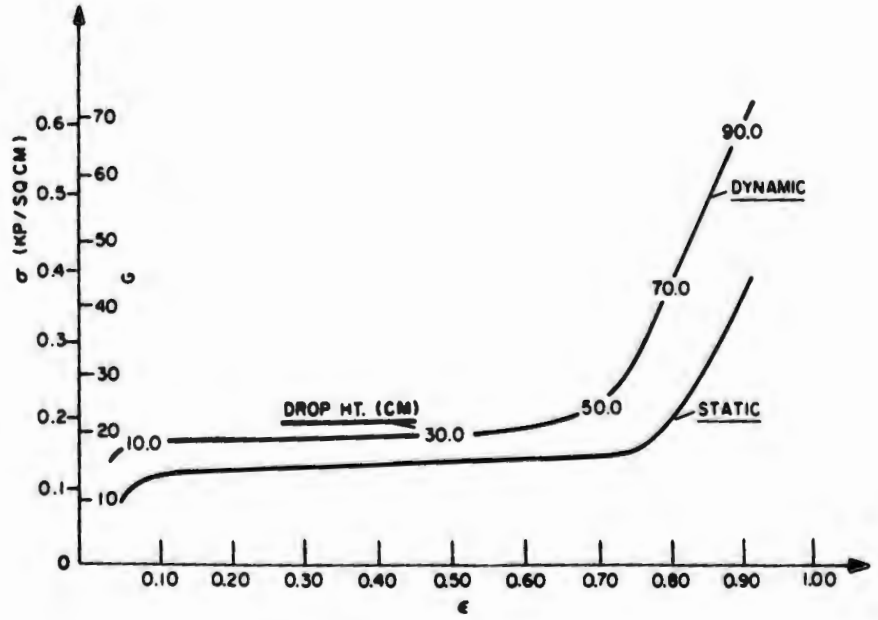

(b)

FIG. 4.58. Stress-strain curves for rigid polyurethane foams: (a) two foams of normal density, thickness 3 cm, static stress 39.5 p/cm², curve 3 – density 35 kp/m³, curve 4 – density 27.3 kp/m³; (b) a superlight hard foam, density 7.3 kp/m³, $Z = 1.2$ Rayl/cm, thickness 3 cm, static stress 10.0 p/cm² [188].

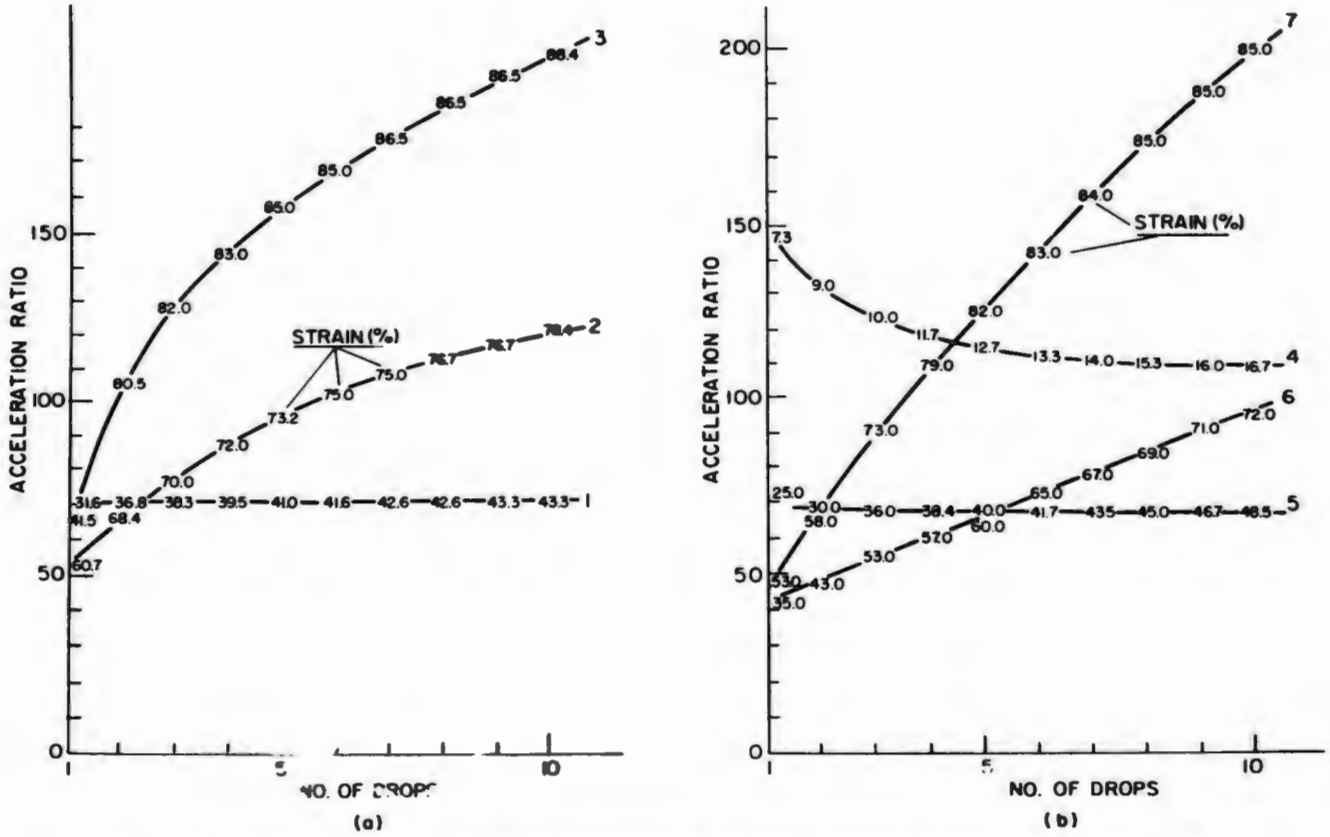

FIG. 4.59. Number of drops *versus* peak acceleration for polyester semi-rigid foams tested at $h/T = 20$: (a) density 54 kp/m³ (b) density 75 kp/m³; static stresses for each curve were: 1 – 10.5 p/cm², 2 – 31 p/cm², 3 – 50 p/cm², 4 – 10.5 p/cm², 5 – 20 p/cm², 6 – 30 p/cm², and 7 – 50 p/cm² [188].

up to about 10 impacts. In effect, even though there be permanent set, polyurethane foams still provide much protection. Perhaps, as with corrugated fiberboard, the concept of foot-falls to failure could be useful here, or the box materials could be rated in the same way as the plastic foams.

Polystyrene foam is more popular in the United States, at least for package-cushioning purposes, than the semi-rigid polyurethane foams. In semi-rigid form, the material is a closed-cell foam with rather strong cell walls. It is available in various nominal densities. Figure 4.60 shows static stress-strain curves for several different densities (expressed as pounds per cubic foot, pcf) of materials in use on both sides of the Atlantic [152,217]. Note that elastic behavior is similar to that of foam rubber compression-curve theory developed by Gent and Thomas [90] and summarized in section 3.3.

Drysdale *et al.* [217] have investigated the properties of several polystyrene foams for packaging. Figure 4.61 compares some materials as absorbers of impact energy. Figure 4.62 shows the typical U-shaped curves predicted by Soper and Dove. Evidently they could be plotted in accordance with Mustin's recommendations. Significant movement of these curves from the first to the second drop is apparent. The authors noted, however, that with the lower-density materials (1.0 pcf nominal) most of the irreversible loss

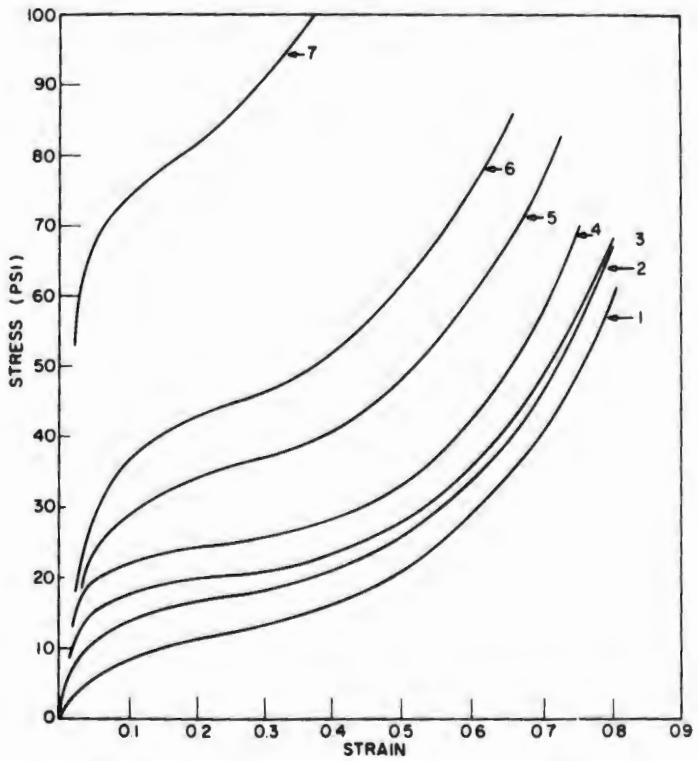

FIG. 4.60. Typical static stress-strain curves for semi-rigid polystyrene foams: approximate nominal densities in pcf: 1 – 0.7, 2 – 1.0, 3 – 1.2, 4 – 1.5, 5 – 2.0, 6 – 3.0, and 7 – 5.0. Curves 1 through 4 from Drysdale, *et al.* [217]. Curves 5 through 7 from Gigliotti [152].

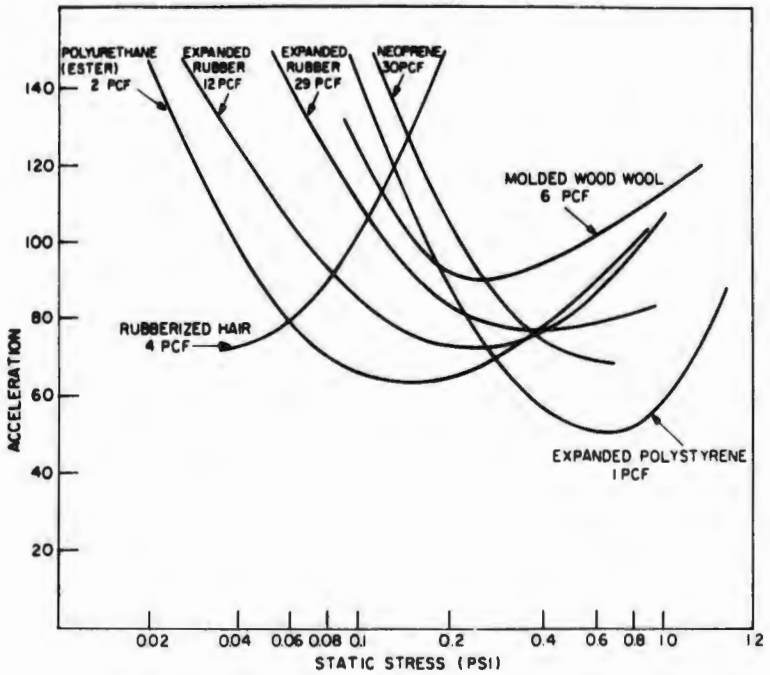

FIG. 4.61. First drop performance of several cushions [217].

occurs on the first drop and that dynamic thickness drift is less on subsequent impacts, so that a constant acceleration level is approached. As an example, the fifth drop on 0.8-pcf material was less severe than the fifth drop on 2-pcf material, although this was not true on the first drop. Defining relaxed strain as the no-load strain remaining one minute after previous compression, they plotted loss of thickness as a function of density for one set of conditions in Fig. 4.63. Relaxed strain as a function of energy per unit initial volume is shown in Fig. 4.64. Useful, thorough information is also given by Mahler and Stockburger [218].

In the United States most of the data on the polystyrene foams are in manufacturer's literature, although Gigliotti has some data [151]. Figure 4.65 contains some dynamic data for expandable polystyrene foams from one manufacturer [219]. Use of fifth-drop data is recommended for design purposes because the results of future drops are more predictable. Data for dynamic deflection and permanant set *versus* static stress for the same materials at the same drop height are given in Fig. 4.66. In order to prevent too much rattle space being developed immediately adjacent to the container contents, the manufacturer recommends making a design that will take all deflection in ribs on the outside of the cushion adjacent to the container walls. Then the depth of the ribs will be determined by the required deflection. Typical rib shapes of optimum strength characteristics are shown in Fig. 4.67. Rib width (across the rib tips) is computed on the basis of the static stress requirement for optimum performance. In finalizing designs, attention must be paid to good molding practice.

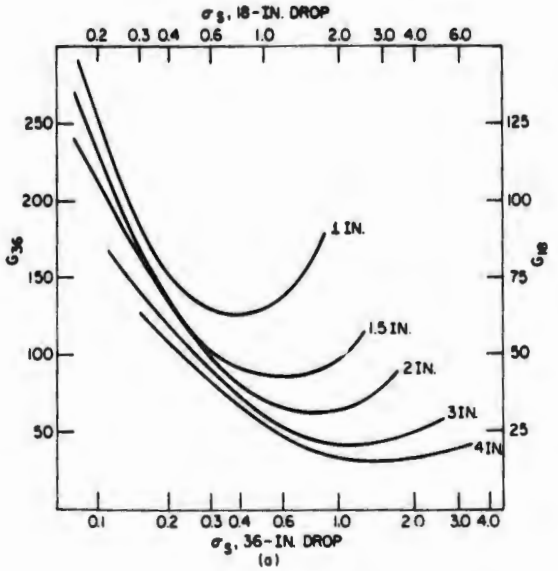

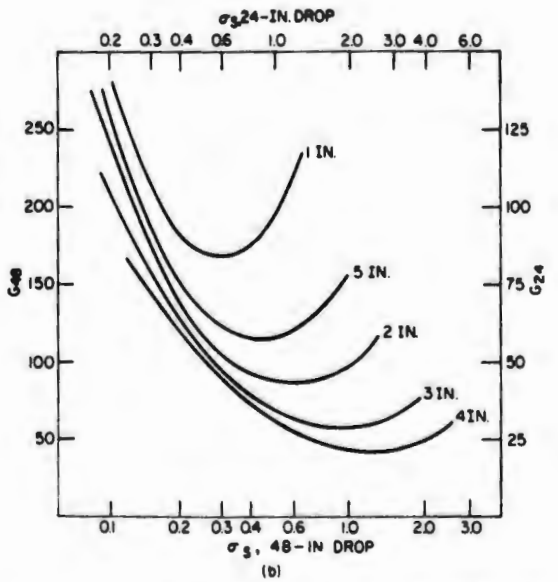

FIG. 4.62. Performance curves for 1.0-pcf polystyrene foam of indicated thickness; a and b are for first drop, while c and d are for second drop on same samples [217].

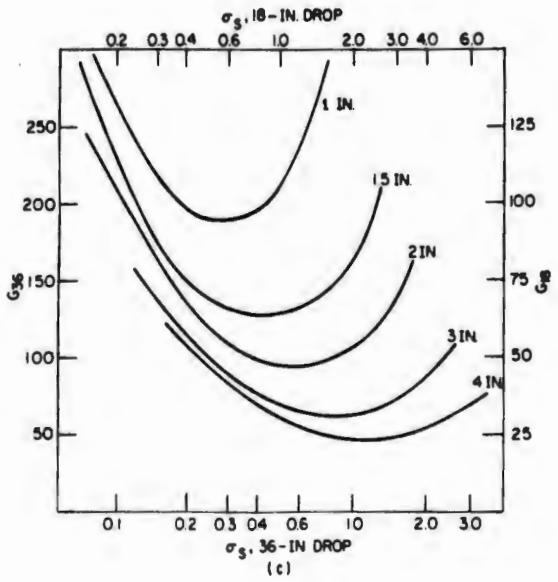

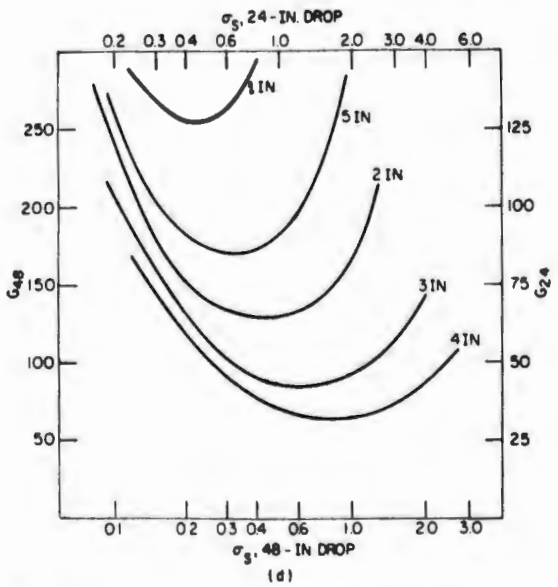

FIG. 4.62 (*Continued*). Performance curves for 1.0.pcf polystyrene foam of indicated thickness; a and b are for first drop, while c and d are for second drop on same samples [217].

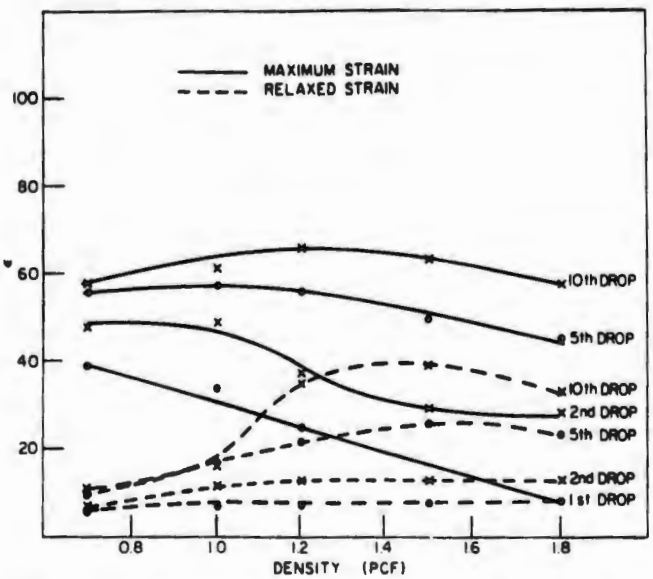

FIG. 4.63. Peak strain during impact and relaxed strain as a function of density; energy per initial unit volume, 7.5 in.-lb/in.^{3} [217].

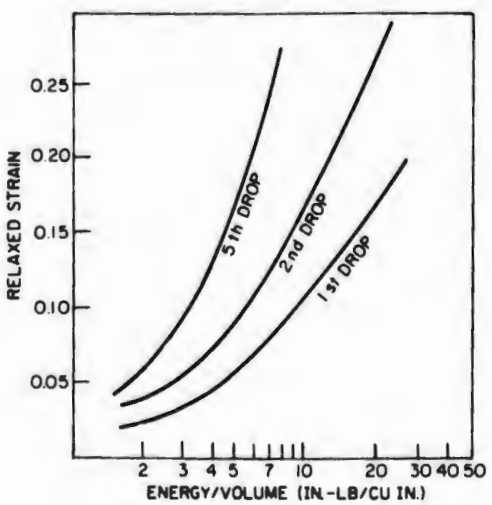

FIG. 4.64. Relaxed strain *versus* energy per initial unit volume for 1.0-pcf polystyrene foam [217].

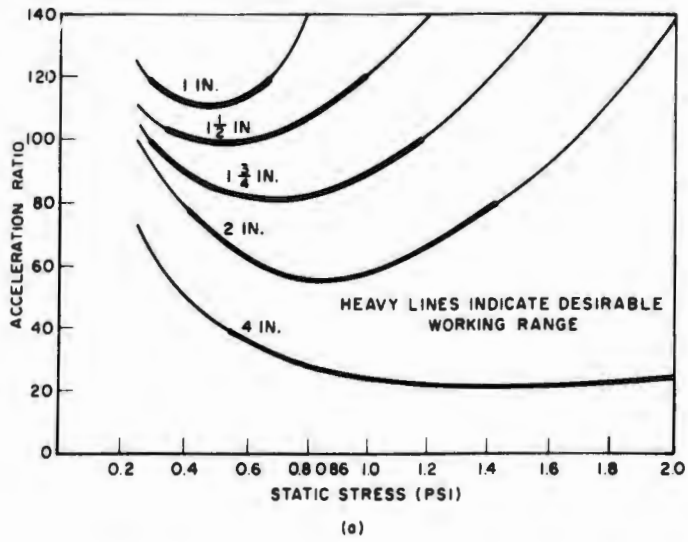

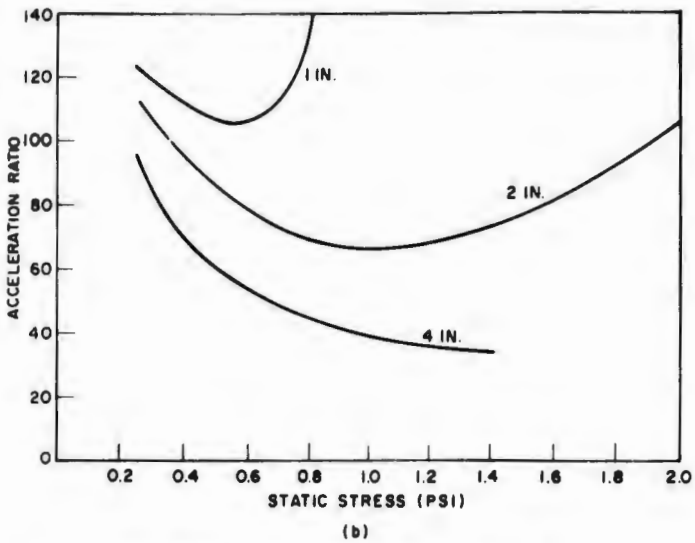

FIG. 4.65. Fifth drop performance of some polystyrene foams: (a) 1.2 pcf, (b) 2.0 pcf, and (c) 3.0 pcf.

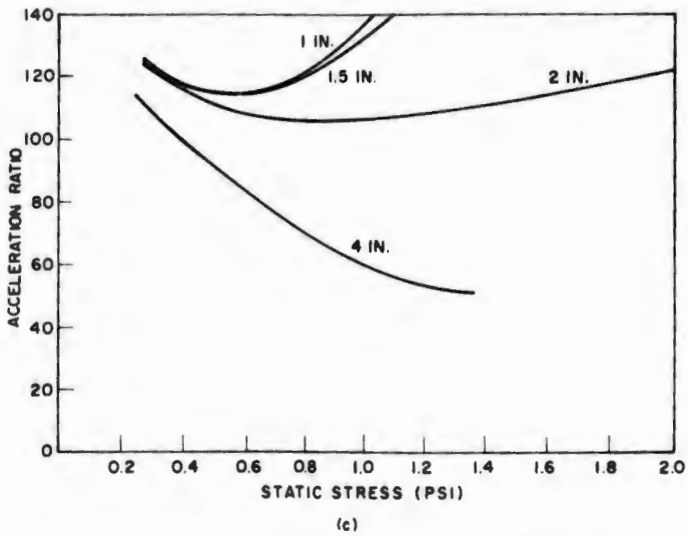

FIG. 4.65 (*Continued*). Fifth drop performance of some polystyrene foams: (a) 1.2 pcf, (b) 2.0 pcf, and (c) 3.0 pcf.

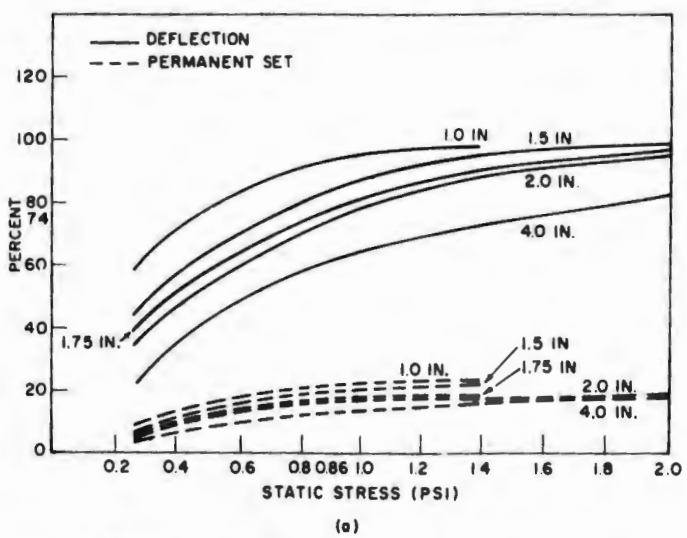

FIG. 4.66. Deflection and permanent set for some polystyrene foams; all data based on fifth drop from 30 in.: (a) 1.2 pcf, (b) 2.0 pcf, and (c) 3.0 pcf [219].

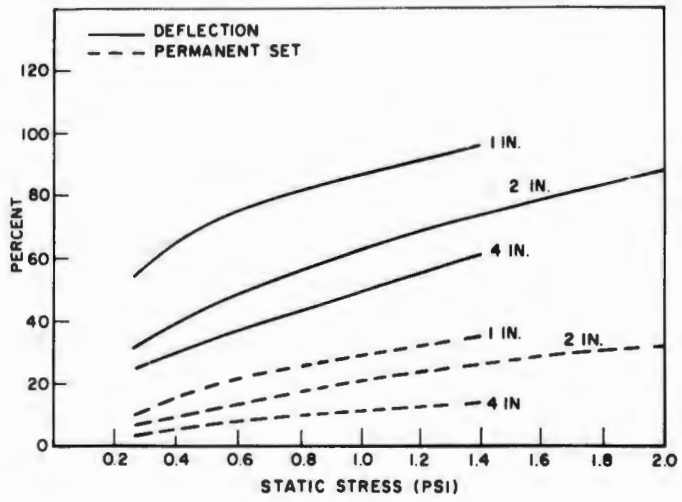

(b)

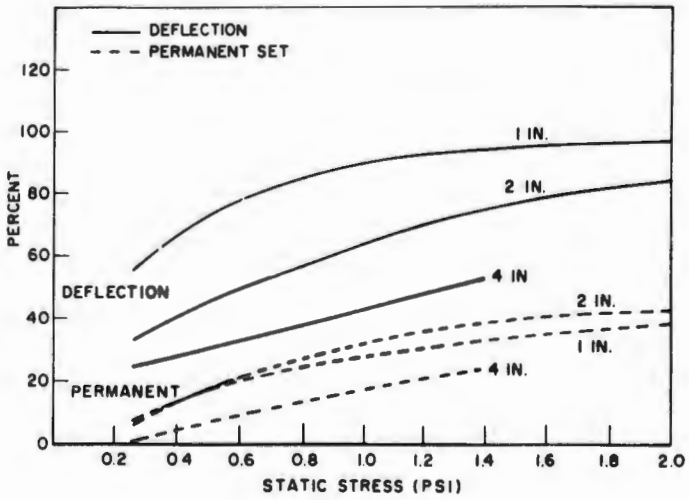

(c)

FIG. 4.66 (*Continued*). Deflection and permanent set for some polystyrene foams; all data based on fifth drop from 30 in.: (a) 1.2 pcf, (b) 2.0 pcf, and (c) 3.0 pcf [219].

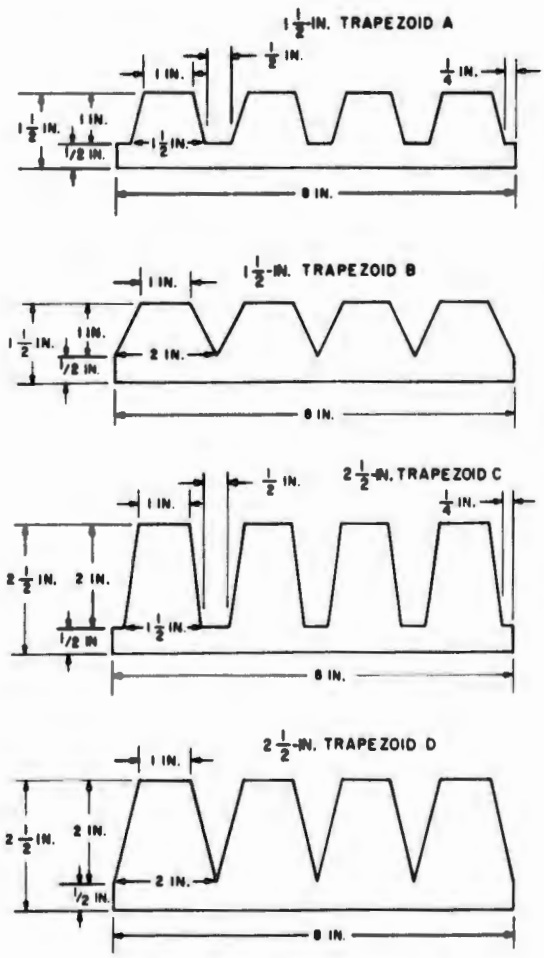

FIG. 4.67. Suggested rib configurations for some polystyrene foams [219].

4.6.3. Rigid Materials. Any material can be used as a shock absorber if the designer will accept an irreversible process such as permanent deformation or disintegration. This section is therefore confined to practical situations where commercially available materials have been examined for possible utility in solving real problems.

It is stipulated that most of the materials and techniques to be discussed are intended for use in the lower ranges of velocity changes. Velocities are subsonic, most of them very much less than Mach 1.

Probably the most sustained and searching inquiry into the cushioning properties of rigid materials has been undertaken at the University of Texas in connection with the classical problem of aerial delivery of equipment and supplies, a technique of great interest to ground troops. The fact that this work has a very practical objective forces concentration on low-cost materials.

The overall approach, sponsored by the U.S. Army Natick Laboratories has produced significant and useful information. This information can be grouped as follows:

1. Searching reviews [220,221] of all the pertinent literature covering shock and response to shock. Brennan's two-volume review [221] contains over 800 abstracts from the open literature alone and was used as a guide in the literature search required for this monograph.
2. A number of excellent papers on response of structures to shock pulses, including plastic irreversible flow of elements of these structures. Several of these will be discussed in the next chapter.
3. A group of reports concerning the dynamic behavior of cushions at impact velocities ranging from 20 feet per second (fps) (equivalent to a 6-foot drop in a vacuum) to around 100 fps. Much of these data will be summarized here.

In 1962 Thompson and Ripperger [202] gave an excellent summary of their progress up to that time, including many of the background considerations guiding their work. From the standpoint of this monograph, it is important to note that they were seeking a material with very low coefficient of restitution. Maximum possible storage of impact energy was desired in order to discourage the load from bounding all over the countryside [202]. See also Stevens [222]. The energy storage time needed, at least, to be very long with respect to the shock pulse duration. There was no technical objection to its being permanent.

Secondly, they were, for obvious reasons, seeking maximum energy absorption for minimum thickness of cushioning [223]. These two factors lead to a definition of the ideal material as one exhibiting a rectangular stress-strain curve such that, when unloading takes place, stress drops vertically at the strain assumed during peak stress. Performance of the materials evaluated was measured against this ideal. A rectangular stress-strain curve (linear elasticity with zero slope) was shown by Mindlin [97] to be the optimum shape for minimum thickness for a given acceleration.

As a result of these considerations, Thompson and Ripperger focused on materials and structures that would show a collapsing-column effect under loading and show large, essentially permanent strains. Honeycomb structure, rigid plastic foams, and axially loaded tubing, among others, meet these definitions. Figure 4.68 demonstrates the significant improvement made possible by using a honeycomb structure as compared with the previously used felt pad shock absorbers.

4.6.3.1. *Honeycombs.* Honeycomb consists of material formed into hexagonal cells and cemented to one or more facing sheets placed across the open ends of the cells. Materials used may be paper or metal, in various combinations. Aluminum or stainless steel are the most common metals used today to satisfy the requirements of the aerospace industry.

It is evident that paper honeycomb must have a lower first cost than an all-metal honeycomb. Therefore, most of the data concern paper materials.

Typical dynamic stress-strain curves for a paper honeycomb with varied maximum strain (achieved by varying sample thickness for constant mass

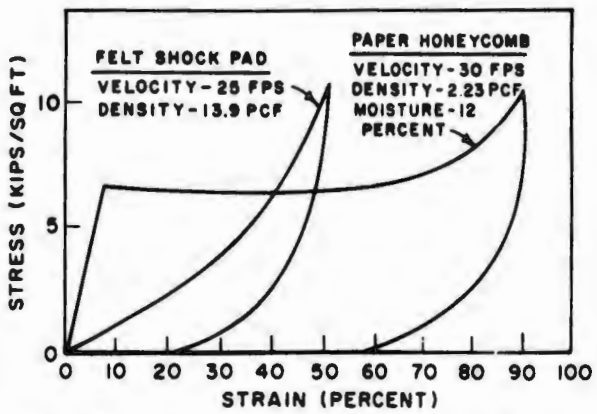

FIG. 4.68. Comparative dynamic performance of paper honeycombs and felt. Thompson and Ripperger [202].

and impact velocity) are shown in Fig. 4.69 [224]. Note that there is an initial peak, followed by a U-shaped portion of the curve and then a rising portion as the cushion begins to bottom out. Practically all paper honeycombs seem to begin bottoming at or slightly above the 70 percent strain point.

Note the honeycomb classification scheme used in Fig. 4.69. The first number is the basis weight of the paper. The second (parenthetical number) is the resin content of the paper in percent, and the third number is the cell size across the flats of the hexagon.

The initial peak stress and the energy absorbed are largely a function of overall density, as shown in Fig. 4.70.

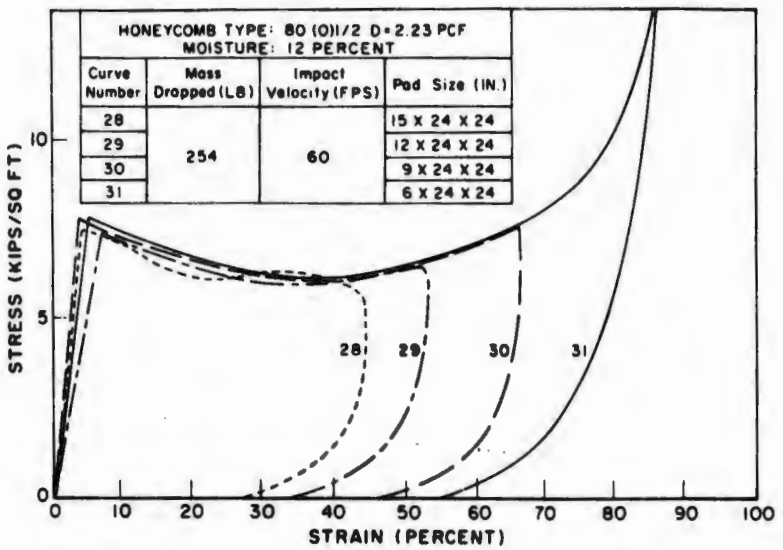

FIG. 4.69. Stress *versus* strain for a paper honeycomb with maximum strain varied. Karnes, *et al.* [224].

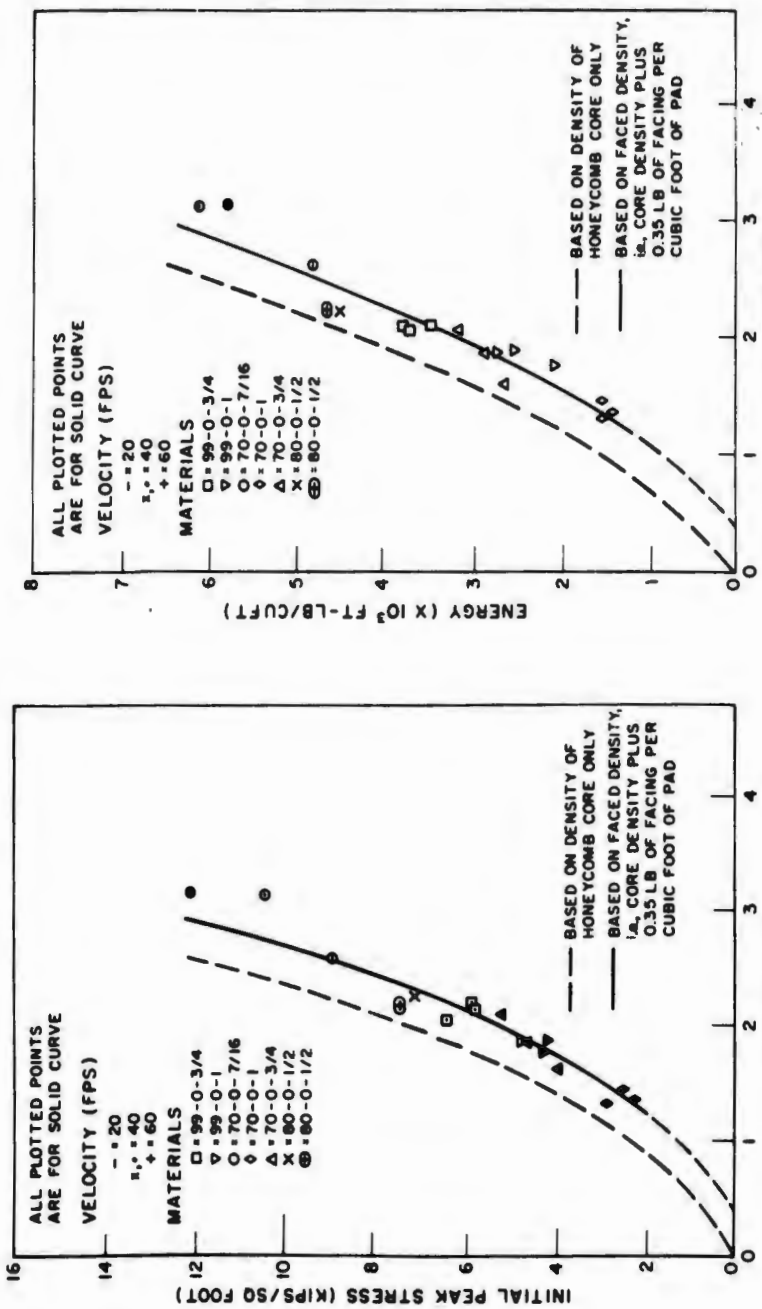

FIG. 4.70. Effect of paper honeycomb density on performance: (a) initial peak stress, and (b) energy absorbed at 70 percent strain [224].

Moisture content does not have a significant effect on performance until very high moisture contents are reached [224]. See Fig. 4.71. Reasonable protection under field storage conditions should usually prove adequate [202].

Honeycombs are essentially strain-rate-insensitive, at least at impact velocities ranging from 30 to 90 fps [224]. In terms of Soper and Dove theory, h/T is greater than 50, and this result is not surprising. Figure 4.72 is illustrative. Here, the cushion thickness and the mass were varied

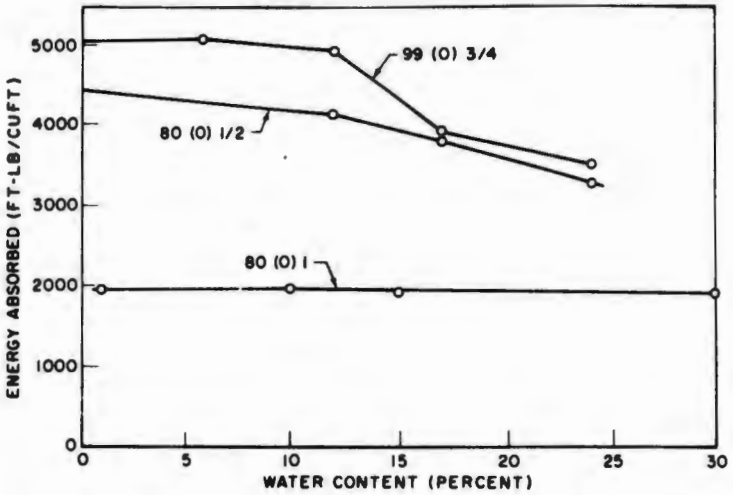

FIG. 4.71. Effect of water content on energy absorbed at 70 percent strain for three paper honeycombs [224].

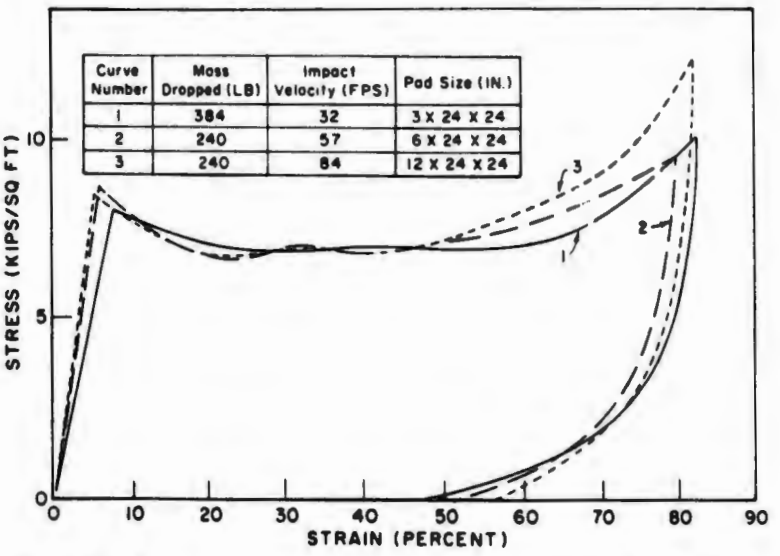

FIG. 4.72. Stress-strain curves for 99(0)3/4 paper honeycomb at 12 percent water content and velocity varied [224].

with impact velocity to produce about the same peak strain on each drop; thus the shapes of the curves above 70 percent strain vary somewhat, but the overall effect in the range of interest is substantially the same. For lighter basis weight papers, there were occasional blow-outs of the cell walls at the edge of the pad but, for pads with large surface area, the effect on stress-strain behavior was negligible.

Because of overall consistency of behavior, it has been recommended that equipment be designed according to the average energy absorbed at 70 percent strain [225,226,227]. Suitable average stress values for a number of different materials are listed in Table 4.18. It is reported that values in the range of interest will not vary by more than plus or minus 10 percent

TABLE 4.18. SUMMARY OF AVERAGED RESULTS ON PAPER HONEYCOMB

Moisture Content (%)	*Honeycomb Type*	*Impact Velocity* (fps)	*Average Stress to 70% Strain* (kips/ft²)	*Total Energy Absorbed to 70% Strain* (ft-lb/ft³)	*Maximum Strain* (%)
		34	6.89	4820	86
0	99(0)3/4	61	7.22	5060	89
		87	6.66	4660	90
		33	7.30	5100	86
0	99(0)3/4	59	7.26	5080	82
		84	7.38	5160	84
		32	6.85	4790	83
12	99(0)3/4	57	7.03	4920	80
		84	7.00	4900	81
		30	5.73	3960	87
17	99(0)3/4	63	5.72	3930	84
		89	6.10	4170	83
		29	4.92	3450	86
24	99(0)3/4	60	5.03	3530	83
		85	5.33	3660	82
0	80(0)1/2	60	6.27	4400	92
		30	6.24	4360	93
12	80(0)1/2	60	5.67	3950	92
		93	5.99	4190	86
18	80(0)1/2	60	5.42	3790	86
24	80(0)1/2	60	4.74	3320	93
1	80(0)1	60	2.75	1930	93
		30	2.94	2060	85
10	80(0)1	62	2.82	1980	87
		88	2.79	1950	83
−5	80(0)1	60	2.75	1920	83
30	80(0)1	60	2.74	1920	83

on a dynamic basis. Dynamic curves are a reasonably consistent 140 to 150 percent of corresponding static values, up to about 190 fps for impact velocity.

Given the allowable acceleration at the interface of the load and the cushion, recommended design procedures [228,229,230] reduce to solution of the following equations:

$$T_c\epsilon = \frac{V_c}{2gG}, \qquad A_c\sigma_a = w(G+1), \tag{4.82}$$

where σ_a is the average stress from Table 4.18.

A typical dynamic stress-strain curve [202] for aluminum honeycomb under incompletely specified test conditions is shown in Fig. 4.73. Note that, quite similarly to the paper honeycombs, bottoming begins at around 70 percent strain but that the energy absorption capacity is considerably larger. For parachute, or (approximately) free-fall delivery, where velocity seldom exceeds 100 fps, the metal honeycombs were ruled out on a cost basis. For higher energies, however, they could be highly satisfactory.

In consonance with the idea behind the last sentence of the preceding paragraph, Soper and Dove [33] give results for cellular magnesium and

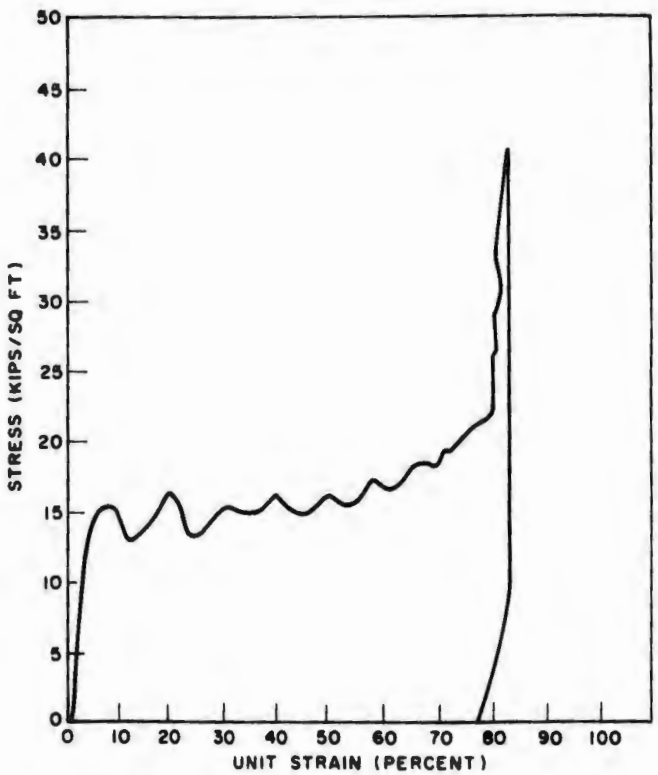

FIG. 4.73. Dynamic stress-strain curve for 2.7-pcf aluminum honeycomb impacted at 26.1 fps [202].

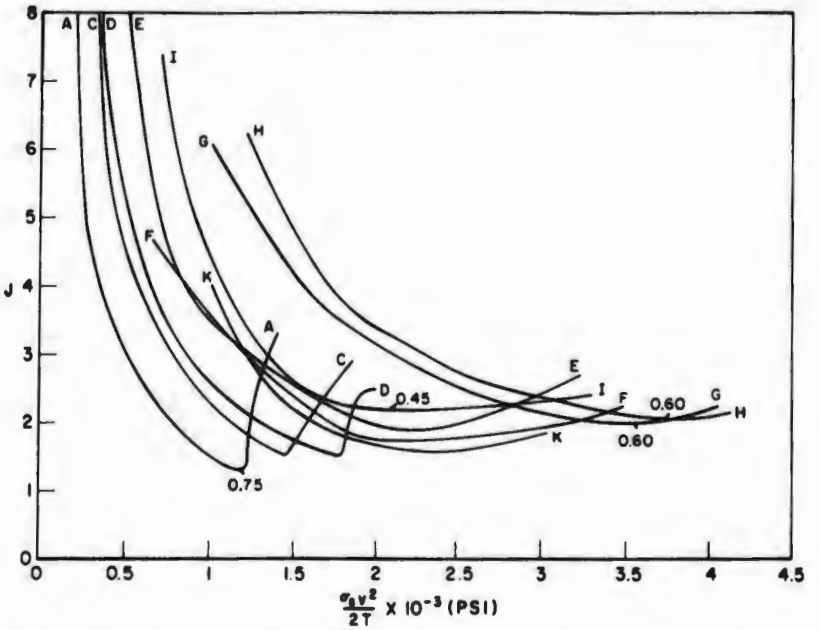

FIG. 4.74. Performance of aluminum honeycomb and cellular magnesium; materials are identified in Table 4.19. Soper and Dove [33].

TABLE 4.19. HIGH-ENERGY ABSORBING MATERIALS INVESTIGATED BY SOPER AND DOVE (HC = ALUMINUM HONEYCOMB)

Designator	*Description*
A	HC + Stafoam, 5.8 pcf
C	HC + Stafoam, 9.0 pcf
D	HC + Stafoam, 8.1 pcf
E	HC + Stafoam, 19.7 pcf
F	HC + Stafoam, 17.3 pcf
G	Cellular Magnesium, 42 pcf
H	Cellular Magnesium, 52 pcf
I	HC + Stafoam, 23.7 pcf
K	HC + Stafoam, 15.4 pcf
L	Silicone Rubber with 44% glass beads, $v/h > 400$
M	Stafoam, 20 pcf
N	Aluminum Foam, 16.4 pcf
O	Aluminum Foam, 24 pcf
P	Aluminum Foam, 20 pcf
Q	Polyrubber and Stafoam, $v/h > 400$
R	Stafoam, 5 pcf

aluminum honeycomb (1-1/8 cell, density 9 pcf) which include approach velocities up to and over 200 fps. Their honeycomb cells were filled with foamed plastic of varying density. The results are plotted as *J versus* energy per unit volume in Fig. 4.74. Materials are identified in Table 4.19. The filler not only increased the energy-absorptive capacity of the material but also smoothed out the approach to bottoming, as illustrated by the smoothness of most of the curves around the optimum point. The curves for cellular magnesium are particularly interesting.

Where the material is not strain-rate-sensitive in the region of interest, design with curves of J-energy per unit volume is straightforward. Thickness is determined from

$$T_c = \frac{Jh}{G_m} = \frac{JV^2}{2a_p}, \tag{4.83}$$

which requires knowledge of the velocity and the peak acceleration allowable, as in all impact problems.

Performance of aluminum honeycombs has been explored by David [231] at impact velocities between 600 and 900 feet per second. A typical load-displacement curve is shown in Fig. 4.75. The very high initial peak is

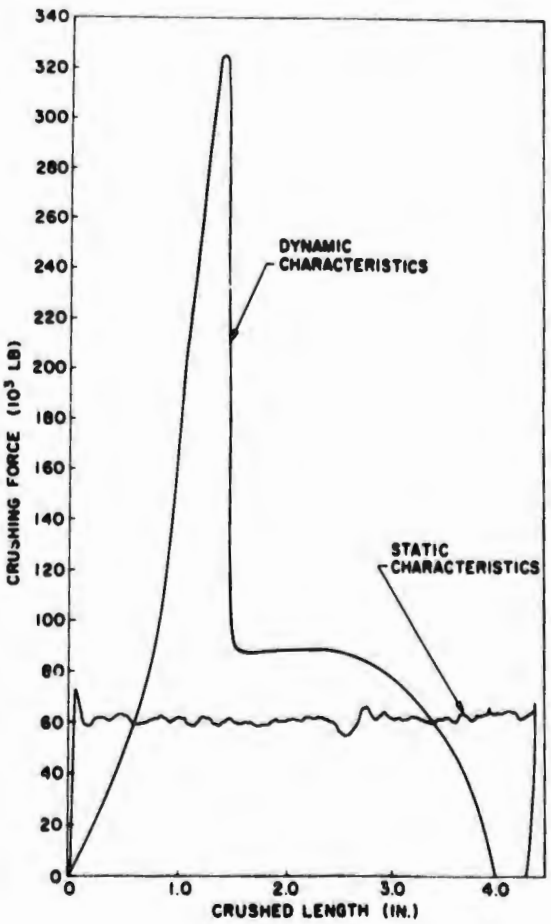

FIG. 4.75. Typical load deflection curve for aluminum honeycomb at impact velocities between 600 and 900 fps; sample about 1 ft in diameter and 6 in. thick. David [231].

charged to an initial smashing of the structure. This smashing destroys the bond of the material to the plate being impacted and occurs before the normal column-collapse effect has time to take place. In the particular tests reported, the after-test appearance of the samples showed about half smashing (or structural disintegration) and half column collapse.

Obviously an engineer's task is not finished until he analyzes relative costs and tries to maximize cost effectiveness. For the air-drop condition this was done by Turnbow and Steyer [232] with the highlights repeated in the summary reports [202,228]. Because of the cost efficiency achievable with paper honeycombs, it was suggested [228] that the optimum combination for air drop involved smaller parachutes (thus increasing impact velocity) and fairly extensive cushioning.

4.6.3.2. *Rigid Foams.* Some elasticity characteristics of rigid plastic foams were treated in section 4.6.2.2. This section will amplify the prior discussion, with particular emphasis on impacts with higher velocity than those encountered in normal package-cushioning work. As before, most of the data were collected on polystyrene and polyurethane foams.

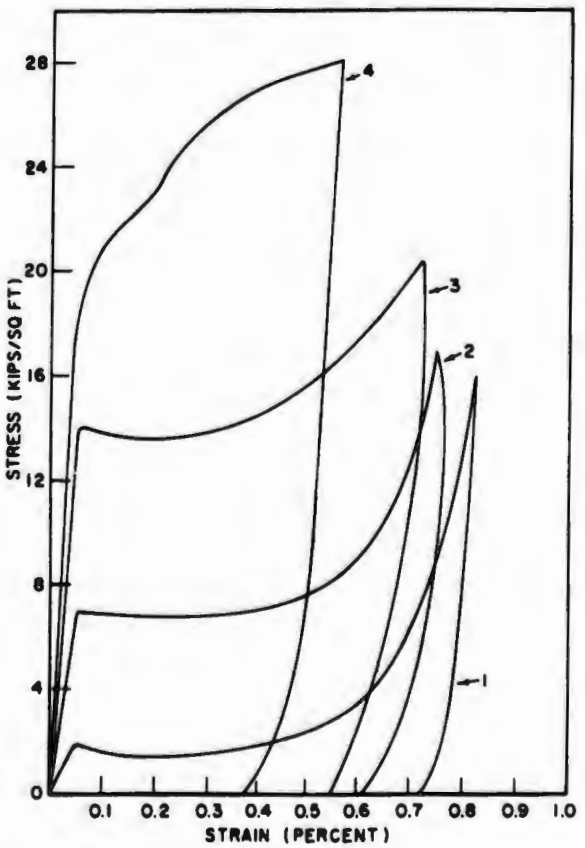

FIG. 4.76. Dynamic stress-strain curves for rigid polystyrene foams: (1) Lockfoam, 2.44 pcf; (2) styrofoam, 1.8 pcf; (3) styrofoam, 3.0 pcf; and (4) styrofoam, 4.5 pcf. Turnbow [233].

At air-drop velocities, polystyrene foams are strain-rate-insensitive. This conclusion by Turnbow [233] is not affected by Carr *et al.* [234] who found that both pulse shape and peak-pulse value affected response shape. Figure 4.76, a composite of several figures from Turnbow, shows dynamic stress-strain curves for a number of different densities. The Lockfoam material is somewhat more brittle than the styrofoams, but is capable of field expansion without special curing equipment. It shattered under impacts of about 60 fps. Except for Lockfoam, the polystyrene foams do not show the initial peak stress characteristic of honeycombs. Limiting maximum strains to 65 percent is recommended [226] in order to avoid danger of bottoming, since materials vary from batch to batch.

Some tests were run on rigid polyurethane foams specially formulated to permit field foaming. The results [235] are shown in Fig. 4.77.

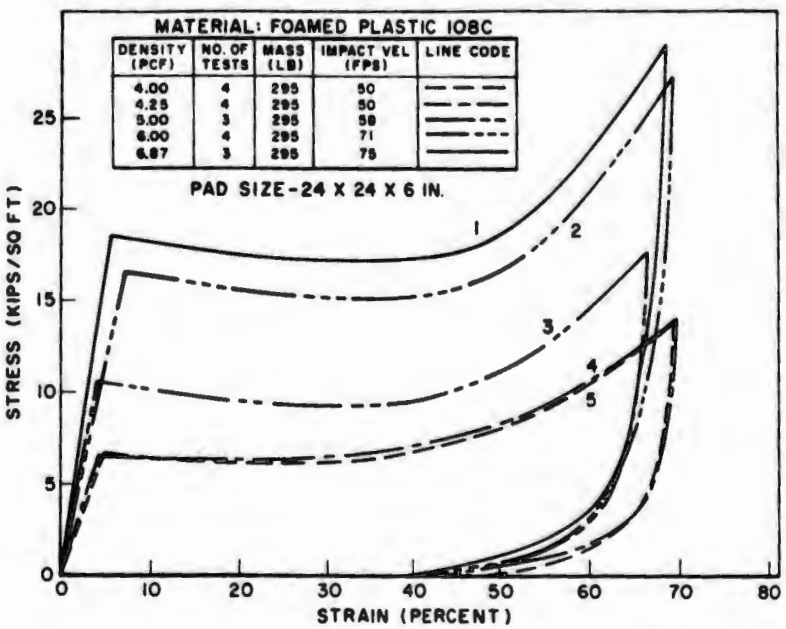

FIG. 4.77. Dynamic stress-strain curves for some rigid polyurethane foams: 1 – 6.87 pcf, 75 fps impact; 2 – 6.00 pcf, 71 fps; 3 – 5.00 pcf, 58 fps; 4 – 4.25 pcf, 50 fps; and 5 – 4.00 pcf, 50 fps. Shield and Covington [235].

Soper and Dove [33] examined some foamed metals and foamed organic or quasi-organic materials. Their results are shown in Fig. 4.78. Here, all impact velocities were on the order of several hundred feet per second.

Daigle and Lonborg [236] investigated a limited number of polystyrene foams and one polyurethane foam. Their results were similar to those previously reported. They also evaluated, in preliminary fashion, an epoxy foam and the same foam with vertical dowel pins. Results were

	Epoxy Foam	*Epoxy Foam with Dowel Pins*
Density, pcf	4.0	6.8
Energy absorbed, ft-lb/ft^3	7300	26,500
Crushing strength, psi	100	340

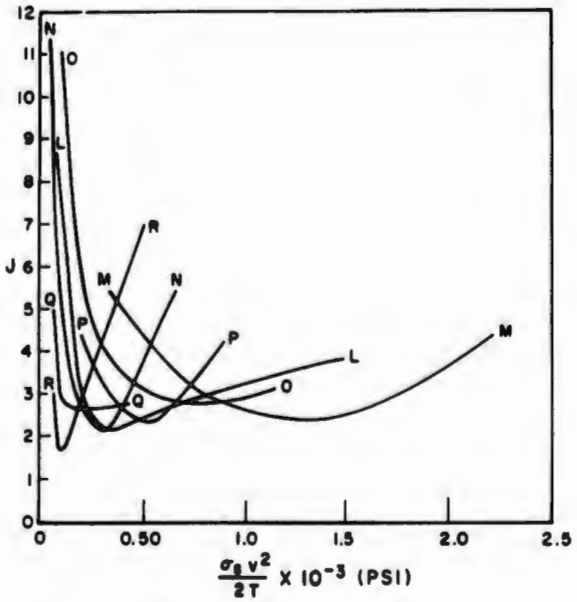

FIG. 4.78. Performance of some metallic- and organic-type foams; materials are identified in Table 4.19. Soper and Dove [33].

4.6.3.3. *Wood.* As is well known, wood will compress under stress. Some of the lighter woods, balsa for example, exhibit a light-weight cellular structure which opens up interesting possibilities in high-velocity work. Ali [210] shows a dynamic stress-strain curve for wood (38 pcf, species unidentified).

Daigle and Lonborg [236] evaluated various balsas and their results are shown in Table 4.20. Grain direction affects performance, as shown in Fig. 4.79.

Ali and Matlock [237] have considered devices in which a length of a wood board, such as a 2-foot long 1 × 4, is forced between shaped compressive jaws, thus compressing the material in a direction normal to the grain. Excellent results are obtained with these devices. Stevens [222] shows a wooden mandrel pushed into tubing.

4.6.3.4. *Tubular Structures or Devices.* Some results for tubular structures that are not, strictly speaking, cushions should be included at this point.

TABLE 4.20. AVERAGES OF PEAK AND MEAN CRUSHING STRENGTHS OF VARIOUS DENSITIES OF BALSA

Density (pcf)	*Peak Crushing Strength* (psi)	*Mean Crushing Strength* (psi)	*Ratio Peak-to-Mean Ratio* (%)
6.5-7.4	1689	1232	137.0
7.5-8.4	2080	1452	143.2
8.5-9.4	1460[a]	965[a]	153.3
9.5-10.4	2750	1624	169.3
10.5-11.4	3070	1780	172.5
11.5-12.4	3055[a]	1715[a]	178.2

[a]Low values believed due to insufficient testing.

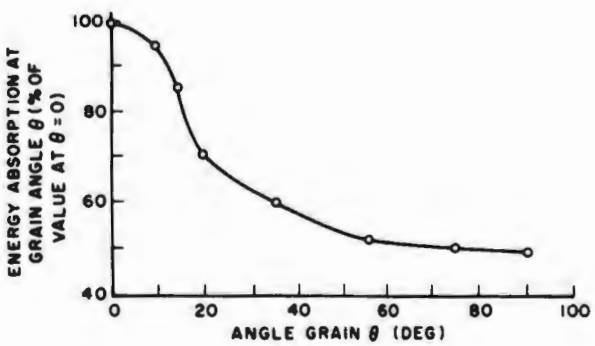

FIG. 4.79. Grain effects on shock-absorbing characteristics of balsa, with density and maximum deceleration held constant. Daigle and Lonborg [236].

Some typical dynamic stress-strain curves are shown in Fig. 4.80, taken from Morgan and Moore [238]. Two of the curves were obtained with cylinders filled with water which was forced out through holes drilled in the sides of the container. Empty food or beverage cans, used drums, *etc.*, could all be sources of material for field improvisation. Cans could also be used for absorbing the energy of point loads where, otherwise, excessive load-spreader structure might be required.

Kroell [239] has some interesting static data for a tubular shock absorber that literally turns itself inside out, thus making available a deflection twice the length of the capsule. One form of the device is shown in Fig. 4.81, while a typical static load deflection curve is shown in Fig. 4.82. Efficiency is obviously very high.

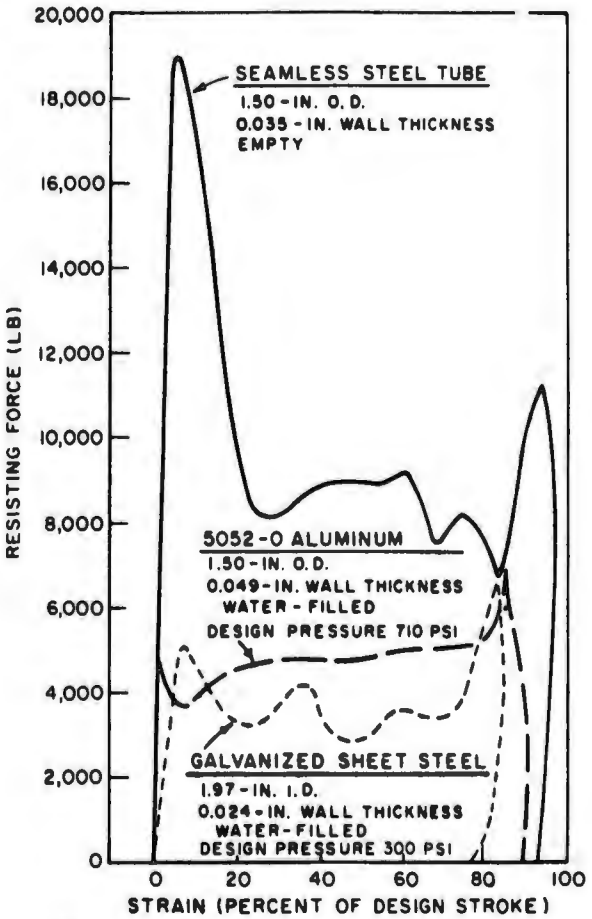

FIG. 4.80. Force strain curves for some tubing. Morgan and Moore [238].

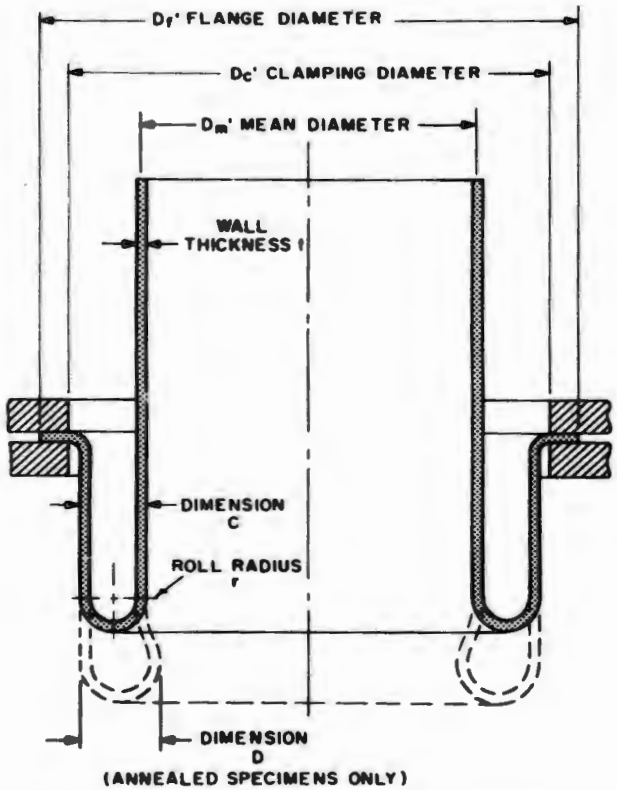

FIG. 4.81. One version of a rolling shock absorber. Kroell [239].

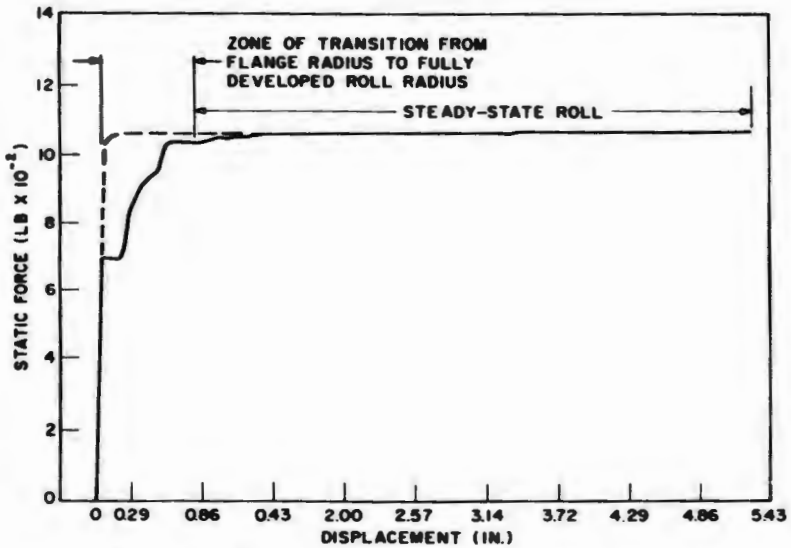

FIG. 4.82. Static force deflection curve for a rolling shock absorber; material was 3003-H14 aluminum alloy tubing with 1-3/4 in. OD and 0.035-in. wall [239].

Chapter 5

RESPONSE OF THE CUSHIONED OBJECT

Chapter 4 dealt with the peak acceleration that is developed at the interface between an object and a cushion while the other end of the cushion is undergoing a step velocity change. For rational design, as long as the object is completely rigid, it is enough to know the peak acceleration. Here is a paradox: a rigid object needs no cushioning. The blacksmith generates extremely high accelerations when he hits the anvil with a hammer, but neither object seems adversely affected.

But no object (including the anvil) is infinitely rigid. The cushion not only reduces the almost infinite acceleration resulting from a step velocity change but also modifies the time in which the original velocity change appears at the interface. We know instinctively that we must consider what the cushion does to the object.

This chapter will explore the little that is known on a mechanically complex subject. Plenty of theory is forthcoming, but very little has been so applied as to satisfy a designer's needs.

5.1. Fundamentals of Response

Consider one of the simplest possible cases, as shown in Fig. 5.1. This is a simplification of the general case of Fig. 2.1, with the system having only one degree of freedom while undergoing plane motion.

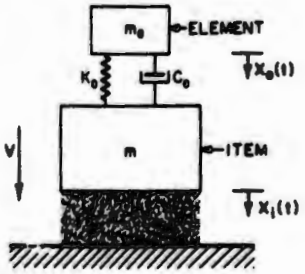

FIG. 5.1. Simple system shown at instant of contact with floor; cushioned item of mass m has an element of mass m_e supported by a linear spring with spring rate k_e and a viscous damper c_e.

The complete system hits the floor with a velocity V. Assume that the element and the item have the same velocity at the instant of impact. This is equivalent to assuming no oscillation of the element during the time of fall. This assumption is true if the system is initially at rest and the velocity change seen by the cushion is an impulsive motion of the base.

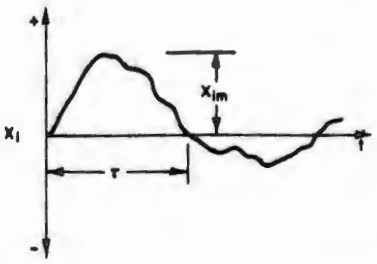

FIG. 5.2. Possible motion $x_i(t)$ of the mass m on its cushion.

The distance-*vs*-time function of the motion of the item—$x_i(t)$—is an initial pulse having magnitude, duration, and shape. The shape is characteristic of the cushion—its elasticity function and dimensions; the magnitude and duration are characterized by the cushion and the initial conditions at time zero, *i.e.*, the instant of contact with the floor. Figure 5.2 is the graph of a possible motion. At the end of the first pulse, $x_i(t)$ becomes negative and the whole assembly tends to rise from the floor. Whether or not rebound occurs, the item will oscillate about its equilibrium position until oscillation subsides. If m_e is negligible with respect to m, the amplitude and duration of each oscillation, as well as the total number of oscillations, will be a function of the damped-force deflection characteristics of the cushion.

Motion of the element will be triggered by the motion of the item. The motion of the element has the distance-*vs*-time function $x_0(t)$, and is characterized by the elasticity characteristics of the element—m_e, k_e, and c_e—and the input motion of the item.

In general terms,

$$x_r(t) = f[x_i(t)], \tag{5.1}$$

where $x_r(t) = x_0(t) - x_i(t)$ is the distance-*vs*-time function of the motion of the element relative to the item. Similarly,

$$\dot{x}_r(t) = f[\dot{x}_i(t)] \tag{5.2}$$

and

$$\ddot{x}_r(t) = f[\ddot{x}_i(t)] \tag{5.3}$$

are functional descriptors of relative output velocity and relative output acceleration.

Now generalize the problem so that there are many elements, each with its own elasticity characteristics, subjected to the motion $x_i(t)$. Figure 5.3 illustrates this situation. As long as the mass of each element is very much smaller than that of the whole system, the response of any one of them is governed by any one of the three prior functional relations. We can examine the behavior of one of them, and generalize from this one to the behavior of all.

Return to the simple system of Fig. 5.1. Suppose that the complete system is dropped from some height and that the cushion then produces an input pulse of maximum displacement x_{im}, whose duration is τ. Figure 5.4 is a very arbitrary graph of what a cushion might produce at the outer boundary of the cushioned item. Define the "shape" of this pulse as a geometric entity

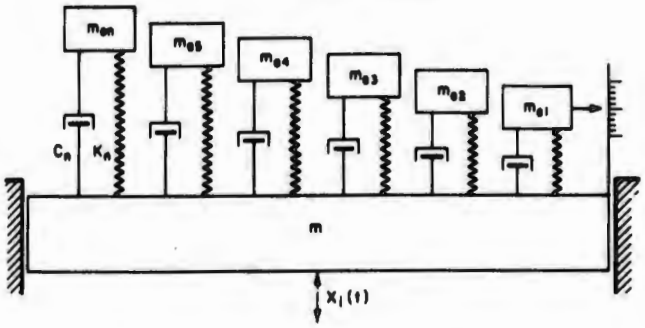

FIG. 5.3. A number of elements, each with their own spring and damping constants, contained in a cushioned mass.

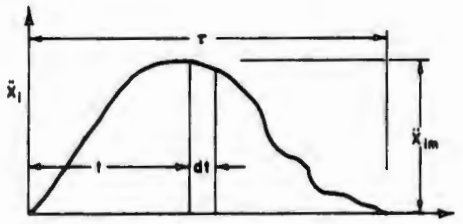

FIG. 5.4. A single input acceleration pulse.

which can be described in terms of pure number as a closed curve in the motion-time plane. Examples of this abstraction are triangles, arcs of circles, conic sections generally, or completely irregular closed curves, as in Fig. 5.4. Whatever the numerical or pure geometric character of this shape, it is dimensionless. Denote the quantitative measure of the shape of the pulse by S.

Since Fig. 5.1 describes all the factors influencing Eq. (5.1), dimensional analysis shows that

$$x_r(t) = f[x_i(t), S, \tau, m_e, k_e, c_e]. \tag{5.4}$$

There are seven variables to be accounted for in finding output motion as a function of input. There are, however, only three dimensions involved: mass, length, and time. According to Buckingham's Pi Theorem, Eq. (5.4) must be expressible in terms of four dimensionless groups. By definition, S is already dimensionless and, therefore, there are only three groups to find. To obtain answers in terms of motion, the ratio of output motion to input motion is one dimensionless group that should be used. Putting this on one side of the equation gives

$$\frac{x_r(t)}{x_i(t)} = f(S, \tau, m_e, k_e, c_e), \tag{5.5}$$

thus leaving two dimensionless groups to be found from the remaining four variables.

Critical damping, *i.e.*, that amount of damping which just stops an oscillatory response, is defined as $c_r = 2\sqrt{k_r\, m_r}$. The dimensionless element damping ratio can then be defined

$$\beta_r = \frac{c_r}{2\sqrt{k_r\, m_r}}. \tag{5.6}$$

The natural frequency of the element is also defined in terms of the circular angle subtended per unit time as

$$\omega_r = \sqrt{\frac{k_r}{m_r}} \text{ radians/sec.} \tag{5.7}$$

The term $\tau\omega_r$ is dimensionless and could be used. We may consider the pulse as half a period of oscillation about the equilibrium position. The natural period of this oscillation would be $2\tau = \tau_n$; hence, the natural frequency of the pulse is

$$\omega_p = \frac{\pi}{\tau}. \tag{5.8}$$

Substituting Eqs. (5.6) through (5.8) in Eq. (5.4) gives

$$\frac{x_r(t)}{x_i(t)} = f(S, \beta_r, \tau\omega_r) = f\left(S, \beta_r, \frac{\omega_r}{\omega_p}\right) \tag{5.9}$$

as the motional response of the element to the input pulse generated by the cushion.

For a given shape of pulse, S is a constant and Eq. (5.9) becomes

$$\frac{x_r(t)}{x_i(t)} = f(\beta_r, \tau\omega_r) = f\left(\beta_r, \frac{\omega_r}{\omega_p}\right). \tag{5.10}$$

If the pulse shape is constant and the element is undamped, then

$$\frac{x_r(t)}{x_i(t)} = f(\tau\omega_r) = f\left(\frac{\omega_r}{\omega_p}\right). \tag{5.11}$$

Evidently similar expressions exist for the velocity and acceleration ratios. Also, what is true at any time must be true for the maximum values of the input and output functions. Hence,

$$\begin{aligned} \frac{x_{rm}}{x_{im}} &= f(\beta_r, \tau\omega_r) = f(\beta_r, \omega_r/\omega_p), \\ \frac{\dot{x}_{rm}}{\dot{y}_{im}} &= f(\beta_r, \tau\omega_r) = f(\beta_r, \omega_r/\omega_p), \\ \frac{\ddot{x}_{rm}}{\ddot{x}_{im}} &= f(\beta_r, \tau\omega_r) = f(\beta_r, \omega_r/\omega_p). \end{aligned} \tag{5.12}$$

The same functional relations will hold for each element of the multi-element model (Fig. 5.3). If there were many such elements, all element responses over the frequency spectrum would be covered. For displacement,

$$R_{dn}(\omega) = x_{rm}/x_{im} \tag{5.13}$$

at all frequencies. For velocity,

$$R_{vn}(\omega) = \dot{x}_{rm}/\dot{x}_{im} \tag{5.14}$$

at all frequencies. For acceleration,

$$R_{an}(\omega) = \ddot{x}_{rm}/\ddot{x}_{im} \tag{5.15}$$

at all frequencies.

In the foregoing equations, the basic symbol $R(\omega)$ refers to any form of response spectrum. The first subscript to R denotes the kind of spectrum: d for displacement, v for velocity, and a for acceleration. A second subscript, invariably n, will be used when the spectrum is normalized, *i.e.*, expressed in dimensionless form.

We are indebted to Pendered's lucid exposition [240] for the line taken in the foregoing paragraphs.

Consistent with the foregoing notational convention, the non-normalized shock response spectra corresponding to Eqs. (5.13) through (5.15) would be written

$$\begin{aligned} R_d(\omega) &= x_{rm}, \\ R_v(\omega) &= \dot{x}_{rm}, \\ R_a(\omega) &= \ddot{x}_{rm}. \end{aligned} \tag{5.16}$$

In these cases, the input disturbance would remain a part of the functional statement. For example, at each element frequency,

$$x_{rm} = f(x_{im}, \beta_e, \omega_e/\omega_p) \tag{5.17}$$

would define the relative displacement functional relation.

As pointed out in chapter 2, the general functional relation covering the response of a system to an input excitation is given by Eq. (2.10). Where the input excitation $f_i(t)$ can be written as a deterministic function, explicit mathematical solutions to Eq. (2.10) can be obtained using the methods found in texts on differential equations; operational calculus, including the Laplace and Fourier transforms, is a useful tool. At present, this monograph will not deal with these methods in depth, but it will show a method usable on any arbitrary disturbance. In chapter 6, the use of Fourier's rule in computing transient behavior will be discussed.

Before covering response to a general excitation, it is convenient to analyze response to an impulsive disturbance, that is, a disturbance that jumps from zero to some finite magnitude and then returns to zero, all in an extremely short interval of time.

Let the simple system of Fig. 2.1 be at rest. At $t = 0$, apply an impulsive excitation such that

$$f_{ii} = \int_0^t f_i(t)\, d\, t. \tag{5.18}$$

Then Eq. (2.10) may be written

$$\ddot{\chi} + 2\beta\omega_n\dot{\chi} + \omega_n^2\chi = \omega_n^2 f_{ii}\delta(t), \tag{5.19}$$

where $\delta(t)$ is the Dirac-delta function defined in Eq. (3.30). Initial conditions are $\chi = \dot{\chi} = 0$ for $t < 0$.

At $t = 0$, there is a finite change in velocity. After $t = 0$ there is no further excitation and the system executes free vibration. To find the initial conditions for this free vibration, integrate Eq. (5.19) over a very short time interval t' using the given initial conditions. The result is

$$\dot{\chi}(t') + 2\beta\omega_n\chi(t') + \omega_n^2 \int_0^{t'} \chi dt = \omega_n^2 f_{it}, \tag{5.20}$$

since the integral of $\delta(t)$ is unity by definition.

Now, as

$$t' \to 0, \chi(t') \to 0$$

and

$$\int_0^{t'} \chi dt \to 0.$$

Hence $\dot{\chi}(t') \to \omega_n^2 f_{it}$. Accordingly, the initial conditions for the free vibration occurring after the impulsive excitation has passed are $\chi = 0$ and $\dot{\chi} = \omega_n^2 f_{it}$ at $t = 0$.

With these initial conditions, the solution of Eq. (5.19) which describes the free vibration is

$$\chi = \frac{\omega_n f_{it}}{\sqrt{1-\beta^2}} e^{-\beta\omega_n t} \sin \omega_d t, \tag{5.21}$$

where

$$\omega_d = \omega_n \sqrt{1-\beta^2}.$$

Figure 5.5 illustrates Eq. (5.21).

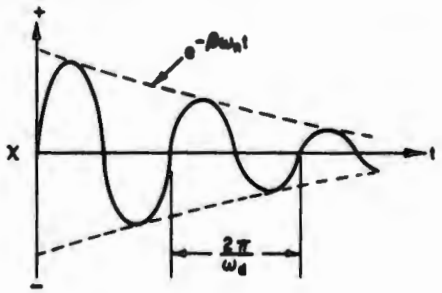

FIG. 5.5. Impulse response of a lightly damped system with one degree of freedom.

Define the impulsive response to a unit impulse as $h(t)$, such that

$$h(t) = \frac{\omega_n}{\sqrt{1-\beta^2}} e^{-\beta\omega_n t} \sin \omega_d t. \tag{5.22}$$

The response to the impulsive input f_{it} is then

$$\chi = f_{it}\, h(t). \tag{5.23}$$

If a unit impulse were applied at $t = \tau$ instead of $t = 0$, then the response would be $h(t - \tau)$, with $h(t - \tau)$ necessarily being zero for $t < \tau$.

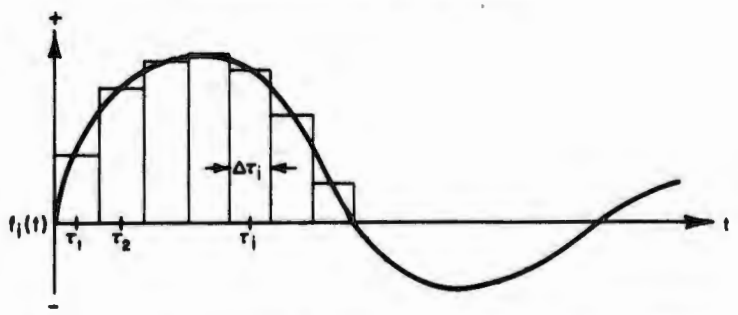

FIG. 5.6. Approximation of a pulse by a sequence of impulses.

Now consider the response to a general excitation, $f_i(t)$, as shown in Fig. 5.6. The continuous function $f_i(t)$ can be approximated by a series of impulses of magnitude $f_{it}\Delta\tau_i$. The change in velocity from each impulsive disturbance is independent of the displacement or velocity then existing and of any forces, such as the spring force, which may be acting at the time. Thus the response of the system to any one of the impulses is

$$\chi_i = f_{it}\Delta\tau_i\, h(t-\tau_i),\ i = 1, 2, \ldots, m. \tag{5.24}$$

Because of system linearity, the individual responses may be added to obtain

$$\chi = \sum_{i=1}^{m} f_{it}\Delta\tau_i\, h(t-\tau_i) \tag{5.25}$$

as the approximate response at $t = \tau_m$. Going to the limit as $\Delta\tau_i \to 0$, Eq. (5.25) approaches the integral

$$\chi = \int_0^t f_i(t)\, h(t-\tau)\, d\tau, \tag{5.26}$$

which, on substituting Eq. (5.22), may be written

$$\chi = \frac{\omega_n}{\sqrt{1-\beta^2}} \int_0^t f_i(t)\, e^{-\beta\omega_n(t-\tau)} \sin \omega_d(t-\tau)\, d\tau. \tag{5.27}$$

It is inherent in the derivation of Eq. (2.10) that the response and excitation functions must be compatible. In most cases, however, the output desired is relative motion, and the input is an acceleration-time function—usually the recording of an acceleration during some dynamic test. Nevertheless, bearing in mind that $\ddot{x}_i(t) = \omega_n^2 x_i(t)$, we can rewrite Eq. (5.27) as

$$x_r = \frac{1}{\omega_d} \int_0^t \ddot{x}_i(t)\, e^{-\beta\omega_n(t-\tau)} \sin \omega_d(t-\tau)\, d\tau. \tag{5.28}$$

This is the form generally used. It can also be seen that substitution of $F_i(t)/m$ for $\ddot{x}_i(t)$ in Eq. (5.28) permits computation of the relative response when the input excitation is a force applied to the base.

Equations (5.26) through (5.28) are various forms of the same integral, called Duhamel's integral. There are versions of this integral with additional

terms designed to take into account motion at $t < 0$, but these more complete versions are not needed here.

As can be seen from Eqs. (5.27) and (5.28), x_r is frequency-dependent. Concentrating on peak values from these equations, but generalizing to all frequencies, leads to the displacement spectrum defined in Eq. (5.16).

Note that the input disturbance in Duhamel's integral is buried under the integral sign, whence it cannot be conveniently extracted. For this and other reasons (including our desire to retain a simple relation between the various forms), shock-response spectra are normally defined mathematically as

$$\begin{aligned} S_d(\omega) &= x_{rm}, \\ S_v(\omega) &= \omega_e x_{rm}, \\ S_a(\omega) &= \omega_e^2 x_{rm}. \end{aligned} \tag{5.29}$$

In Eqs. (5.29) it must be recognized that the velocity and acceleration response spectra are generally not the true maximum responses. The velocity response maxima, for example, occur at other times than the displacement maxima, and damping further increases the discrepancy. This velocity shock spectrum is more properly called a pseudo-velocity spectrum. Acceleration response spectra from Eqs. (5.29) are exact if there is zero damping. Otherwise they may differ slightly.

Even though the responses may not be exact, they are usually good enough for practical purposes, and this is the form they usually take in the current literature.

We can also normalize the shock spectra of Eqs. (5.29). The usual way to normalize is to consider the reference excitation as the excitation which would occur if the peak value (displacement, velocity, or acceleration) had been reached very slowly. The equivalent static displacement can be found directly from Eq. (2.5) by omitting the transient terms involving $\ddot{x}_r$ and $\dot{x}_r$. The result is

$$x_{st} = \frac{\ddot{x}_{im}}{\omega_e^2} = \frac{m_e}{k_e} \ddot{x}_{im}. \tag{5.30}$$

For a drop test Eq. (5.30) may be written

$$x_{st} = \frac{\omega_c}{\omega_e^2} \sqrt{2gh}, \tag{5.31}$$

where ω_c is the natural frequency of the cushion.

Then the normalized shock spectra may be defined

$$\begin{aligned} S_{dn}(\omega) &= \frac{x_{rm}}{x_{st}} = \frac{\omega_e^2}{\ddot{x}_{im}} x_{rm} = A_m x_{rm}, \\ S_{vn}(\omega) &= \frac{\omega_e x_{rm}}{\dot{x}_{st}} = \frac{\omega_e^2}{\ddot{x}_{im}} x_{rm} = A_m x_{rm}, \\ S_{an}(\omega) &= \frac{\omega_e^2 x_{rm}}{\ddot{x}_{st}} = \frac{\omega_e^2}{\ddot{x}_{im}} x_{rm} = A_m x_{rm}, \end{aligned} \tag{5.32}$$

where A_m was called amplification factor by Mindlin [97].

It is clear that the magnitude of A_m depends on the shape of the input pulse when peak value is held constant. Some examples are given in Fig. 5.7.

Define

$$G_e = A_m\, G_m,$$

where G_e = equivalent static acceleration of the element response, and

G_m = maximum value of the disturbing acceleration.

A spectrum in G_e is synonymous with the acceleration shock response spectrum. This definition is the one used by Mindlin; the concept was first introduced by Biot [241].

Setting G_s as the safe value of acceleration for the element of the packaged article determined by static-strength test or by the usual static-strength calculations for materials, we obtain the criterion of successful shock absorption:

$$G_e = A_m\, G_m \leq G_s. \tag{5.33}$$

G_s is the static fragility rating of the material. This term may be somewhat misleading since the higher G_s is, the more durable is the article. Nevertheless, Eq. (5.33) shows that item fragility can never be completely separated from the performance of an individual cushion. Not understanding this fact—and thinking that the minimum contract design strength must be enough to withstand the maximum allowable dynamic shock—has caused more overdesign than bears thinking about.

Response spectra can be computed numerically from the dynamic stress-strain curve applicable to initial input conditions. The first step is to determine the acceleration-time history of the motion so that it can be substituted into Duhamel's integral.

It was shown in section 4.2 that the general equation of motion for velocity shock was

$$m\ddot{x}_i = mg - f(x_i), \tag{5.34}$$

where $f(x_i)$ is the load-displacement function. After integrating once, Eq. (5.34) becomes

$$\dot{x}_i^2 = 2gh - \frac{2}{m}\int_0^{x_i} f(x_i)\, d\, x_i. \tag{5.35}$$

Solve Eq. (5.35) for dt, remembering that

$$\dot{x}_i = \frac{dx_i}{dt}$$

and integrate. The result is

$$t = \int_0^{x_i} \frac{dx_i}{\dot{x}_i} = \int_0^{x_i} \frac{dx_i}{\sqrt{2gh - \frac{2}{m}\int_0^{x_i} f(x_i)\, dx_i}}. \tag{5.36}$$

This equation gives the time at which each deflection x_i occurs. By continuing the integration, we obtain the rise time t_m, that is, the time at which the peak acceleration occurs. If the pulse is symmetrical, doubling this time

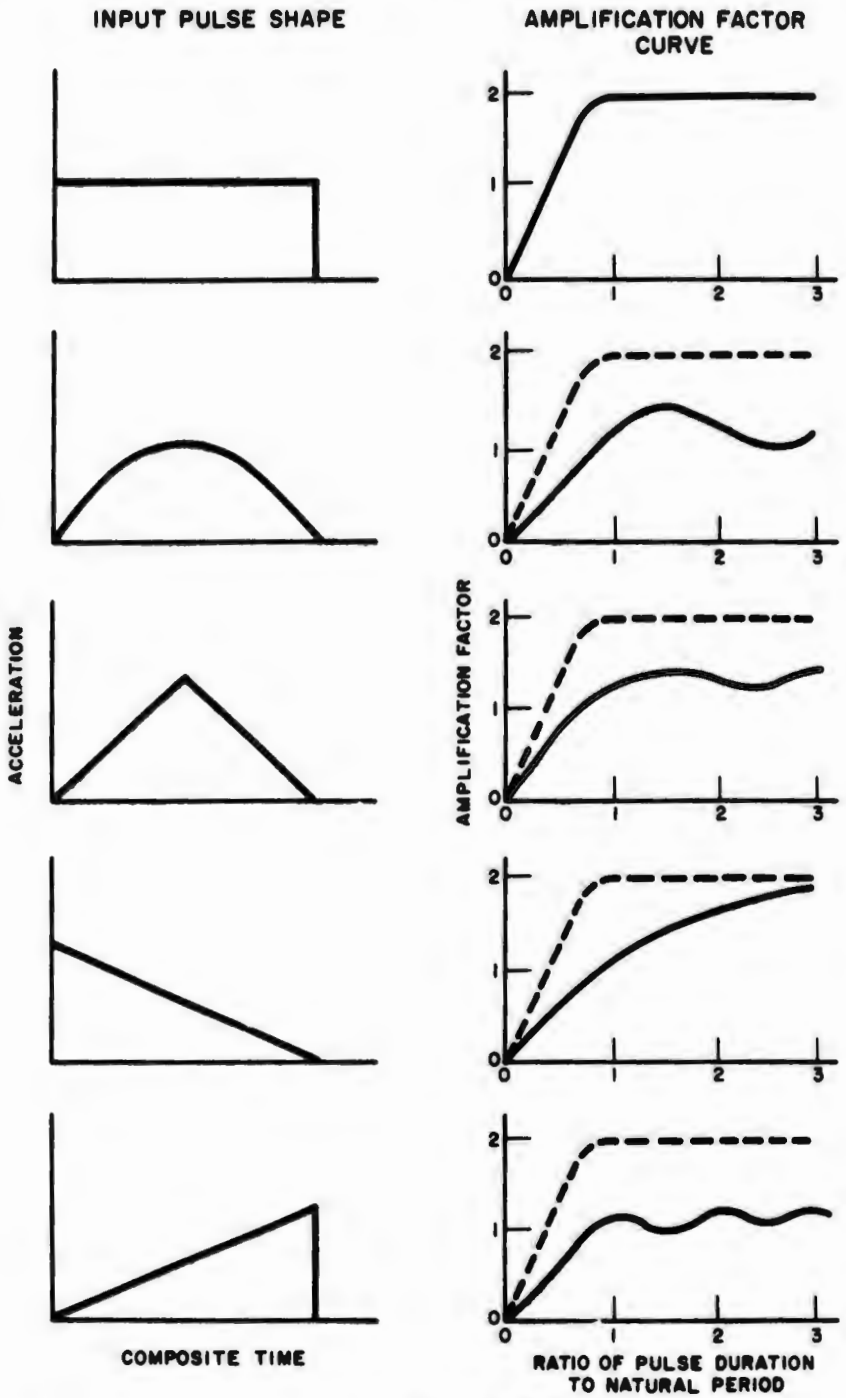

FIG. 5.7. Typical normalized shock spectra; dashed curves indicate why square wave can be considered the limiting case.

will give the total pulse duration τ. Otherwise, similar operations are conducted on the unloading curve; then simple addition will give pulse duration.

Mindlin [97] gives a concise numerical integration procedure, using mechanical quadrature, which gives both acceleration and time. The method (provided that some programming precautions are taken toward the end of the integration to avoid dividing by zero) is adaptable to machine computation and applicable to a pulse of any shape. Once t_m and τ are known, x_{rm} can be determined by taking these values as limits of integration in Duhamel's integral, Eq. (5.28).

Using the basic procedure just outlined, Mindlin [97] computed acceleration-time pulses for a number of different elasticity functions. Results for various values of the ratio of ϵ_b/ϵ_1 (see section 4.3) for undamped tangent elasticity are plotted in Fig. 5.8. The ordinate of the curve is the ratio of cushion acceleration to the acceleration which would have developed had the cushioning been linear, and the abscissa is the natural frequency for very small excursions (linear) multiplied by pulse duration. The curve for $\epsilon_b/\epsilon_1 \to \infty$ is the purely linear case. Ayre [242] compiled a number of response spectra for different input pulses.

Figure 5.8 promises an infinity of shock spectra for a nonlinear cushion. However, the optimum ratio of ϵ_b/ϵ_1 is identified in section 4.3 as 1.35. The pulse shape would then fall somewhere between the curves for $\epsilon_b/\epsilon_1 = 1.0$ and $\epsilon_b/\epsilon_1 = 2.0$. By concentrating on the spectrum for the shock pulse at optimum thickness and static stress, much useful information would be achieved at a considerable reduction in overall labor.

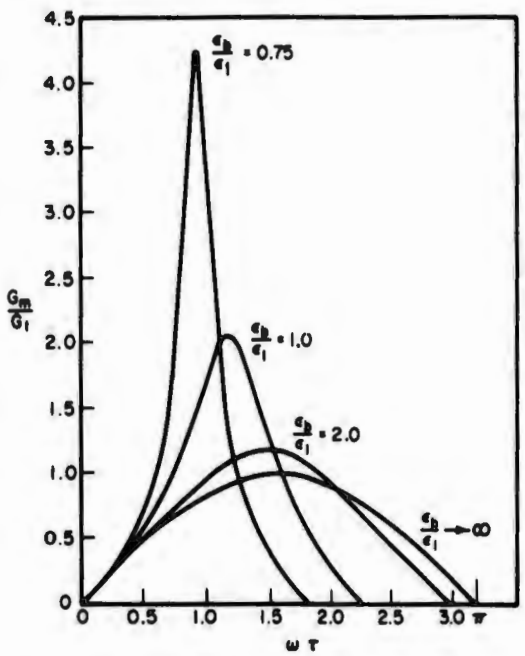

FIG. 5.8. Acceleration-time pulses for tangent elasticity. Mindlin [97].

Duhamel's integral is independent of the pulse shape. In certain cases this integral can be found in closed form without much trouble. Mindlin analyzed several of these cases and some of his results will be discussed later in this section. In most cases, however, the analyst proceeds directly from the measured acceleration-time record, or assumes a pulse of some arbitrary shape, and computes the shock spectrum directly using an analog or digital computer. Elegant mathematics is sacrificed to speed.

Several schemes exist for computing shock response spectra by analog computer. Rubin [243] has a diagram of operational flow, and Morrow and Riesen [244] developed a device specifically to compute shock spectra. More recently, Painter and Parry [245] describe an improved version using solid-state circuitry. In these devices the acceleration pulse is recorded on tape and then processed through the analyzer. Results are recorded and then the input parameters are changed. For each set of input parameters, the maximum output is recorded and the results are plotted as the shock spectrum.

Whenever a valid equation can be written it can be solved on a digital computer. Duhamel's integral can be so solved. O'Hara's method [246] consists of breaking Eq. (5.28) into pairs of recursion equations

$$\omega_e(x_r)_{n+1} = A_1\omega_e(x_r)_n + A_2(\dot{x}_r)_n + A_3(\ddot{x}_f)_n + A_4\Delta(\ddot{x}_f)_n,$$
$$(\dot{x}_r)_{n+1} = A_5\omega_e(x_r)_n + A_6(\dot{x}_r)_n + A_7(\ddot{x}_f)_n + A_8\Delta(\ddot{x}_f)_n, \qquad (5.37)$$

where $(x_r)_n = x_r$ at time t_n,

$(\dot{x}_r)_n = \dot{x}_r$ at time t_n,

$(x_r)_{n+1} = x_r$ at time $t_n + \Delta t$,

$(\dot{x}_r)_{n+1} = \dot{x}_r$ at time $t_n + \Delta t$,

$\Delta t = t_{n+1} - t_n$, usually taken in equal increments,

$$A_1 = a + \beta_e\, b,$$

$$A_2 = b,$$

$$A_3 = \frac{1}{\omega_e}(A_1 - 1),$$

$$A_4 = \frac{1}{\omega_e} \cdot \left\{\frac{1}{\omega_e \Delta t}[(1 - 2\beta_e^2)b + 2\beta_e^2(1 - a)] - 1\right\},$$

$$A_5 = -b,$$

$$A_6 = a - \beta_e b,$$

$$A_7 = -\frac{b}{\omega_e},$$

$$A_8 = \frac{A_3}{\omega_e \Delta t},$$

$$b = (e^{-\beta_e \omega_e \Delta t} \sin \omega_d \Delta t)\sqrt{1 - \beta_e^2},$$

$$a = e^{-\beta_e \omega_e \Delta t} \cos \omega_d \Delta t,$$

$(\ddot{x}_i)_n = \ddot{x}_i$ at t_n, and

$\Delta(\ddot{x}_i)_n$ = increment in $\ddot{x}_i$ in time period $t_n + \Delta t$.

It is understood that canned programs are available. Suitably small increments of time are selected, the test record is digitized (which can be done automatically) and the digitized data are fed to the computer. The output is plotted as the shock spectrum.

The simplest shock spectrum is that of a linear undamped element excited by the half-sine pulse characteristic of linear undamped cushioning examined by Mindlin [97]. By straightforward methods, it can be shown that

$$A_m = \frac{\omega_e/\omega_p}{\omega_e/\omega_p - 1} \sin \frac{2n\pi}{\omega_e/\omega_p - 1}, \quad 0 \leq t \leq \tau, \tag{5.38}$$

where n is a positive integer chosen to make the sine term as large as possible while the argument remains less than π.

After rebound, A_m is given by

$$A_m = \frac{2 \cdot \omega_e/\omega_p \cdot \cos \dfrac{\pi\omega_e}{2\omega_p}}{1 - \dfrac{\omega_e^2}{\omega_p^2}}, \quad t \geq \tau. \tag{5.39}$$

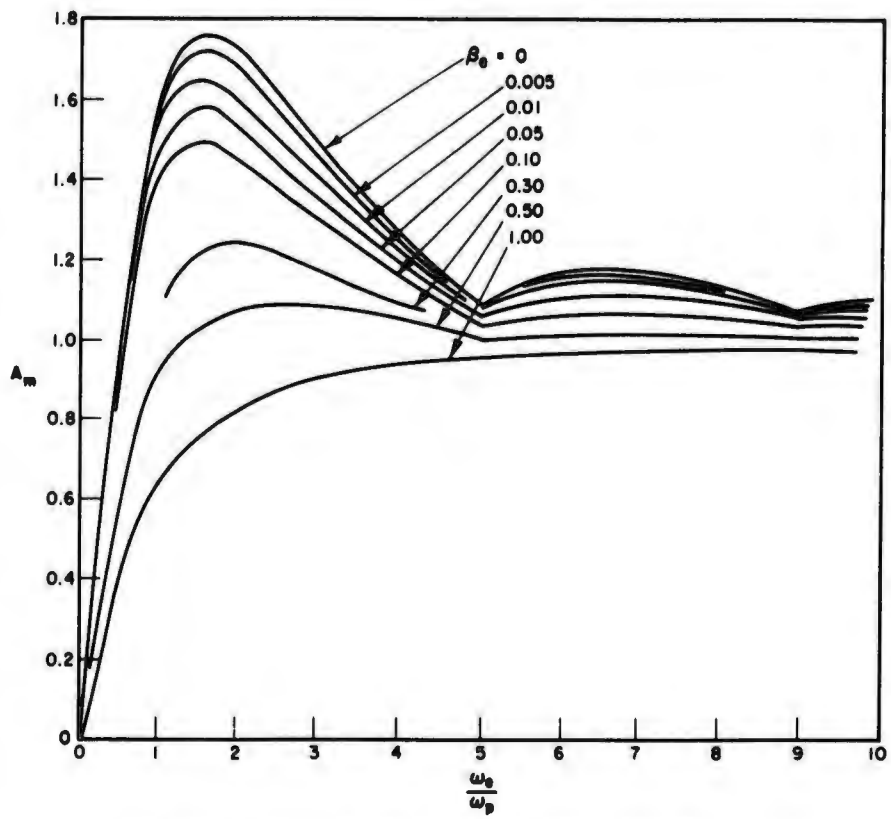

FIG. 5.9. Response spectra to half-sine input pulses [97].

For $\omega_e/\omega_p \leq 1$, Eq. (5.39) gives the larger value of A_m, while for $\omega_e/\omega_p \geq 1$, Eq. (5.38) gives the larger value. Figure 5.9 is a plot of the larger of the two values of A_m for various damping ratios. When impact duration is shorter than one half of the natural period of element vibration, maximum response occurs after the system has bounced. Element damping reduces A_m, whose peak value is 1.76 at $\omega_e/\omega_p = \pi/2$.

The undamped shock spectrum can be seen to be the worst-case response and is reasonably accurate for lightly damped elements.

Mindlin [97] also considered response spectra resulting from damped sinusoidal inputs. He plotted six families of curves, one for each of a selected value of cushion damping, with each family containing several values of element damping. To emphasize the effect of cushion damping on peak acceleration ratio, Crede [3] rearranged the plots for a single element damping ratio but with varying amounts of cushion damping. This latter plot is reproduced in Fig. 5.10. The high amplification is the result of resonant vibration of the element which is excited by the continuing transient vibration of the item on the lightly damped isolator. Note, however, that amplification is plotted as A_0 since Mindlin was careful to stipulate that his reference acceleration was not the maximum developed by the cushion but, rather, the maximum which would have been reached had the damping in the cushion been zero.

The curves presented so far have assumed that element mass is negligible compared to item mass. McCalley [247] points out, however, that mass will

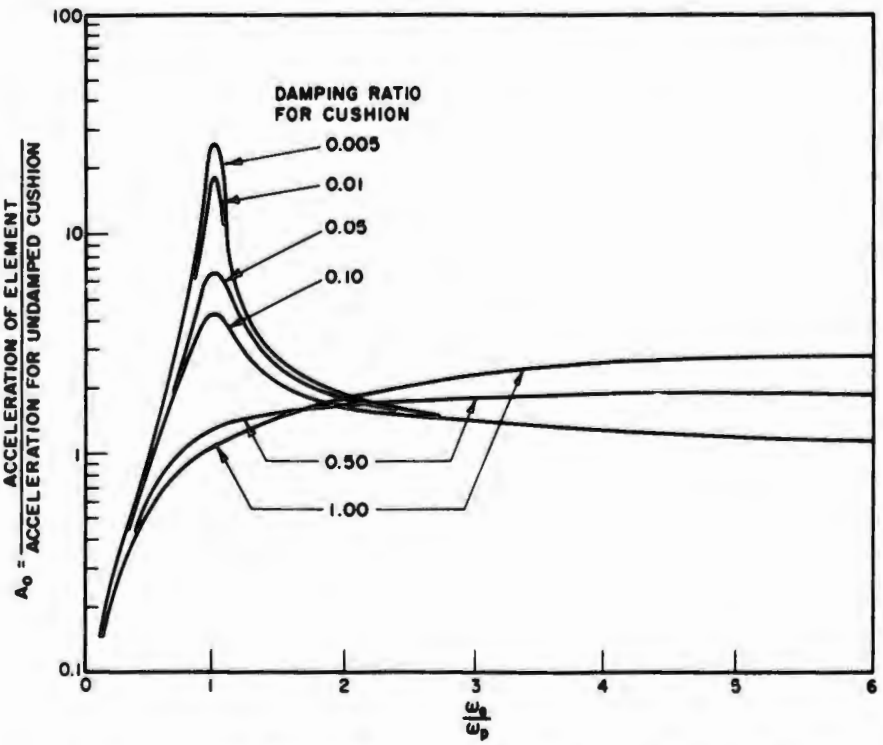

FIG. 5.10. Response spectra for damped sinusoidal input pulses. Crede [3].

affect the results actually achieved. As an example, maximum A_0 for a one percent-damped element on a one percent-damped linear cushion, as computed when element mass is neglected, is only 10; whereas Fig. 5.10 shows the actual amplification as 17.

The curves of Fig. 5.10 assume that there is no rebound. A necessary but not sufficient condition for rebound with linear elasticity has also been derived by Mindlin [97] as

$$G_m > 1 + \frac{m_3}{m}, \tag{5.40}$$

where m_3 is the total mass of the system, *i.e.*, object, cushion and outer container. Actually, acceleration on the rebound is the G_m that should be considered. Damping in the cushion strongly affects this value, as shown in Fig. 5.11.

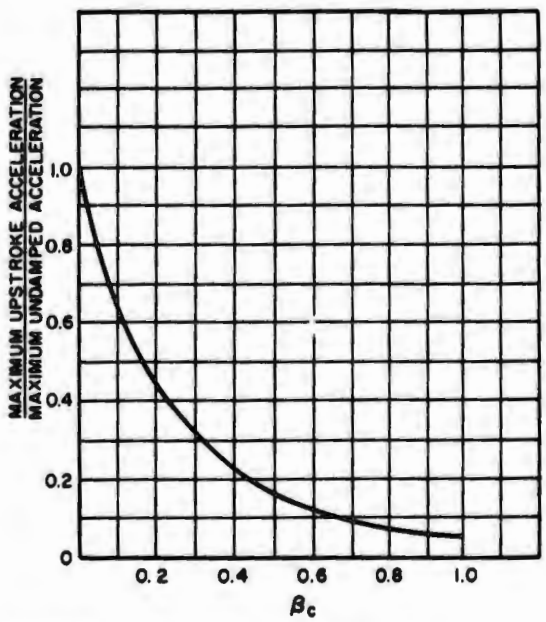

FIG. 5.11. Effect of cushion damping on maximum upstroke acceleration, linear elasticity. Mindlin [97].

5.2. Shock Spectrum Asymptotes

The behavior of shock spectra in general can best be illustrated by plotting several on one set of coordinates, as in Fig. 5.12 from Kornhauser [248].

Note that, for very long pulses, all the shock spectra, except that for the square pulse approach an asymptotic value of 1.0. This means that for long shock pulses the computations of section 4 are sufficient. The single exception, the square wave, rises quickly to its peak value of 2 and remains there. For all other undamped elements, the behavior is very similar. Where there is damping in the cushion, the secondary excursions of the A_m

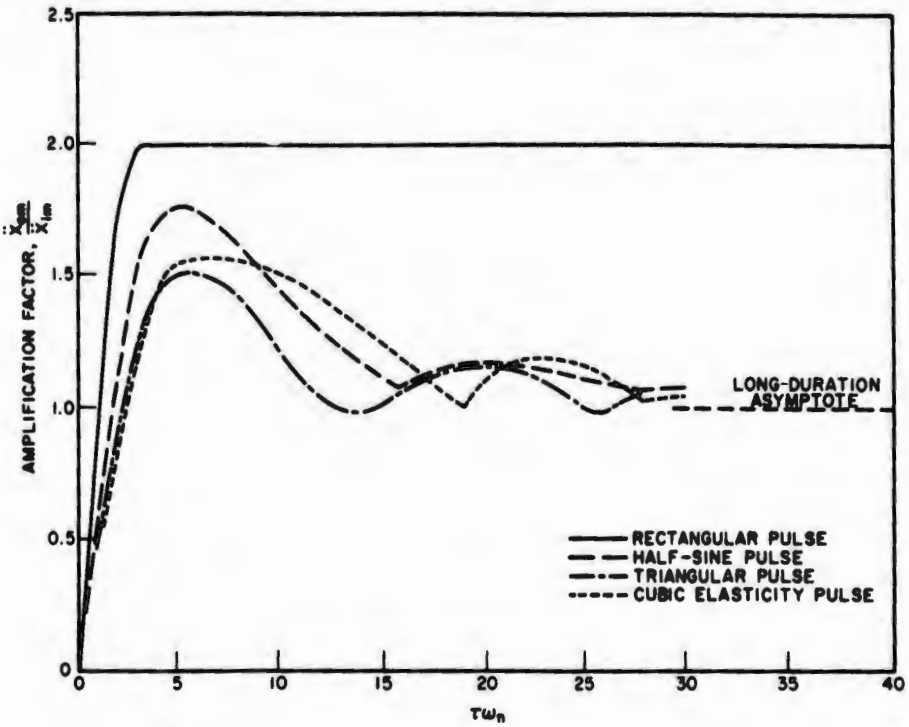

FIG. 5.12. Normalized shock spectra. Kornhauser [248].

curve disappear rapidly and the frequency ratio for which amplification becomes less than about 1.1 arises earlier. More important, however, the value of the asymptotic value of A_m tends to increase. Mindlin [97] examined this problem for various amounts of damping in a linear cushion. The value of the asymptote is 2.0 for a critically damped cushion. For more reasonable damping fractions, say 0.3 or less, the asymptote appears indistinguishable from 1.0.*

Thus, for all real systems the asymptotic value of A_m is 1.0, regardless of input pulse shape; this value is approximated for any frequency ratio roughly exceeding 8.0. This is useful not only in design engineering but also in investigating specific cushioning materials, since the computing procedure may be terminated after a reasonable number of frequency ratios have been checked.

At the other end of the shock spectrum, the amplification curve is linear to all intents and purposes. As noted by Mindlin, the initial slope of the amplification factor curve is directly proportional to the area under the acceleration-time curve. For instance, the slope in Fig. 5.9 is 2 when the input pulse is

*Unless Mindlin is very carefully read, the foregoing statement may appear incredible. In the curves plotted, however, he used as a reference input pulse the pure sine wave obtained from an undamped linear cushion and arrives at an asymptotic amplification factor of 4 for the critically damped linear cushion. One half of this amplification factor is due to the fact that the peak input acceleration from a critically damped cushion is twice the acceleration from an undamped cushion. There is no inconsistency.

a half-sine wave. The slope, on the same scale, for a square wave is π and for a triangular pulse is $\pi/2$.

In this region, say for $\omega_e/\omega_p \leq 1.0$, A_m can be estimated directly from

$$A_m = C\,\frac{\omega_e}{\omega_p}, \tag{5.41}$$

where C is 2.0 for a half-sine wave, $\pi/2$ for triangular, and π for rectangular.

This leads to an interesting consideration, first explored by Mindlin. For lightly damped elements, say $\beta_e \leq 0.10$, the amplification factor is given by

$$A_m = 2\,\frac{\omega_e}{\omega_p}. \tag{5.42}$$

Combining Eq. (5.42) with our criterion for failure of an element, Eq. (5.33) gives

$$2\,\omega_e\sqrt{\frac{2h}{g}} \leq G_s. \tag{5.43}$$

This may be written

$$f_e \leq \frac{1.1\,G_s}{\sqrt{h}}, \tag{5.44}$$

where f_e is the element natural frequency in cycles per second and h is the drop height in inches. In effect then, the element needs no cushioning, provided that its natural frequency meets the criterion of Eq. (5.44).

A physical reason for Mindlin's observation can be deduced. The undamped equation of motion for the simple system of Fig. 5.1 is

$$\ddot{x}_r + \omega_e^2\,x_r = -\,\ddot{x}_i(t). \tag{5.45}$$

Recalling that x_r is defined as the difference between x_0 and x_i, Eq. (5.45) can be written

$$\ddot{x}_0 + \omega_e^2(x_0 - x_i) = 0. \tag{5.46}$$

The acceleration solution, with the usual initial conditions, is

$$\ddot{x}_0 = -\,(\dot{x}_0 - \dot{x}_i)\,\omega_e \sin \omega_e t, \tag{5.47}$$

for which the maximum value is

$$\ddot{x}_{om} = (\dot{x}_0 - \dot{x}_i)\,\omega_e. \tag{5.48}$$

At $t = 0$, $\dot{x}_0 = \dot{x}_i$. For a true impulse $\dot{x}_0$ does not change during the excitation. Hence, $\dot{x}_0$ is the common velocity prior to impact, and $\dot{x}_i$ is the velocity following impact. The term $(\dot{x}_0 - \dot{x}_i)$ is, therefore, the change of velocity of the item during the excitation. Integrating the acceleration-time curve at the cushion-object interface, shows that the change in velocity is equal to the area under this curve. If this area is A_a, the peak output acceleration is

$$\ddot{x}_{om} = \omega_e A_a, \tag{5.49}$$

which may be written

$$\frac{\ddot{x}_{om}}{\omega_e A_a} = 1. \tag{5.50}$$

Crede [249] suggested that this idea be extended to longer pulses, and that the function

$$\frac{\ddot{x}}{\omega_e A_a} = f(\tau\omega_e) = f\left(\frac{\omega_e}{\omega_p}\right) \tag{5.51}$$

be plotted. Typical Crede spectra are shown in Fig. 5.13, which confirms the short-pulse relationship of Eq. (5.50). The main advantage claimed was that the effect of pulse shape on the spectrum was reduced materially as compared with the normal spectrum. This is true for short pulses and, to a lesser extent, for intermediate-length pulses. The behavior of long pulses is partly disguised by rapid approach of the spectra to zero.

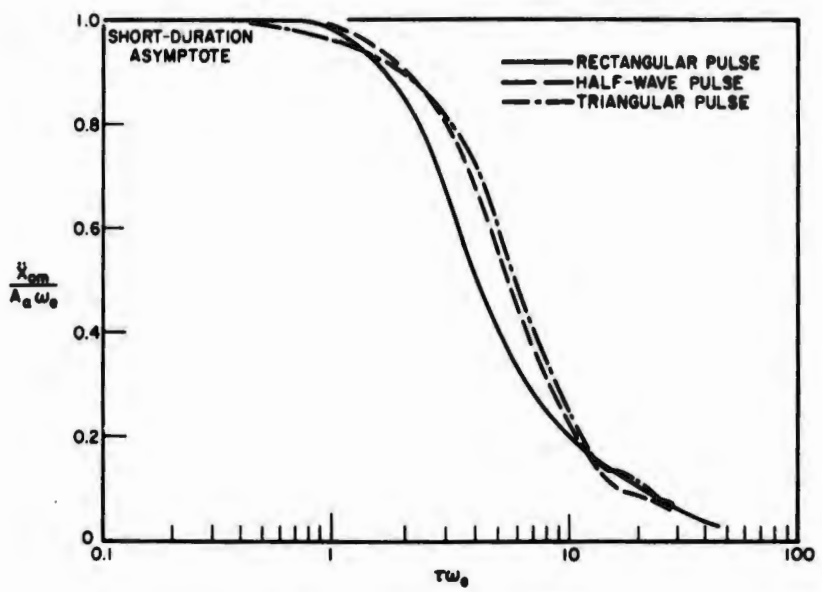

FIG. 5.13. Crede spectra [249].

For velocity shock, as in package testing, the velocity change can be directly related to impact and rebound velocities. Pendered [240] shows that

$$A_a = (1 + c_r)\sqrt{2gh} = (1 + c_r)V = V + V_r, \tag{5.52}$$

where c_r is the coefficient of restitution of the material* and V_r is the rebound velocity. Thus the ordinate on the Crede spectrum can be constructed without laborious integration of the acceleration-time function.

In particular, it should be noted that a "poor man's" Crede spectrum can be constructed with a minimum of calculation and effort. Where an article is damaged in test, the Crede-spectrum approach can show the way to logical corrective action.

*The coefficient of restitution is defined as the ratio of upward velocity to downward velocity in a drop test, being zero for inelastic materials and 1.0 for perfectly elastic materials.

Note that none of the plotted Crede spectrum curves rise above the asymptotic value 1.0. Hence [240]:

$$G_s\, g \geq (1 + c_r)\, \omega_e \sqrt{2gh}, \tag{5.53}$$

as a condition of no failure of an element. This reduces to

$$f_e \leq \frac{2.2\, G_s}{(1 + c_r)\sqrt{h}}, \tag{5.54}$$

which should be compared to Eq. (5.44). Mindlin's version is obviously a special case. The general case is independent of input pulse shape.

5.3. Damage Sensitivity

So far, we have considered two types of shock spectra: the conventional spectrum defined in terms of amplitude, duration, and shape; and Crede spectra based on area, duration, and shape.

Combine the variables of the general functional relation, Eq. (5.4), omitting the damping term. Then

$$\ddot{x}_{om} = f(\ddot{x}_{im}, S, A_a, m_e, k_e). \tag{5.55}$$

The output pulse is thus defined in terms of input peak value, shape, and area. These can be arranged in dimensionless form to write, for a given pulse shape,

$$\frac{\ddot{x}_{om}}{A_a \omega_e} = f\left(\frac{\ddot{x}_{om}}{\ddot{x}_{im}}\right). \tag{5.56}$$

Define the average height, $\ddot{x}_a$, of the input acceleration pulse such that

$$\ddot{x}_a = \frac{A_a}{\tau}. \tag{5.57}$$

Equation (5.56) can then be written

$$\frac{\ddot{x}_{om}}{A_a \omega_e} = \frac{\ddot{x}_{om}}{\ddot{x}_{im}} \cdot \frac{\ddot{x}_{im}}{\ddot{x}_a \tau \omega_e}. \tag{5.58}$$

Pendered's [240] plot of Eq. (5.56) for three different pulse shapes is shown on normal coordinates in Fig. 5.14 and on logarithmic coordinates in Fig. 5.15. (The term "damage-sensitivity" applied to the curves was coined by Kornhauser, see below.)

The slope of the line joining a point on one of the curves of Fig. 5.13 to the origin gives the term

$$\frac{\ddot{x}_{im}}{\ddot{x}_a \tau \omega_e}$$

and is thus a measure of pulse duration $\tau\omega_e$. On log-log paper, the inverse of this term is a series of logarithmically spaced lines oriented at 45 degrees to the main axes, and the slope of the inverse term can be read directly from the intercept of the appropriate line with the

$$\frac{\ddot{x}_{om}}{\ddot{x}_{im}}$$

axis.

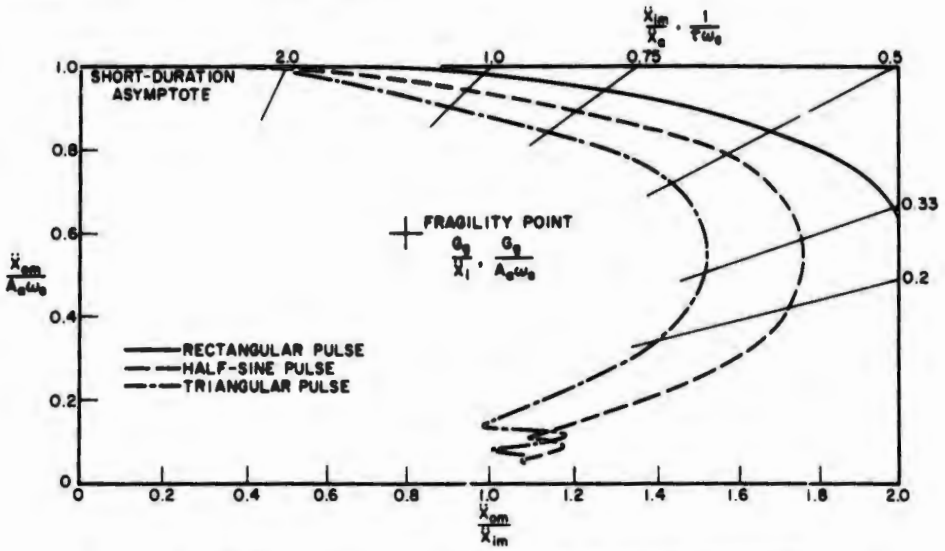

FIG. 5.14. Pendered's damage-sensitivity curves on normal coordinates [240].

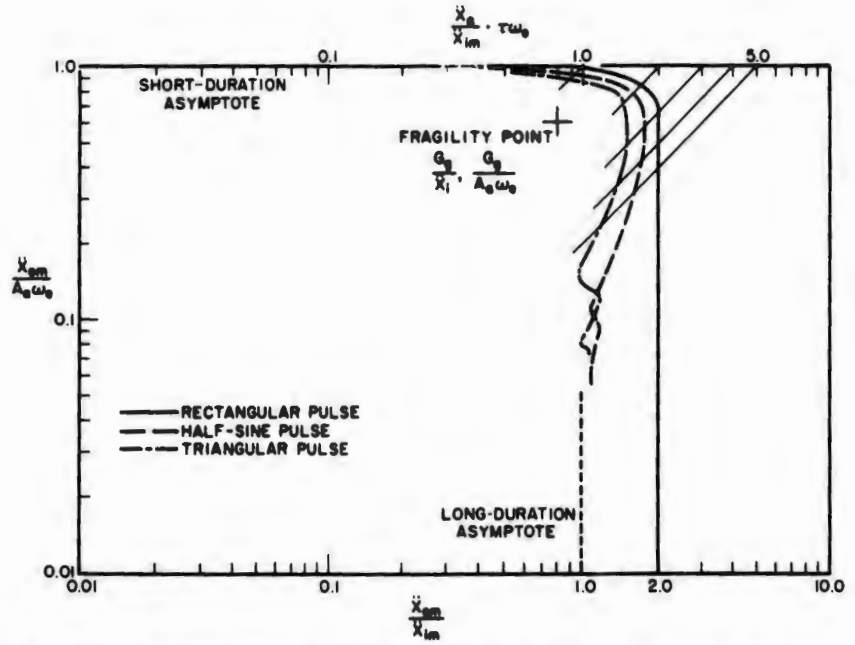

FIG. 5.15. Pendered's damage-sensitivity curves on logarithmic coordinates [240].

Note that, with the exception of the rectangular pulse, the curves display two asymptotes and that, even in the intermediate regions, the curves lie inside a narrow band.

Curves similar to Pendered's were first suggested by Kornhauser [248], who plotted the velocity change (pulse area) and average acceleration necessary to give a predetermined displacement to the system and called the

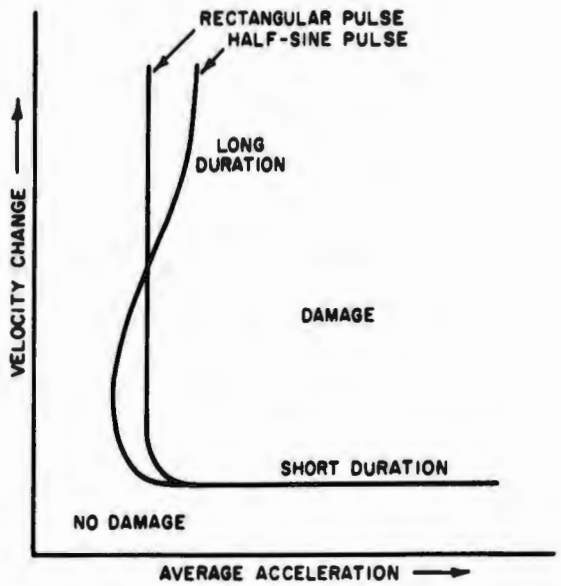

FIG. 5.16. Kornhauser's damage-sensitivity curve [248].

result a damage-sensitivity curve. This results in the type of plot shown in Fig. 5.16. It can be seen that Kornhauser's plots are, with minor exceptions, the inverse of Pendered's who considered Kornhauser's designation appropriate to his own curves.

Pendered goes on to note that, for defined pulse parameters, it is possible to plot a point with the coordinates

$$\frac{G_s g}{\ddot{x}_{lm}} \quad \text{and} \quad \frac{G_s g}{A_a \omega_e^2},$$

where G_s is static fragility of a given component. If (and only if) this point lies inside the sensitivity curve, damage will ensue. Note that the ordinate of the damage-sensitivity curve can be expressed as

$$\frac{\ddot{x}_{lm}}{(1 + c_r)\,\omega_e \sqrt{2gh}},$$

so that one axis of the spectrum can be computed quite easily.

Instead of plotting in terms of the velocity change of the pulse, one could plot in terms of the displacement across the cushion. This approach is recommended by Parfitt and Snowdon [250]. A typical plot from their work is shown in Fig. 5.17.

Parfitt and Snowdon note that, in those common cases where cushion displacement must also be limited, the most effective mount is one whose characteristic curve lies far from the origin: that is, the shock-acceleration ratio and cushion-displacement ratio are simultaneously small. In this connection, note the fine performance of the heavily damped linear mount as compared with a lightly damped linear mount and with stiffening and softening mounts exposed to a rounded velocity step.

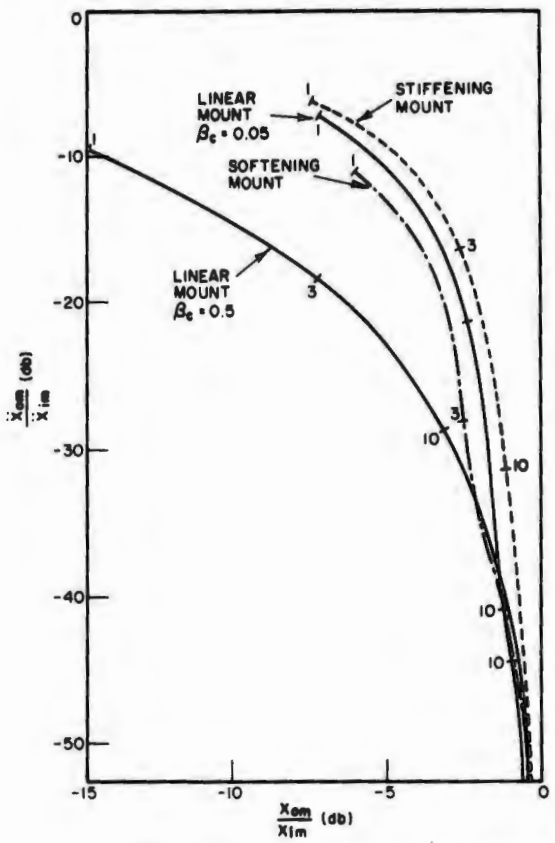

FIG. 5.17. Shock and deflection ratios for several mounts. Parfitt and Snowdon [250].

5.4. Permanent Deformation

In this monograph, prior discussions concerning fragility have all assumed that response as a function of displacement could be an adequate measure of the fragility of an item. This response was usually expressed as an acceleration. This seems reasonably valid for elements which could fail either as the result of fracture or by collision with adjacent components. Acceleration could, possibly, be a valid descriptor of damage sensitivity where failure is the result of permanent deformation of some element. But is it? The question assumed importance in the work at the University of Texas on cushioning for air drop because it was observed that failure in most vehicles was usually of the permanent-deformation type.

Ripperger and Fowler [251] have done work in this area. The details are in reports by Huckaby [252], Luke [253], Fowler [254], Reifel [255], and Richter [256]. The highlights are summarized in a final report by Ripperger [228] on the whole subject of impact sensitivity. Only the key results are given here.

Consider the small cantilever beam shown in Fig. 5.18. Assume that beam mass is negligible compared with tip mass and that relative tip displacements are small compared with length, so that rotational effects can be

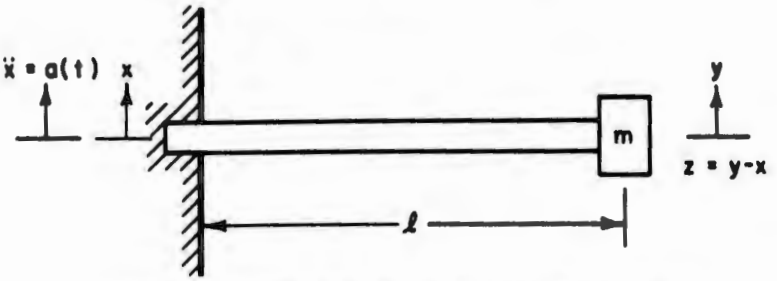

FIG. 5.18. Cantilever beam with a tip mass. Fowler [254].

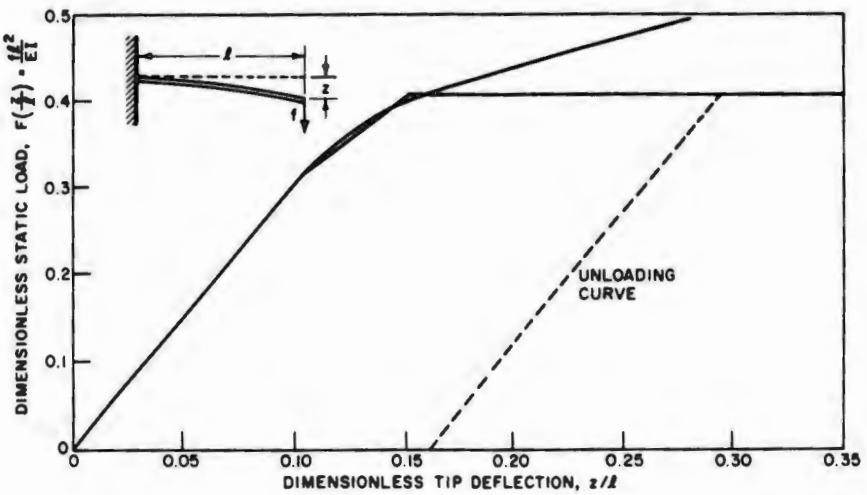

FIG. 5.19. Dimensionless static load *versus* dimensionless tip deflection for a mild-steel cantilever and corresponding straight-line approximation [254].

ignored. Internal damping of the beam is very small or non-existent so that strain-rate effects may be ignored. The stress-strain curve is the static-stress/strain curve for a mild-steel cantilever beam which, for purposes of the study, was approximated by three straight-line functions. The unloading curve is parallel to the loading curve up to the yield point of the beam. These latter assumptions are shown in Fig. 5.19.

Using dimensional analysis, Fowler developed the following functional statement for the permanent deformation of the beam

$$\frac{\delta_p}{\delta_y} = f\left(\frac{\ddot{x}_1 \tau^2}{\ell}, \frac{t_m}{\tau}, \frac{A_a}{\ddot{x}_a \tau}, \frac{\tau}{\tau_e}, \frac{\delta_y}{\ell}\right), \tag{5.59}$$

where δ_p = permanent deflection deformation,

δ_y = deflection at the yield point,

t_m = rise time to peak amplitude of $\ddot{x}_1$,

ℓ = beam length, and

τ_e = natural period of the beam.

Compare this relation with the general relation of Eq. (5.4); it can be seen that this is a special form of response function which, as before, takes into account the significant system variables of pulse shape and magnitude and the significant variables of the element.

These significant variables were then programmed into a computer and subjected to sixteen different pulse shapes, the first ten of which were variations of the triangular pulse with different rise times. The time peak varied from $t_m = 0$ to $t_m = \tau$. The latter is often called a terminal peak sawtooth pulse. The next five pulses were arbitrary forms of step functions, while the sixteenth was a shape closely simulating the pulse due to paper honeycomb.

The effects of individual groups on total response can be studied by keeping other groups constant. In this way, effects of rise time, pulse amplitude, element natural frequency and pulse duration were all studied theoretically, using a digital computer. For triangular pulses, the effect of rise time is shown in Fig. 5.20. Note that the peak value occurs at about $t_m = (\tau_e/4)$. This pulse approximates the first quarter period of a pure sine-wave pulse with natural period τ_e and will cause the most permanent deformation.

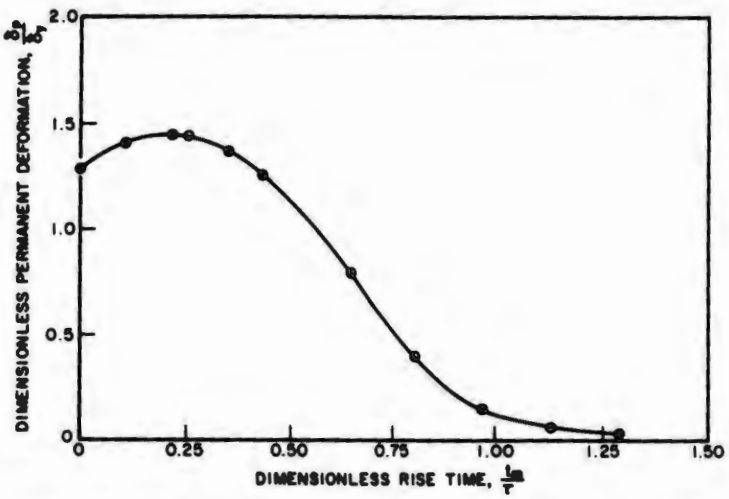

FIG. 5.20. Permanent deformation *versus* rise time for triangular pulses [254].

Three different pulses were selected in order to investigate the effect of pulse shape. The analytical results are plotted in Fig. 5.21. In the computed data, the rectangular pulse had the same values of $\ddot{x}_i$ and τ as did the triangular pulses, so that the velocity change was double. Measured results with a half-sine-wave pulse are shown in Fig. 5.22.

Considering the probable interaction of all variables, it can be seen that there should be a boundary between permanent deformation and no permanent deformation. Both the analytical and the experimental results confirmed the existence of this boundary. The experimental results are shown in Fig. 5.23. Note that the effects of $\ddot{x}_i$, τ, and l cannot be separated. For

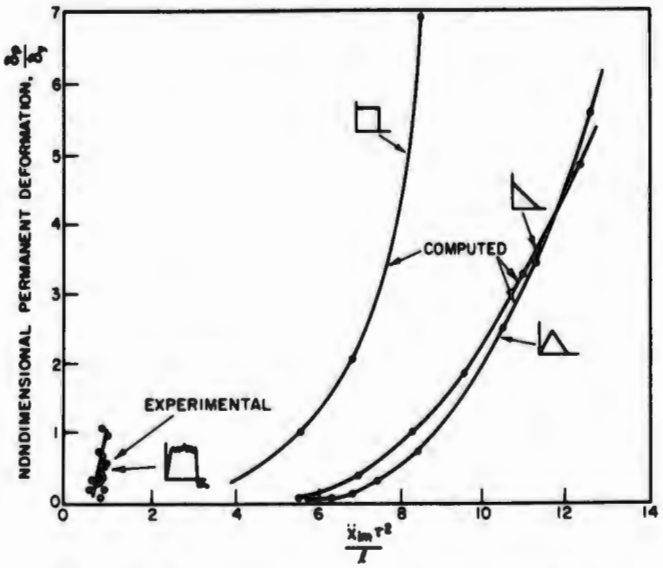

FIG. 5.21. Permanent deformation produced by three acceleration pulses [254].

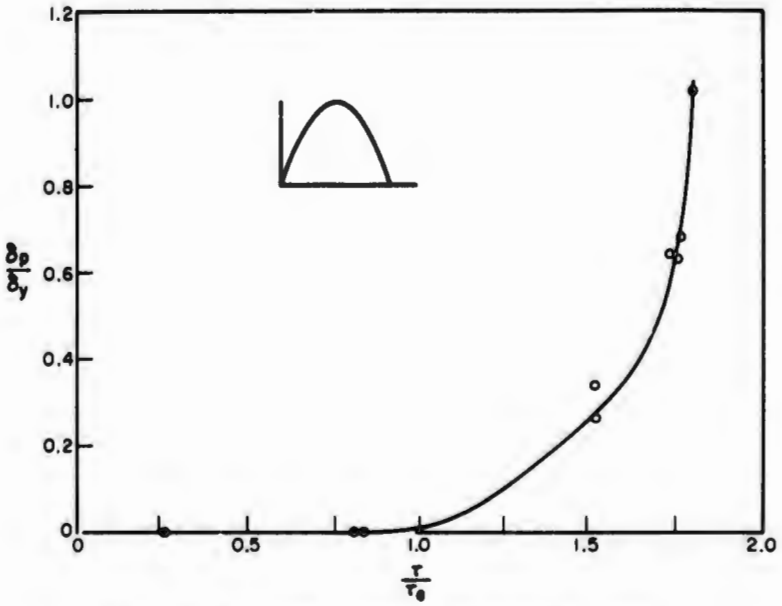

FIG. 5.22. Measured permanent deformations produced by a half-sine pulse [254].

a given pulse shape and a given beam, the permanent deformation increases as either $\ddot{x}_i$ or τ increases, after a certain minimum value of $\ddot{x}_i$ is exceeded.

Reifel [255] considered the effects of damping (in a more conventional spring-mass system) on the onset of permanent deformation. He found that sensitivity to permanent deformation of the spring is strikingly reduced by the introduction of damping in the element support system.

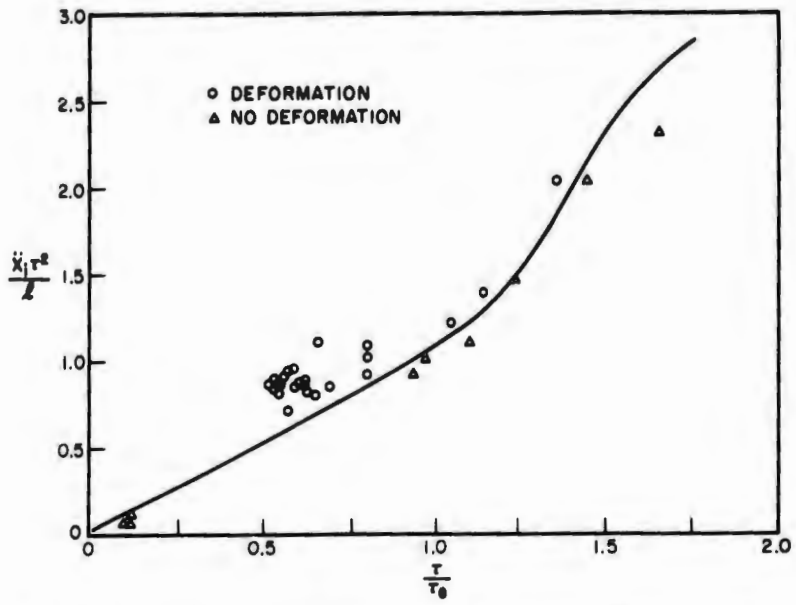

FIG. 5.23. Boundary between deformation and no-deformation regions [254].

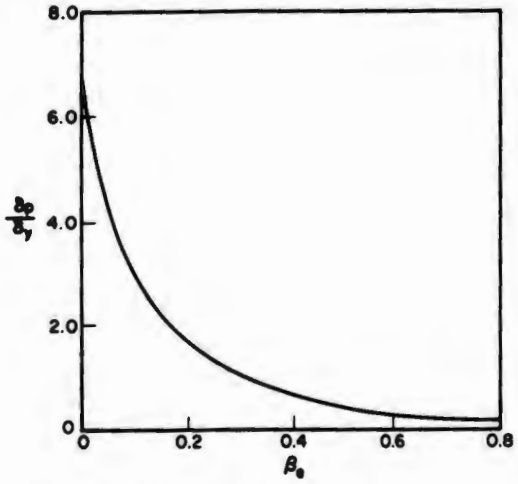

FIG. 5.24. Permanent deformation for a rectangular pulse with variable damping factor, $\tau/\tau_e = 1.287$; peak acceleration over yield force = 1.212. Reifel [255].

Figure 5.24 shows a typical result for a specific rectangular pulse with the percentage of critical damping varied. Figure 5.25 compares the effect of only 10 percent critical damping on a triangular pulse with $\tau/\tau_e = 1.287$. A reduction of 50 percent in the overall permanent deformation must be considered beneficial.

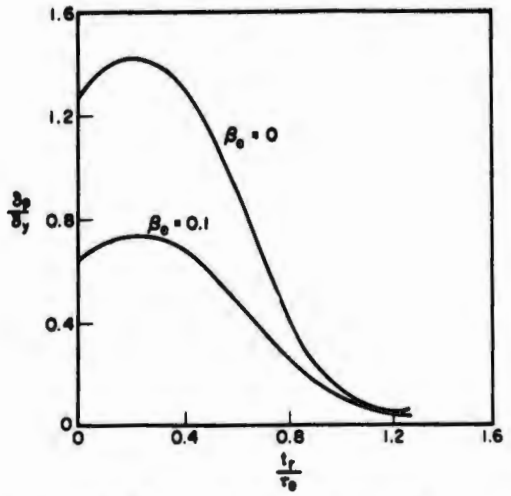

FIG. 5.25. Effect of second element damping on permanent deformation [255].

For triangular pulses, with amplitude and rise time fixed, permanent deformation seems to increase with pulse duration, indicating that permanent deformation is also affected by pulse decay time.

No correlation between conventional shock-spectra values and the amount of permanent deformation could be found. Actually, this result is not surprising since, in a shock spectrum, the element springs are assumed linear while these studies deliberately explored the plastic, nonlinear range. A shock spectrum can, at best, indicate the acceleration and forces which would be developed if the system were linear, undamped, and able to move without limit. As such, it can only indicate crudely whether permanent deformation is likely to occur. It cannot render a go/no-go verdict; it cannot be used when damage is measured by quantitative, permanent deformation. It is not a Rubicon that tells us to stop, before we have to cross it.

5.5. Collision

This section briefly discusses the possibility of collision between adjacent elements. Consider the system shown in Fig. 5.26. The rigid base is subjected to a shock motion in the direction shown, and the two masses respond to this motion. The distance between the two masses at any time is P. This distance is the static distance between the two masses plus the dynamic change Δ_c of this distance under excitation. P is called the proximity and Δ_c the proximity criterion. The ability of an excitation to create relatively large values of Δ_c is a measure of its ability to cause proximity failures, *i.e.*, failures by collision.

This concept is due to Schell [257,258], whose very recent efforts can only be briefly mentioned here. Schell points out that, while a complete history of the proximity criterion would be ideal, most investigators are more concerned with its extreme values, positive or negative. By restricting attention to extreme values and varying the frequencies of the element springs, the proximity-criterion concept is expanded to the proximity spectrum.

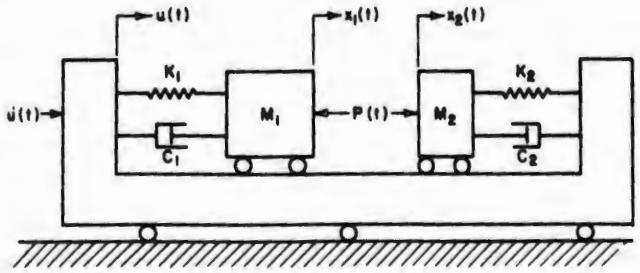

FIG. 5.26. Model used in deriving proximity spectra. Schell [257].

The proximity spectrum is a special form of response spectrum which—like the proximity criterion—depends not only on the element masses, springs, and damping, but also on the input-pulse shape. Figures 5.27 and 5.28 represent reasonably typical sets of results of a very extensive and complicated computing program. The ordinate is the difference Δ of the displacements of the two systems divided by the product of squared pulse duration τ^2 and the peak acceleration E_p of the input pulse. The abscissa is the normalized product of frequency f_2, of the second mass and pulse duration τ. Each curve is plotted for a separate value of normalized product τf_1, where f_1 is the frequency of the first mass.

Figure 5.27 is the undamped proximity spectrum for the terminal peak sawtooth excitation. This is a highly special case, which only involves algebraic addition of the individual shock spectra. The square-wave results, as shown in Fig. 5.28, are very much more complicated.

Both plots, however, show that the proximity spectrum becomes nearly constant at some value of f_2. They also show that when f_1 is small, the spectrum becomes nearly constant only when f_2 also is small. The basic reason for this phenomenon is that, as f_2 increases, the response of m_2 becomes smaller and smaller, eventually becoming substantially insignificant. Thus the entire proximity spectrum will be due to the response of m_1 at the frequency f_1.

In the square-wave plot, Fig. 5.28, there are peaks and valleys and sudden trend reversals. Schell recommends that the plots be separated into separate plots for separate values of τf_1, so that the results can be studied without built-in confusion.

Schell attributes these reversals, at least for the undamped case, to the fact that the maximum and minimum spectral values in the spectra occurring during the initial pulse and the free vibrational spectra occurring thereafter exhibit opposite trends. Thus, a point occurs on the curves where the one becomes greater or lesser than the other. Since the plots are only the maximum and minimum values without regard to the time when they occur, a sudden trend reversal results. Where the minimum curve departs from the maximum curve, minima occur during the initial pulse, but sudden changes in trends still occur. These changes can be explained by the following: (a) the minima occur at a time when the response of system 1 is zero,

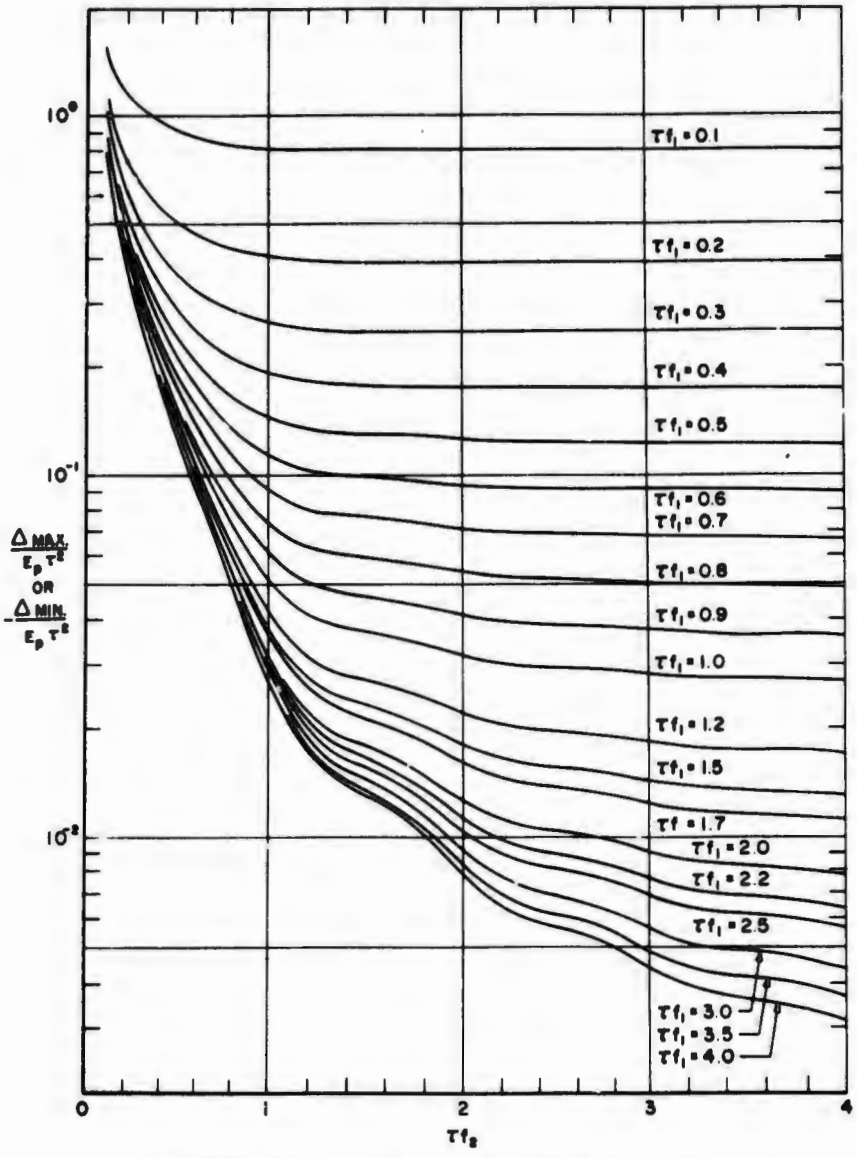

FIG. 5.27. Undamped proximity spectra for terminal peak sawtooth pulse [257].

and the response of system 2 is maximum, in which case the phase relationship is correct for producing the smallest of the possible minima for the two frequencies involved; (b) the phase relationship is such that the largest of the minima is produced; or (c) intermediate minima are produced.

The concept of a proximity spectrum is still too new to have been carried beyond the preliminary theoretical stages of investigation, so that its ultimate utility cannot be estimated at this time. Nevertheless, the proximity spectrum is one more tool for analyzing the damage potential of a given shock.

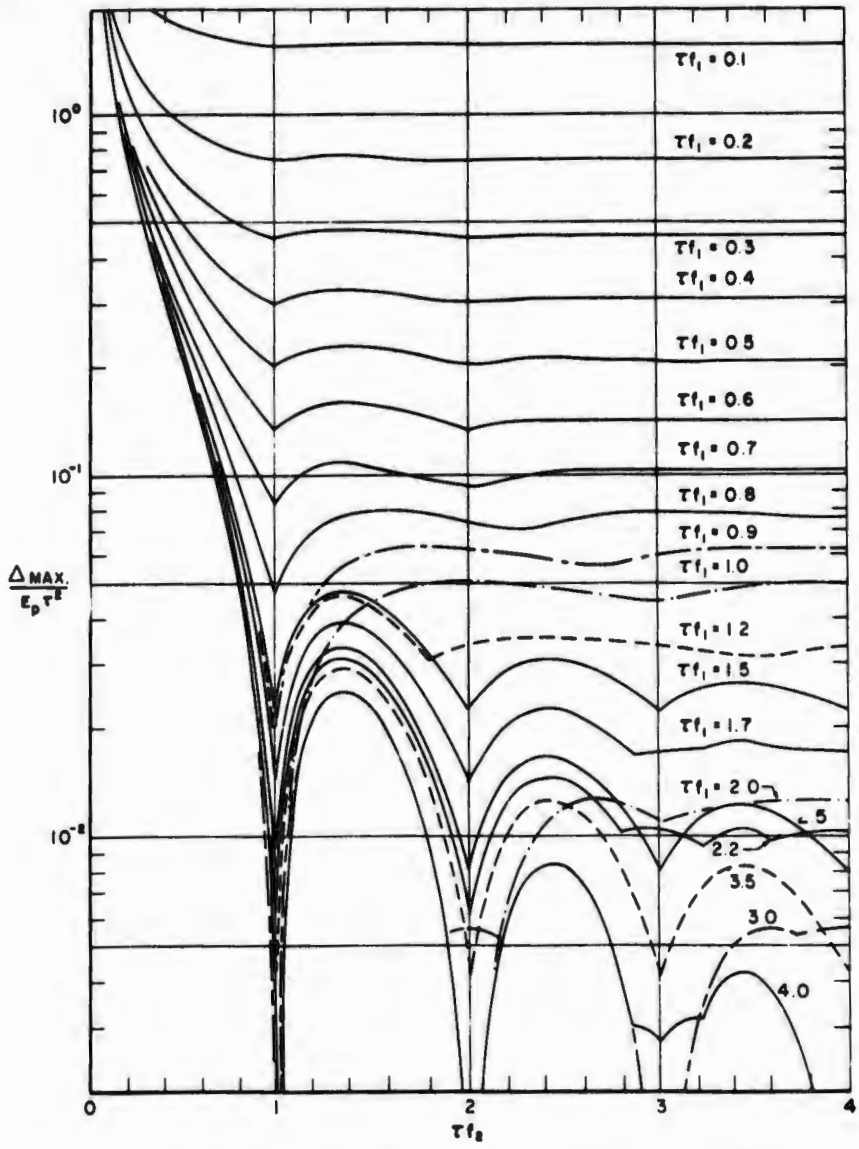

FIG. 5.28. Undamped proximity spectra for square-wave input [257].

5.6. Other Forms of the Shock Spectrum

For the most part, the shock and response spectra that have been shown are primarily limited to the zero-rebound case. There are other forms in which spectra may be reported or analyzed, depending on what is especially interesting at any time. These may be categorized into a few simple concepts:

1. (a) When the analysis gives two spectra, there is a spectrum of what occurs during the shock pulse ("initial" or "during" spectrum), and (b) a spectrum of what occurs afterward ("residual" or "after" spectrum). The

terms "during" and "after" were coined by Morrow [1]. As previously noted, the equations of motion for "after" spectra are dependent on whether the system has left the floor.

2. If the first part of the analysis concerns peak response of the element in one direction and the second part concerns peak response in the opposite direction, we obtain positive and negative spectra. This is of interest when the investigator knows that specific elements are more sensitive to disturbances in tension than to disturbances in compression. Normally, however, it is enough to know the absolute value of the peak response, regardless of the direction of the response. Negative spectra are important in analysis of proximity failure.

Finally, of course, there is no reason why response spectra cannot be computed for systems with several degrees of freedom. A typical situation which might be of particular interest is shown in Fig. 5.29. Morrow [1] defines the response of the second mass m_2 as the "second-order spectrum." He then shows how to derive its probable behavior, using simple rules that apply when

$$m_2 << m_1,$$

and

$$f_1 \neq f_2.$$

He suggests that applying these rules usually makes it unnecessary to compute second-order or (especially) higher-order spectra.

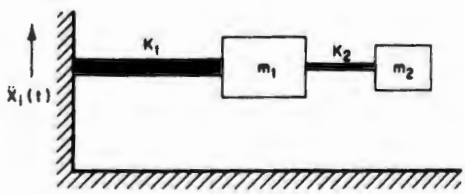

FIG. 5.29. Resonant member with two degrees of freedom.

Richter [256], however, has computed second-order spectra for half-sine, triangular, and rectangular pulses and an irregular pulse analogous to that produced by honeycomb. A number of different frequency and mass ratios were investigated. Some first- and second-order spectra are shown in Fig. 5.30. Note that the second-order spectrum becomes very similar to the first-order spectrum as k_2 increases with respect to k_1. When m_2 approaches m_1 (not plotted), first- and second-order spectra seem indistinguishable.

5.7. A Look at the Future

Writing in 1950, Walsh [4] said: "Cushion A is better than cushion B, in the large majority of cases, if A produces a lower spectrum than B." He was the first to state explicitly the importance of the shock spectrum in selecting optimum cushioning, although the idea is implicit in Mindlin's classic analysis.

This simple statement has recently led to some interesting theoretical studies of how to define the optimum isolator. Blake [259] reports the results of a mathematical search for the best possible load-deflection curve

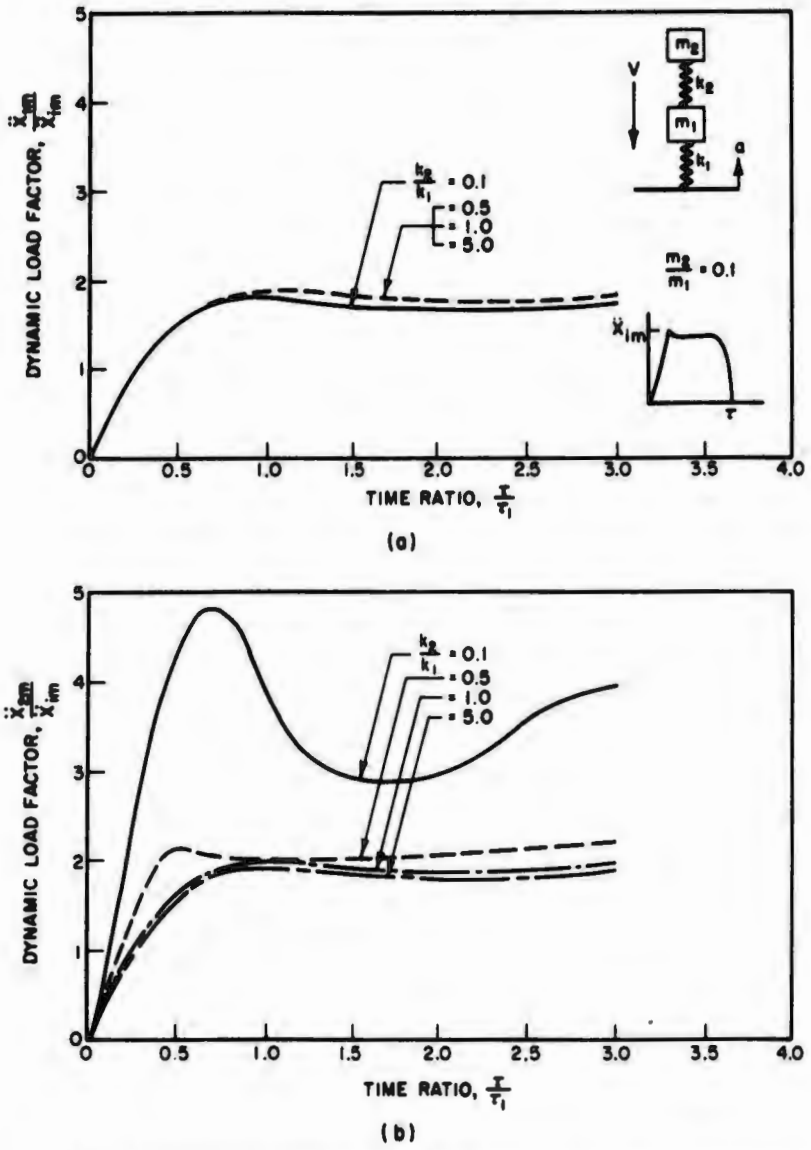

FIG. 5.30. Acceleration response spectra for an irregular pulse typical of paper honeycomb: (a) first-order spectrum, and (b) second-order spectrum. Richter [256].

that will describe an isolator in terms of the severity of transmitted shock. In making this approach Blake considered only the effects of a single pulse, but he considered that the vibratory components of response deserved greater emphasis than was attainable with a conventional shock spectrum. With these and still deeper considerations in mind, he has begun to discover some mount characteristics that seem optimal for certain pulsed inputs. Eventually, this should lead to an objective meaning of the "goodness" of a cushion and an estimate of how far cushions may be improved.

Liber and Sevin [260] have been considering an analogous problem, except that they considered inputs with strong reversals of stress direction, characteristic of ground shocks on hardened installations. So far, they have come up with answers somewhat different from those given by Blake's effort. They give an interesting definition of the optimum characteristics of the mount as a special problem in linear programming. This, it seems, has not previously been attempted in shock and vibration technology.

The use of linear programming leads to tradeoff limit diagrams, of which Fig. 5.31 may be considered typical. This procedure of plotting maximum acceleration ratio *versus* maximum displacement ratio was recommended by Parfitt and Snowdon [250] (see Fig. 5.17) for cases where both acceleration and space available are practical design constraints.

It is too early to predict whether either of the approaches just mentioned will produce anything usable on a day-to-day basis, especially since neither considers the character of real materials available today.

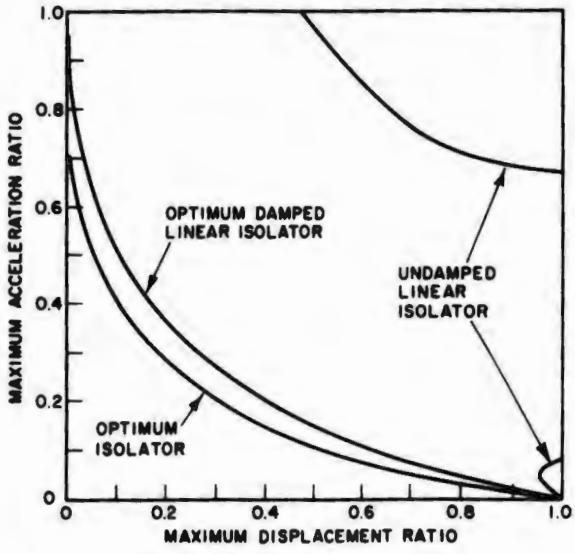

FIG. 5.31. Trade-off limit diagram for a particular input pulse. Liber and Sevin [260].

5.8. The State of the Art

The previous sections have shown that the problem of object fragility is really a problem of the fragility of key elements and that the subject of fragility cannot be separated from cushion performance. Further, it has been shown that the shock-response spectrum is one measure of cushion performance that is essential to rational design. Several specialized forms of the conventional shock spectrum have been introduced as improved methods of presenting cushion data. Two special forms of response spectra, one measuring permanent deformation and the other measuring susceptibility to collision among the elements, have been discussed.

With one exception, every curve presented was theoretical in character. This is a measure of the state of the art, and which may be described as all theory and no practice. Mindlin's classic monograph [97] stated almost twenty years ago that knowledge of three things was essential to rational design of cushions:

1. The magnitude of the maximum acceleration that the cushioning permits the packaged object to reach,
2. The form of the acceleration-time relation so that element response could be computed, and
3. The strengths, natural frequencies of vibration, and damping of structural elements of the packaged article.

As of today, we are only beginning to collect good data on the first of these.

There are many reasons why progress has been so slow. Walsh's remark (see "A Look at the Future") emphasizes the importance of filling the enormous gap in the area of shock spectra. It has been shown that one of the inhibitory factors in cushion shock spectral determinations is the vast number of curves that may be drawn for nonlinear materials. However, since an easy method of operating very close to optimum thickness and static stress has been shown, shock spectra computations could be confined to the optimum coordinates in the acceleration/static-stress plane. Considerable progress could then be made.

It has been shown that item fragility cannot be separated completely from cushion performance. After all, what is a cushion for? For simple structures, it might be possible to use specific test results, such as the square-wave decelerator discussed by Schuler [261,262]. Pendered [263] and Mindlin [97] also discuss the possibility of making centrifuge tests to evaluate static strengths of some elements, and vibration tests to evaluate natural frequencies. Such tests presented many difficulties. Pendered thinks that information qualitatively better than what is now being used could be derived from the shock tests that all equipment must undergo as a part of its qualification for service.

For really complex structures, it seems unlikely that practical designs—particularly package designs—will be based on valid element fragilities for a very long time. Even the extensive work at the University of Texas could not produce readily usable ways to determine objectively the fragility of reasonably simple structures—trucks, for instance. Ellis, Ripperger, and Thompson [229] conclude that some cut-and-try testing will always be inevitable. Availability of shock spectra, plus knowledge of the test failure, can reduce the number of experiments drastically.

But now the path has been shown; we have only to follow it.

Chapter 6

VIBRATION ISOLATION

The second main function of cushions is isolation of vibration. With very few exceptions, every object produced encounters vibration. Even a piece of furniture, which sits undistrubed in its final location, is vibrated during its journey from factory to owner.

The subject of vibration isolation—like the subject of shock—will be developed from basic principles. The information available concerning specific materials or problems will also be summarized.

6.1. Basic Principles of Vibration Isolation

The basic principles of vibration isolation can be found in almost any textbook on differential equations. In addition, Crede's exposition [3] is very lucid. Den Hartog [25] and Timoshenko [29] both give rigorous derivations, and McLachlan's short book [27] is a most valuable adjunct. Chapters 2 and 3 of the Shock and Vibration Handbook [26] are excellent refreshers.

Since this wealth of background information exists, the concepts needed to analyze vibratory systems will not be rigorously derived here. Instead, a brief review will be undertaken, chiefly to ensure consistent terminology. The lead given by Crandall [24] will be followed, since the concepts of random vibration and mechanical impedance and mobility follow logically from his approach.

The system considered is that shown in Fig. 2.2. Equation (2.10) is the general differential equation. The response sought is the absolute motion, x_0, of the mass m. According to Table 2.1, the generalized excitation $f_i(t)$ can be applied either to the mass, with the base immobile, or to the base.

Assume that the excitation is a simple harmonic function with frequency ω, amplitude A, and phase angle ϕ, such that

$$f_i(t) = A \cos(\omega t + \phi). \tag{6.1}$$

Equation (6.1) can be written in the form

$$f_i(t) = A^* e^{i\omega t}, \tag{6.2}$$

provided that only the real part of Eq. (6.2) is used and that the complex amplitude A^* is given by

$$A^* = A e^{i\phi}. \tag{6.3}$$

With the Eq. (6.2) excitation function, it can be shown that, in terms of the absolute output motion x_0, the complete solution to Eq. (2.10) is given by

$$x_0 = B^* e^{(-\beta\omega_n t + i\omega_d t)} + \frac{A^* e^{i\omega t}}{1 - \left(\frac{\omega}{\omega_n}\right)^2 + i2\beta\frac{\omega}{\omega_n}}, \tag{6.4}$$

where $\omega_d = \omega_n\sqrt{1-\beta^2}$ is the damped natural frequency.

The term involving B^* is the complementary function and the term involving A^* is the particular integral. Eq. (6.4) is evidently consistent with the overall solution requirement of Eq. (2.11). The term involving B^* is a free-vibration solution, with the value of B^* depending on the initial conditions. Note that a solution involving only free-vibration response to a particular form of disturbance is shown in Eqs. (5.18) through (5.21).

Where the input disturbance continues for a substantial time, the free-vibration term tends to zero, leaving only the steady-state term. Hence, the steady-state solution to Eq. (2.10) is given by

$$x_0 = \frac{A^* e^{i\omega t}}{1 - \left(\frac{\omega}{\omega_n}\right)^2 + i2\beta\frac{\omega}{\omega_n}} = \frac{f_i(t)}{1 - \left(\frac{\omega}{\omega_n}\right)^2 + i2\beta\frac{\omega}{\omega_n}}. \tag{6.5}$$

Note that the absolute response is the input function divided by a quantity related to the natural frequency and damping of the cushion.

The dimensionless ratio of the steady-state output to the steady-state excitation is called the complex frequency response, or the complex magnification factor, and is expressed as

$$H(\omega) = \frac{x_0}{f_i(t)} = \frac{1}{1 - \left(\frac{\omega}{\omega_n}\right)^2 + i2\beta\frac{\omega}{\omega_n}}. \tag{6.6}$$

For the force-excitation case, $H(\omega)$ is the complex ratio of the force in the spring to the exciting force. $H(\omega)$ is also the ratio of dynamic displacement to static displacement from an exciting force that is applied very slowly. For the motion-excitation case, $H(\omega)$ is the complex ratio of the force in the spring to the inertia force that would be imposed on the mass if it were rigidly attached to the moving foundation.

The absolute value of $H(\omega)$ is

$$H = |H(\omega)| = \left\{\left[1 - \left(\frac{\omega}{\omega_n}\right)^2\right]^2 + \left[2\beta\frac{\omega}{\omega_n}\right]^2\right\}^{-1/2} \tag{6.7}$$

H is called the magnification factor throughout this monograph. The omission of "complex" signifies absolute value. The value of H depends on frequency. Figure 6.1 shows the relationship. Damping reduces H at all frequencies.

In many applications, the engineer is interested in other ratios. For instance, complex transmissibility,

$$T(\omega) = \left[1 + i2\beta\frac{\omega}{\omega_n}\right]\left[1 - \left(\frac{\omega}{\omega_n}\right)^2 + i2\beta\frac{\omega}{\omega_n}\right]^{-1}. \tag{6.8}$$

In the force-excitation case, $T(\omega)$ is the complex ratio of the force transmitted to the foundation by the spring and dashpot to the exciting force. For the

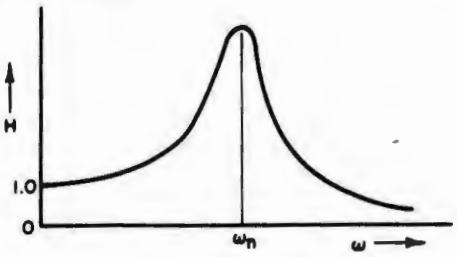

FIG. 6.1. Typical magnification-factor curve for a lightly damped system.

motion-excitation case, it is the ratio of the absolute displacement of m, x_0, to the input displacement, x_i.

Again—omitting "complex"—the absolute value of $T(\omega)$ or transmissibility, is

$$T = |T(\omega)| = \left\{\left[1 + 2\beta\frac{\omega}{\omega_n}\right]^2\left[\left(1 - \frac{\omega^2}{\omega_n{}^2}\right)^2 + 4\beta^2\frac{\omega^2}{\omega_n{}^2}\right]^{-1}\right\}^{1/2}. \tag{6.9}$$

Note that magnification factor and transmissibility are related to one another by a single factor such that

$$T(\omega) = \left(1 + i2\beta\frac{\omega}{\omega_n}\right) \cdot H(\omega) \text{ (for complex values)},$$

and (6.10)

$$T = \left(1 + 2\beta\frac{\omega}{\omega_n}\right) \cdot H \text{ (for absolute values)},$$

so that magnification factor and transmissibility are equal if, and only if, the system is undamped. Figure 6.2 shows transmissibility *versus* frequency for the systems of Fig. 2.2 where the forcing function is harmonic.

For the undamped case, transmissibility reaches its maximum when $\omega/\omega_n = 1.0$ and at a frequency ratio always less than unity when the damping ratio is greater than zero. By differentiation of Eq. (6.9) we obtain

$$\left.\frac{\omega}{\omega_n}\right|_{T=max} = \frac{1}{2\beta}\left[-1 + (1 + 8\beta^2)^{1/2}\right]^{1/2}. \tag{6.11}$$

This value can be substituted in Eq. (6.9) to give maximum transmissibility, T_m; this is found to be

$$T_{max} = 4\beta^2\left[16\beta^4 - 8\beta^2 - 2 + 2(1 + 8\beta^2)^{1/2}\right]^{-1/2}. \tag{6.12}$$

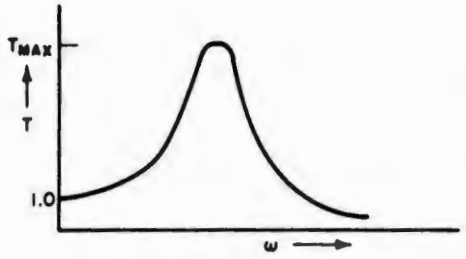

FIG. 6.2. Transmissibility of a lightly damped system with one degree of freedom.

Writers often use the quality factor Q instead of the damping ratio, borrowing from the analogous discipline of electrical circuitry. Q is formally defined as

$$Q = \frac{1}{2\beta} = \frac{\sqrt{km}}{c}. \tag{6.13}$$

From Eq. (6.13), the previous two relations can be written

$$\left.\frac{\omega}{\omega_n}\right|_{T=max} = Q[-1 + Q^{-1}(Q^2 + 2)^{1/2}]^{1/2}, \tag{6.14}$$

and

$$T_{max}{}^{-1} = [1 - 2Q^2 - 2Q^4 + 2Q^3(Q^2 + 2)^{1/2}]^{1/2}. \tag{6.15}$$

For small values of β (*i.e.*, large values of Q), T_{max} is approximated by

$$T_{max} \approx (2\beta)^{-1} = Q. \tag{6.16}$$

When the damping in the system is light ($Q \geqslant 10.0$ or $\beta \leqslant 0.05$), the resonance peak in the magnification factor occurs at $\omega = \omega_n$ and the curve of H *versus* frequency is approximately symmetrical for small variations in ω about ω_n. The peak amplitude is approximately the value of Q. The amplitude falls to $1/\sqrt{2}$ times this value at the points P_1 and P_2 with frequencies $\omega_n[1 \pm (2Q)^{-1}]$ shown in Fig. 6.3. These points are called the half-power points because the power that can be absorbed by a dashpot from a simple harmonic motion at a given frequency is proportional to the square of the amplitude. The frequency difference between the half-power points is called the bandwidth B of the system, defined as

$$B = \omega_n(Q)^{-1} = 2\beta\omega_n. \tag{6.17}$$

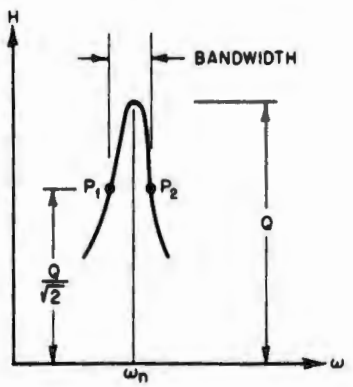

FIG. 6.3. Bandwidth of a lightly damped system with one degree of freedom.

Another ratio, particularly useful in foundation-excitation cases is the complex ratio of the relative displacement of mx_r, to the foundation displacement x_i. This ratio is

$$\frac{x_r}{x_i} = \left(\frac{\omega}{\omega_n}\right)^2 H(\omega). \tag{6.18}$$

The absolute values are given by

$$\left|\frac{x_r}{x_i}\right| = \left(\frac{\omega}{\omega_n}\right)^4 H. \tag{6.19}$$

In some cases of foundation excitation, the input acceleration $\ddot{x}_i$ is given and the response (output) acceleration $\ddot{x}_0$ is desired. From basic considerations

$$\frac{\ddot{x}_0}{\ddot{x}_i} = T. \tag{6.20}$$

The response relative motion is given by

$$\frac{x_r}{\ddot{x}_i} = \left|-\frac{1}{\omega_n^2} \cdot \frac{x_r}{x_i}\right| = \frac{1}{\omega_n^4} \cdot H. \tag{6.21}$$

6.2. Complex Modulus Usage

Chapter 3 defines the complex modulus as the ratio between stress and strain of a viscoelastic material exposed to a sinusoidal disturbance. The complex modulus E^* has two elements, the storage modulus E_r and the loss modulus E_l, such that

$$E^* = E_r + i\,E_l = E_r\left(1 + i\,\frac{E_l}{E_r}\right) = E_r(1 + i\tan\delta), \tag{6.22}$$

where tan δ is the loss tangent.

The general equation of motion for a system subjected to base-motion excitation is

$$m\ddot{x}_0 + c\dot{x}_0 + kx_0 = kx_i(t). \tag{6.23}$$

Let the input motion be sinusoidal such that

$$x_i(t) = x_i^* = x_{im}e^{i\omega t}. \tag{6.24}$$

Then the output motion, $x_0(t)$ is sinusoidal also, but of different phase, so that

$$x_0(t) = x_0^* = x_{om}e^{i(\omega t+\phi)} = x_{om}^*e^{i\omega t}. \tag{6.25}$$

The correspondence principle (discussed in detail in Chapter 3) permits writing damped equations without an explicit damping term, since the damping is accounted for by the complex modulus. Hence, Eq. (6.23) may be written

$$m\ddot{x}_0^* + C_3E^* = C_3E^*\,x_i^*, \tag{6.26}$$

where C_3 is a shape factor converting complex modulus (in pounds per square inch) to a complex spring rate with dimensions of pounds per inch. When the surface area under stress is A_c and the thickness is T_c, then $C_3 = A_c/T_c$.

Equation (6.26) leads to

$$(C_3E^* - \omega^2 m)x_{om}^* = C_3E^*x_{im}, \tag{6.27}$$

from which

$$T(\omega) = \frac{1}{1 - \dfrac{m\omega^2}{C_3E^*}} = \frac{1 + i\tan\delta}{1 - \dfrac{m\omega^2}{C_3E_r} + i\tan\delta}. \tag{6.28}$$

Define E_{rn} as the value of the storage modulus at the natural frequency of the cushion. Then,

$$\omega_n^2 = C_3 \frac{E_{rn}}{m}. \tag{6.29}$$

Substituting Eq. (6.29) in Eq. (6.28) gives

$$T(\omega) = \frac{1 + i \tan \delta}{1 - \left(\frac{\omega}{\omega_n}\right)^2 \frac{E_{rn}}{E_r} + i \tan \delta}. \tag{6.30}$$

the absolute value of which is

$$T = \left\{ \frac{1 + \tan^2 \delta}{\left[1 - \left(\frac{\omega}{\omega_n}\right)^2 \frac{E_{rn}}{E_r}\right]^2 + \tan^2 \delta} \right\}^{1/2}. \tag{6.31}$$

The foregoing derivation is due to Snowdon [58-60]. By the correspondence principle, and Eq. (6.10),

$$H(\omega) = \left[1 - \left(\frac{\omega}{\omega_n}\right)^2 \frac{E_{rn}}{E_r} + i \tan \delta\right]^{-1},$$

and (6.32)

$$H = \left\{\left[1 - \left(\frac{\omega}{\omega_n}\right)^2 \frac{E_{rn}}{E_r}\right]^2 + \tan^2 \delta\right\}^{-1/2}.$$

Figure 6.4 plots shear transmissibility of three solid rubbers on the assumption that undamped natural frequency is 5 cps.

In the previous section it was assumed that the masses of the spring and of the damper are negligible. Similarly, the cushion mass has so far been assumed negligible in this section. Snowdon [61] examined the effects of mass on transmissibility, using a modified form of the Love [6] longitudinal-vibration theory for a rod of uniform cross section. Snowdon points out that an expression for transmissibility can be found in the general form

$$T^{-1} = \left| \left(\cos N^* T_c - \frac{m}{m_c} N^* T_c \sin N^* T_c \right) \right|, \tag{6.33}$$

where T_c = cushion thickness

m_c = cushion mass, and

$N^* = p_. + iq_1$.

The complex quantity, N^*, is given by the relations

$$p_1 = \frac{n_1 T_c}{\sec \delta} \left(\frac{E_{rn}}{E_r} \cdot \frac{1 + \sec \delta}{2} \right)^{1/2} \tag{6.34}$$

and

$$q_1 = -\frac{n_1 T_c}{\sec \delta} \left(\frac{E_{rn}}{E_r} \cdot \frac{\sec \delta - 1}{2} \right)^{1/2}, \tag{6.35}$$

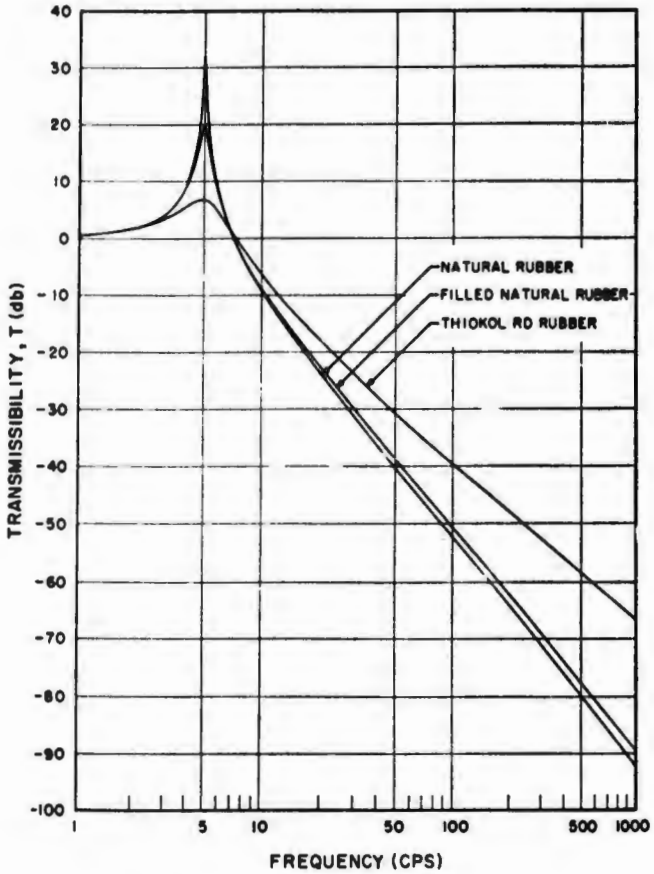

FIG. 6.4. Transmissibility of three rubbers, mass effect ignored. Snowdon [61].

where

$$n_1 = \omega \left(\frac{\rho}{E_{rn}}\right)^{1/2}$$

and ρ is the density of the material.

Since Eq. (6.33) is expressed in terms of the circular functions of a complex number, the equation must be expanded by the multiple-angle formulas and the denominator grouped into real and imaginary parts. Equation (6.33) then becomes:

$$T^{-2} = \left[\cos p_1 \cdot \cosh q_1 - \frac{m}{m_r}(p_1 \cdot \sin p_1 \cdot \cosh q_1 - q_1 \cdot \cos p_1 \cdot \cosh q_1)\right]^2 + \left[\sin p_1 \cdot \sinh q_1 + \frac{m}{m_r}(p_1 \cdot \cos p_1 \cdot \sinh q_1 + q_1 \cdot \sin p_1 \cdot \cosh q_1)\right]^2. \tag{6.36}$$

Snowdon computed a number of transmissibility curves at different density ratios. Figure 6.5 shows the transmissibilities of the three materials illustrated in Fig. 6.4 for the ratio $m/m_r = 50$. Effects of varying the mass ratio for natural rubber are shown in Fig. 6.6.

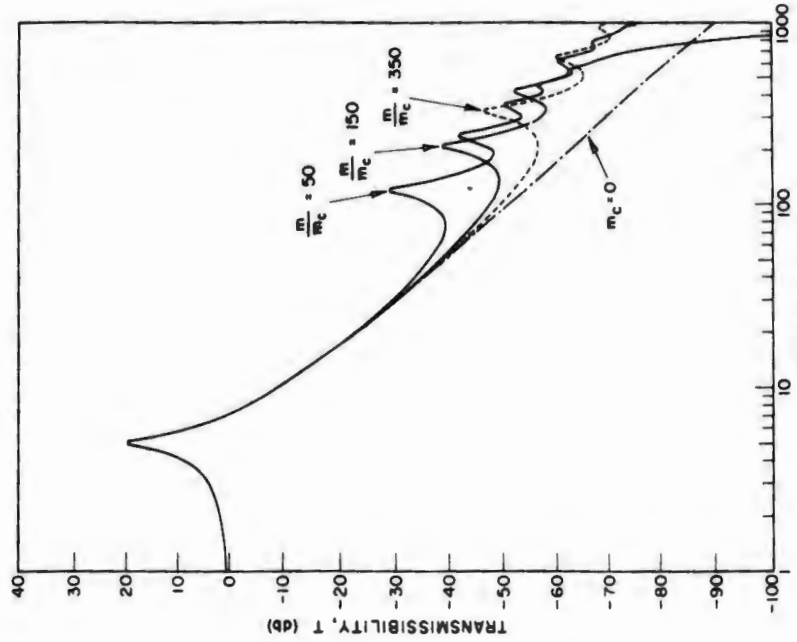

FIG. 6.6. Effect of varying m/m_r on occurrence of wave effects in natural rubber [61].

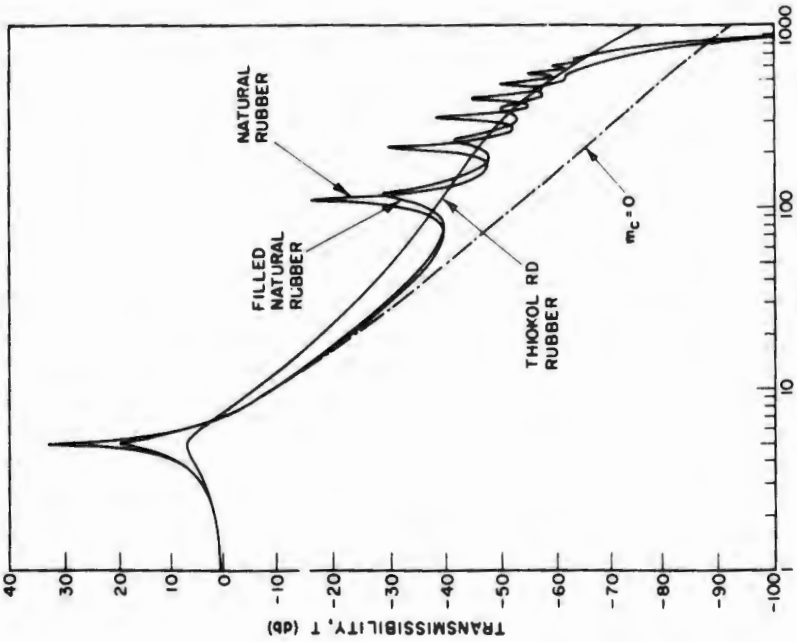

FIG. 6.5. Wave effects in rubbers: natural frequency assumed to be 5 cps, $m/m_r = 50$ [61].

The transmissibility of natural rubber at some high frequencies is increased by about 20 db, because of wave resonances, although peak transmissibility remains small. The transmissibility of high-damping Thiokol RD rubber, however, is increased only slightly by wave effects; the simple theory accurately predicts the frequency-dependence of the transmissibility of this and all other high-damping materials.

For quick analysis, the simple theory involving massless cushions provides a very good approximation, particularly in the range $0 \leqslant \omega/\omega_n \leqslant 10.0$, even with light damping.

The complex modulus is only absolutely correct for relatively small excursions over the range of linear behavior of the material. Effects of nonlinearities on resonance will be discussed in a later section.

6.3. Using Fourier's Rules

It will be recalled that Fourier's rules were referred to in Chapter 3, particularly when deriving expressions for relaxation and creep functions. They will be used (though not derived) in this section.

Consider the system of Fig. 2.1, which has one degree of freedom. Now let the steady-state excitation be a complicated wave. Fourier's first rule states that any periodic wave can be expressed as the sum of a number of simple harmonic functions having different amplitudes, phases, and frequencies. In other words, the steady-state excitation, $f_i(t)$, can be written as the real part of

$$f_i(t) = \sum_{m=1}^{m} A_m^* \, e^{i\omega_m t}, \; m = 1,2,\ldots,m, \tag{6.37}$$

where ω_m is the natural frequency of the mth wave and A_m^* is its complex amplitude.

Because of the linearity of the simple system, solutions may be obtained by superposition. Hence, the steady-state solution is

$$x_0 = \sum_{m=1}^{m} H_m(\omega) \cdot A_m^* \cdot e^{i\omega_m t}, \tag{6.38}$$

where

$$H_m(\omega) = \left[1 - \left(\frac{\omega_m}{\omega_n}\right)^2 + i2\beta\,\frac{\omega_m}{\omega_n}\right]^{-1}. \tag{6.39}$$

The output motion, x_0, is a complicated wave that stems from the input complicated wave but may look very different, since each component of the input wave has had its amplitude and phase altered differently.

When $f_i(t)$ has a natural period t_n, the ω_m in the foregoing equations will all be positive multiples of the fundamental excitation frequency, $\omega_b = 2\pi/t_n$. Hence Eq. (6.39) may be written

$$H_m(\omega) = \left[1 - \left(\frac{m\omega_b}{\omega_n}\right)^2 + i2\beta\,\frac{m\omega_b}{\omega_n}\right]^{-1}. \tag{6.40}$$

The absolute value is given by

$$H^{-2} = |H_m(\omega)|^{-1} = \left[1 - \left(\frac{m\omega_b}{\omega_n}\right)^2\right]^2 + \left[2\beta\,\frac{m\omega_b}{\omega_n}\right]^2. \tag{6.41}$$

Any series of the form

$$f(t) = \sum_{-m}^{m} A_m^* e^{im\omega t} \tag{6.42}$$

is called a Fourier series in the exponential form. The coefficients A_m for a given $f(t)$ may be evaluated from the integral

$$A_m^* = \frac{1}{t_n} \int_t^{t+t_n} f(t) e^{-im\omega t}\, dt. \tag{6.43}$$

There are other forms of representation of the Fourier series such as the trigonometric form with two sub-forms, the cosine series, and the sine series; these are not reviewed here.

Consider that $f_i(t)$ is represented by the real part of the Fourier series

$$f_i(t) = \sum_{m=0}^{m} A_m^* e^{im\omega t}. \tag{6.44}$$

Note that this equation is the same as Eq. (6.42) since there are no negative multiples of natural frequency. Information concerning the phases of the constituents is contained in the coefficients A_m^*. Solutions in terms of complex frequency response or in terms of the magnification factor will be the same as those of Eqs. (6.40) and (6.41).

Although any complicated wave can be resolved into its Fourier series components, it can be seen from Eq. (6.41) that deterministic analysis of even a two-component wave could be arduous. On the other hand, the statistical characteristics of the wave are adequately measured by the mean square of the amplitude, $\overline{y^2}$, defined as

$$\overline{y^2} = \frac{1}{\tau} \int_0^{\tau} y^2 dt. \tag{6.45}$$

Applying this definition to a Fourier-series excitation, and recalling that only the real part of the series is of interest, leads to

$$\overline{f_i^2} = \frac{1}{\tau} \int_0^{\tau} \left[\sum_{m=0}^{m} A_m^* e^{im\omega t} \right]^2 dt. \tag{6.46}$$

Since the A_m^* are defined as complex numbers, Eq. (6.46) can be written

$$\overline{f_i^2} = \frac{1}{4\tau} \int_0^{\tau} \left[\sum_{m=0}^{m} (A_m^* e^{im\omega t} + A'_m e^{-im\omega t}) \right]^2 dt, \tag{6.47}$$

where A'_m is the complex conjugate of A_m. Integrating Eq. (6.47) gives

$$\overline{f_i^2} = \sum_{m=1}^{m} \frac{1}{2} A_m^* A'_m = \sum_{m=1}^{m} \frac{1}{2} (|A_m^*|)^2. \tag{6.48}$$

Accordingly, the mean square of the response motion is

$$\overline{x_0^2} = \sum_{m=1}^{m} \frac{1}{2} H_m^2 (|A_m^*|)^2. \tag{6.49}$$

Equations (6.48) and (6.49) can be combined to give

$$\overline{x_0^2} = H_m^2 \overline{f_i^2}. \tag{6.50}$$

Similar reasoning, using Eqs. (6.19), (6.20), and (6.21), leads to

$$\overline{x_0^2} = T_m^2 \overline{x_i^2},$$

$$\overline{\ddot{x}_0^2} = T_m^2 \overline{\ddot{x}_i^2},$$

$$\overline{x_r^2} = H_m \omega_n^2 \overline{\ddot{x}_i^2} \tag{6.51}$$

and

$$\overline{x_r^2} = \left(\frac{\omega}{\omega_n}\right)^4 H_m \overline{x_i^2},$$

where T_m is transmissibility corresponding to H_m.

Consider a system with one degree of freedom, under a transient excitation. Assume that $f_i(t)$ looks something like the solid-line pulse of Fig. 6.7 such that $f_i(t) = 0$ for $t < 0$. Select a time τ that is large compared to the duration of $f_i(t)$ and then construct a periodic function $f_i(\tau)$ that coincides with $f_i(t)$ in the interval $-\tau \leq t \leq \tau$ and then repeats indefinitely with period -2τ. As in Fig. 6.7 where the dotted curve represents the artificial periodicity.

Since $f_i(\tau)$ is periodic, the response can be obtained by following Fourier's rules. Expand $f_i(\tau)$ in a Fourier series. The result is

$$f_i(\tau) = \sum_{-\infty}^{\infty} A_m^* e^{im\omega_b t}, \quad \omega_b = \pi/\tau, \tag{6.52}$$

where the A_m^* are now given by

$$A_m^* = \frac{1}{2\tau} \int_{-t}^{\tau} f_i(\tau) e^{-im\omega_b t}\, dt. \tag{6.53}$$

If Eq. (6.52) is taken to the limit, the result is known as the Fourier integral transform, $F_i(\omega)$, of $f_i(t)$, defined as

$$F_i(\omega) = \lim_{t \to \infty} (2\tau A_m^*) = \int_{-\infty}^{\infty} f_i(t) e^{-i\omega t}\, dt. \tag{6.54}$$

Operating as before, the approximate steady-state response $x_0(\tau)$ to $f_i(\tau)$ is given by

$$x_0(\tau) = \sum_{m=-\infty}^{m=\infty} A_m^* H_m(\omega) e^{im\omega_b t}. \tag{6.55}$$

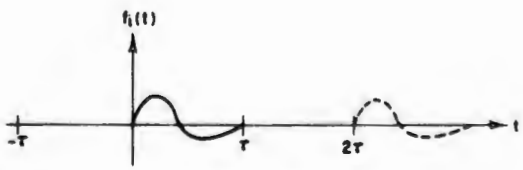

FIG. 6.7. A transient excitation artificially converted to a periodic excitation with period 2τ.

To obtain an exact solution let τ and ω_0 approach infinity. In performing this operation, hold $m\omega_b = \omega$ constant during a limiting process in which the sums in Eqs. (6.55) and (6.52) approach integrals. Multiply and divide by 2τ and set $m\omega_b = \omega$ and $\omega_b = \Delta\omega$. Then, from Eq. (6.52):

$$f_i(\tau) = \sum_{m=-\infty}^{m=\infty} (2\tau A_m^*) e^{i\omega t} \frac{\Delta\omega}{2\pi}. \tag{6.56}$$

Substituting Eq. (6.54) in Eq. (6.56), and proceeding to the limit, gives

$$f_i(\tau) = \frac{1}{2\pi} \int_{-\infty}^{\infty} F_i(\omega) e^{i\omega t}\, d\omega. \tag{6.57}$$

Repeating the limit process for Eq. (6.55) gives

$$x_0(\tau) = \frac{1}{2\pi} \int_{-\infty}^{\infty} H(\omega) \cdot F_i(\omega) e^{i\omega t}\, d\omega. \tag{6.58}$$

It is clear that the Fourier integral transform of the output motion is defined as

$$F_0(\omega) = \int_{-\infty}^{\infty} x_0(t) e^{-i\omega t}\, dt. \tag{6.59}$$

Hence, Eq. (6.58) may also be written

$$x_0(t) = \frac{1}{2\pi} \int_{-\infty}^{\infty} F_0(\omega) e^{i\omega t}\, dt, \tag{6.60}$$

from which

$$F_0(\omega) = H(\omega) \cdot F_i(\omega). \tag{6.61}$$

That is to say, the Fourier transform of the response is the Fourier transform of the excitation multiplied by the complex magnification factor.

The Fourier integral solution for a transient pulse is derived from a superposition of steady-state responses to simple harmonic excitations. The Duhamel-integral solution (derived in Chapter 5) is built up from a superposition of free-vibration solutions to a sequence of impulsive disturbances. For a given excitation $f_i(t)$, the two methods of representing the response must be identical. To see the connection, apply the Fourier-integral method to an impulsive disturbance.

Let the impulsive disturbance be the Dirac-delta function $\delta(t)$ used in the derivation of Duhamel's integral and defined in Eq. (3.30). In accordance with Eq. (6.54), the Fourier transform of the excitation is

$$F_i(\omega) = \int_{-\infty}^{\infty} \delta(t) e^{-i\omega t}\, dt. \tag{6.62}$$

Since $\delta(t) = 0$ for $t \neq 0$, and its integral is unity at $t = 0$, Eq. (6.62) can be written

$$F_i(\omega) = 1. \tag{6.63}$$

Accordingly, using Eq. (6.61), the Fourier transform of the response is

$$F_0(\omega) = H(\omega). \tag{6.64}$$

In Chapter 5 the response to an impulsive input was defined as $h(t)$ and called response to a unit-impulse function. Thus, from Eq. (6.60),

$$h(t) = \frac{1}{2\pi} \int_{-\infty}^{\infty} H(\omega) e^{i\omega t} \, d\omega, \tag{6.65}$$

which states that the unit impulse response is the Fourier transform of the complex frequency response. Using the relation suggested by Eq. (6.59), one can also write

$$H(\omega) = \int_{-\infty}^{\infty} h(t) e^{-i\omega t} \, dt, \tag{6.66}$$

showing that $h(t)$ and $H(\omega)$ are Fourier-transform pairs.

The Fourier transform has not been a popular method of finding what a transient does to a system, although it has some advantages. Rubin [243] and O'Hara [264] both discuss its utility, and point out that a fixed relation exists between the Fourier spectrum and the undamped shock spectrum after the initial pulse has occurred:

$$F_0(\omega) = \omega_n \cdot S_d(\omega), \tag{6.67}$$

where $S_d(\omega)$ is taken after the initial transient; the system being undamped.

In effect, Eq. (6.67) indicates that the pseudo-velocity of the after, or residual, shock spectrum is identical with the Fourier amplitude spectrum of the pulse. Gertel and Holland [265] recently gave an excellent short review of the relative utility of the two approaches.

In this section, some properties of the Fourier rules applicable to practical problems have been shown. Statistical concepts such as mean-square excitation and response have been defined.

In all of these examples, as in the previous two sections, the complex frequency response $H(\omega)$ has been proved central in all operations. For all practical purposes, $H(\omega)$ can be considered an almost universal transfer function relating output to input and thus, in many ways, reducing the cushion to a "black box."

6.4. Random Vibration

This section will consider time-varying functions so complicated that they conceal function periodicity.* An example of such a function is shown in Fig. 6.8. These very complicated functions seem to include all frequencies and exhibit very wide fluctuations in amplitude from moment to moment.

Because the fundamental period is not discernible, Fourier's rules cannot be used directly to determine magnitude at any instant. The investigator must therefore fall back on statistical descriptions of the motions.

Most of the approaches taken are an almost direct borrowing from the analysis of noise in communications circuits, the study of which was pioneered by Rice [266]. Robson's book [267] is an excellent review of the fundamentals.

---

*Periodicity cannot be discerned with the tools now available in a convenient time frame. This does not mean that periodicity is unobservable in the sense used by modern physicists; if it were, there would be little reason for proceeding further.

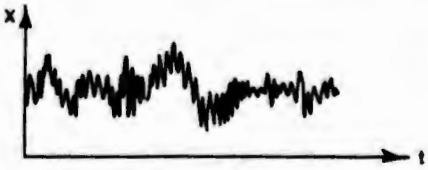

FIG. 6.8. A random vibration.

6.4.1. Statistical Analysis of a Fluctuating Quantity. To apply statistical methods to observed quantities which vary with respect to some reference, it is necessary to assume that the value of any observation of the variable is random. That is, one must assume that variation in observed values from one observation to the next is the result of chance.

The statistician usually collects observed data (which are necessarily sample data) and arranges these data in groups according to the frequency of occurrence of each value (or range of values). When enough data are accumulated, he tries to match the sample data to a mathematical function. The function is then used to estimate the behavior of the total population from which the samples have been drawn.

This mathematical function, found by empirical curve-matching techniques, is called a distribution function. Some writers call it a probability density function. The distribution function $p(y)$ of the variable y is defined as

$$p(y) = f(y), \tag{6.68}$$

where $p(y)$ = number of occurrences of y within a sufficiently small range, and

$f(y)$ = some mathematical function of y.

By basic definition, probability is the integral of the distribution function. Further, by the same basic definition, the certainty that no event will occur has a probability of zero and the certainty that all possible events will occur has a probability of 1.0. To satisfy this definition, the form of $f(y)$ must be such that the integral $P(y)$ of the distribution function $p(y)$ satisfy the relation

$$P(y) = \int_{y_{min}}^{y_{max}} f(y) \cdot dy = 1.0, \tag{6.69}$$

where $P(y)$ = probability of y,

y_{min} = least conceivable value of y, and

y_{max} = largest conceivable value of y.

In theory any distribution function meeting the criterion of Eq. (6.69) may be used, providing the function fits the empirical data. For convenience, buttressed by reasons advanced later, vibration analysts consider that the value of a random vibration at a given instant fits the normal, or Gaussian, distribution function. This distribution function is defined as

$$p(y) = \frac{1}{s_y\sqrt{2\pi}} e^{-1/2(y - y_{av}/s_y)^2}, \tag{6.70}$$

where y_{av} = mean value of y, and

s_y = standard deviation of y such that $s_y = (\overline{y^2})^{1/2}$.

In vibration work it is always possible to set $y_{av} = 0$. Now let $z_1 = y/s_y$. Equation (6.70) can then be transformed to the standardized normal distribution function

$$p(z_1) = \frac{1}{\sqrt{2\pi}} e^{-(1/2)z_1^2}, \tag{6.71}$$

where z_1 may assume all values along the real number line. Equation (6.71) is plotted in Fig. 6.9. The function is symmetrical about its mean and is uniquely determined by the standard deviation which, by definition, is the square root of the variance.

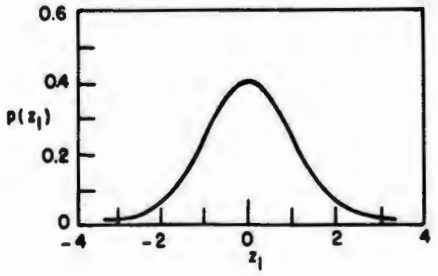

FIG. 6.9. Normal or Gaussian distribution function.

The criterion of Eq. (6.69) is met by writing

$$P(z_1) = \frac{1}{\sqrt{2\pi}} \int_{-\infty}^{\infty} e^{-(1/2)z_1^2} dz_1 = 1.0. \tag{6.72}$$

Although the integration limits are shown as being infinite, one is not justified in assuming that the real population also has infinite limits. A distribution function is no more than the result of an empirical curve-matching procedure; no absolute conclusions can be drawn concerning the limits of the population.

In the normal distribution, the probability that z_1 will have some magnitude $+z_2$ or less is given by

$$P(z_2) = \frac{1}{\sqrt{2\pi}} \int_{-\infty}^{z_2} e^{-(1/2)z_1^2} \, dz_1. \tag{6.73}$$

$P(z_2)$ is called the probability (or cumulative probability function) of z_2. Since z_1 may have positive or negative values, the probability that the absolute value of z_1 is equal to or less than $\pm z_2$ is

$$P(|z_2|) = \frac{2}{\sqrt{2\pi}} \int_0^{z_2} e^{-(1/2)z_1^2} \, dz_1 = erf\left(\frac{z_2}{\sqrt{2}}\right), \tag{6.74}$$

where

$$erf(y) = \frac{2}{\sqrt{\pi}} \int_0^y e^{-z^2} \, dy,$$

and $erf(y)$ is known as the error function of y.

The probability that $|z_1|$ exceeds a stipulated value $|z_2|$ (exceedance probability) is given by

$$P(|z_1| > |z_2|) = 1 - P(|z_2|) = erfc\left(\frac{z_2}{\sqrt{2}}\right), \tag{6.76}$$

where *erfc* (y) is called the complementary error function of y.

Values of the integrals given in Eqs. (6.73) and (6.74) are tabulated in numerous standard texts and special statistical publications. Canned digital computer routines are readily available.

The statistician is not entitled to state that a random variable fits a particular distribution function until sufficient data have been accumulated, the function has been postulated, and various tests of the goodness of fit have been performed. However, when the statistician knows that there are particular scientific factors influencing the data collected, he can usually make some rational deductions concerning the most likely distribution function, thus obtaining an *a priori* distribution function or probability. Similar reasoning tells him that the instantaneous value of y in random vibration work is a Gaussian variable.

The reason for assuming that the instantaneous value of y is normally distributed lies in the powerful Central Limit Theorem of mathematical statistics. With some qualifications, this theorem states that any random variable tends to become Gaussian if each value is in itself the resultant of a very large number (tending to infinity) of independently caused random variables—no matter what their individual distribution functions may be.

Strictly speaking, the statistical distribution is concerned with the value at a specific instant, taken from a very large number of records. Data analysis is very laborious, particularly if several instants are taken in order to ensure that a sound picture of the distribution at a given instant is developed.

All the samples available may have been taken from some larger sample; for instance, the complicated wave shown in Fig. 6.8. It would be much easier to deal with the sample record if the distribution of y-values over the duration of the record were not only the statistics of the whole sample but also the statistics applicable to any arbitrarily chosen instant. It happens that this simplification is possible provided that the wave being sampled has two properties:

1. The sample is drawn from a stationary process. That is, no translation of the time origin will affect the statistical properties of the wave.
2. The sample is drawn from an ergodic process. That is, the sample analyzed is "typical" of the process from which it is drawn.

The investigator cannot be sure that these conditions are met before the data are analyzed, though he can make it more probable by careful design and sample selection. Sometimes he can do nothing but hope for the best.

6.4.2. Determining the Variance of a Random Variable. Assuming *a priori* that the record of Fig. 6.8 is a random normal variable taken from a stationary and ergodic process, it can be seen that the variance $\overline{y^2}$ must be determined since the Gaussian distribution function is uniquely determined

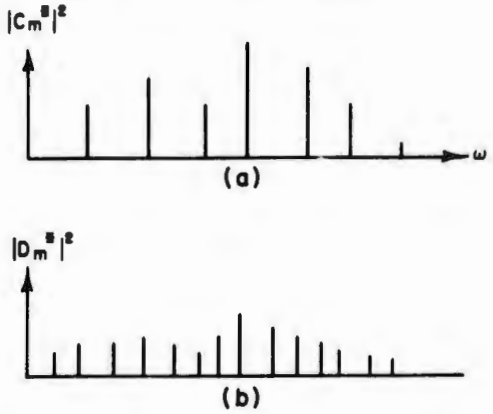

FIG. 6.10. Spectral lines for a random vibration: (a) period τ and (b) period 2τ. Miles and Thompson [268].

by this quantity. This section will deal with the basic theory of measuring random-vibration variance.

Assume that the sample record is on magnetic tape whose ends can be spliced together to form a loop of arbitrary fixed length.* The loop can be cycled through the playback device an indefinite number of times. With the loop, the sample has been made periodic with the loop period equal to 2τ, or twice the arbitrarily chosen fundamental period of the sample motion. Fourier's rules can be used to analyze this periodic motion. Specifically, the quantity $y(t)$ will be described, for a specific loop length, by

$$y(t) = \sum_{m=-\infty}^{\infty} C_m^* e^{im\omega_b t}, \quad \omega_b = \frac{\pi}{\tau}, \tag{6.77}$$

where

$$C_m^* = \frac{1}{2\tau} \int_{-\tau}^{\tau} y(t) e^{-im\omega_b t}\, dt. \tag{6.78}$$

Then, using Eq. (6.48), the variance is

$$\overline{y^2} = 2 \sum_{m=1}^{\infty} |C_m^*|^2 \tag{6.79}$$

A graph of $|C_m^*|^2$ *versus* frequency is shown in Fig. 6.10(a).

If the loop period is doubled, then the number of lines will be doubled, as in Fig. 6.10(b). With the change in period, the Fourier coefficients will take on new values, D_m^*. Since $y(t)$ is unchanged, the mean-square value must remain unchanged; a situation which leads to

$$\Sigma |C_m^*| = \Sigma |D_m^*|. \tag{6.80}$$

*This loop need not be actually fabricated. A shuttling mechanism on the tape deck will perform adequately while satisfying the concept of a loop. The area of a splice might sometimes develop spurious signals.

Since the period has been doubled,

$$C_m^* = 2D_m^*. \tag{6.81}$$

The increment in the variance, divided by the frequency increment, remains approximately constant, or

$$\frac{\Delta\overline{y^2}}{\Delta\omega} = \frac{|C_m^*|^2}{\omega_0} = \frac{2|D_m^*|^2}{\omega_0} = W(\omega_m), \tag{6.82}$$

where $W(\omega_m)$ is called the discrete power spectral density of the quantity represented by the variable y.

As the length of the loop is increased, $|C_m^*|^2$ decreases correspondingly but $W(\omega_m)$ remains finite. In the limiting case, as $T \to \infty$ or $\Delta\omega \to 0$, the spectrum becomes continuous and the discrete values of $W(\omega_m)$ approach the smooth, continuous, power-density spectrum, defined as

$$W(\omega) = \lim_{\Delta\omega \to 0} \frac{\Delta\overline{y^2}}{\Delta\omega} = \frac{d\overline{y^2}}{d\omega}, \tag{6.83}$$

or

$$\overline{y^2} = \int_0^\infty W(\omega)d\omega. \tag{6.84}$$

In other words, the variance of $y(t)$ can be found by determining $W(\omega_m)$ at various frequencies and then summing.

In practice, $W(\omega)$, is estimated by feeding the sample record through a spectrum analyzer that transmits only those frequency components within the passband

$$\overline{\omega} \pm \frac{1}{2}\Delta\omega.$$

The output of the analyzer, $\Delta\overline{y^2}$, is indicated by a mean-square meter, and the mean-power spectral density is computed by dividing the meter reading by $\Delta\omega$; this operation can be incorporated in the calibration of the meter. The complete power spectral density can be estimated by changing the passband central frequency, $\overline{\omega}$. A typical set of passbands in a commercially available instrument is shown in Table 6.1.

The principle of determining a power spectral density spectrum is relatively simple. There are some experimental pitfalls, but most of these have been recognized and procedures are fairly standard.

Note that, in all of the foregoing, the fluctuating quantity y was perfectly general. Hence, there can be several different types of power spectral density derived for the same motion. The more common forms are absolute displacement (input and output), relative displacement, and acceleration (input and output). Uses of specific forms are discussed in the remainder of this chapter.

6.4.3. Response of a Simple Resonator to Random Excitation. For a simple harmonic function, it was shown in section 6.1 that

TABLE 6.1. TYPICAL SET OF PASS BANDS IN A SPECTRUM ANALYZER

$\bar{\omega}$	$\bar{\omega} \pm \frac{1}{2}\Delta\omega$	$\bar{\omega}$	$\bar{\omega} \pm \frac{1}{2}\Delta\omega$	$\bar{\omega}$	$\bar{\omega} \pm \frac{1}{2}\Delta\omega$
		125	112-140	1250	1120-1400
16	14-18	160	140-180	1600	1400-1800
20	18-22.5	200	180-225	2000	1800-2250
25	22.5-28	250	225-210	2500	2250-2800
31.5	28-35	315	280-350	3150	2800-3500
40	35-45	400	350-450	4000	3500-4500
50	45-56	500	450-560	5000	4500-5600
63	56-71	630	560-710	6300	5600-7100
80	71-88	800	710-880	8000	7100-8800
100	88-112	1000	880-1120	10000	8800-11200

$$\frac{x_0}{f_i} = H(\omega),$$

$$\frac{x_r}{x_i} = \left(\frac{\omega}{\omega_n}\right)^2 \cdot H(\omega),$$

$$\frac{x_0}{x_i} = T(\omega), \tag{6.85}$$

$$\frac{\ddot{x}_0}{\ddot{x}} = \left(1 + i2\beta\frac{\omega}{\omega_n}\right) \cdot H(\omega), \text{ and}$$

$$\frac{x_r}{\ddot{x}_i} = \frac{1}{\omega^2} \cdot H(\omega).$$

These concepts were then extended to the mean-square values of functions which could be described by Fourier series so that

$$\frac{\overline{x_0^2}}{\overline{f_i^2}} = H^2,$$

$$\frac{\overline{x_0^2}}{\overline{x_i^2}} = \frac{\overline{\ddot{x}_0^2}}{\overline{\ddot{x}_i^2}} = T^2,$$

$$\frac{\overline{\ddot{x}_r^2}}{\overline{\ddot{x}^2}} = \frac{1}{\omega_n^4} \cdot H, \tag{6.86}$$

and

$$\frac{\overline{x_r^2}}{\overline{x_i^2}} = \left(\frac{\omega}{\omega_n}\right)^4 H.$$

Finally, in the previous section, it was shown that the power spectral density spectrum was a measure of the mean square of a random function. While the proof is quite complicated (see, for example, Miles and Thompson

[268]), it can be seen that it is logical to write the following power spectral density ratios for a simple resonator

$$\frac{W_{ox}(\omega)}{W_{ix}(\omega)} = \frac{W_{oa}(\omega)}{W_{ia}(\omega)} = T^2,$$

$$\frac{W_{rx}(\omega)}{W_{ia}(\omega)} = \frac{1}{\omega_n^4} \cdot H, \tag{6.87}$$

and

$$\frac{W_{rx}(\omega)}{W_{ix}(\omega)} = \left(\frac{\omega}{\omega_n}\right)^4 \cdot H.$$

Subscripts i and o stand for input and output, respectively. Where the subscript r is used, the power spectral density refers to relative motion $x_r = x_0 - x_i$. The additional subscripts x and a denote displacement and acceleration, respectively. Equations (6.87) thus describe the interrelations between five different kinds of power spectral densities.

Combining Eqs. (6.84) and (6.87) produces

$$\overline{x_0^2} = \int_0^\infty T^2 \cdot W_{ix}(\omega) \cdot d\omega,$$

$$\overline{x_r^2} = \int_0^\infty \frac{H}{\omega_n^4} \cdot W_{ia}(\omega) \cdot d\omega, \tag{6.88}$$

and

$$\overline{\ddot{x}_0^2} = \int_0^\infty T^2 \cdot W_{ia}(\omega) \cdot d\omega.$$

Other combinations are possible but these are the ones most frequently used.

In evaluating the foregoing integrals, note that the units used for power spectral density in writing Eqs. (6.87) are square inches/radian/second or g^2/radian/second. If the input data are in terms of square inches/cps or g^2/cps, each ω must be multiplied by a constant, $1/2\pi$.

If the instantaneous value of the input is Gaussian, then the instantaneous value of the output must also be normally distributed. Using Eq. (6.74) gives

$$P(|x_r|) = erf\frac{x_r}{\overline{x_r}\sqrt{2}}. \tag{6.89}$$

Similar relations can be written for x_0 and $\ddot{x}_0$.

Expose the simple resonator to white noise, that is, excitation with equal power spectral density at all frequencies. Denote the acceleration power spectral density for this white noise by $W_{ia}(c)$. Then the relative-motion response can be shown to be

$$\overline{x_r^2} = \frac{\pi}{4\beta\omega_n^3} \cdot W_{ia}(c) = \frac{\pi Q}{2\omega_n^3} \cdot W_{ia}(c). \tag{6.90}$$

Similarly, for absolute motion,

$$\overline{x_0^2} = \frac{\pi\omega_n}{4\beta} \cdot W_{ia}(c) = \frac{\pi Q\omega_n}{2} \cdot W_{ia}(c), \tag{6.91}$$

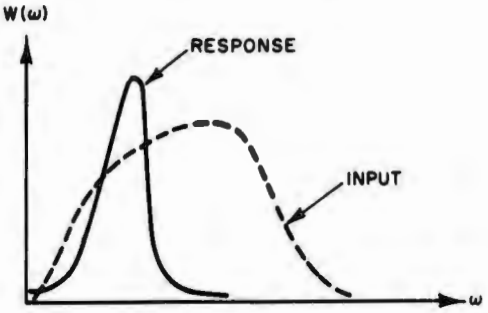

FIG. 6.11. Response of a narrow-band oscillator to broadband excitation [268].

and for acceleration,

$$\overline{\ddot{x}_0^2} = \frac{\pi\omega_n}{2\beta}(1 + 4\beta^2) \cdot W_{ia}(c) = \frac{\pi\omega_n(Q^2 + 1)}{Q} \cdot W_{ia}(c). \tag{6.92}$$

Strictly speaking, these results are valid only if the input is white noise; this is physically impossible because it needs infinite power. However, if the resonator is narrow-band and the excitation power spectral density curve is only approximately flat in this region, then Eqs. (6.90) through (6.92) give a very close approximation to the responses. Figure 6.11 indicates behavior where excitation bandwidth is broad compared with response bandwidth. The cushion acts as a filter, and the cushioned system receives energy only in the neighborhood of its natural frequency.

It is possible, though unlikely, that the input spectral density has a peak within the bounds of the bandwidth of the simple resonator.

Assume that this peak is at ω_n and the bandwidth of the input motion is B, defined in Fig. 6.3 and Eq. (6.17). The quantity B/ω_n is a measure of the power content of the power spectral density in the neighborhood of ω_n. Hence, the input motion may be regarded as responding to some outside, unspecified force. On this basis, it may be reasoned that the power spectral density in the region of this bandwidth will have a response such that

$$\frac{W_{ia}(\omega B)}{W_{ia}(\omega)} = \left(\frac{\omega}{\omega_n}\right)^2 H, \tag{6.93}$$

where $W_{ia}(\omega B)$ is the power spectral density in the bandwidth.

It has been shown [269,270] that the acceleration response is then

$$\overline{\ddot{x}_0^2} = \frac{\pi\omega_n}{4\beta} \cdot \frac{1 + 4\beta^2}{1 + \dfrac{1}{\omega_n}} \cdot W_{ia}(\omega), \tag{6.94}$$

while the relative-motion response is

$$\overline{x_r^2} = \frac{\pi}{4\omega_n^3\beta\left(1 + \dfrac{1}{\omega_n}\right)} W_{ia}(\omega). \tag{6.95}$$

As can be seen from Fig. 6.11, this refinement should rarely be needed.

Let us now turn to examining some of the other statistical information which can be developed concerning random vibration. Consider a random oscillation $y(t)$. The mean value of this oscillation is stipulated to be zero and the distribution of its value at any instant is assumed to fit the normal distribution function.

Rice [266] has shown that the number of times n_0 that the value of $y(t)$ passes through zero per unit time is, on the average

$$n_0 = \frac{1}{\pi}\left[\frac{\int_0^\infty \omega^2 \cdot W(\omega) \cdot d\omega}{\int_0^\infty W(\omega) \cdot d\omega}\right]^{1/2}. \tag{6.96}$$

The quantity n_0 is often called the number of zero crossings per unit time.

Since the motion is oscillatory, there are occasions when the value of $y(t)$ is increasing, *i.e.*, when the function $y(t)$ has a positive slope. Take any value of $y(t)$, say y. Rice has also shown that the average number per unit time n_y that $y(t)$ passes through y while $y(t)$ is increasing in value is

$$n_y = \frac{1}{2}\, n_0 \exp\left[-\frac{1}{2}\left(\frac{y}{s_y}\right)^2\right]. \tag{6.97}$$

Since the motion is oscillatory, what went up must come down; there must be maximum, or peak values of $y(t)$. The number per unit time of positive peaks n_{yp} of $y(t)$ equal to or infinitesimally greater than y is found by equating the derivative of Eq. (6.97) to zero and ignoring the sign. The result is

$$n_{yp} = \frac{1}{2}\,\frac{n_0 y}{s_y^2} \cdot \exp\left[-\frac{1}{2}\left(\frac{y}{s_y}\right)^2\right] \cdot dy. \tag{6.98}$$

When the responding system is excited by white noise, the average number of zero crossings per unit time is found to be

$$n_0 = \omega_n/\pi, \tag{6.99}$$

which is also the number of zero crossings that would occur if the system were undamped and vibrating freely.

When a lightly damped system is exposed to broadband excitation, the behavior is similar to that of a general system exposed to white noise. The response resembles that shown in Fig. 6.12. The response wave appears to be a sine wave with a natural frequency ω_n but with a slowly varying but random amplitude.

Applying Eq. (6.98) to this case, using Eq. (6.99), gives

$$n_{yp} = \frac{\omega_n y}{2\pi\, s_y^2} \exp\left[-\frac{1}{2}\left(\frac{y}{s_y}\right)^2\right] dy, \tag{6.100}$$

as the average number per unit time of positive peaks of $y(t)$ equalling or very slightly exceeding y. Multiplying by the natural period of the response motion, $t_n = 2\pi/\omega_n$, results in

$$t_n n_{yp} = \frac{y}{s_y^2} \exp\left[-\frac{1}{2}\left(\frac{y}{s_y}\right)^2\right] dy = z_1 e^{-(1/2)z_1^2}\, dz_1. \tag{6.101}$$

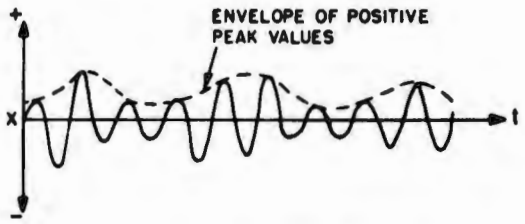

FIG. 6.12. Narrow-band response to random noise (a random sine wave).

There can be but one positive peak per cycle. Hence, Eq. (6.101) can be taken as one means of expressing the distribution function of the peaks of a random sine wave, *i.e.*, of the distribution function of the envelope of peak magnitudes.

Setting z_p as a peak value of the standardized variate z_1, the distribution function implied by Eq. (6.101) can be written explicitly as

$$p(z_p) = z_p e^{-(1/2)z_p^2}, \tag{6.102}$$

which is known as the Rayleigh distribution function and is also called the two-dimensional error distribution. Equation (6.102) is plotted in Fig. 6.13.

To meet the essential definition of a probability function, the limits of integration are set at zero and plus infinity. The probability that a peak value is equal to or less than some stipulated value, say z_p is

$$P(z_p) = 1 - \exp\left[-\frac{1}{2} z_p^2\right]. \tag{6.103}$$

Although Eq. (6.103) implies that z_p may have an infinite value, it is emphasized again that very large values may not be physically realizable because of such limitations as strength or available space.

6.4.4. Space Requirements. For random vibration, the collision-free space required must be expressed in probability terms. The answer must be found in the field of extremal statistics; most of what follows was derived from Gumbel's comprehensive text [271]. Some aspects of this problem were recently considered by Gray [272].

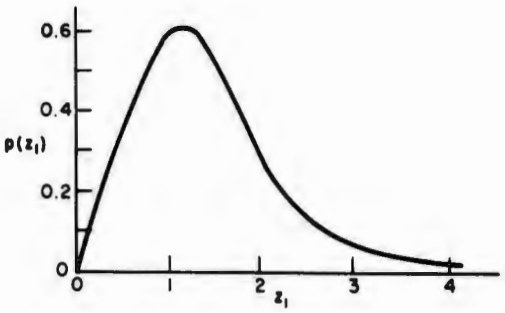

FIG. 6.13. Rayleigh, or two-dimensional error, distribution function.

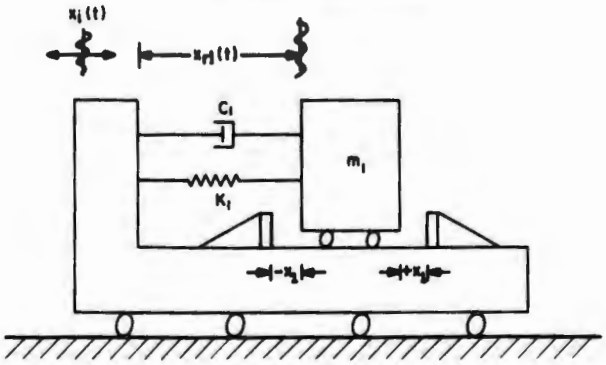

FIG. 6.14. Simple single oscillator with fixed travel limits; impedance of base infinite.

Consider the simple single oscillator system shown in Fig. 6.14. The relative response motion $x_{r1}(t)$ of the mass m_1 is a function of the input motion $x_i(t)$ of the base member, whose mechanical impedance is assumed infinite. When $x_i(t)$ is random, stationary and ergodic, the output motion is characterized by

$$\overline{x_{r1}^2} = \frac{95.6}{f_{n1}^4} \int_0^\infty H^2 \cdot W_{ia}(f) \cdot df, \tag{6.104}$$

where $\overline{x_{r1}^2}$ = variance of $x_{r1}(t)$, in.^{2},

$W_{ia}(f)$ = input acceleration spectral density, g^2/cps,

f_{n1} = undamped natural frequency of the oscillator, cps, and

H = magnification factor, see Eq. (6.7).

Equation (6.104) is a conversion of the second of Eqs. (6.88).

When the oscillator is lightly damped ($\beta \leq 0.1$) and the input is white noise ($W_{ia}(f) = W_{ia}(c)$ = a constant), Eq. (6.104) becomes

$$\overline{x_{r1}^2} = 150.1 \frac{Q_1 W_{ia}(c)}{f_{n1}^3}, \tag{6.105}$$

where $Q_1 = (2\beta_1)^{-1}$. When Eq. (6.105) is used for broadband excitation with narrow-band response, the error is negligible when the upper frequency limit of integration is about four or more times the natural frequency of the oscillator.

The original problem may now be restated in terms of Fig. 6.14. We wish to know the probable time when $|x_{r1}(t)|$ will exceed the distance x_1. To generalize the resulting equations, let z_2 be the maximum value of the standardized variate, such that $z_2 = x_1/\sqrt{\overline{x_{r1}^2}}$. Set $z_1 = x_{r1}(t)/\sqrt{\overline{x_{r1}^2}}$ as the standardized value of $x_{r1}(t)$ and let z_p be a peak value of z_1. Using Eq. (6.98), the average number of peaks z_p equalling or very slightly exceeding a stipulated value of z_1 per unit of time is

$$n_{zp} = n_0 z_p \exp\left[-\frac{1}{2} z_p^2\right] dz_1, \tag{6.106}$$

where n_0 is the average number of zero crossings per unit time. For narrow-band response, n_0 will be twice f_{n1}. Note that the factor 1/2, appearing in Eq. (6.98), has been dropped because, in this problem, we are interested in both positive and negative peaks.

If z_p is considered to be the extreme value after each zero crossing, there can be but one such value per crossing. Regard each zero crossing as the start of an independent experiment that will produce one, and only one, extreme value z_p. It is evident heuristically that the distribution function for z_p may be written

$$p(z_p) = z_p \exp\left[-\frac{1}{2} z_p^2\right]. \tag{6.107}$$

In other words, the distribution of z_p is a Rayleigh distribution.

The probability that z_p is greater than z_2 can be written

$$P(z_p > z_2) = 1 - P(z_2). \tag{6.108}$$

According to Gumbel [271], the mean time t_e to first exceedance of z_2 can be written

$$t_e = \frac{1}{n_0[1 - P(z_2)]} = \frac{1}{n_0} \exp\left[\frac{1}{2} z_2^2\right]. \tag{6.109}$$

Equation (6.109) simply restates the truism that, if an event has a probability P, one has to make on the average $1/P$ trials for the event to happen once. The specific form of the relation is derived from the familiar binomial distribution.

The mean time to first exceedance is a variable which is limited to the left (since an exceedance need not occur) and unlimited to the right. The standard deviation of t_e, s_{te}, may be found from

$$s_{te} n_0 = \sqrt{(t_e n_0)^2 - t_e n_0} \approx t_e n_0 - \frac{1}{2}. \tag{6.110}$$

The actual time τ to first exceedance is a variable. The probability $P(\tau)$ that exceedance occurs before or at time τ is given by

$$P(\tau) = 1 - [P(z_2)]^{\tau}. \tag{6.111}$$

When z_2 is larger than about 3.0, Eq. (6.111) may be written, with good accuracy,

$$P(\tau) = 1 - \exp[-\tau/t_e], \tag{6.112}$$

which is recognizable as the probability obtained from a Poisson distribution. For large values of τ/t_e, the probability rapidly approaches certainty; that is, $P(\tau)$ approaches 1. Expansion of Eq. (6.112) into a power series will show that for small values of τ/t_e the probability is closely approximated by

$$P(\tau) \approx \tau/t_e. \tag{6.113}$$

In most design situations, the probability $P(\tau)$ and the period of exposure τ are specified and the desired clearance needs to be determined. Solving Eq. (6.109) for z_2 and using t_e from Eq. (6.112) or from Eq. (6.113) leads to

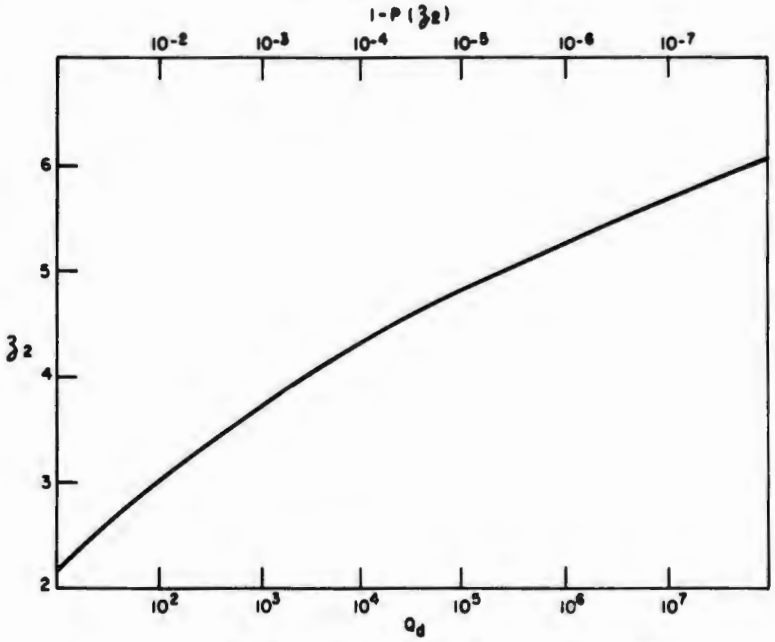

FIG. 6.15. Design quotient *versus* required value of z_2.

$$z_2 = (2 \log Q_d)^{1/2} = \left\{2 \log \frac{\tau n_0}{-\log [1 - P(\tau)]}\right\}^{1/2} \approx \left\{2 \log \frac{\tau n_0}{P(\tau)}\right\}^{1/2}, \quad (6.114)$$

where Q_d is called the design quotient. Figure 6.15 is a plot of required z_2 *versus* various values of the design quotient. The numbers at the top of the graph represent the probability that any given peak will exceed z_2.

In a given design problem, the time of exposure may be fixed; we wish to know the characteristic largest value of z_1 seen during this time τ. This value, z_c, is defined as that value which is expected to be exceeded once in a given number of trials (n_0 in our case) and is defined by the general probability relation

$$P(z_c) = 1 - \frac{1}{\tau n_0}. \quad (6.115)$$

Substituting Eq. (6.108) and solving for z_c leads to

$$z_c = \sqrt{2 \log \tau n_0}, \quad (6.116)$$

which may be written, for narrow-band response,

$$z_c = \sqrt{2 \log 2\tau f_{n1}}. \quad (6.117)$$

As an example of the utility of Eq. (6.117), suppose that the natural frequency of an oscillator is 20 cps and the specified time of exposure to a random signal is 30 minutes. Then the characteristic largest value is about 3.8 standard deviations of the response motion. Desirability of redesign is made apparent by using the simple equation.

Although the characteristic largest value is formally defined by Eq. (6.115), comparison between Eqs. (6.109) and (6.116) shows that mean time to first exceedance and characteristic largest value are essentially equivalent concepts with the Rayleigh distribution.

The most probable, or modal, largest value of z_1, z_m, in a Rayleigh distribution is given by the solution of

$$\tau n_0 = \frac{1}{2} z_m^2 \left[1 - 1/z_m^2\right] + 1/z_m^2 , \tag{6.118}$$

from which a first-approximation solution is

$$z_m \approx z_c = \sqrt{2 \log \tau n_0} . \tag{6.119}$$

Hence the most probable largest value is very close to the characteristic largest value.

Where exposure time and space available are fixed, the designer must control natural frequency of the oscillator if exceedance is to be avoided with a stipulated probability. For small values of the ratio τ/t_e, Eq. (6.114) may be written

$$\frac{1}{2} \frac{x_1^2}{\overline{x_{r1}^2}} = \log \frac{\tau n_0}{P(\tau)} , \tag{6.120}$$

where $\overline{x_{r1}^2}$ is frequency-dependent and also contains damping terms because of the complex frequency response. The term n_0 is also frequency-dependent. For practical purposes, an oscillator with a discrete natural frequency would be quite narrow-band with respect to broadband excitation; so it should be sufficient to substitute Eq. (6.105). Then, Eq. (6.120) transforms to

$$f_{n1} = \left[\frac{300\, Q_1 W_{ts}(c)}{x_1^2} \log \frac{2\tau f_{n1}}{P(\tau)}\right]^{1/3} . \tag{6.121}$$

Although transcendental, this equation is reasonably tractable, even for hand computation. Note that the higher the assumed value of Q_1, the higher the natural frequency and the safer the design.

Consider the problem posed by Fig. 6.16. If the relative motion $x_{r2}(t)$ is large enough in the inward direction, collision will occur. That is, it will occur at the moment when $x_{r2}(t)$ is greater in one direction than the static equilibrium distance x_3 between masses m_1 and m_2.

The essential difference between Figs. 6.14 and 6.16 is that, in the former, bottoming can occur in either direction while, in the latter, two-mass collision can occur only in a single direction.

Motion of mass m_1 is described by Eq. (6.104) or Eq. (6.105). Motion of mass m_2, $x_{r2}(t)$, is covered by the same equations, with simple one-for-one substitution of the quantities indicated in the figure.

Since $x_{r1}(t)$ and $x_{r2}(t)$ are random variables, $x_{r3}(t)$ is also a random variable. The problem of whether $x_{r3}(t)$ could become large enough to cause collision was first explored by Skoog and Setterlund [273] whose approach was later amplified by Himelblau and Keer [274]. Equations (6.122) through (6.125) follow the latter reference.

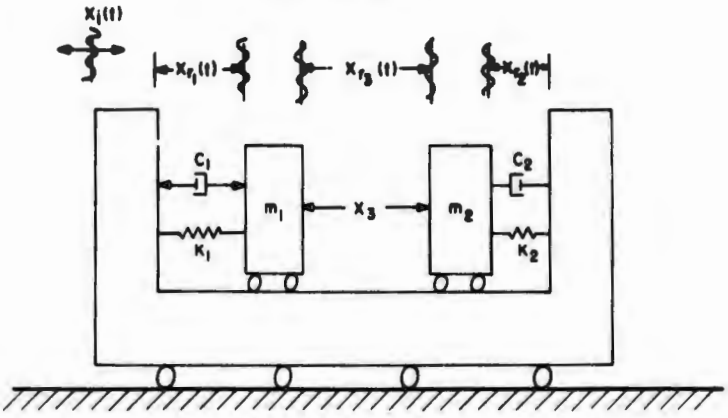

FIG. 6.16. Two oscillators connected through a common base of infinite impedance.

The variance $\overline{x_{r3}^2}$ of $x_{r3}(t)$ is given by

$$\overline{x_{r3}^2} = \overline{x_{r1}^2} - 2R + \overline{x_{r2}^2}, \tag{6.122}$$

where the cross-product R is

$$R = \frac{95.6}{(f_{n1}f_{n2})^2} \int_0^\infty H_1 H_2 W_{ia}(f) \cos(\phi_1 - \phi_2)\, df, \tag{6.123}$$

and the phase angles are

$$\tan \phi_{1,2} = \frac{2\beta_{1,2}(f/f_{n1,n2})}{1 - (f/f_{n1,n2})^2}. \tag{6.124}$$

Where both responses are narrow-band, and the excitation is broadband, Eq. (6.123) becomes

$$R = 300.3 \frac{[W_{ia}(c)/(f_{n1}f_{n2})^2]\,[(Q_1/f_{n1}) + (Q_2/f_{n2})]}{\left[\frac{1}{f_{n1}} + \frac{1}{f_{n2}}\right]^2 + Q_1 Q_2 \left[\frac{f_{n1}}{f_{n2}^3} + \frac{f_{n2}}{f_{n1}^3}\right] + \frac{1}{f_{n1}f_{n2}}\left[\frac{Q_1}{Q_2} + \frac{Q_2}{Q_1}\right]}. \tag{6.125}$$

With the value of $\overline{x_{r3}^2}$ established, pertinent probability values can (with one significant exception) be taken using the probability equations developed for the single-oscillator condition. The single exception is that wherever the term n_0 appears, it should be taken as one half the value developed from using Eq. (6.96) since interest is concentrated only on motion in a single direction.

Table 6.2 gives some numerical values for bottoming probability and collision probability for several values of z_1.

In developing the probability equations of this section, extensive use was made of Gumbel's comprehensive text [271]. A key assumption was made that each zero crossing was the start of a statistically independent experiment; this may not always be warranted. Gray [272] makes the point, however, that the assumption of statistical independence provides an upper

TABLE 6.2. PROBABILITY OF BOTTOMING, P_1, AND OF COLLISION, P_2, FOR SEVERAL VALUES OF A STANDARDIZED VARIATE

z_1	P_1	P_2
0	1.000	0.500
1	0.317	0.159
2	4.55×10^{-2}	2.28×10^{-2}
3	2.70×10^{-3}	1.35×10^{-3}
4	6.33×10^{-5}	3.17×10^{-5}
5	5.73×10^{-7}	2.87×10^{-7}
6	1.97×10^{-9}	9.86×10^{-10}
7	2.56×10^{-12}	1.28×10^{-12}
8	1.24×10^{-15}	6.22×10^{-16}
9	2.28×10^{-19}	1.13×10^{-19}
10	1.52×10^{-23}	7.62×10^{-24}

bound on the prevailing probabilities. Hence, the equations given here provide a safe design margin.

6.5. Mechanical Impedance and Mobility

Previous discussions have been aimed at systems with one degree of freedom. Much is applicable to systems with multiple degrees of freedom, by means of the concept of normal modes. This concept leads to solutions in terms of differential equations using eigenvalue techniques. Another very powerful technique for such systems, borrowed from electrical engineering, is called mechanical impedance and mobility and has this major advantage: one can change one parameter of a complete system without solving the complete set of differential equations over again.

Impedance and mobility are not much used in work with cushions; but one should be able to transfer cushion data to impedance terms for analysis of more complex systems. Methods of measuring impedance are well established, and it is possible to obtain cushioning data from impedance measurements. Some elementary details are therefore presented here.

The complex modulus has been defined as the ratio of stress to strain in a body subjected to a sinusoidal motion. Impedance, by contrast, is defined as the ratio of the force to the velocity in a linear system excited by a sinusoidal force. Let the velocity at some point in a system be

$$V^* = Ve^{i\omega t}, \tag{6.126}$$

and let the force causing this velocity be

$$F^* = Fe^{i(\omega t+\phi)} = Fe^{i\phi}e^{i\omega t}, \tag{6.127}$$

where ϕ is the phase angle. Then the complex impedance is

$$Z^* = \frac{F^*}{V^*} = \frac{F}{V}e^{i\phi} = Ze^{i\phi}, \tag{6.128}$$

which, using Euler's formula, may also be written

$$Z^* = Z(\cos\phi + i\sin\phi) = Z_r(1 + i\tan\phi) = Z_r + iZ_i, \tag{6.129}$$

where $Z = |Z^*| = (Z_r^2 + Z_i^2)^{1/2}$,

$\tan\phi = Z_i/Z_r$.

Mobility, M^*, is the reciprocal of impedance so that

$$Z^*M^* = 1. \tag{6.130}$$

Impedance and mobility are called phasor quantities and they can be plotted in the same manner as vectors but in the phasor plane, often called the impedance plane. Since both force and velocity are vector quantities, both place and direction of measurement must be stipulated. When both force and velocity are measured at the same point in a system and in the same direction, the resulting impedance is called driving-point impedance. All other cases (including those for which the velocity is measured at the driving point, but in a direction other than the force) are called transfer impedances.

Elementary impedances for single elements of a system are given by:

1. For mass,

$$Z^* = i\omega m. \tag{6.131a}$$

2. For a damper,

$$Z^* = c. \tag{6.131b}$$

3. For a spring,

$$Z^* = -i\frac{k}{\omega}. \tag{6.131c}$$

Complex impedances for individual elements of a system can be added to give the impedance of the complete system. Hixson [275] derives Eqs. (6.131) and gives a table of impedance formulas for many simple mechanical models involving various combinations of mass, spring, and damper. He also summarizes the rules for combining and simplifying very complex systems so that an estimate of vibration behavior can be made. In this monograph the discussion will be limited to the simplest possible case: the massless cushion with a single spring and dashpot shown in Fig. 2.2.

The complex impedance for this simple cushion is

$$Z^* = c - i\frac{k}{\omega}, \tag{6.132}$$

which can be separated directly into its real and imaginary parts

$$Z_r = c,$$

$$Z_i = -\frac{k}{\omega}, \tag{6.133}$$

so that, in terms of amplitude and phase,

$$Z = \left(c^2 + \frac{k^2}{\omega^2}\right)^{1/2} \tag{6.134}$$

and

$$\tan \phi = -\frac{k}{\omega c}.$$

Both of these are measurable quantities. The real and imaginary portions of the complex impedance are equal at a certain frequency, ω_0, called the characteristic frequency. Using Eqs. (6.131), this characteristic frequency is

$$\omega_0 = \frac{k}{c}, \tag{6.135}$$

so that

$$\tan \phi = -\frac{\omega_0}{\omega}. \tag{6.136}$$

When the characteristic frequency is known, the isolator is completely described.

Note that the complex modulus for a cushion of thickness T_c and surface area A_c is given by

$$E^* = \frac{T_c}{A_c}(k + i\omega c), \tag{6.137}$$

from which

$$\begin{aligned} E_r &= kT_c/A_c, \\ E_i &= \omega c T_c/A_c, \end{aligned} \tag{6.138}$$

and

$$\tan \delta = \frac{\omega c}{k} = \frac{\omega}{\omega_0}.$$

Thus, if the mechanical impedance parameters of a given cushion have been measured, then the complex moduli may be calculated from

$$\begin{aligned} E_r &= \frac{T_c}{A_c}\omega Z \sin \phi, \\ E_i &= \frac{T_c}{A_c}\omega Z \cos \phi, \end{aligned} \tag{6.139}$$

and

$$\tan \delta = -\cot \phi.$$

A frequently used form of impedance head contains a force transducer and an accelerometer. The absolute values of complex moduli can be calculated directly by making the substitutions $a = \omega V$ and $Z = \omega F/a$, so that

$$\begin{aligned} E_r &= \frac{T_c \omega^2 F}{A_c a} \sin \phi, \\ E_i &= \frac{T_c \omega^2 F}{A_c a} \cos \phi. \end{aligned} \tag{6.140}$$

From a practical standpoint in design and test work, the analyst starts with the complex moduli for the cushion and wishes to convert to impedance or mobility in order to analyze a more complex structure. These relations are

$$Z = \frac{A_c E_t}{\omega T_c \sin \delta} = -\frac{A_c E_r}{\omega T_c \cos \delta},$$
$$\tan \phi = -\cot \delta. \tag{6.141}$$

The foregoing simplified explanation of the relation between impedance and complex moduli is taken from Burgess [62], who was careful to note that Nolle [76] had previously found the relation between loss angle and impedance angle.

6.6. Nonlinear Response

The foregoing discussions are reasonably correct for some nonlinear cushions, provided that the disturbance is small. Most cushions are nonlinear, particularly in their response to large disturbances. This section will review some of the basic phenomena of nonlinear oscillations.

Take an isolator whose stress-strain curve exhibits stiffening characteristics; see curve A in Fig. 6.17. When the strain exceeds some value ϵ_1, the stress exerted by the cushion is greater than would be obtained from a continuation of the straight line. Since the natural frequency is a function of the ratio between stress and strain, the natural frequency would also be increased during that portion of the vibratory cycle when $\epsilon > \epsilon_1$.

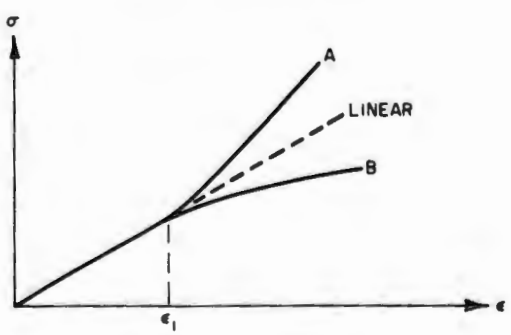

FIG. 6.17. Nonlinear stress-strain functions: A is hardening curve, and B is softening curve.

The result is shown in Fig. 6.18 for a hardening system. The vertically rising peak of the response curve is bent towards the right. If the forcing frequency be continually increased towards resonance, each added frequency element increases the system response until a peak value is reached. As frequency is increased beyond this peak value, the response cannot follow the solid curve, for this would require a decrease in frequency. Accordingly, the response jumps on a straight line down to the only value it can assume following the arrows. When the excitation begins at a high frequency and is gradually reduced, the response follows the solid line until such time as

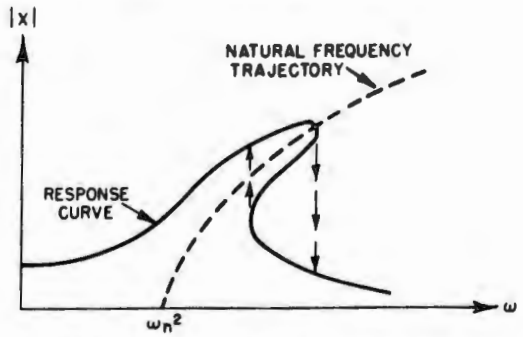

FIG. 6.18. Response of a hardening system.

following the solid curve would require an increase in frequency. At this point, the response shifts upward as indicated by the arrows to the higher curve. The change of amplitude is not instantaneous; usually several cycles of vibration are required to establish the change.

The following general remarks may be made concerning nonlinear behavior:

1. Vibration amplitude determines the extent of the nonlinearity effect and therefore governs the extent to which the peak of the damped response curve is deflected from the vertical.
2. The amount of damping determines not only the maximum value of the response but also the frequency for this maximum response.
3. Maximum-response amplitude and frequency depend on whether the forcing frequency is being swept from a lower to a higher frequency or the reverse.
4. The region between the vertical tangents to the theoretical response curve is called the region of instability. If we could excite response at a steady amplitude corresponding to a point along the theoretical line, then any disturbance of the system would cause a jump to either of the more stable response amplitudes.

Consider a system with a general elastic restoring force, but with linear damping, exposed to a sinusoidal exciting force so that the equation of motion is

$$a_1\ddot{x} + a_2\dot{x} + a_3 f(x) - F\cos\omega t = 0. \tag{6.142}$$

There are many ways to attack such equations. Abramson [68] summarizes most of these; further examples are given in the books on nonlinear vibrations cited in Chapter 2.

One procedure, called the Ritz method involves satisfying the equation in the average. Assuming a solution of Eq. (6.142) of the form

$$x_{av} = A\cos(\omega t - \phi), \tag{6.143}$$

in which x_{av} is the average value of x, and using the Ritz method leads to a pair of equations for the two unknowns A and ϕ,

$$\left[f(A) - \frac{a_1}{a_3}\omega^2\right]^2 + \left(\frac{a_2}{a_3}\omega\right)^2 = \left(\frac{F}{a_3 A}\right)^2 \tag{6.144}$$

and

$$\tan \phi = \frac{a_2}{a_3} \cdot \frac{\omega}{f\left(A - \frac{a_1}{a_2}\omega^2\right)}, \tag{6.145}$$

where

$$f(A) = \frac{1}{\pi A} \int_0^{2\pi} f(A \cos y) \cos y \, dy,$$

and y is an integration variable. The form of $f(A \cos y)$ is dictated by the form of $f(x)$.

Equation (6.144) describes response curves of the form shown in Fig. 6.18, and Eq. (6.145) gives corresponding phase-angle relationships. From these two equations, certain special relations are also found. Equations for these relations are listed below.

1. The undamped-free-vibration curve or natural-frequency trajectory:

$$f(A) = \frac{a_1}{a_3}\omega^2. \tag{6.146}$$

2. The undamped response curves:

$$a_1\omega^2 = a_3 f(A) \mp \frac{F}{A}. \tag{6.147}$$

3. The locus of vertical tangents of the undamped response curves:

$$\frac{a}{c}\omega^2 = f(A) + A\frac{\partial f(A)}{\partial A}. \tag{6.148}$$

4. The damped response curves:

$$\frac{a_1}{a_3}\omega^2 = f(A) - \frac{a_2^2}{2a_1a_3} \mp \left\{\left[\frac{F}{a_3A}\right]^2 - \frac{a_2^2}{a_1a_3}\left[f(A) - \frac{a_2^2}{4a_1a_3}\right]\right\}^{1/2}. \tag{6.149}$$

5. The locus of vertical tangents to the damped response curves:

$$\left[f(A) - \frac{a_1}{a_3}\omega^2\right]\left[f(A) + A\frac{\partial f(A)}{\partial A} - \frac{a_1}{a_3}\omega^2\right] = -\left(\frac{a_2}{a_3}\omega\right)^2. \tag{6.150}$$

In practical design, the maximum response amplitude is of prime interest. This resonance amplitude occurs at the point where the natural frequency trajectory crosses the damped response curve. Solving Eqs. (6.146) and (6.149) simultaneously leads to

$$\frac{b\omega}{c} = \frac{F}{a_3A}$$

and (6.151)

$$\phi = \pi/2.$$

The first of Eqs. (6.151) defines a hyperbola in the response diagram defining the locus of resonance amplitudes. The coordinates of the intersection of the free-vibration curve and the hyperbola define not only the maximum amplitude but also the frequency at which this amplitude occurs. Equation (6.151)

also states that the phase angle at maximum amplitude is $\pi/2$; this is identical with the linear case.

As in the linear case, the effects of reasonably small amounts of damping are almost negligible except near resonance. Hence, one could achieve a reasonable approximation of the response curve by computing only the undamped response curves and the hyperbola and then drawing the portions between, using the crossing point as the maximum. These operations are illustrated in Fig. 6.19.

Snowdon [60] makes the particular point that conventional transmissibility curves based on small dynamic strains still provide an extremely useful first approximation for large-strain behavior because, in well-designed mounting systems, the natural frequencies and the resonant frequencies fall well below the critical frequencies of the isolated object.* Further, the bending of the transmissibility curve to the right or left for the same energy input indicates that the transmissibility would be less than that calculated on the basis of a linear approximation.

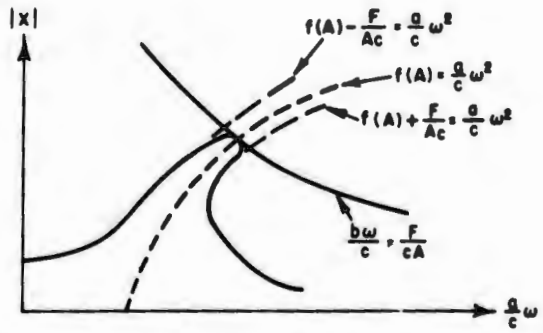

FIG. 6.19. Resonant amplitude of a nonlinear function.

Thus conventional transmissibility curves are definitely needed for cushions as a part of input-design data. It is important, however, that these curves be identified for the range of exciting amplitudes that appear reasonably valid.

6.7. Estimating Natural Frequency

For a linear system, the natural frequency is a unique value determined by the spring rate and the mass supported, or

$$\omega_n = \sqrt{\frac{k}{m}} = 19.6\sqrt{\frac{k}{W}},$$
$$f_n = \frac{\omega_n}{2\pi} = 3.13\sqrt{\frac{k}{W}}. \tag{6.152}$$

The last relation is valid numerically when k is in weight units per inch of deflection.

*Where the cushion has also been designed as a shock isolator as in a package, this statement does not hold true except for items with high fragility index.

In terms of a diffuse cushion, Eqs. (6.152) transform to

$$\omega_n = 19.6\sqrt{\frac{E}{\sigma_s T_c}} = 19.6\sqrt{\frac{E_r}{\sigma_s T_c}},$$
$$f_n = 3.13\sqrt{\frac{E}{\sigma_s T_c}} = 3.13\sqrt{\frac{E_r}{\sigma_s T_c}}, \tag{6.153}$$

where E is the modulus of elasticity and E_r is the real part of E^*. Damped natural frequencies are given by

$$\omega_d = \omega_n\sqrt{1-\beta^2} = \sqrt{\frac{|E^*|}{\sigma_s T_c}},$$
$$f_d = \frac{\omega_d}{2\pi} = \frac{1}{2\pi}\sqrt{\frac{|E^*|}{\sigma_s T_c}}. \tag{6.154}$$

For nonlinear systems, the slope of the stress-strain curve is no longer a straight line. The undamped natural frequency for any small excursions about the static load position will be given by [3]:

$$\omega_n = 19.6\sqrt{\frac{dF/dx}{w}} = 19.6\sqrt{\frac{d\sigma/d\epsilon}{\sigma_s T_c}}, \tag{6.155}$$

which can be written

$$\omega_n = 19.6\sqrt{\frac{E'}{\sigma_s T_c}} = 19.6\sqrt{\frac{E'_r}{\sigma_s T_c}} \tag{6.156}$$

provided that the elastic moduli (E' and E'_r) are determined in the region of the equilibrium position.

Table 6.3 gives some natural frequencies for various nonlinear elasticity functions.

TABLE 6.3. NATURAL FREQUENCIES FOR CERTAIN CLASSES OF ELASTICITY

Name	*Function* σ	*Natural Frequency* $\omega_n = 19.6\,(\sigma_s T_c)^{-1/2}\,Q$ Q
Tangent	$\frac{2}{\pi}\,a_1\epsilon_b \tan\frac{\pi}{2}\frac{\epsilon}{\epsilon_b}$	$\sec\frac{\pi}{2}\frac{\epsilon}{\epsilon_b}\sqrt{a_1}$
Algebraic	$a_1\epsilon\left(1-\frac{\epsilon}{\epsilon_b}\right)^{-1}$	$\left(a_1\frac{\epsilon}{\epsilon_b}\right)^{1/2}(1-\epsilon/\epsilon_b)^{-1}$
Logarithmic	$a_1\epsilon_b\left[\log\left(1-\frac{\epsilon}{\epsilon_b}\right)\right]$	$[-a_1(1-\epsilon/\epsilon_b)^{-1}]^{1/2}$
Air[a]	$P_a(1-\epsilon)^{-n}$	$[nP_a(1-\epsilon)^{-(n+1)}]^{1/2}$
Cubic	$a_1\frac{\epsilon}{\epsilon_b}+a_2\left(\frac{\epsilon}{\epsilon_b}\right)^3$	$\left(\frac{\epsilon}{\epsilon_b}+\frac{3a_2}{\epsilon_b{}^3}\epsilon^2\right)^{1/2}$

[a] n = 1.0 for isothermal compression and 1.4 for adiabatic compression.

6.8. Data on Real Materials

Despite the wealth of tools available for analysis, there are few data available in the literature in a form usable by designers. It seems that most of the vibration testing which has been performed is related to specific design projects, and the results are not readily retrievable. This paucity of information and many putative reasons for it have been discussed by Zell [179].

It will have been noted that all of the theoretical formulas depend on an assumption that the "spring" will operate in tension as well as compression. This is not necessarily true of cushions. The following include some of the variations from the ideal:

1. The cushion is bonded to the exciting surface and the load. In effect, the cushion becomes the elastomeric element in a mount. If the disturbances are small, tension and compression moduli are substantially equal and the test results can be analyzed by conventional theory. If the disturbance is large, however, and if the cushion is a foam or otherwise exhibits a collapsing-column effect, then the compression and tension moduli are different, as shown in Section 3.5. Several resonant points may appear because of the differences in moduli; these resonances would not be related to the wave-effect phenomena predicted by Snowdon [61].
2. The load is sandwiched between two layers of cushioning. Here the cushion acts in compression in both directions. When the test is run with the elements of the response system arranged vertically, then the downward force exerted by the load is greater than the upward force because of gravity. When the cushion is precompressed, the force on the cushion being compressed during a given cycle is increased by relief of the compression stress in the other cushion. Nevertheless, this configuration is reasonably typical of real packages and was selected as the test configuration by Zell [179]. There are further complexities involved in this configuration; they are discussed in Section 6.8.2.
3. The cushion is placed under a small, known precompression and vibrated by a moving head in such fashion that the head never leaves the cushion surface. This method is valid only for small inputs, but many valuable data can thus be obtained. Venning's [91] method of obtaining complex elastic moduli for the first portion of the curve for polyurethane foam is based on this technique.

Data obtained by any of these techniques are only as valid as the test technique allows them to be. Some form of vibration testing of individual designs will probably always be required.

6.8.1. Cushion Mounts. For the purpose of this monograph, a cushion mount is any combination of cushion and face plates for which vibration data have been obtained in compression and tension. In practice, these mounts are also loaded in shear and, where shear data are available, the results are also summarized.

What is perhaps the most comprehensive effort to use foam cushions for shock and vibration protection of installed equipment has been led by personnel of the Naval Air Development Center at Johnsville. This work includes laboratory evaluation and design studies; also, service test under

instrumented conditions, aided by practical service experience with specific designs installed in operational high-performance naval aircraft. The sole conclusion that can be drawn is that a properly designed foam mount surpasses the conventional point isolator mounts by several orders of magnitude when measured by the only significant criterion: equipment failure rate. From these results it seems inevitable that every designer faced with the problem of mounting equipment in a larger structure must consider the use of foam mounts, particularly where severe shocks and strong vibration are part of the environment.

The very superior performance of foam equipment mounting bases, as compared with the conventional point isolator mounting bases, is partly (at least) due to some assumptions that underly the design specification for the latter [276]. For example, this specification permits, in one configuration, a maximum overall height of the isolator of 1-5/8 in. with minimum rated load. It requires the use of snubbers, so that maximum travel before bottoming is 3/8 in.

The bottoming distance is therefore less than 25 percent of the available height. A foam, on the other hand, does not really bottom (although it may become very stiff) at 80 percent of its available thickness. Cohen [277] reasoned that this lack of travel was at the root of the problem; because mount-bottoming occurs at about a 2g acceleration input and this is well within the normal naval aircraft environment. Shock transmissibility in the vertical direction for a 3.8-pcf foam mount, compared with a conventional point isolator base, is shown in Fig. 6.20 (static stress, 0.18 psi). Typical vertical-vibration transmissibility for a 6.5-pcf polyurethane foam at the same static stress is shown in Fig. 6.21, while lateral transmissibilities for the same foam are shown in Fig. 6.22. Note that, as expected, natural frequency

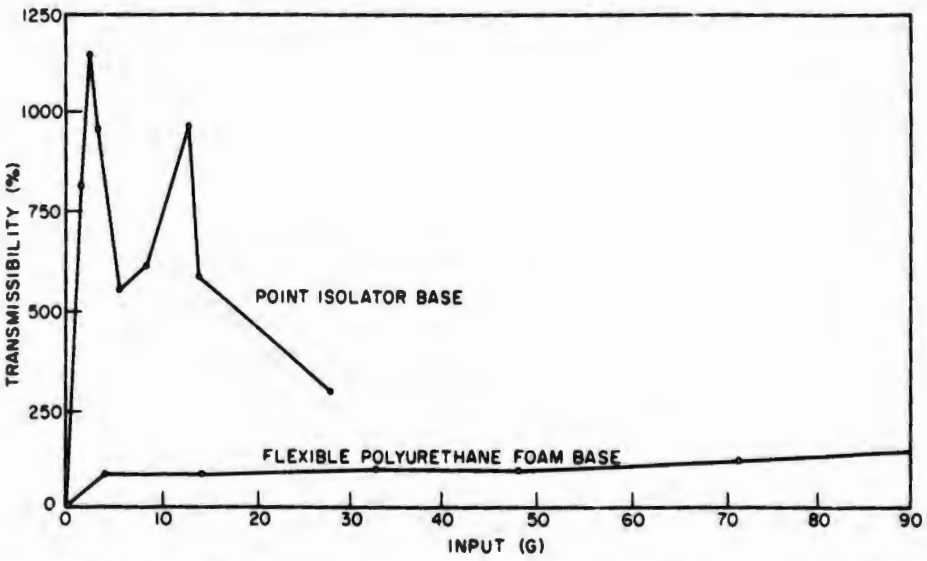

FIG. 6.20. Shock transmissibility for a foam mount compared with a conventional mount; foam density 3.8 pcf, thickness 1 in. Cohen [277].

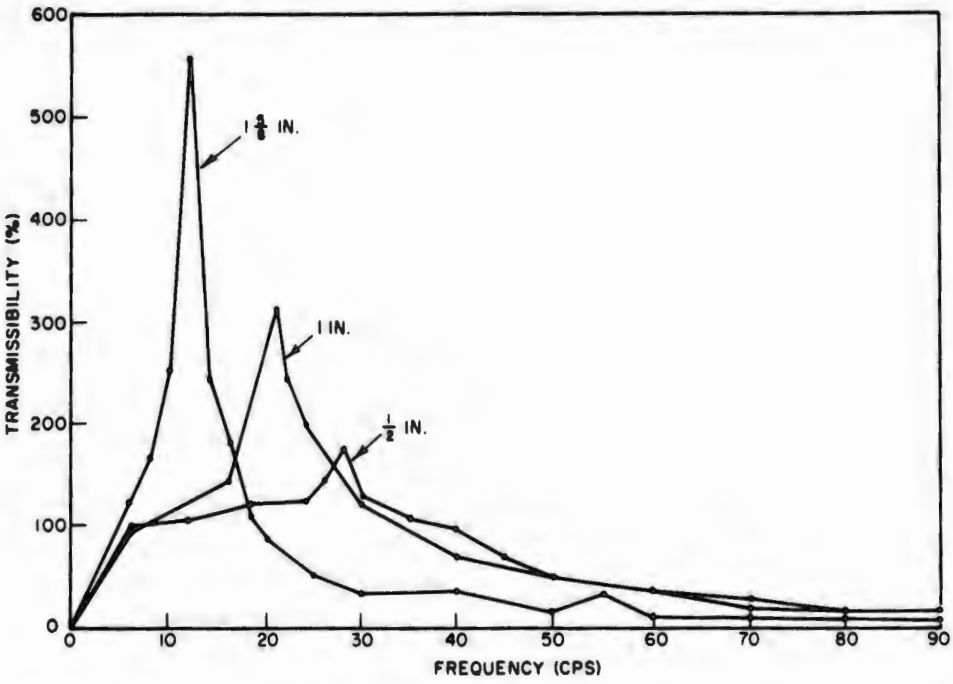

FIG. 6.21. Vertical-vibration transmissibility *versus* thickness of 6.5-pcf polyurethane foam; static stress 0.18 psi [277].

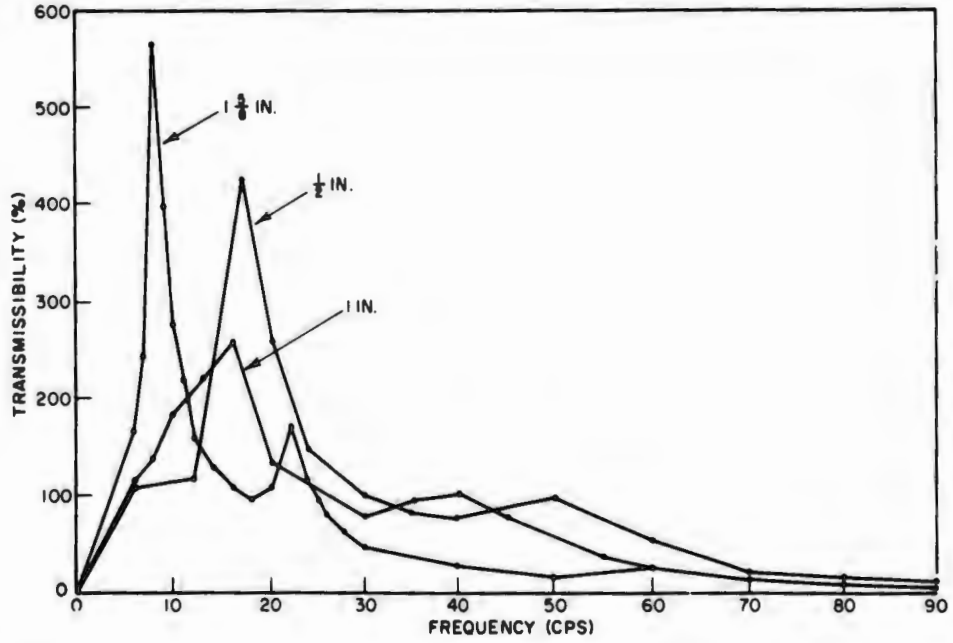

FIG. 6.22. Lateral-vibration transmissibility frequency for different thicknesses of 6.5-pcf polyurethane foam; static stress 0.18 psi [277].

rises as thickness is decreased. Input test syllabus was that of the referenced specification [276], *i.e.*,

5-14 cps,	0.100 in. double amplitude (d.a.)
14-23 cps,	1 g
23-74 cps,	0.036 in. d.a.
74-1000 cps,	10 g.

Vertical- and lateral-vibration transmissibilities for different foam densities are shown in Figs. 6.23 and 6.24.

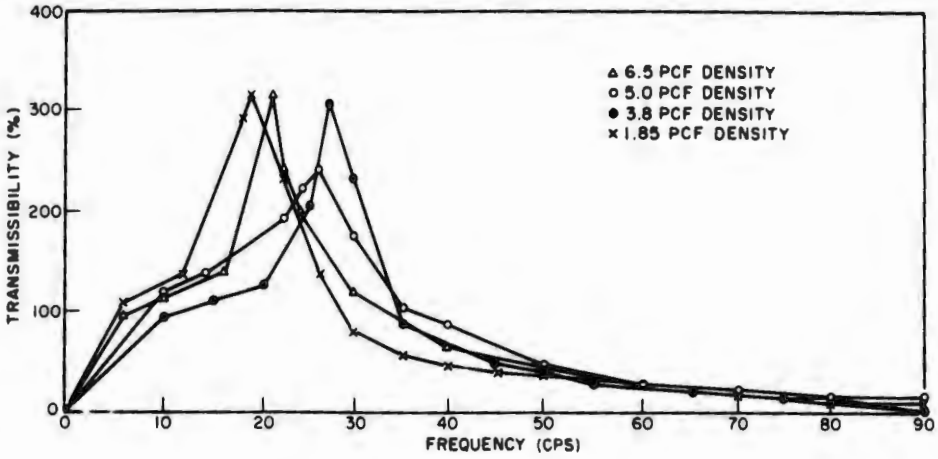

FIG. 6.23. Vertical-vibration transmissibility *versus* frequency for different densities of 6.5-pcf polyurethane foam; thickness 1 in., static stress 0.18 psi [277].

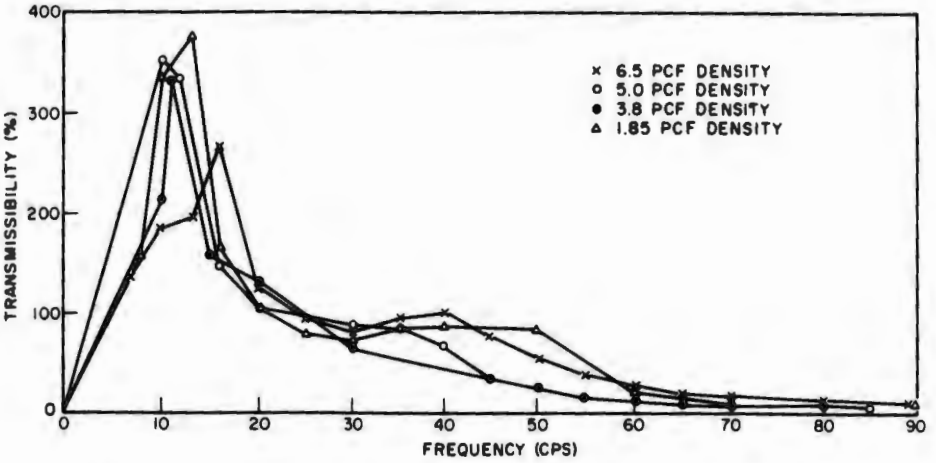

FIG. 6.24. Lateral-vibration transmissibility *versus* frequency for different densities of 6.5-pcf polyurethane foam; thickness 1 in., static stress 0.18 psi [277].

Cohen's work has been extended by Calcaterra [278] in the form of a design guide. Note that this design guide is only one of two papers reviewed – the other being Mustin's [171] – that recognized the importance of the contribution to cushion design made by Soper and Dove [33,67]. For an 8- by 8- by 1-9/16-in. sample of 3.8-pcf foam, resonant frequency *versus* static stress with several different steady-state input amplitudes is shown in Fig. 6.25. Peak transmissibility *versus* static stress for the same foam and three different input acceleration amplitudes is shown in Fig. 6.26.

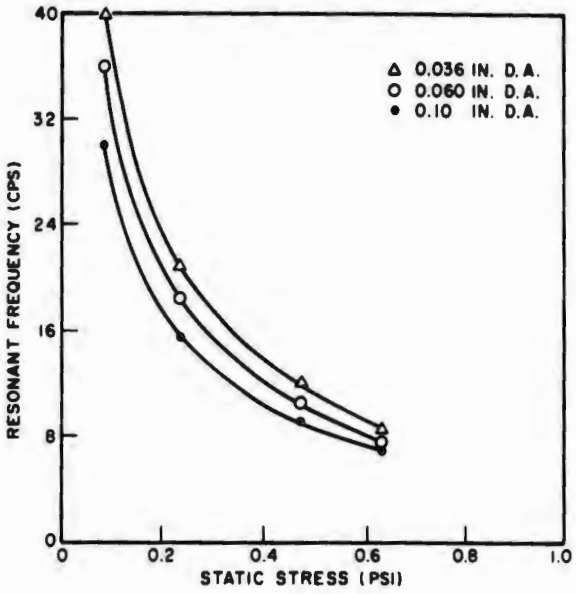

FIG. 6.25. Resonant compression frequency *versus* static stress with different vibration inputs for 3.8-pcf polyurethane foam; thickness 1-9/16 in. Calcaterra [278].

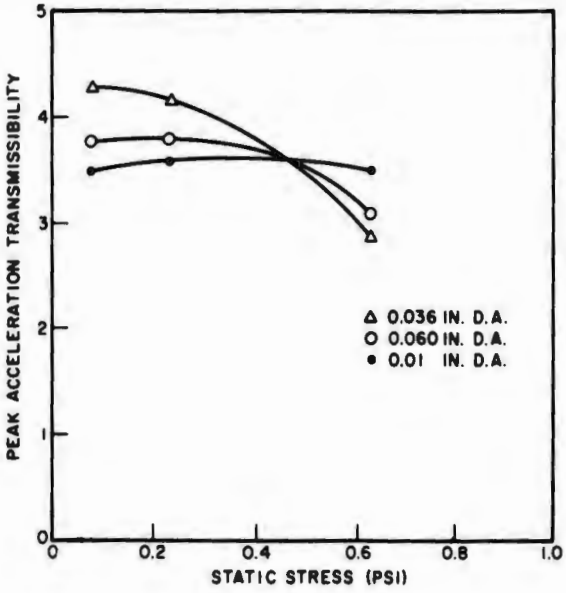

FIG. 6.26. Peak transmissibility at resonance *versus* static stress with different vibration inputs for 3.8-pcf polyurethane foam; thickness 1 in. [278].

Calcaterra [279] also reports the results of tests of various foam isolators placed at various locations in an A-3D aircraft with measurements being made during takeoff, landing, turn, sea-level flight, cruise at altitude, pullout, catapult shots, and arrested landings. A comparison of conventional mounts with foam mounts is given in Fig. 6.27, which shows that the two types of isolators are comparable in vibration isolation over a wide frequency range. The ordinate of these curves is "effective transmissibility," defined as the square root of the ratio of output to input power spectral density ("effective" because of the nonlinearity of the foam mounts). A comparison of measured responses for foam and conventional mounts for an arrested landing is given in Fig. 6.28. The peak input pulses are typical for the cockpit area of this aircraft. Inputs as high as 13g were measured in the vertical-stabilizer area, where aircraft structural attenuation would naturally be less.

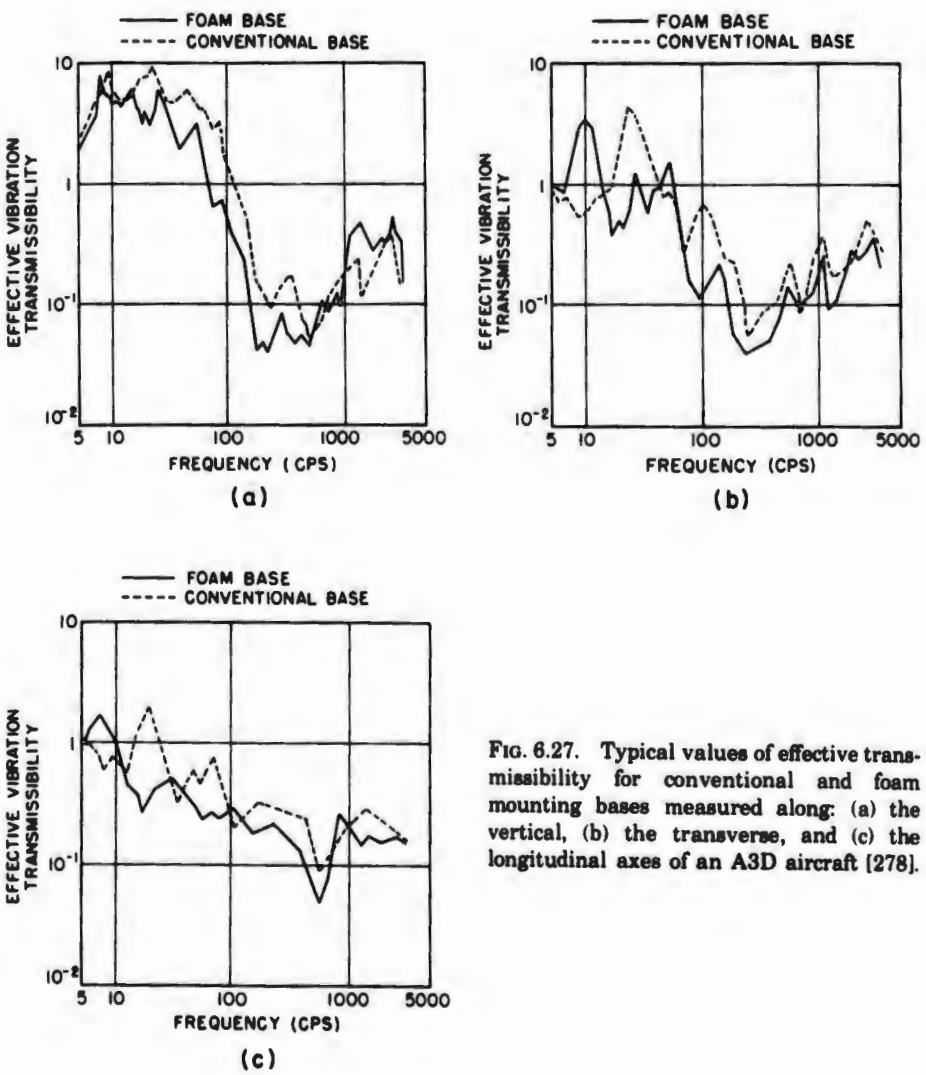

FIG. 6.27. Typical values of effective transmissibility for conventional and foam mounting bases measured along: (a) the vertical, (b) the transverse, and (c) the longitudinal axes of an A3D aircraft [278].

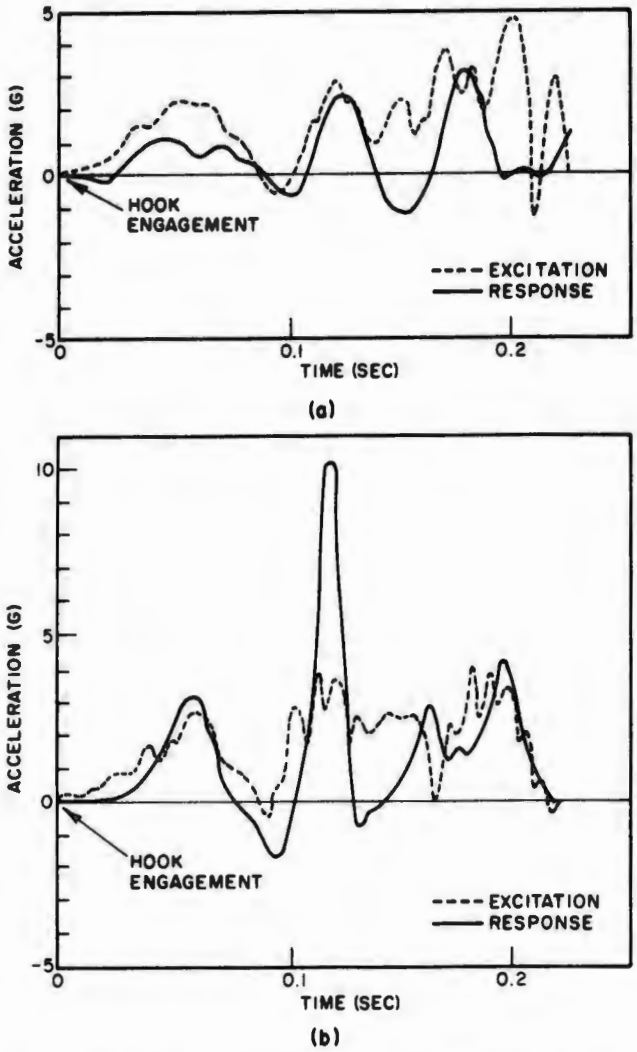

FIG. 6.28. Typical responses for vertical foam and conventional mounting bases during arrested landing: (a) foam mounting base, and (b) conventional mounting base. Calcaterra [279].

Some care is required in fabricating these mounts, largely to assure an adequate bond between the foam and the metal mounting plates. Cohen [277] found that he could test mounts at rated load with a 90-g sinusoidal shock wave in shear without encountering separation, provided that he used the correct adhesive on properly cleaned metal. He was not the first to use polyurethane foam in both compression and shear. Hardigg's Hardi-Pads [159] are glued between an inner and outer container. Unfortunately, the data available are rather inadequate.

Foam isolators were also used for the instrumentation capsule used on Edwards Air Force Base high-speed track sleds [280]. For all of these tracks,

speeds are so high and rail anomalies so unpredictable that random-vibration technology is the only useful analytical tool. Burgess [281] has described the environment and developed [282,283] a resilient slipper for these sleds to reduce the generally Gaussian input from the rails. Because of the heat of friction, the resilient material used was stainless-steel knitted wire mesh bonded to stainless-steel backing sheets. Figure 6.29 shows rms accelerations *versus* sled velocity for the conventional slipper without isolator and for the proposed resilient slipper. The acceleration values shown were obtained by numerically integrating the response acceleration spectral-density curves and taking the square root of the result.

Burgess [62] has also investigated the problem of distributed media for shock and vibration isolation of installed electronic equipment. In this work he determined complex moduli for certain solid elastomers, some with very small closed holes scattered throughout the matrix, Jacobsen's [192] silastic with Teflon inclusions, a polyurethane foam, and a fibrous silicone rubber. He noted that thickness to achieve a specified natural frequency was given by

$$T_r = \frac{g\,E_r}{4\pi^2\,\sigma_s\,f_n^2} = 9.86\,\frac{E_r}{\sigma_s\,f_n^2}. \tag{6.157}$$

On this basis, for the materials investigated, he computed the values shown in Table 6.4. Using these results, and considering the weight penalty involved, he concluded that only foams and similar materials offered real promise as distributed shock and vibration isolators.

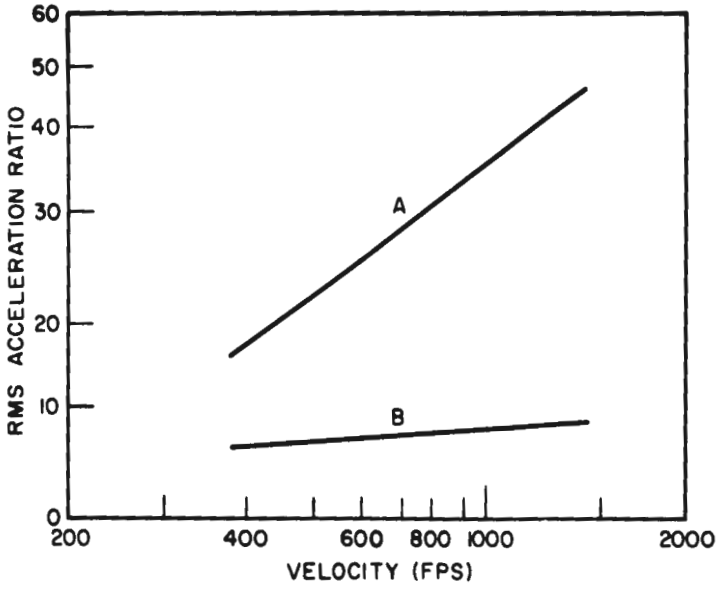

FIG. 6.29. Rms acceleration *versus* sled velocity: A with conventional slipper, and B with resilient slipper. Burgess [282].

TABLE 6.4. THICKNESS OF VARIOUS MATERIALS FOR A SPECIFIED NATURAL FREQUENCY

Material	T_c, *Approximate Thickness Required* (in.)			
	$\sigma_s = 0.1$ psi		$\sigma_s = 1.0$ psi	
	$f_n = 10$ cps	$f_n = 40$ cps	$f_n = 10$ cps	$f_n = 40$ cps
BTR Rubber	980	60	98	6
Microporous nitrile rubber	440	30	44	3
Silastic with Teflon rods	440	30	44	3
Homogeneous silastic	340	25	34	2.5
Silastic with air-filled holes	130	8.5	13	0.85
Neoprene latex foam	30	2.5	3	0.25
Polyurethane foam	5	0.37	0.5	0.04
Fibrous silicone rubber	5	0.32	0.5	0.03

6.8.2. Simulated Packages. The major available work on vibration properties of cushions using the simulated-package technique is that of Zell [179].

In using the simulated-package technique several variables that may affect the results obtained must be recognized. In Fig. 6.30, the upper cushion is placed in contact with the mass in its static position. Figure 6.31 shows how a pair of linear undamped cushions would respond to a sinusoidal excitation. The response of the cushioned mass is inherently nonlinear despite the linearity of the material.

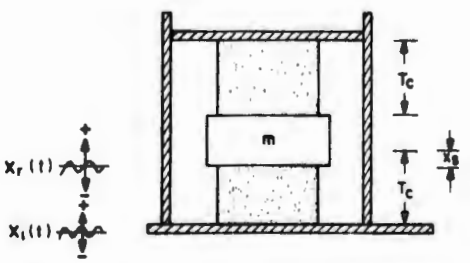

FIG. 6.30. Package cushion with upper cushion not precompressed; x_s is static deflection produced by mass m (single-degree-of-freedom response assumed).

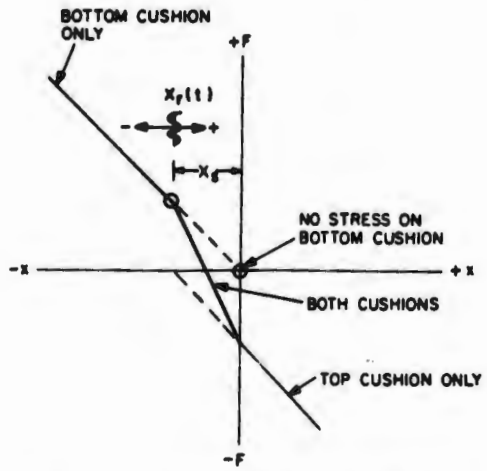

FIG. 6.31. Force on mass *versus* deflection of the Fig. 6.30 configuration; response inherently nonlinear even when cushions are linear and massless.

Figure 6.32 shows the configuration used by Zell. Here a static preload is applied through the upper plate of the test rig. The upper cushion is compressed a distance Δx_u produced by this preload, whereas the lower cushion is compressed a total distance $x_s + \Delta x_l$. When the cushions are linear and massless, $\Delta x_u = \Delta x_l$. When the cushions are nonlinear, Δx_u is not expected to equal Δx_l unless the preload produces strains in the linear range of the material. Figure 6.33 illustrates the response of linear massless cushions to sinusoidal excitation. The response is linear as long as the peak-to-peak value of $x_r(t)$ is less than $2\Delta x$, but becomes nonlinear when $2\Delta x$ is exceeded.

A third possible condition which might exist is shown in Fig. 6.34. Here, the static deflection of the lower cushion under the influence of mass m is not compensated for in the test rig. In addition, the lower cushion has taken a set, x_d, over and above the initial static deflection, x_s. The response is shown in Fig. 6.35. As soon as the upward moving mass overcomes distance

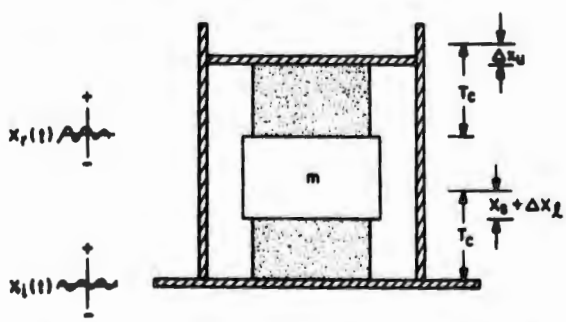

FIG. 6.32. Package cushion when preload is applied to top and bottom cushions.

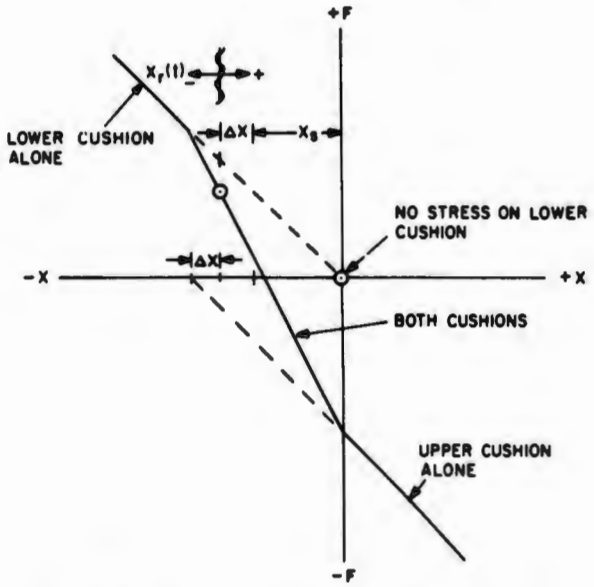

FIG. 6.33. Response of linear massless undamped cushions in the Fig. 6.32 configuration.

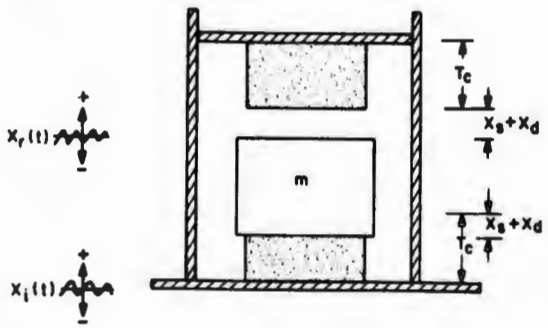

FIG. 6.34. Uncompensated configuration; distance x_d is a set assumed by the lower cushion.

x_s, the upward cushion force drops to zero and the mass is in free flight upward until brought to rest by the force of gravity or until it contacts the upper cushion. (Figures 6.31, 6.33, and 6.35 ignore gravity for the sake of clarity.)

Figure 6.34 shows a degenerate case of the configurations in Figs. 6.30 and 6.32. In an actual package, the additional deflection, x_d, of the lower cushion can arise from drift or creep during storage. This topic is discussed in more detail in Chapter 8.

A situation like that shown in Fig. 6.35 can arise in vibration-testing real cushions, all of which have marked damping characteristics. Where $x_i(t)$ is a relatively high-frequency oscillation, the cushion may not have time to recover before force direction changes. Such a situation is shown in Fig. 6.36; this is for the configuration of Fig. 6.32 with the peak-to-peak value of $x_r(t)$ less than $2\Delta x$. (Compare Fig. 6.36 with Fig. 3.6.)

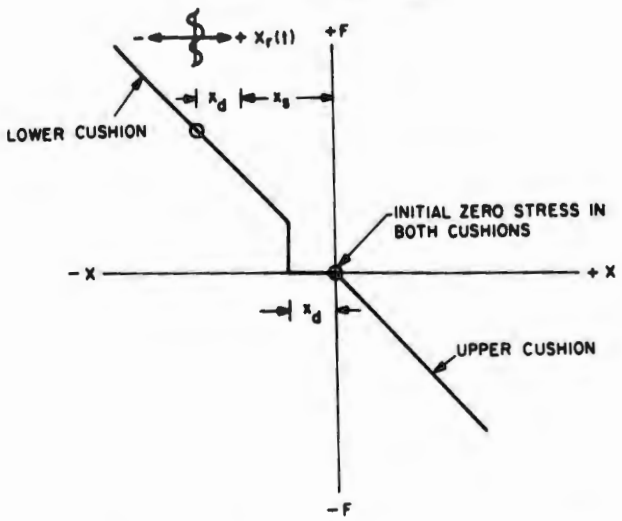

FIG. 6.35. Response of the Fig. 6.34 configuration; mass is in free flight over distance x_d.

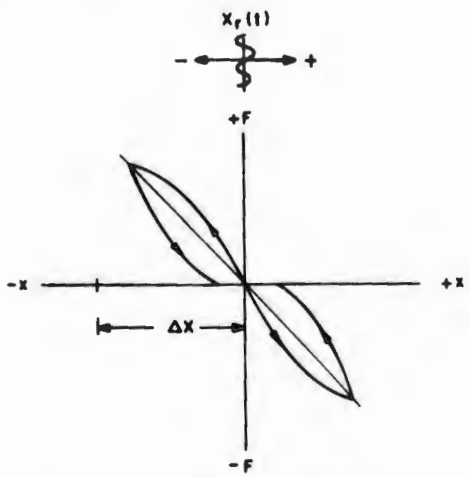

FIG. 6.36. Force *versus* deflection for a pair of linear damped cushions.

Finally, free flight can be induced simply because $x_r(t)$ is so large as to induce substantial permanent set in either or both members of the cushion pair.

All the foregoing factors demonstrate why information is scarce and why the designer must use available data with caution and insight.

Zell [179] began with a test syllabus based on a military specification [284] that was being considered by the American Society for Testing and Materials as a package-cushioning vibration-properties test. This test syllabus requires exposure to the following frequencies and amplitudes:

2-5 cps,	1.0 in. d.a.
5-25 cps,	1 g peak acceleration
25-50 cps,	0.04 in. d.a.
50-300 cps,	5 g peak acceleration.

Working initially with polystyrene foam, Zell found that trying to hold to these extreme conditions produced drastic permanent set of the material even when the total test period was 15 minutes but only about 5 minutes at resonance. Remaining tests were run at much lower amplitudes.

Figure 6.37 shows typical results for 2-pcf polyether urethane foam at a thickness of 2.9 in. and a static stress of 0.16 psi. Note that the measured peak transmissibilities lean to the left as the response moves into the softening range of the foam and then lean to the right as the response amplitude extends into the hardening area of the dynamic stress-strain function.

Figures 6.38 through 6.41 show the results for various polystyrene foams at different static stresses and thicknesses. Note that, except in Fig. 6.38, these static stresses were at the lower end of the optimum static-stress values obtained from shock-testing the foams. When testing 0.8-pcf polystyrene at the indicated optimum shock stress of 1.5 psi, thickness losses in the upper and lower cushions were 18 and 36 percent respectively. At 0.7 psi, however, the losses were reduced to 8 and 10 percent.

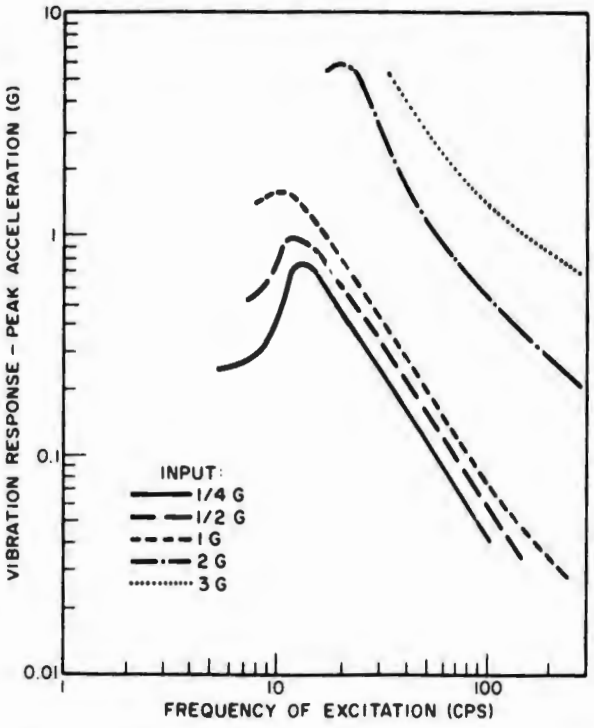

FIG. 6.37. Response for 2.9-in.-thick polyether urethane foam; density 2 pcf, static stress 0.16 psi. Zell [179].

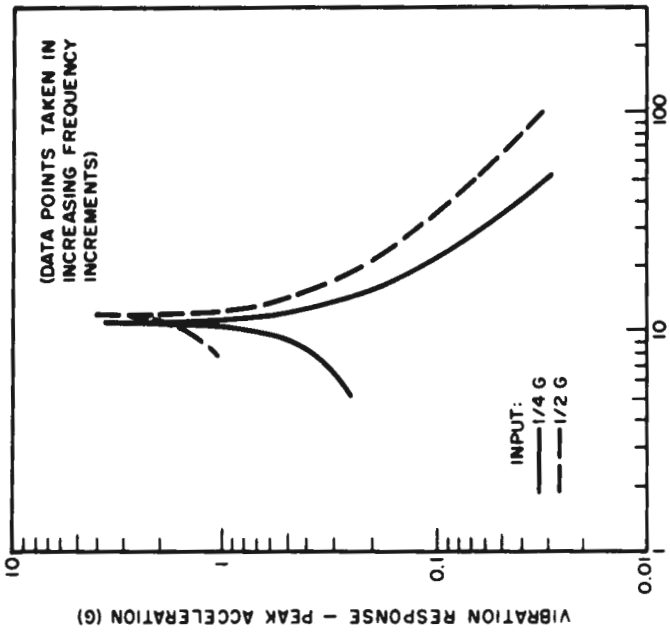

FIG. 6.39. Response for 5-in.-thick polystyrene foam; density 0.8 pcf, static stress 0.7 psi [179].

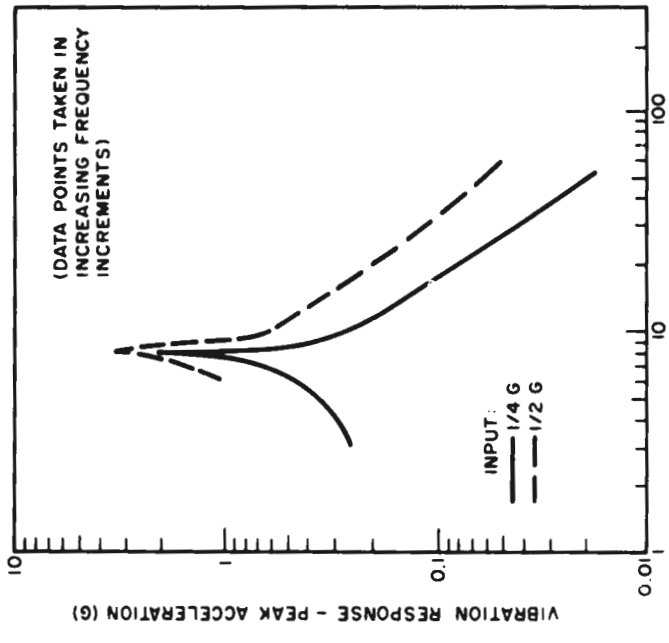

FIG. 6.38. Response for 5-in.-thick polystyrene foam; density 0.8 pcf, static stress 1.5 psi [179].

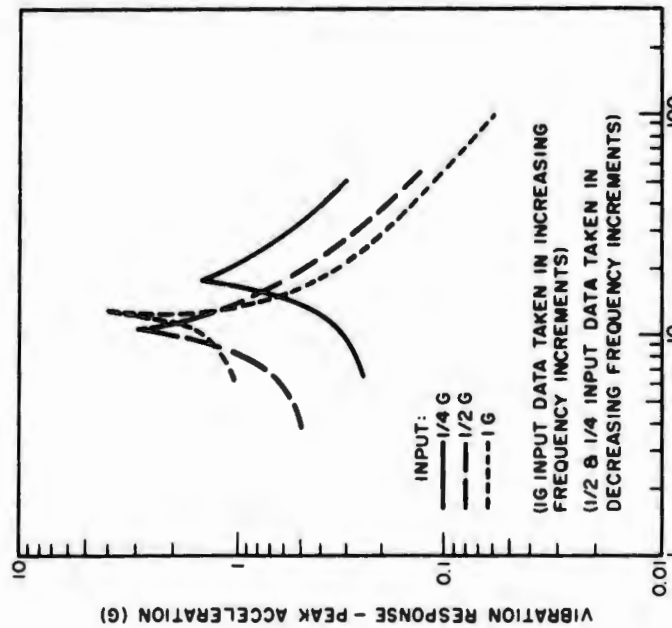

FIG. 6.41. Response for 3-in.-thick polystyrene foam; density 1.1 pcf, static stress 0.6 psi [179].

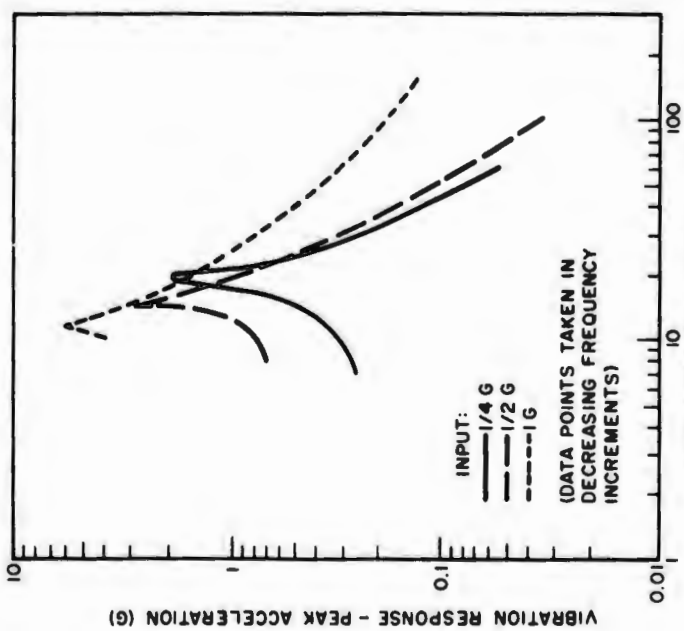

FIG. 6.40. Response for 5-in.-thick polystyrene foam; density 0.5 pcf, static stress 0.6 psi [179].

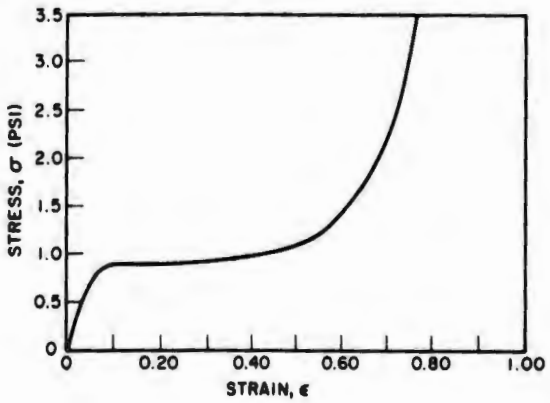

FIG. 6.42. Stress-strain curve for the polyurethane foam checked by Henny and Leslie [285].

In discussing his results with polystyrene foam, Zell tentatively suggested that the 0.8-pcf foam was demonstrating a linear spring characteristic but nonlinear damping. However, one can argue the opposite from the same set of data. Since, for a given static stress,

$$\omega_n = f\left(\frac{E_r}{T_c}\right), \tag{6.158}$$

a reduction in elastic modulus at a given deflection matched to an equal reduction in thickness (through cushion creep) would leave the natural frequency unchanged.

Henny and Leslie [285] have also reported results on a polyurethane foam whose static stress-strain curve is shown in Fig. 6.42. Results for various static stresses and inputs are shown in Fig. 6.43. When the input vibration spectrum of Fig. 6.44 was applied with a bearing stress of 0.81 psi, the results were as shown in Fig. 6.45. Isolation occurred at all frequencies above 6 cps. These authors also noted that a package designer must compromise between the shock data and the vibration-response data. For the 2-inch-thick polyurethane foam (Fig. 6.45) they recommended a static stress between 0.23 and 0.30 psi as the best compromise to meet the requirements of Fig. 6.44.

More recently, Zell and his co-workers have explored the results obtainable from the Fig. 6.32 configuration in greater depth and with two additional materials.* All these tests have been run at a constant peak input acceleration of $2g$, with varied frequency. Since $x_i(t)$ is essentially sinusoidal, maximum displacement is directly ascertainable by using the familiar relationship

*The work discussed here was not available at first writing. The graphs first became available in manuscript review. The approach taken was considered so basic as to warrant rewriting Section 6.8.2 despite the publication delays involved. As of this writing, the polyethylene foam data are scheduled to be published in a Picatinny Arsenal Report tentatively titled "Vibration Testing of Resilient Package Cushioning Materials; Polyethylene Foam." The polystyrene-acrylonitrile co-polymer data are scheduled to follow in a separate report, which will be prepared after additional testing. Particular thanks are due for permission to use the data in advance of publication. The reader will appreciate that any conclusions drawn are my own and are not necessarily related to those which Zell may draw with all the data before him.

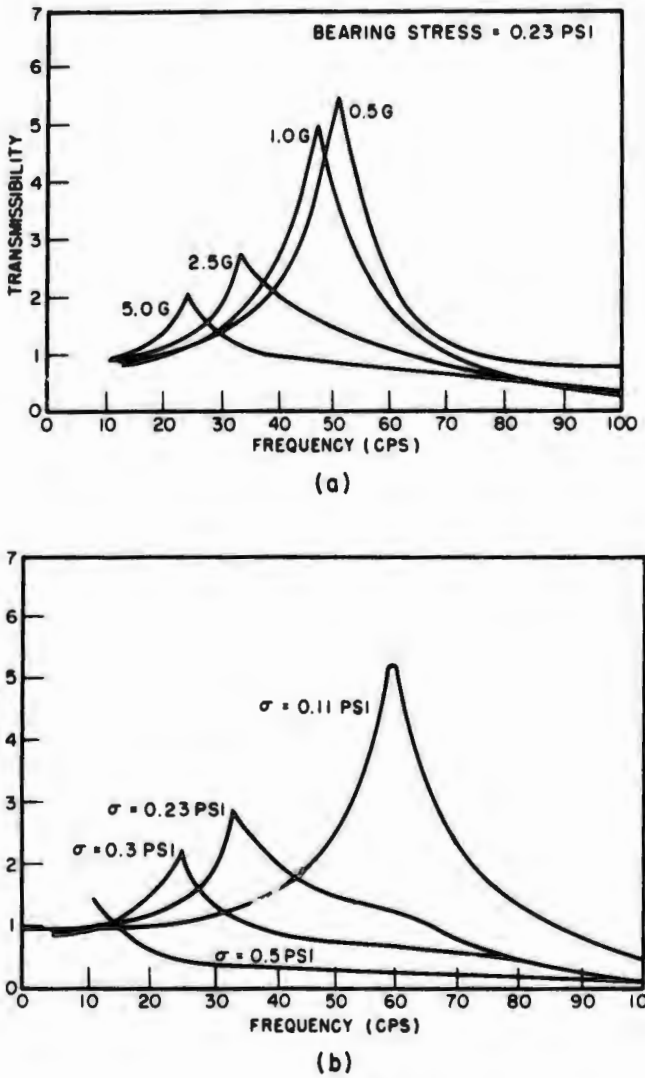

FIG. 6.43. Transmissibility curves for a polyurethane foam: (a) static stress 0.23 psi and various input amplitudes, and (b) input 2.5 g and various static stresses [285].

$$x = \frac{\ddot{x}}{\omega^2} = \frac{\ddot{x}}{(2\pi f)^2}, \tag{6.159}$$

which may be written

$$x = \frac{Gg}{(2\pi f)^2} \approx 10\,\frac{G}{f^2}\ \text{in.}, \tag{6.160}$$

where f is frequency in cps, and G is a multiple of the engineering value of the acceleration of gravity, $g = 386$ in./sec/sec.

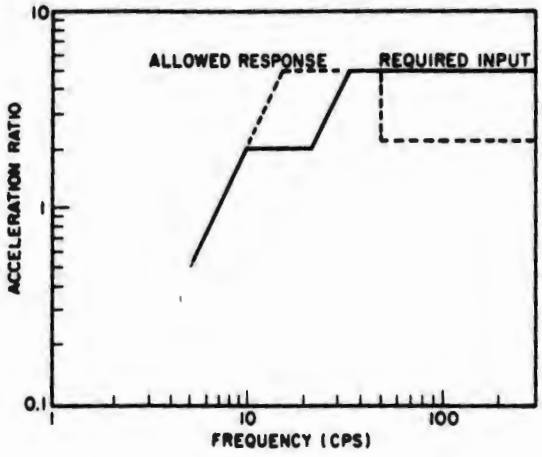

FIG. 6.44. A required test syllabus [285].

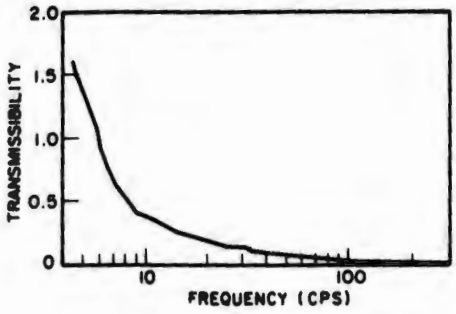

FIG. 6.45. Results of exposing a 2-in.-thick polyurethane foam to the test syllabus of Fig. 6.44; static stress 0.81 psi [285].

Figure 6.46 plots results obtained with 2.1-pcf polyethylene foam with 1.0-psi static stress. Testing began at 200 cps and was run in decreasing frequency intervals with the amplitude at zero between successive data points. Sample dimensions were $8 \times 8 \times 2$ inches. Peak response amplitude of $11g$ was noted at about 11 cps. Testing was continued down to about 6 cps, at which point a set of 3/16 inch became evident. The frequency change procedure was then reversed, using the same sample throughout; these results are also shown. This figure clearly illustrates the anomaly introduced by dynamic set of a given material.

Figure 6.47, on the other hand, used one sample for the increasing frequency sweep and another sample for the decreasing sweep. This figure shows behavior that is in consonance with classical theory, summarized in Section 6.6.

Figures 6.46 and 6.47 demonstrate rather dramatically the difficulty of making firm predictions of service behavior based on idealized laboratory tests.

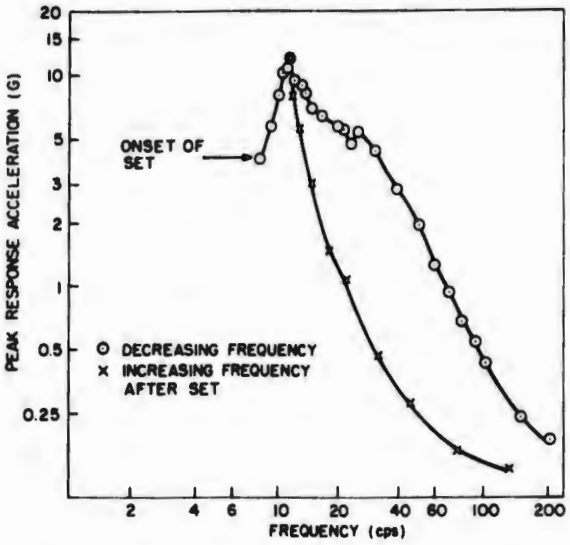

FIG. 6.46. Response *versus* frequency for polyethylene foam, density 2.1 pcf; samples 8 × 8 × 2 in., static stress 1.0 psi, 2 g input; same sample used throughout, showing effect of set; amplitude at zero between data points. Zell.

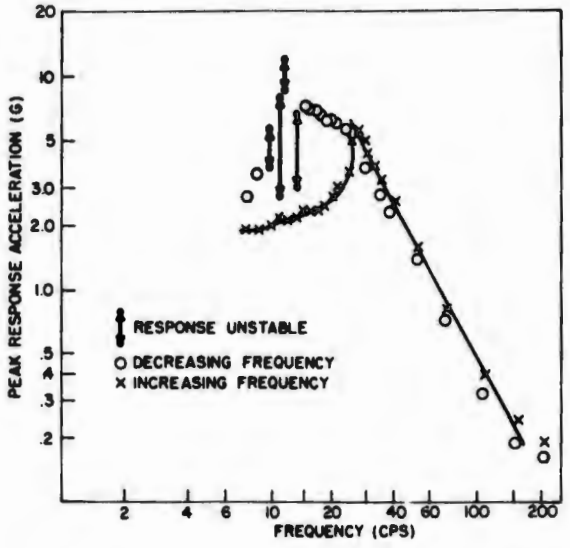

FIG. 6.47. Response *versus* frequency for same foam (8 × 8 × 2 in. sample) as in Fig. 6.46 except samples were changed between increasing frequency sweep and decreasing frequency sweep; static stress 1.0 psi, amplitude at zero between data points. Zell.

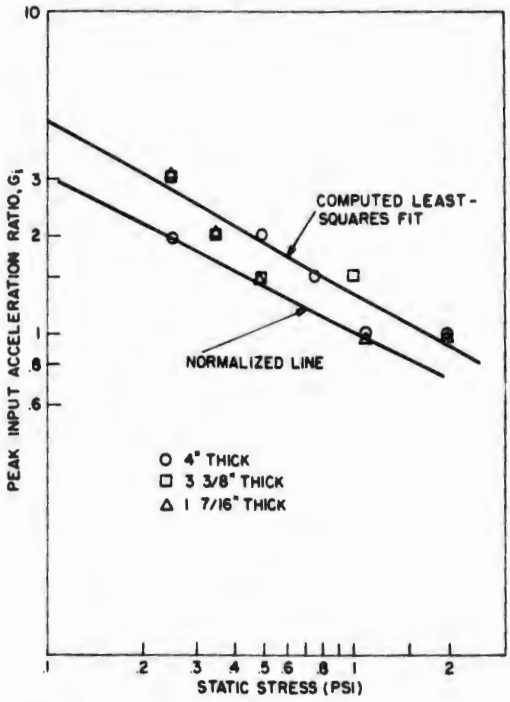

FIG. 6.48. Input vibratory acceleration producing dynamic set *versus* static stress, for 2.1-pcf polyethylene foam. Zell.

Considerable effort was devoted to finding what combination of input motion and static stress would produce dynamic set. The results, which seem largely independent of thickness, are shown in Fig. 6.48. The equation for the least-squares fit to the available data is

$$G_i = 1.3\,\sigma_s^{-0.54}, \tag{6.161}$$

where G_i = input acceleration amplitude (dimensionless).

The closeness of the slope of the line to $-1/2$ suggests that the true slope from a very large population might well be $-1/2$. Refitting the data to the *a priori* relation results in the normalized line shown. This latter line seems to provide a lower bound to the data available and therefore could be used as the design curve with some confidence. The equation for the normalized line is

$$G_i = \sigma_s^{-1/2}. \tag{6.162}$$

In plotting the results obtained from extensive tests at many frequencies and thicknesses (while generally maintaining the 8- by 8-inch plan for the samples), the investigators found a consistency of relationship between two quantities. The first quantity, "effective modulus" E_f, is the modulus at resonance of a linear cushion having the same resonant frequency as the actual nonlinear system under given test conditions. The second quantity, "forcing strain" ϵ_f, is the ratio of peak input motion to cushion thickness.

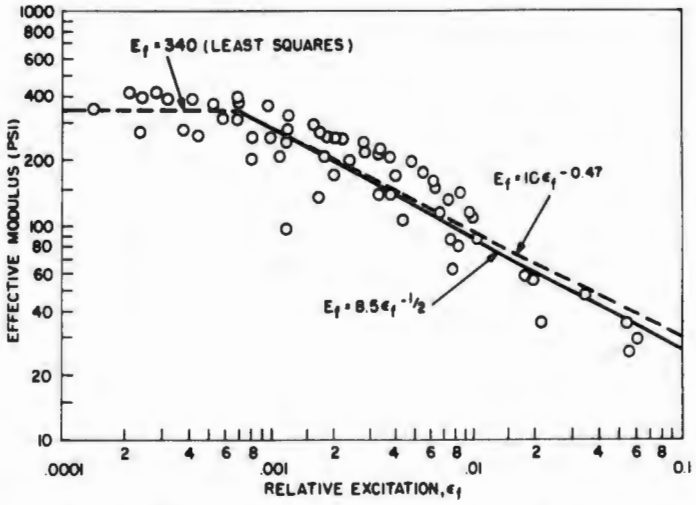

FIG. 6.49. Effective modulus *versus* forcing strain for four different thicknesses of 2.1-pcf polyethylene foam, note apparent material linearity at low forcing strains, *i.e.*, at high frequencies. Zell.

Since the input motion is always sinusoidal, ϵ_f and E_f can be defined mathematically as

$$\epsilon_f = \frac{x_i}{T_c} = \frac{Gg}{\omega_n^2 T_c} = \frac{Gg}{(2\pi f_n)^2 T_c} \approx 10\,\frac{G}{f_n^2 T_c}, \tag{6.163}$$

$$E_f = \frac{\omega_n^2 \sigma_s T_c}{g} = \frac{(2\pi f_n)^2 \sigma_s T_c}{g} \approx 0.1\ \sigma_s T_c f_n^2. \tag{6.164}$$

For both the polyethylene foam and the styrene co-polymer they found that E_f is a constant for lower values of ϵ_f and then tends to follow an exponential regression line of the form

$$E_f = a\epsilon_f^{-b}, \tag{6.165}$$

where a and b are empirically obtained from least squares. Specific results for polyethylene foam are shown in Fig. 6.49. Again, the slope of the empirical line being close to $-1/2$ suggests an approximation in the form

$$E_f = a'\epsilon_f^{-1/2}, \tag{6.166}$$

where, for polyethylene foam, a' is 8.5.

For the styrene co-polymer, it was found that the constant for the approximate regression line is $a' = 12.5$. E_f has a constant value of 270 psi when $\epsilon_f \leq 2 \times 10^{-3}$.

Combining Eqs. (6.164) and (6.166) leads to a prediction of natural frequency for varying E_f in the form

$$f_n \sigma_s = c(GT_c)^{-1/2}, \tag{6.167}$$

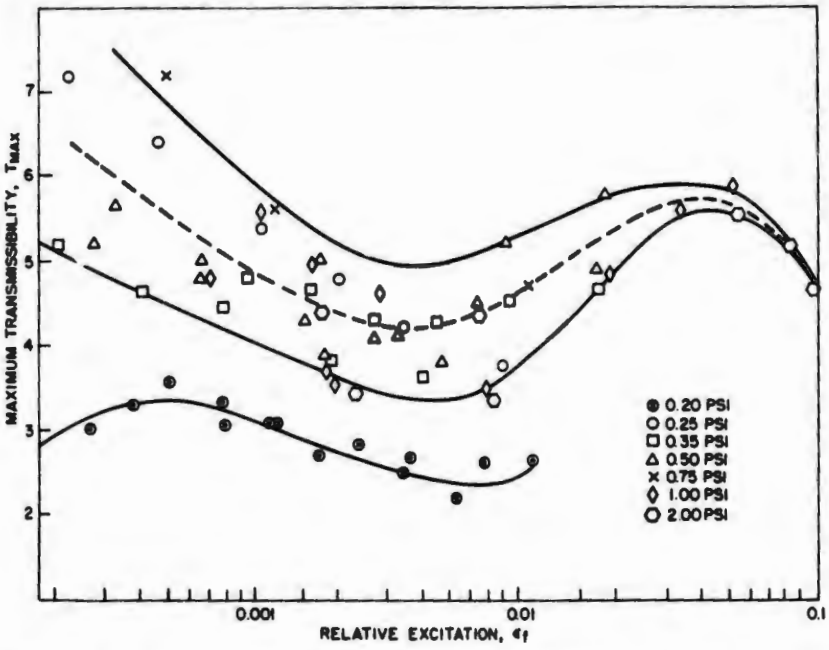

FIG. 6.50. Maximum transmissibility *versus* forcing strain for four thicknesses of 2.1-pcf polyurethane foam. Zell.

where

$$c = \frac{a'}{2\pi}\sqrt{g}.$$

For polyethylene foam, $c = 26.7$; for the styrene co-polymer, $c = 39.3$.

Plotting transmissibility against forcing strain does not produce such simple curves. Data from four thicknesses and varying static stresses for polyethylene foam are summarized in Fig. 6.50.

The work performed to date by Zell and his co-workers represents a significant improvement in methods of attacking the complex problem of cushion performance in the simulated package mode. Note that the definition of E_f given in Eq. (6.164) can be shown to be the same as the definition of the storage modulus at the natural frequency of the cushion given by Eq. (6.29). Evidently, therefore, Fig. 6.49 is a plot of the storage modulus at the natural frequency of polyethylene against a parameter representing cushion deflection. As pointed out in Chapter 3, this is the goal to be sought in considering the complex moduli of nonlinear materials.

Equation (6.31) gives transmissibility in terms of the complex modulus. Transmissibility at resonance can be estimated with reasonable accuracy from

$$T_{max} = (1 + E_r^2/E_i^2)^{1/2}, \tag{6.168}$$

which is a restatement of Eq. (6.31) assuming that peak transmissibility occurs at a frequency ratio of 1.0. Naturally, this is not accurate for heavily damped materials but such inaccuracies would undoubtedly be masked by

inherent material variability. Hence, the simplified equation could be used in preliminary design.

Since the test procedure evaluates the maximum transmissibility at a fixed input acceleration and variable frequency, the loss modulus at a given excitation level is

$$E_l = E_f(T_{max}^2 - 1)^{-1/2}. \tag{6.169}$$

It would be interesting to see a plot of the loss modulus, so derived, against ϵ_f; a usable relation is badly needed. It must be admitted that the loss modulus so determined may not be translatable to other cushion shapes, because of the strong effect of shape on the effective air damping. Shape-factor corrections could undoubtedly be determined in due course.

6.8.3. Precompressed Single Cushions. As noted in the first part of Section 6.8, successful results are obtained with this configuration only if the response is such that the load does not part company with the cushion.

North American Aviation [164] exposed a firm (nominal density around 3 pcf) latex hair sample 3 inches thick to the following vibration spectrum:

2 cps,	0.25 in. d.a.
3 cps,	0.45 in. d.a.
5-16.5 cps,	0.5 in. d.a.
16.5 to 200 cps,	7 g peak.

Three static stresses were used: 0.266, 0.284, and 0.363 psi. Under these conditions, the differences in stresses and amplitudes produced no significant difference in results, so one transmissibility curve was enough (Fig. 6.51). This curve is repeated in Franklin and Hatae [161], who also show one transmissibility curve for 2.2-pcf polyester urethane, presumably obtained from the same form of test syllabus.

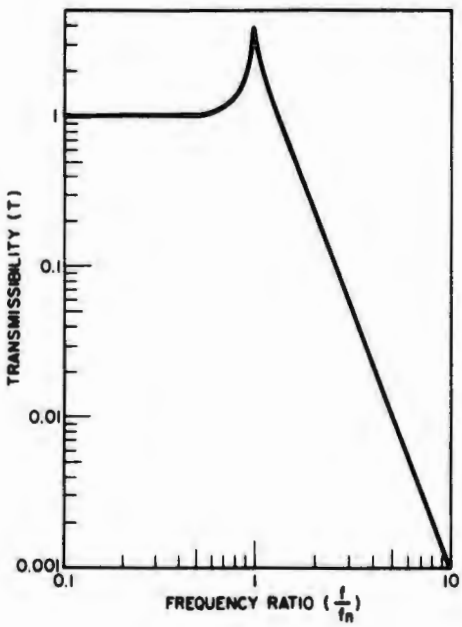

FIG. 6.51. Transmissibility of firm rubberized hair. North American Aviation [164].

Keast and Baruch [184] have computed the transmissibilities of a number of packaging materials. Since their chief aim was to observe the effects of extreme environments on these materials, their results will be discussed in the next chapter.

Felt has been rather neglected in shock isolation work in recent years and its popularity as a vibration isolator has apparently declined, except for applications made in a traditional manner. Lehmberg's [286] data on the six SAE grades of felt provide much valuable practical information. Tyzzer and Hardy [287] found useful results with 10-, 22-, and 49-pcf felts for vibration isolation.

Finally, as a reminder that the property of vibration isolation is not confined to carefully fabricated materials, Ezzat [288] has found that dry Oregon Pine sawdust is a good isolator for all except low-frequency, low-amplitude vibrations.

6.9. The State of the Art

Vibration theory is far ahead of the availability of data on which sound designs can be based. Few cases are recorded of rational designs based on specific efforts to control vibration characteristics with cushions. As far as packaging is concerned, the number of such designs is negligible.

This is unfortunate. Hatae [289] has correctly labeled vibration as the true frontier for package designers. Morrow [290,291] suggested almost nine years ago that packages be designed on the basis of the vibration to be isolated, letting the shock values fall where they may. He noted, in particular, that the Q of the system can be established as satisfactorily by designer's choice as by vibration test, provided that the designer separates the suspension resonance and the first resonance of the equipment by at least an octave.

My own observation over a number of years convinces me that it is far more common for packaged items to fail in shock from hard bottoming of the cushion than from exceeding an arbitrarily chosen peak acceleration. Perhaps, in some golden age when we have adequate statistical data on the shipping environment, designers will calculate thickness on the basis of preventing bottoming under root-mean-square shock intensity, except for very high-value items which might be protected for three or more standard deviations. Then they can concentrate on the vibration problem.

Mains [292] states that shock intensity practically has to have the characteristics of a random variable, noting that one must think of a punch press or a drop hammer to visualize a structure for which shock loading is anything but random.

Undoubtedly a major current difficulty is the selection of a reasonable vibration-test amplitude and syllabus. The commonly used military standard [284] is known to be based on an envelope of worst conditions, and many test syllabi do not recognize the effects on the forcing structure of the mass of the object being vibrated. For heavy loads, as pointed out by O'Hara [264], the impedance of the supporting structure—be it rail car, truck, or ship deck—cannot be considered infinite.

There has been a tendency to regard field vibration as random and then equate more convenient sinusoidal testing through a cumulative fatigue

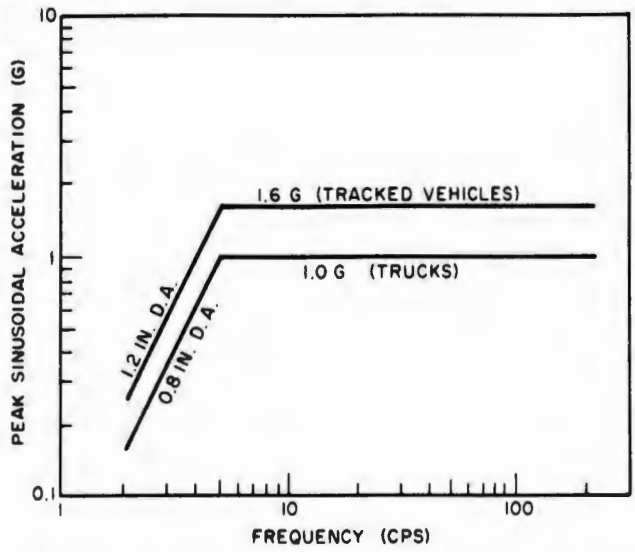

FIG. 6.52. Equivalent sinusoidal vibration spectrum for wheeled and tracked vehicles on the Munson road. Zell [179].

function such as the Miner-Palmgren [293,294] linear hypothesis. One such effort was discussed recently by Kasuba [295]. In general, as shown by Gertel [296], this results in a sinusoidal amplitude which is 2.17 times the root-mean-square random amplitude. Results for vehicles traveling over the Munson Road course at Aberdeen are shown in Fig. 6.52. It is now felt, despite my own contribution using Miner-Palmgren a few years ago [269,270], that these amplitudes are too high to measure the vibration behavior of cushions. Doubts of the validity of a connection through Miner-Palmgren are supported by lack of a clearly defined endpoint for compression cushions, such as exists when a fatigued metal sample breaks.

Lee [297] instrumented three different heavy packages (80-400 lb). These packages were placed in a standard 4 × 4 truck which was then driven over a potholed paved course used as a standard in Great Britain for testing vehicle suspensions. After records of the response of the store were taken, the package was placed on an LAB low-frequency package-vibration tester which was operated in the nonsynchronous linear mode. Table travel was one inch double amplitude.

The packages were not fastened to the truck or the table, although cables were used to encourage a response with a quasi-single degree of freedom and keep the packages within the confines of the test area. The results are shown in Fig. 6.53. Note that 1 minute on the tester seems roughly equivalent to 5 minutes in the truck. The inevitable conclusion is that the severe rough-road environment produces shocks, not steady-state vibration.

The foregoing statements do not mean to deny the existence of a very severe environment in moving military cargo over rough roads. All we can say, and that only tentatively, is that the vibratory behavior of cushions should be evaluated at small amplitudes and that the large-amplitude package "vibration" tests should be considered as shock tests.

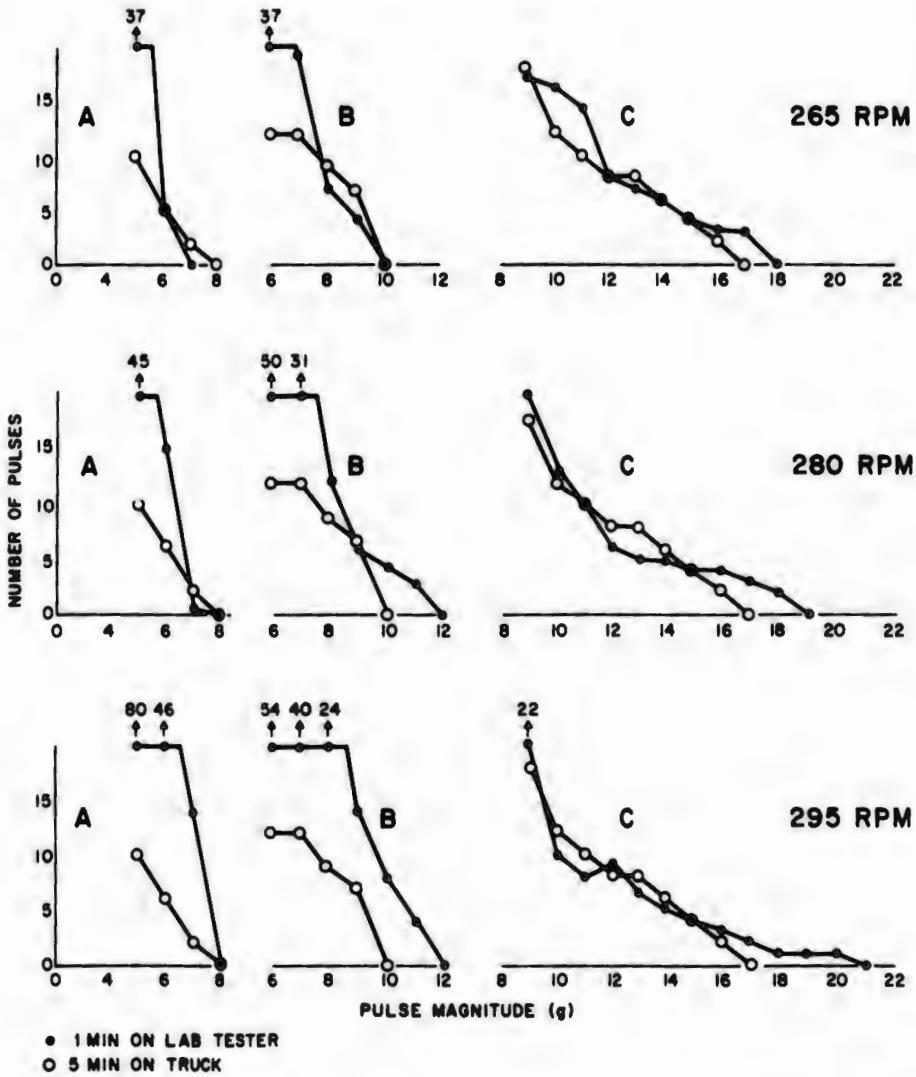

FIG. 6.53. Distribution of shock amplitudes inside packages on a truck passing over a rough road and on an LAB tester. Lee [297].

Chapter 7

EXTREME ENVIRONMENT PERFORMANCE

Extreme environment as used in this chapter means very low or very high temperatures, plus (in the case of low temperatures) the low ambient pressures associated with high altitude or outer space.

As shown in Chapter 3, most of the materials usable as cushions exhibit viscoelastic properties. Thus, merely on theoretical grounds, one would expect considerable stiffening of the material as the temperature is reduced. At the glass transition temperature T_g peculiar to the elastomeric substance, near-maximum stiffness would be achieved. As temperature is lowered below T_g, stiffness would remain reasonably constant until the material became so brittle as to fail through fracture. (The well-known brittleness of rubber at very low temperatures is typical.)

As temperatures increase, the dynamic moduli become progressively lower until the temperature region called the rubbery plateau is reached. Here the material is stabilized for a specific range of temperatures peculiar to the material; the width of the plateau being a function of polymer cross-linkage. At the top end of the rubbery-plateau region the material behaves as a thermoplastic; its shock and vibration isolation characteristics are largely nonexistent, or, in many cases, irreversible.

High altitude or outer space will reduce the quantity of air trapped in a matrix. Where a material has properties that are markedly dependent on this air, these properties will be changed. For closed-cell foams these changes may be drastic, such as cell wall rupture. Changes may also occur in the loss modulus, provided that air plays a prominent role in the loss modulus (as it does in open-celled foams).

The limited data confirm some theoretical prophecies.

Early attempts to estimate low-temperature effects on cushions were largely in terms of the effects on the static stress-strain curves. Jordan and Witting [298] produced a number of curves for conventional package-cushioning materials which indicated stiffening and, at −70°C, ruled out a number of materials as probably unsuitable for use in such an environment.

Hatae [299] plotted static stress-strain curves for polyurethane foam at 165°, 120°, 70°, 30°, 0°, −30°, and −50°F. The degree of softening between +70° and +165° was not nearly so marked as the hardening between 0° and −30°. The difference between −30° and −50° was not very marked. This latter observation is not surprising since Fig. 4.56 indicates that the glass temperature for polyether urethane foams is about −40°F and for the polyester foams is about −4°F.

Wilson [170] reports static stress-strain data on some 27 different cushions at −65°F and +165°F. Some of these results are repeated in Gigliotti [152] and some were given at a Shock and Vibration Symposium [169].

Eller [300] investigated 19 different polyurethane foams at −20°, −40°, and −67°F. These results are also reproduced in Gigliotti [152], who also gives some data on resilient polystyrene foams. Statically, at least, these latter materials are relatively unaffected by wide temperature fluctuation.

North American Aviation [164] plotted stress-strain curves for a firm rubberized hair and found that the stiffness approximately doubled in going from room temperature to −50°F. On the other hand, drop tests conducted at this temperature resulted in little or no increase in peak acceleration. This may be explained by the theoretically allowable stiffness range for a given drop test, as shown in Table 4.9.

Gordon and Wheeler [301] investigated polyester urethane, latex foam, closed cell rubber, sponge rubber, neoprene sheet, expanded polyvinyl chloride (pvc), and 11.6-pcf felt at 20°, 10°, 0°, −10°, −20°, −30°, and −40°C. They plotted their results in the form of curves for *J versus* energy per unit volume. For all the cellular materials the entire curve was lowered, at first; then the left-hand side of the curve (corresponding to low energy per unit volume) rose rapidly and eventually the whole curve rose rapidly. As temperature is reduced the materials become not only harder but also less resilient. Hence the initial improvement in performance. As temperature is lowered even further, however, stiffness increases more rapidly and eventually overwhelms the decreased resilience effect.

Gordon and Wheeler make the special point that a large increase in cushion stiffness may not show up as an increased acceleration, particularly where

TABLE 7.1. MINIMUM "SAFE" TEMPERATURE FOR CUSHIONED PACKAGES

Material	*Minimum "Safe" Temperature* (°C)	
	Gordon and Wheeler [301]	*Letchford* [302]
Polyester urethane foam	−10	−10
Latex foam (open-celled)	−20[a]	−20
Closed cell rubber	−20	—
Neoprene sheet	0	—
Expanded pvc	−10	—
Polyether polyurethane	—	−30
Felt	−34[b]	—
Rubberized hair	—	−40
Plastic bonded hair	—	−40
Latex bonded wood wool	—	−50[b]
Latex bonded glass fiber	—	−50[b]

[a] Stiffness increase not sharp. Possibly usable to −34°C.
[b] Limit of data taken. Material appears safe to some lower but unspecified temperature.

the design has been set close to the optimum point. The "safe" temperature for a package designed to operate at room temperature was defined as the lowest temperature achieved before drastic increase in peak acceleration begins. This definition led to the compilation shown in Table 7.1. Letchford [302] noted similar effects and his results are also included in Table 7.1. All three authors cautioned that their data were valid only for materials that are substantially dry initially and throughout the test program.

Mazzei [303] has examined the effects of wetting rubberized hair and testing at room temperature and after freezing the drip-dry matrix at −40°F. At ambient temperatures, water actually lowered optimum peak acceleration but, after freezing, produced a drastic increase in the optimum room-temperature loading range. However, at high static loadings (say, double the optimum), lower accelerations were recorded, indicating that ice could play a beneficial role under certain circumstances.

Tolley [304] has asked this question: Can static tests be used to predict low-temperature dynamic performance? Using a polyurethane foam, he showed that a number of static properties changed drastically at a temperature that seemed characteristic of that foam. For polyurethane foam he

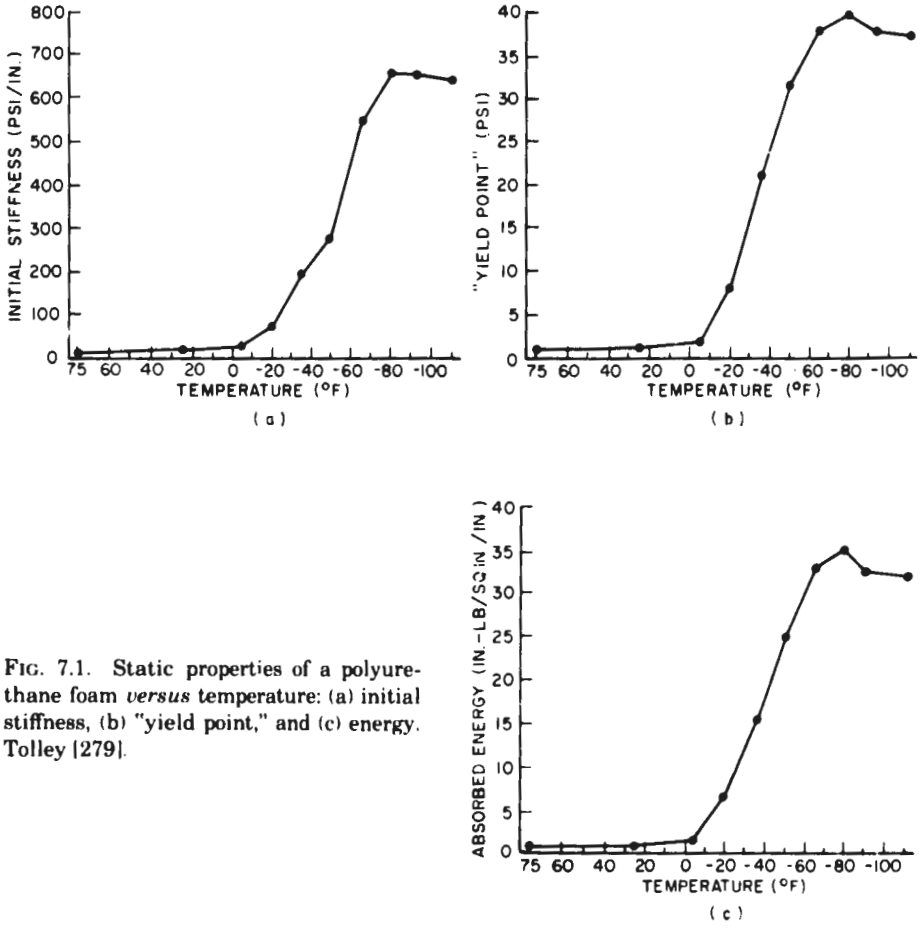

FIG. 7.1. Static properties of a polyurethane foam *versus* temperature: (a) initial stiffness, (b) "yield point," and (c) energy. Tolley [279].

checked initial spring rate (the slope of the stress-strain curve prior to column collapse), the yield point (the stress at which the strain becomes nonlinear), and energy per unit volume up to a strain of 1/3 the original thickness of 3 inches. These results are shown in Fig. 7.1.

As a design input, Tolley was seeking 25g max at −65°F with an 8-inch drop height. Static stress for the particular design was 0.5 psi, and 15 percent precompression was necessary. Figure 7.2 shows how this result was achieved with the particular foam covered in Fig. 7.1, with a density of 4.1 ± 0.14 pcf. Figure 7.3 shows the range of peak accelerations for various drop heights and temperatures with this foam.

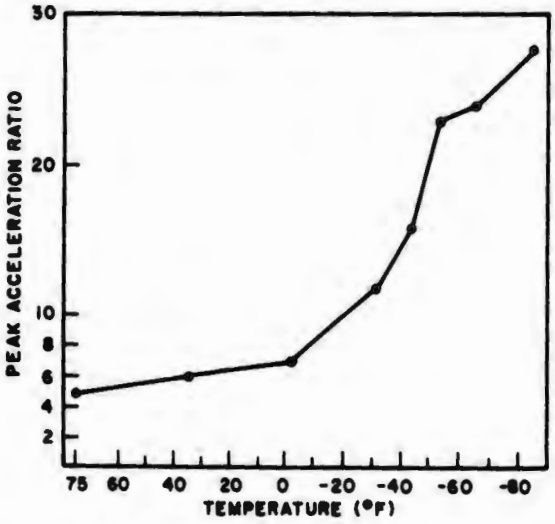

FIG. 7.2. Peak acceleration *versus* temperature for a polyurethane foam at an 8-in. drop height. Tolley [304].

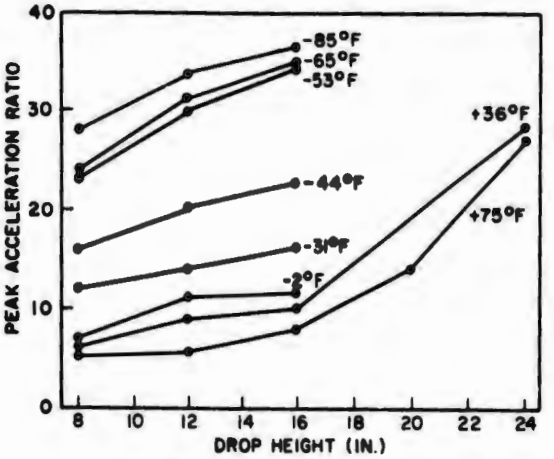

FIG. 7.3. Peak acceleration *versus* drop height for a particular polyurethane foam design at various temperatures [304].

Note that the results of Fig. 7.2 show a sharp rise in peak acceleration in the neighborhood of −10°F—the temperature at which the static properties also show a sharp rise. Thus, the static properties can be used to evaluate the lower bound for maintaining room-temperature performance characteristics. From previous studies of viscoelasticity mentioned in this monograph, we see that −10°F must be near the glass transition temperature of the polymer and that the results achieved apparently show a gratifying confirmation of theory.

Tolley also investigated some 17 different materials; he reports that the only ones that performed as well at −65°F as they did at +65°F were some silicone rubber foams and a fiberglass pad of unspecified properties.

Soper and Dove [33] also investigated low- and high-temperature shock performance of two special rubber compounds at initial strain rates of 400 sec^{-1}. The two "rubbers" were a polyrubber-Stafoam mix and a silicone rubber filled with glass beads. Temperatures were +160°, +60°, and −60°F. The results are shown in Fig. 7.4. These authors further suggested that the optimum design for performance over a wide temperature range was dictated by the upper bound of all the J curves for the range considered. This is shown by the heavy line in Fig. 7.4 for 65 percent polyrubber and 25 percent Stafoam.

Cohen [277] was more interested in input shocks expressed in terms of input acceleration than in drop height. Measured shock transmissibility for a 1-in. thick 5-pcf polyurethane foam pad at 250° and −60°F is shown in Fig. 7.5. Static stress was 0.2 psi. Input acceleration was a half-sine

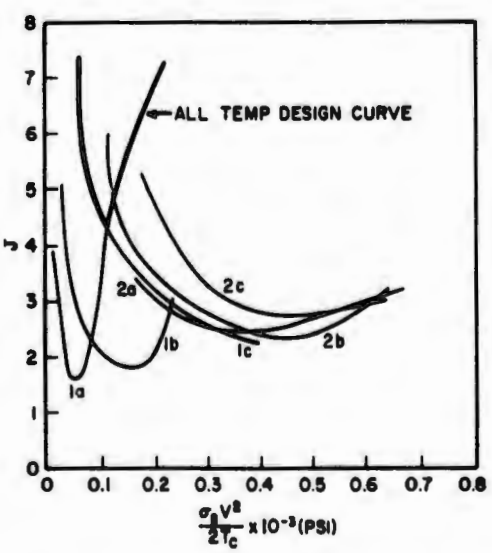

FIG. 7.4. Performance of special rubbers at various temperatures: curves 1 are 65 percent polyrubber, 25 percent Stafoam; curves 2 are a silicone rubber filled with glass beads; curves 1a and 2a are measured at 160°F., curves 1b and 2b at 80°F, and curves 1c and 2c at −60°F; initial strain rate 400 sec^{-1}. Soper and Dove [33].

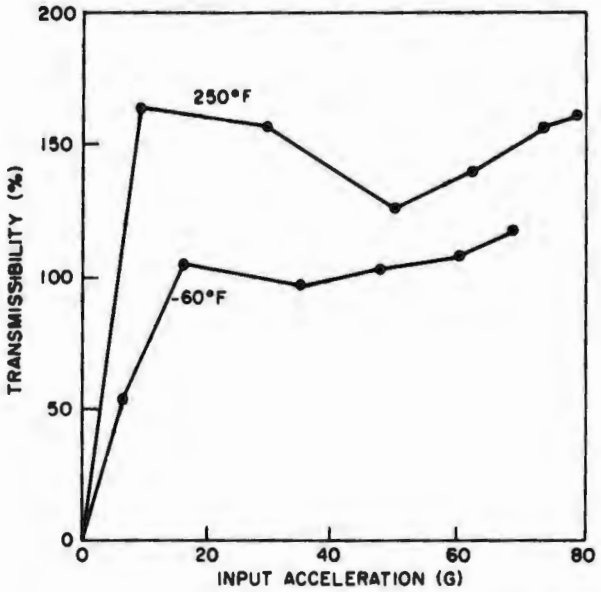

FIG. 7.5. Vertical shock transmissibility at high and low temperature for a 5-pcf polyurethane foam; static stress 0.2 psi, thickness 1 in. Cohen [277].

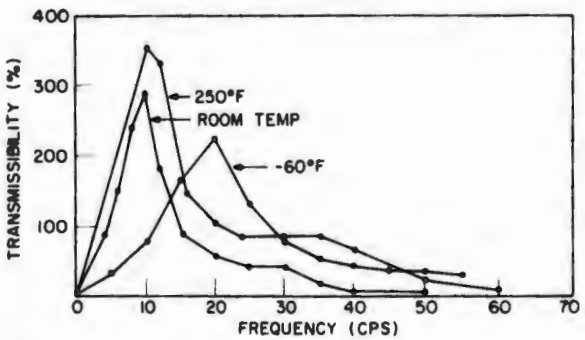

FIG. 7.6. Lateral vibration transmissibility at low, room, and high temperature for 5-pcf polyurethane foam, 1-in. thick [277].

pulse. By contrast, at room temperature transmissibility was under 50 percent for input shocks less than 8g—a shock figure considered less than might be expected as a part of the aircraft shock envelope. Note that at 8g transmissibility is only about 55 percent at −60°F, thus confirming that peak acceleration need not rise excessively.

Cohen checked vibration transmissibility at several temperatures. Figure 7.6 gives lateral transmissibilities at room temperature, +250° and −60°F. Note that peak transmissibility actually decreased at −60°F, although, as expected, natural frequency increased.

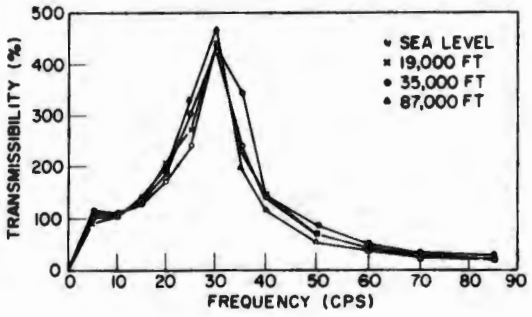

FIG. 7.7. Vertical-vibration transmissibility of polyurethane foam at different altitudes; static stress 0.225 psi, thickness 1 in. [277].

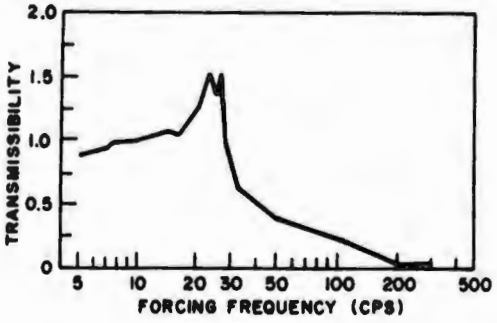

FIG. 7.8. Vibration response of a polyurethane foam to high-stress vibration at −65°F; static stress 0.81 psi, thickness 2 in. Henny and Leslie [285].

Cohen also exposed polyurethane foam to several simulated altitudes, as shown in Fig. 7.7. In these tests the sample was only 4 × 5 × 1 in., and static stress was 0.225 psi. One might expect a substantial increase in transmissibility due to lack of an air damping factor. Cohen suspected that the high transmissibilities at sea level might have been the result of using a much smaller sample than the normal aircraft mount installation. If so, this would be one more proof that air in foam cushions cannot be ignored.

Henny and Leslie [285] exposed the foam whose static stress-strain curve is given in Fig. 6.42 to the vibration spectrum given in Fig. 6.44. The results, at −65°F, for 2-in.-thick material at 0.81 psi static stress, are shown in Fig. 7.8. Note that, despite considerable stiffening, transmissibility did not exceed 1.5.

Keast and Baruch [184] studied the properties of a number of materials at very low temperatures and pressures. These included glass fiber, latex bound hair, polyether polyurethane foam, silicone rubber foam, and paper honeycomb. Temperatures were +75°, −65°, and −200°F. Measurements were made at sea level pressures and at 10^{-4} mm Hg (a virtual vacuum).

Temperature alone had little or no effect on the vibration performance or stress-strain characteristics of glass fiber materials but a vacuum effectively changed the material from a good vibration absorber to a poor one. Results are summarized in Table 7.2.

Unfortunately, the Keast and Baruch report does not stipulate the input vibration amplitudes, but they were apparently small.

Considerable difficulty was encountered in testing polyurethane foam as a free cushion at low temperatures, because of the tendency of the material

TABLE 7.2. TRANSMISSIBILITY OF A GLASS FIBER MAT.
SUPPORTED MASS 3.72×10^{-4} SLUG/IN.^{2}.
SURFACE AREA 16 IN.^{2}. THICKNESS 1 IN.

Property	*Ambient Pressure*			10^{-4} mm Hg		
	T = Ambient	*T* = −65°F	*T* = −200°F	*T = Ambient*	*T* = −65°F	*T* = −200°F
Resonant frequency (cps)	32	32	45	32	34	42
Damping ratio, β	0.40	0.31	0.29	0.083	0.072	0.057
Transmissibility, max	1.7	2.0	2.2	6.1	7.0	8.8
Damping coefficient (slugs/in.^{2} sec)	0.060	0.046	0.027	0.012	0.0114	1.011

to curl. Finally, Keast and Baruch cemented the sample to an aluminum plate, thus effectively producing a cushion mount. They found a transmissibility of 1.0 at all frequencies up to 1000 cps at −65° and −200°F.

For polyurethane foam, pressure and temperature both strongly affect the dynamic stress-strain curves (see Figs. 7.9 and 7.10), but not for rubberized hair (see Fig. 7.11). The different effects of room temperature (+73°F) and −65°F are shown in Fig. 7.12. The difference seems to be due more to sample variability than to softening. At −200°F, the material simply disintegrated during the course of testing.

Dynamic stress-strain curves for silicone rubber foam remained almost unchanged at −65°F, as compared with room temperature conditions. At −200°F, however, the material was almost as stiff as the polyurethane foam at the same temperature. Vacuum adversely affected vibration transmissibility (which was not very good in the first place); see Table 7.3.

Paper honeycomb was not affected significantly by temperature changes.

To summarize: most cushions become considerably stiffer as temperature drops; with the glass temperature T_g playing a key role in the temperature

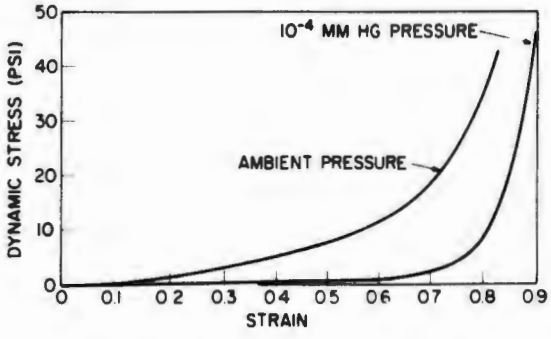

FIG. 7.9. Effect of vacuum on dynamic stress-strain characteristics of polyurethane foam. Keast and Baruch [184].

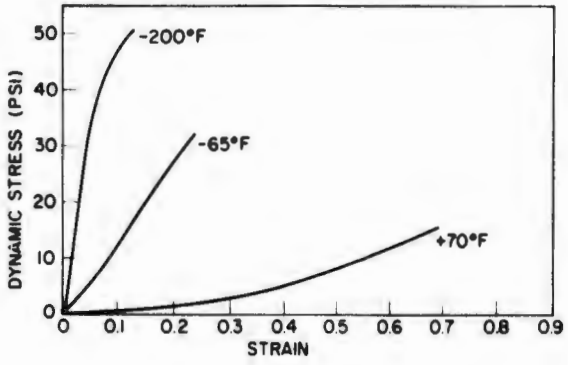

FIG. 7.10. Effect of temperature on dynamic stress-strain characteristics of polyurethane foam [184].

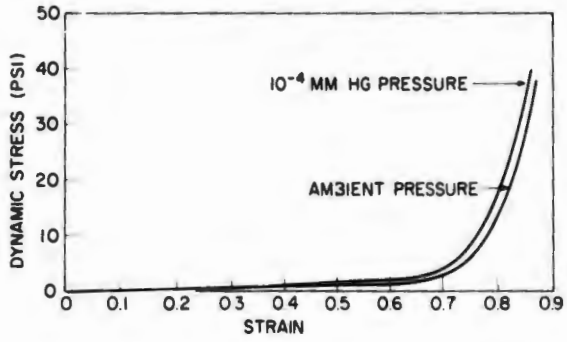

FIG. 7.11. Effect of vacuum on dynamic stress-strain characteristics of rubberized hair [184].

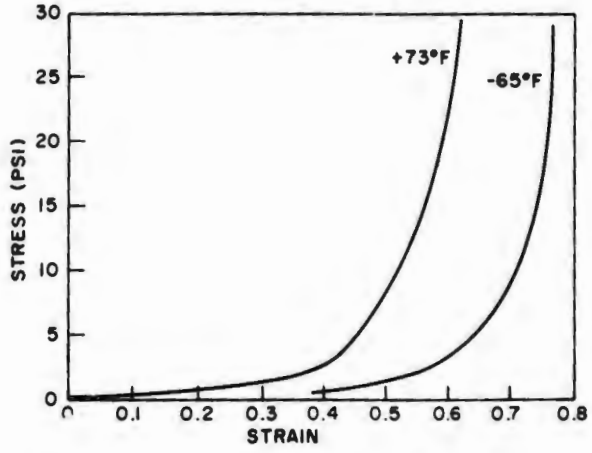

FIG. 7.12. Dynamic stress-strain curves for rubberized hair, at two different temperatures [184].

level at which maximum stiffness is found. As regards shock, peak accelerations do not rise as rapidly as the stiffness parameter. Systems designed for room temperature service do not show very large changes in peak acceleration until they reach the neighborhood of T_g. The minimum safe temperatures of Table 7.1 indicate the approximate location of the point at which the acceleration increase rate undergoes an abrupt change. This point is in the neighborhood of T_g.

Vibration transmissibility is also affected by temperature changes; the most noticeable effect being a change in natural frequency. There are changes in transmissibility but not as large as might be expected. For small vibration amplitudes, materials which have a strong air-damping effect at large excursions do not necessarily have the same effect at small excursions. Air effect must be determined empirically and is probably a function of sample size.

TABLE 7.3. TRANSMISSIBILITY OF A SILICONE FOAM.
SUPPORTED MASS 2.01×10^{-3} SLUG/IN.^{2}.
SURFACE AREA 16 IN.^{2}. THICKNESS 1 IN.

Property	*Ambient Pressure*			10^{-4} mm Hg		
	T = Ambient	*T* = −65°F	*T* = −200°F	*T = Ambient*	*T* = −65°F	*T* = −200°F
Resonant frequency (cps)	19	47	50	22	45	50
Damping ratio, β	4.5×10^{-2}	1.2×10^{-1}	2.6×10^{-1}	3.5×10^{-2}	1.1×10^{-1}	2.7×10^{-1}
Transmissibility, max	11.1	4.35	2.15	14.3	4.5	2.1
Damping coefficient (slugs/in.^{2} sec)	2.2×10^{-2}	1.4×10^{-1}	3.4×10^{-1}	2×10^{-2}	1.3×10^{-1}	3.4×10^{-1}

There seems some possibility that, for small excursions, time and temperature superposition could be used to good effect to develop expressions for natural frequency and transmissibility as a function of static stress and thickness. This would effect a considerable reduction in the number of curves required. Plotting master curves of complex moduli as a function of frequency and temperature would reduce the load even further. Transmissibilities could be computed directly for a specific design, using Snowdon's [60] formula, Eq. (6.31).

The foregoing must be considered as tentative opinions stated as possible guides for future work. There are not enough data to warrant firm conclusions.

Chapter 8

DRIFT AND CREEP

Drift is defined as the percentage loss in thickness of a material under stress. Some investigators use the phrases dynamic drift and static drift to differentiate between thickness loss due to repetitive shock or vibration stresses, and long-term thickness loss due to static stress.

Dynamic drift occurs with practically all cushions but is particularly marked with quasi-resilient and rigid cushions. Dynamic drift of these materials has been discussed in Chapters 4 and 6. Schmidt and Hoffmann [188] strongly imply that dynamic drift of polyurethane foams can be controlled by preworking the material enough to ensure constant air drag. Zell [179] observes that dynamic drift of closed-cell polystyrene foams seems associated, also, with cell wall rupture and consequent modification of air-cushioning effect. With lighter-weight rubberized hairs, dynamic drift is apparently associated with progressive felting of the hair-rubber matrix.

Drift under static load is something common to all materials. It is usually ignored with metals at normal temperatures, because the rate and absolute magnitude are very low. More properly, this phenomenon should be called creep, since it involves a change in strain under constant stress. The variables affecting creep in a viscoelastic material can be identified as:

1. the stress applied;
2. the material's own creep characteristics, *i.e.*, the specific damping constants when the material is regarded as a generalized Maxwell body (see Chapter 3);
3. the temperature at which the measurements are made; and
4. the time of the exposure.

Perhaps we should also consider changes in density of the material during the experiment, and the relative humidity at which the measurements were made. The physical properties of many organic materials, especially cellulosic materials, are intimately related to water content; for accurate work, relative humidity should always be controlled.

In section 3.2.4 on the uses of time and temperature superposition, it was suggested that a drift master curve could be plotted for a given material exposed to a given static stress using the following relation

$$\log \frac{(1-\epsilon)\rho T}{\rho_0 T_0} = f\left(\log \frac{t}{a_T}\right). \tag{8.1}$$

This procedure would permit shortening test time by elevating the temperature to the region of the material's rubbery plateau.

Since relaxation modulus can be plotted by the reduced-variable technique, and since creep and relaxation moduli are interrelated (Chapter 3), perhaps we could plot a single master curve in a form such as

$$\log\left(\frac{\sigma_c T\rho}{T_0\rho_0}\right) = f\left(\log\frac{(1-\epsilon)t}{a_T}\right). \tag{8.2}$$

However, no evidence was found to support this hypothesis.

As it is, drift tests are very time-consuming, and none of the available data indicate that reduced-variable technique was employed. A typical test set up for measuring drift of package-cushioning materials is shown in Fig. 8.1. After the cushion and measuring platen are installed, thickness is read. Then the weight box containing a sufficient quantity of lead shot to produce the desired static stress is eased down onto the cushion and the thickness is read promptly. Generally speaking, a substantial portion of the drift occurs during the first few hours.

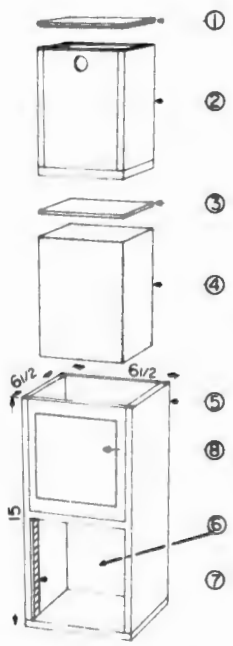

FIG. 8.1. Kerstner creep box: 1- cover, 2- weight box with total weight adjusted with lead shot, 3- measuring platen, 4- cushion, 5- outer plywood box, 6- clear plastic window, 7- measuring scale, and 8- record card.

Table 8.1 contains some results extracted from the sources indicated. While these data are indicative, rather than conclusive, it can be seen that very large creep losses can occur with some materials. Blake's results [305,306,307] are particularly interesting because his static stresses were the optimum for particular drop heights and thicknesses.

For polystyrene foam, Drysdale *et al.* [217] found that creep was very small if the material had not previously been compressed. Table 8.2 lists recommended maximum loadings to keep creep below 5 percent and 10 percent for a 100-hour period. Figure 8.2 shows measured creep of 0.1-pcf polystyrene foam with various static loads after the material has undergone one impact from a height of 36 inches with a drop-test static stress of 0.165 psi.

TABLE 8.1. SOME CREEP TEST RESULTS[a]

Material	Density (pcf)	Static Stress (psi)	Creep, % Loss in Thickness				Ref.
			24 Hr	1 Wk	1 Mo	6 Mo	
Rubberized hair	1.80	0.090	10.0	10.5	13.0	22.7	31
Rubberized hair	1.80	0.180	24.5	31.6	36.5	46.0[b]	31
Rubberized hair	2.70	0.180	8.0	9.0	10.5	17.8	31
Rubberized hair	2.70	0.362	10.0	14.0	16.5	24.8	31
Rubberized hair	2.70	0.542	22.1	26.4	29.5	36.0[c]	31
Rubberized hair	Soft	0.180	30.0	30.4	37.7	49.0	161
Rubberized hair	Soft	0.090	10.0	12.0	14.0	23.0	161
Rubberized hair	Medium	0.180	39.0	42.0	46.0	52.0	161
Rubberized hair	Firm	0.180	8.0	10.0	12.0	17.0	161
Rubberized hair	Firm	0.194	12.0	15.0	20.0	20.0	161
Rubberized hair	Firm	0.362	12.0	17.0	18.0	23.0	161
Rubberized hair	Firm	0.542	27.0	28.0	29.5	40.0	161
Rubberized hair	Firm	0.400	30.0	32.0	37.0	40.0	161
Rubberized hair	1.6	0.050	4.0	5.0	5.0	–	305
Rubberized hair	1.6	0.055	4.0	5.0	6.0	–	305
Rubberized hair	3.7	0.065	4.0	5.0	5.0	–	305
Rubberized hair	5.9	0.058	3.0	3.0	3.0	–	305
Polyurethane foam (ester)	2.4	0.382	5.0	6.6	10.0	11.6[c]	161
Polyurethane foam (ester)	2.2	0.400	2.5	5.2	6.0	7.0[c]	161
Polyurethane foam (ester)	2.2	0.120	5.0	10.0	13.0	14.0	161
Polyurethane	2.4	0.382	5.0	6.5	10.0	10.6[c]	31
Polyurethane	2.2	0.400	4.4	5.0	6.0	7.0[c]	31
Polyurethane	DR Chemfoam	0.65	66.0	68.0	68.0	–	305
Polyurethane	LP Reclaim	0.350	3	3	3	–	305
Polyurethane	LP Reclaim	0.400	4	5	5	–	305
Polyurethane	LP Reclaim	0.500	5	5	6	–	305
Polyurethane	7B Reclaim	0.150	2	2	2	–	305
Polyurethane	7B Reclaim	0.200	3	3	3	–	305
Polyurethane	7B Reclaim	0.250	4	4	5	–	305
Polyurethane	PE Reclaim	0.600	2	2	2	–	305
Polyurethane	PE Reclaim	0.650	3	3	3	–	305
Polystyrene	Tyrilfoam	0.420	0	0	0	–	306
Polystyrene	Tyrilfoam	0.750	0	0	0	–	306
Polystyrene	Tyrilfoam	0.850	0	0	0	–	306
Polystyrene	Celluliner 20	0.470	0	0	0	–	306
Polystyrene	Celluliner 20	0.630	0	0	0	–	306
Polystyrene	Celluliner 20	0.800	0.7	0.7	0.7	–	306
Polystyrene	Celluliner 30	0.500	0	0	0	–	306
Polystyrene	Celluliner 30	0.640	0	0	0	–	306
Polystyrene	Celluliner 30	0.650	1.0	1.0	1.0	–	306
Polystyrene	Celluliner 30	0.800	0.7	1.4	1.4	–	306
Polystyrene	Celluliner 40	0.700	0	0	0	–	306
Polystyrene	Celluliner 40	0.750	0	0	0	–	306
Polystyrene	Celluliner 40	0.850	1.0	1.0	1.0	–	306
Polystyrene	Ololite	0.800	0	0	0	–	306

[a] Room temperature, uncontrolled unless otherwise indicated.
[b] Test terminated at 5 mo.
[c] Test terminated at 4 mo.

TABLE 8.1 (*Continued*). SOME CREEP TEST RESULTS[a]

Material	*Density* (pcf)	*Static Stress* (psi)	*Creep, % Loss in Thickness*				*Ref.*
			24 Hr	*1 Wk*	*1 Mo*	*6 Mo*	
Polystyrene	Ololite	0.730	0	0	0	–	306
Polystyrene	Ololite	0.750	0.8	0.8	0.8	–	306
Polystyrene	Tyrilfoam	0.60	0.4	0.4	0.4	–	307
Polystyrene	Tyrilfoam	0.806	0	0	0	–	307
Polystyrene	Celluliner 20	0.60	0.5	1.0	1.5	–	307
Polystyrene	Celluliner 20	0.806	0.4	0.5	0.7	–	307
Polystyrene	Celluliner 30	0.806	0.5	0.5	0.5	–	307
Polystyrene	Celluliner 40	0.806	0.3	0.3	0.3	–	307
Polystyrene	Dylite #1	0.600	0.5	1.0	1.0	–	307
Polystyrene	Dylite #2	0.600	0	0	0	–	307
Polystyrene	Dylite #2	0.806	0	0.3	0.3	–	307
Polystyrene	KRB Chemfoam	0.500	2	2	2	–	305
Polystyrene	KR-1 Chemfoam	0.650	0	0	0	–	305
Neoprene	NF Chemfoam	0.050	0.7	0.7	0.7	–	305
Polyethylene	Ethafoam	0.350	0	0	0	–	305
Polyethylene	Ethafoam	0.550	2	3	3	–	305
Polyethylene	Ethafoam	0.600	3	3	3	–	305
Cellulose fiber felt	Tufflex U-150	0.080	4.7	5.2	5.8	–	306
Cellulose fiber felt	Tufflex U-200	0.080	5.4	6.8	6.8	–	306
Cellulose fiber felt	Tufflex U-300	0.050	8.6	8.6	8.6	–	306
Cellulose fiber felt	Tufflex U-300	0.080	8.7	8.7	8.7	–	306
Cellulose fiber felt	Tufflex U-300	0.110	13	13	14	–	306

[a] Room temperature, uncontrolled unless otherwise indicated.

TABLE 8.2. SAFE STRESSES FOR 100-HOUR EXPOSURE OF POLYSTYRENE FOAMS

Uncompressed			*Compressed*		
Density (pcf)	*5% Creep*	*10% Creep*	*Density* (pcf)	*5% Creep*	*10% Creep*
0.77	4.2	7.0	0.74	2.1	2.8
0.93	4.2	<6.9	1.01	2.1	2.8
1.17	4.2	6.9-9.7	1.27	2.8	4.2
1.36	12.4	<18	1.32	7.0	<9.5
1.77	12.4	<18	1.60	7.0	12.5

One problem with respect to creep is that at present there is no universally accepted endpoint establishing acceptable creep performance. Schmidt and Hoffmann [188] imply that 5 percent creep in about one year may be a good general measure. Figure 8.3 is a plot for polyurethane foams showing density *versus* the static stress which would produce 5 percent creep in 10^4 hours at 55 percent relative humidity and storage temperature under 22°C.

Excessive static stress can produce catastrophic creep failures. Eller, Stein, and Chatten [308] exposed a number of foam materials to static stresses great enough to cause 20- to 25-percent initial strain on the cushion. The

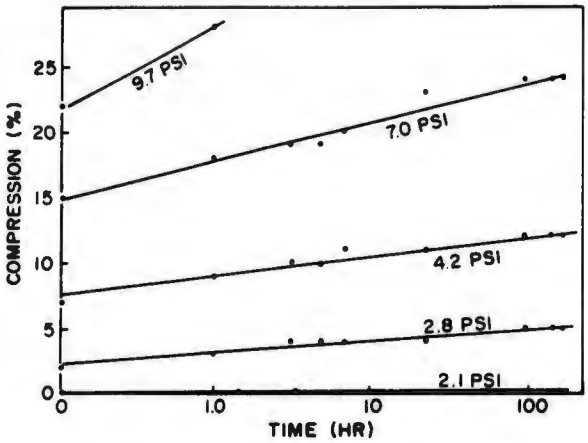

FIG. 8.2. Creep of 0.1-pcf polystyrene foam with various static loads, after impact from 36-in. height with 0.165-psi static stress. Drysdale, *et al.* [217].

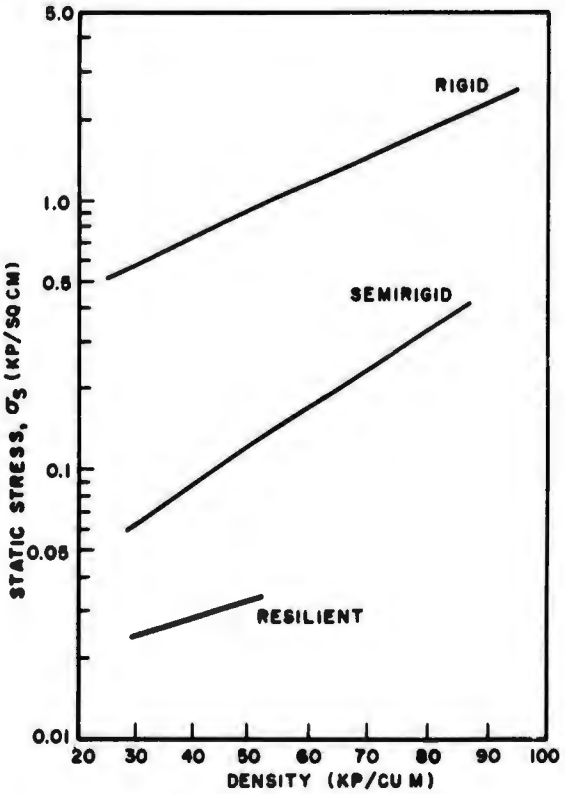

FIG. 8.3. Allowable static stress (*i.e.*, with 5 percent/year creep, temperature ≤ 22°C) *versus* density of polyurethane foams. Schmidt and Hoffmann [187].

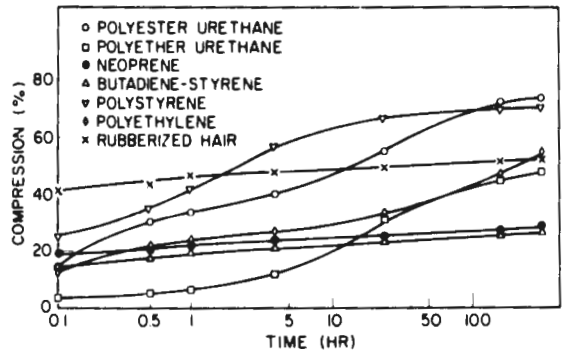

FIG. 8.4. Creep of cushions with static stress sufficient to cause 20 to 25 percent initial strain. Eller, Stein, and Chatten [308].

results are shown in Fig. 8.4. Note the sharp rise in the polyurethane creep values. For a cushion with a constant-stress plateau, such as polyurethane foam, static stress close to the knee will eventually creep over the knee and then proceed across the plateau at least until the stiffening portion of the stress-strain curve is reached.

When a resilient polyurethane foam with a pronounced knee in the static stress-strain curve is loaded close to the knee and the stress is not uniform, a catastrophic failure can occur quite rapidly. If one corner of the pad is overstressed, this corner will creep to failure first. The overstress is then gradually transferred across the pad, and the entire pad is reduced in thickness by about 70 or 80 percent. Design shock and vibration isolation characteristics, of course, are substantially lost. It is particularly important, therefore, to ensure good balance on polyurethane foam cushions. Indeed, this is a goal that should be sought for all cushions, since both static and dynamic properties depend on uniformity of stress.

Creep performance of cushions required to support a static load may well be a more limiting factor in design than either: (a) the optimum static stress for minimum shock acceleration, or (b) the vibration isolation characteristics of a pad with certain dimensions. The data available are scanty, and do not give a firm picture of the allowable static stresses for certain materials; nor do they provide means of evaluating creep at different temperatures.

Chapter 9

CONCLUSIONS

The literature reviewed in preparing this monograph generally falls into one of three broad groups; individual papers may fall in all three. These groups are:

1. Studies of the properties of continuous, deformable media under stress;
2. Analyses, some highly mathematical, of the forces exerted by materials on objects being isolated; and
3. Data concerning the performance of specific materials or classes of materials.

The purpose of this chapter is to summarize the highlights of these studies and draw any possible conclusions.

9.1. Theory

Stress passes through a cushion in waves. Wave velocity is a function of the cushion's mechanical constants. The waves are reflected in a complex manner from all interfaces, including the edges of the cushion. Simplification and better understanding are achieved by assuming that the stress wave is plane. Conditions for the validity of this assumption are that the stress be applied parallel to some arbitrarily selected axis and be uniformly distributed over the face of the cushion.

As a plane stress wave passes through a cushion, waves are generated at the edges behind the wave front. It has been shown, however, that the waves will not penetrate further than a distance about the same as the thickness of the material. Hence, if surface dimensions are large compared to cushion thickness, surface stress can be considered uniform.

The behavior of cushions can be fitted into a consistent pattern when analyzed in terms of modern viscoelastic theory. This is a very active field; it has recently been extended to cover nonlinear behavior and large-strain behavior, leading to practical application. From a very large reservoir of theoretical studies, only a limited number of concepts need be drawn at this time; the most pertinent are presented below.

The strain behavior of a cushion is a function of the stress, time, and temperature. All three variables must be considered in any problem although, for most shock applications, temperature rise in the cushions can be ignored; this reduces the problem to studying and recording the effects of ambient temperature.

Performance of cushions at any one temperature can be equated to performance at any other temperature through an empirical shift factor. If we know the temperature T_g at which the material begins to behave in a

glassy fashion, we can predict the shift factor for most elastomeric materials by a single empirical equation; this is accurate within the limits of experimental error from T_g to $T_g + 100°C$, a range that covers most ambient temperatures.

Below T_g most materials are very stiff and the damping is relatively small. As the temperature is raised, stiffness decreases through a transition zone and then stabilizes in a rubbery-plateau region. In the rubbery-plateau region stiffness remains constant until a temperature is reached at which the material becomes plastic and flowing. Stiffness characteristics have gone (as least for shock-isolation purposes) and the loss may be irreversible. As the temperature increases, damping increases, reaching a peak value just past the transition temperature. After peaking, damping diminishes, reaching a new minimum at the boundary between the transition and rubbery-plateau regions.

Exactly the same phenomena are observed when the time of stress application is changed, while the temperature is kept constant. As the time of application is shortened (frequency increasing), the material becomes stiffer and behaves exactly as it does when the temperature is lowered.

This parallel between temperature and time means that they can be superposed. As shown in a well-proven theory, there is a unique relationship between a physical property, such as stiffness, and temperature, or time (which may be expressed as strain rate or as frequency) and the empirical shift factor. This principle governs all mechanical constants: dynamic stress-strain, stiffness under vibration, damping capacity, and creep—whether determined in tension, compression, or shear. For example, suppose that we make vibration tests at a certain temperature over a limited frequency range. Then, by making the same tests at a different temperature, we produce the same effect as if we had altered the range; thus, we can obtain the equivalent of full-range tests by temperature change. This principle is of prime importance in extending knowledge of the behavior of cushions, particularly in vibration and creep.

Cushions, especially those with good energy-absorption characteristics at low impact velocities, have creep characteristics; *i.e.*, they increase in strain under constant load. They also show relaxation properties, *i.e.*, gradual reduction in the stress required to maintain a constant strain. It is clearly established that these characteristics are a consequence of the viscoelastic nature of the materials.

For a vibratory input, especially for small strain, the concept of a complex elastic modulus is a very important aid to understanding and predicting cushion behavior. The complex modulus combines in a single quantity the stiffness and damping characteristics of a given material, thus permitting simplified analysis; at the same time, it takes into account the fact that stress behavior depends on time as well as on strain.

While relatively few investigators actively use the complex-modulus concept with cushioning materials, much of the accomplished work is consistent with the tenets of complex-modulus theory which is a direct outcome of the viscoelasticity concept. Although complex moduli are usually used for small excursions due to sinusoidal disturbance, they can also be used for large excursions such as shock motions, with the help of Fourier's rules.

Further, although complex modulus began with the assumption of a linear response, we can now apply the concept to nonlinear materials with enough accuracy for engineering purposes.

Tension and shear moduli for elastomeric foams can be predicted with good accuracy from knowledge of the foam density and tension modulus (Young's modulus) of the unfoamed material. Compression resistance also depends on foam density but must usually be determined experimentally, since much of the overall behavior is directly related to collapse of somewhat randomly oriented columns (often with differing cross sections). Euler's column rules (which are related to Young's modulus of the material itself) apply to this effect but, in the absence of a specific structural model, prediction is difficult.

The foregoing rules particularly apply to open-celled foams. They also apply to closed-cell foams, with the addition of terms appropriate to the compression of air in the closed cells. Maintenance of behavior as a closed-cell foam is directly related to cell wall strength.

With open-celled foams, the behavior of the foam itself can be isolated from the behavior of the air trapped in the matrix of the material. At very slow compressions, the air within the material is not compressed; as the rate of compression is increased, the air is subjected to pressure which is changed by ability of the air to escape from free surfaces of the cushion.

This ability is a function of the cushion geometry. Thus many cushioning materials must be expected to exhibit a shape factor, whose importance depends on foam density, cell size, and degree of interconnection between the cells. Surprisingly enough, some non-cellular materials (notably, bound fiberglass) also show strong air-damping effects. Control of the air-resistance properties of specific materials, perhaps through measurement of the specific drag of the matrix, is apparently one way to control the damping factor.

There are indications that, at least for polyurethane foams, air-resistance characteristics become stabilized after prework or a few reasonably large dynamic strains. This has been attributed to rupture of very thin membranes (which are not necessarily continuous but do restrict air flow) between the larger threads of polymer forming the main structure of the foam. This suggests a way to control the properties of the material.

To make further progress in understanding, specifying, designing, and using foam cushioning materials, we must apply the lessons of viscoelastic theory. This conclusion is inevitable.

9.2. Mathematical Analyses of Shock and Vibration Behavior of Cushions

The response of a cushion to shock or oscillatory input depends directly on the dynamic stress-strain relation of the cushion. Shock is a special case of vibration and can be analyzed by techniques developed for the vibration-isolation condition.

For velocity-shock isolation, the optimum point for design is the least material thickness for a stipulated peak acceleration. It is indicated by the point on the dynamic stress-strain curve where the ratio of dynamic stress to energy absorbed per unit volume is a minimum. But because of

the viscoelastic nature of cushions, it is unlikely that a single dynamic stress-strain curve for the material exists until very high impact velocities, or very high-frequency vibrations, are encountered. Hence, the minimum ratio of stress to energy per unit volume, called J_0, is represented, not by a single point but by a line in a surface whose coordinates are stress, strain, and some function of time.

The time function is quite often expressed in terms of the first derivative of the strain, *i.e.*, strain rate. It can be measured by dividing the velocity at the start of cushion distortion by the undistorted thickness of the cushion. In packaging work it is more convenient to convert strain rate to a dimensionless number: height of drop divided by cushion thickness.

For each value of J_0 in the J surface there is a corresponding value of the optimum static stress. Actual static stress may be allowed to vary from about 60 to about 140 percent of optimum without significant effect on peak acceleration, all other input conditions remaining the same. This phenomenon is one of the key explanations for the following observed behavior of cushions:

1. As the material stiffens with decreasing temperature, peak acceleration does not rise as rapidly as the temperature until the glass temperature of the cushion is reached; then, peak acceleration jumps to a new and reasonably stable value.
2. Considerable change in drop height can occur before significant change in peak acceleration.

Both features, peculiar to nonlinear cushion materials, provide unexpected safety margins. Further, they allow the designer to deviate from the optimum static stress (for such purposes as giving the cushion dimensions convenient to manufacture) without undue concern over the acceleration value.

While J and J_0 are functions of the dynamic stress-strain curve of the material, they can be measured in terms of the static stress, velocity (or drop height), and thickness without detailed knowledge of the dynamic stress-strain curve. Further, it seems well established, at least for package-cushioning materials, that the variables can be separated so that the designer can select thickness and optimum static stress by means of empirical equations.

The data which have been analyzed to show that the variables of minimum thickness and optimum static stress can be separated have limited applicability, as do all data concerning cushions. The approved method of obtaining the data does not seem to assure a constant shape factor for the material, nor does it take into account the following factors which affect real designs:

1. Precompression of the cushion caused, in packages for example, by a top pad placed on the store;
2. Friction by side pads which will serve to increase peak acceleration through additional damping effects;
3. Confinement of the edges of bottom pads, say, by an outer container that restricts the flow of air from the cushion matrix—this may have a surprisingly large effect even when the outer container is a non-rigid corrugated fiberboard box; and
4. Using semicircular shapes or other geometric figures.

Nonetheless, the suggested design method using separated variables gives a sound point of departure. Further calculations can be made, as required by the complexity of any design problem.

The data used to derive J curves can also be used to derive families of dynamic stress-strain curves. The latter are undoubtedly more useful in complex design problems, particularly when it is not feasible to make a realistic full-scale test with an adequate sample, making extensive analysis necessary.

It has been implied that the concept of separating variables is the best method of approaching an optimum design. This may or may not be true; it is too early to tell. However, other methods may be cumbersome, requiring many curves and some interpolation.

The foregoing discussion has been based on an implicit assumption of a system with one degree of freedom, such as a perfectly flat drop on a uniformly stressed cushion.

When it comes to analyzing situations involving nonlinear geometries in addition to nonlinear materials, we must use the applicable stress-strain curve. (Suppose, for example, that the drop is not completely flat, involving combined rotations and translations.) There are analytical techniques, reinforced by computers, that permit solution of very complex problems. Equations have been written and programmed for nonlinear damped elasticity for the familiar rotational-drop test on the assumption that the outer container is rigid and the cushioned object is also rigid. The nonlinear elasticity characteristics need not be described by mathematical expressions but can be programmed for a curve follower or for an equation of any complexity.

To sum up: the state of the art is well equipped to estimate the peak shock developed at the interface between cushion and cushioned object, but not how elements of the cushioned object respond to peak shock and the associated wave form; here, practice lags far behind theory. In most practical cases, shock isolators are rated in terms of the shock spectrum. The shock spectrum is the response of a system with one degree of freedom to the shock pulse developed by the cushion. With modern tools, response is readily computable over a wide range of element natural frequencies.

Shock spectrum theory clearly establishes that designing for minimum thickness for a given peak acceleration at the cushion load interface is not necessarily the best way to protect a complex item. This gap between theory and practice demands closure.

The definition of shock spectrum implies some of the difficulties involved in determining response. This difficulty, coupled with the fact that nonlinear materials may have an infinity of shock spectra, means that there are practically no usable spectral data on cushions. It is essential to rational design that these data be accumulated. Further, it would appear most useful to begin by accumulating the data with the cushions loaded at optimum thickness and static stress. The need for such an approach was stressed at the very beginning of rational design (over twenty years ago), yet nothing concrete has yet been accomplished in this area.

Part of the problem has been the lengthy computations required to develop a single shock spectrum. Very accurate digital-computer programs have been developed within the past several years; some automatic analog computers have also been designed.

The shock spectrum by its very nature is only a rough indicator of cushioned-item response. Nevertheless, a cushion with a low shock spectrum is better than a cushion with a high shock spectrum.

A conventional shock spectrum is only one of several ratings for cushioning materials. A particular form of spectrum due to the late C. E. Crede has the advantage of being easily computable and quite useful in indicating the direction that corrective action should take when there is a test failure. Another form of response spectrum is the damage-sensitivity spectrum. Here, the sensitivity of individual elements of the cushioned object to damage can be computed as coordinates and plotted on graph paper. If a point is inside the envelope curve, the corresponding element is subject to damage. If the point is outside, the element will be safe with that cushion.

A major obstacle to our making a broad use of the shock spectrum is the assumption that the elements of the cushioned object are supported on springs that remain linear throughout their travel range and do not bottom. Because much shock damage consists of permanent deformation, there has been an effort to develop special response spectra that will predict when this will occur and how badly. The theory of such spectra is not nearly so simple or well developed as that of the simple shock spectrum. But it contains the germ of a rational way to predict fragility in certain elements of cushioned objects.

Another form of damage occurs in the collision of adjacent components. Recently, the proximity spectrum concept has been advanced as a possible way to predict this sort of damage. Proximity spectra for half-sine and triangular pulses could be very useful in packaging work; proximity spectra for step pulses, such as the square wave, would apply to high-velocity impacts on rigid or quasi-resilient cushions. Proximity-spectrum theory is relatively new in shock; however, in vibration, collision probabilities have been worked out for input and response.

Fragility of an item under shock can only be expressed in terms of the fragility of individual elements, and these fragilities cannot be divorced from the behavior of specific cushions. Shock spectra, and the various specialized forms of response spectra, show what a cushion does to a cushioned object; also, they suggest means of estimating item fragility.

The tools needed to analyze the behavior of cushions under vibratory stress have existed for some time. This is true for sinusoidal inputs (periodic with many forcing frequencies) or random inputs (disturbances so complicated that periodicity cannot be readily detected). A measure of cushion response is provided by the complex magnification factor, or by its absolute value, the magnification factor. Other measures of response, such as relative-motion response or absolute-displacement response (transmissibility) are functions of the magnification factor. Magnification factor and transmissibility can be computed from the complex moduli of the materials.

In general, a cushion's natural frequency is controlled by the static stress on the cushion and by its thickness. Stress and thickness therefore affect

magnification factor and transmissibility, which are functions of natural frequency.

The concept of mechanical impedance and mobility provides a powerful tool for the analysis of complex systems, particularly those with multiple degrees of freedom. If the complex modulus for a cushion and its dimensions are known, then conversion to impedance terms is straightforward. Similarly, impedance techniques can be used to excellent advantage in finding complex-modulus values for cushions. This is another argument for further concentration on the complex modulus.

Most of the foregoing statements concerning vibration behavior are based on linear theory, which is not necessarily applicable to cushions, particularly where excursion is large. Most usable materials stiffen with increasing strain. For these materials the familiar family of transmissibility curves, evenly distributed about the vertical axis of the natural frequency of the system, is distorted. Distortion occurs to the right for stiffening materials, to the left for softening; the natural-frequency axis becomes a trajectory. In linear systems, the peak value of transmissibility is a function of cushion damping only. With nonlinear systems peak value of transmissibility is a function of input amplitude, frequency, and damping; but peak value is less than it would be if the system were linear. Thus analysis on the basis of a linear response determines the envelope of possible peak responses.

For specific cushion thicknesses and inputs, that is, for specific designs, response curves can be drawn with reasonable accuracy. Recent work, as yet unpublished, promises near-term ability to predict maximum transmissibility and associated frequency in a simple manner.

There is not at present a consensus on what constitutes a sound method of evaluating the vibration performance of cushions. For example, tests based on military specifications requiring a sinusoidal equivalent of a rough-road environment have been found to produce shock motions, not vibratory response.

9.3. Behavior of Materials

Materials usable as cushions can be divided into three categories: resilient, quasi-resilient, and rigid. In analyzing the utility of materials, three broad ranges of impact velocity have been investigated:

1. Low velocities, resulting from drops of a few feet, typical of the packaging environment;
2. High velocities, resulting from drops of up to 20 feet, typical of parachute delivery; and
3. Very high but subsonic velocities typical of explosive impacts. Data in this category are rather scanty.

Most data are concerned with the behavior of resilient and quasi-resilient materials used for packaging, although a good collection of data covers paper honeycombs for air-drop shock absorption. Almost all of the data, however, are concerned with peak acceleration at the interface between the cushion and the object; practically none with shock spectral effects.

For delicate items, the data show that soft open-celled plastic foams, bound fibers such as animal hair, vegetable fiber and fibrous glass, reclaimed rubber

and plastic foams, hair or cellulosic felts and a host of other materials can be used. Practical utility is based on the energy-absorptive capacity of the material, creep characteristics, and (especially for military work) extreme-temperature performance.

Data on extreme-temperature performance are scanty. Much of this scarcity is due to not making sufficient use of viscoelastic theory, so as to give a consistent approach. However, it does seem that although most materials stiffen as the temperature drops, there is little increase in peak acceleration (other conditions being equal) until the region of the glass temperature is reached. From this there arises the concept of the lowest "safe" temperature for a cushion, that is, the lowest temperature attained before a room-temperature design is no longer approximately valid. Several materials continue to be "safe" down to $-40°C$, although most plastic foams become "unsafe" at $-10°C$ to $-20°C$.

Data on drift of package-cushioning materials is far from complete although some developments show promise. For any given material, enough tests must be run to establish the maximum practical load for a given creep over a given time. Creep is a function of the materials properties (including cross linking, in the case of polymers). For the polyurethane foams there is a set of curves giving maximum static stress for 5 percent creep in about one year, related to the density of the foam. Data on other materials are not so satisfactory, since the time and creep end points have not been established.

Among quasi-resilient materials, there is plenty of available data on polystyrene foams. These data indicate considerably more shock and vibration isolation utility for this material than might be expected. The semi-rigid polyurethane foams perform especially well, even after a number of drops, if the original static stress is properly set.

The most popular (and a very versatile) quasi-resilient cushion material is corrugated fiberboard; the available data only begin to sample its properties. A double layer of corrugated fiberboard (such as occurs at the bottom of a conventional box) continues to give protection up to 30 or 40 severe drops. When formed into accordion or rat trap pads, corrugated fiberboard gives as much protection as any of the resilient materials, but the structure has limited durability.

Among the nonresilient materials, paper honeycomb seems the most popular, at least for air-drop cushioning. But there are indications that metal honeycombs absorb more energy per unit volume; honeycombs filled with plastic or rubbery materials are even better, in this respect.

In short, we have a large choice of materials with known properties. The choice for a given application depends on design constraints and goals.

9.4. General

More than 300 written contributions have been drawn upon in writing this monograph. This shows that much solid work, by some of the world's best minds, has been devoted to the subject of cushioning.

One of the first papers to discuss velocity-shock isolation was Mindlin's "The Dynamics of Package Cushioning." This classic is almost invariably referenced in any serious work on velocity shock isolation; it is referred to here many times.

However, in the general field of cushions, too many packaging studies have avoided such deeper issues as damping, shape, and viscoelasticity. Their authors have let slip from their hands the ownership of a fascinating and difficult field. Too many engineers and physicists still do not consider packaging respectable. So, cookbook answers are given to questions that need the best thinking.

This refusal to take packaging seriously has hampered the shock and vibration experts, for the packagers have much to teach them even if it is not expressed in elegant mathematical terms. Package cushions are excellent shock and vibration isolators, but only recently have their properties begun to be exploited in non-packaging applications.

Finally, both classes of expert have widely ignored what the polymer scientists have to say. The fact that only one engineering study of cushions used the principle of time and temperature superposition (which has been recognized since 1943) is a good example.

The three disciplines must be brought together. May this monograph be a letter of introduction.

Appendix I

METHODOLOGY

In this monograph we have tried to include every paper having an identifiable bearing on the problem of cushions, within the bounds established in the introduction.

First, the known bibliographies were consulted. Of particular value here was Brennan's [221] monumental work which brought the literature up through 1956, thus appreciably shortening search time. Van der Toorn's [172] bibliography was particularly helpful. Gigliotti's report [152], Ali and Benson [220], Strachwitz [309], a report from the Central Packaging Branch, Ministry of Aviation [310], Curtis [311] and The Package Cushioning Design Handbook [148]; all have pertinent bibliographies which were reviewed.

Finally, the abstract journals from 1955 onward were read. In particular, Engineering Index and Packaging Abstracts were both read through December 1965.

It was found that pertinent references were included in a surprisingly large number of technical and quasi-technical journals and periodicals. Table I-1 lists by journal the open source material consulted in preparing this monograph.

A special search was made of abstracts available in the Defense Documentation Center. Over 300 references to cushions were found, as well as over 300 citations to viscoelasticity studies in the past five years. The complete file of Shock and Vibration Bulletins at the Shock and Vibration Information Center was reread.

Each paper and report identified as having possible bearing on the problem was read and annotated with the needs of this monograph in mind. Citations in each paper were also checked for possible further contributions to understanding.

In addition to the foregoing, and possibly more important to the timeliness of this writing, many workers identifiably active in early 1966 were asked about the direction of their work and any conclusions that they cared to draw.

Thus, this overview represents a determined effort to attain completeness. However, the great volume of the literature and its scattered availability make it very possible that some significant paper or report may have been missed; any comments on such omissions will be gratefully received.

For the sake of coherence, the author used his own judgment concerning what was significant in the light of today's knowledge. This monograph therefore contains an element of bias; nevertheless, every reasonable effort has been made to present a balanced view of every topic.

TABLE I-1. DISTRIBUTION OF PERIODICAL REFERENCES

Journal	*No. of Citations*
J. Acoust. Soc. Am.	10
J. Am. Chem. Soc.	2
Aeron. Quart.	1
Am. J. Math.	1
J. Appl. Mech.	4
J. Appl. Phys.	1
Arch. Rat. Mech. Anal.	1
ASTM Bulletin	1
Bell System Tech. J.	2
Br. J. Appl. Phys.	2
Bull. Seismological Soc. Am.	1
J. Chem. Phys.	2
J. Colloid Sci.	1
Electrical Communication	1
Engineering	1
Experimental Mechanics	1
Ind. Eng. Chem.	1
Industrial Packaging	1
Materials Handling Engineering (Flow)	6
Mech. Engineering	1
Modern Materials Handling	1
Modern Packaging	10
Neue Verpackung	1
Noise Control	3
Ost. Ing.-Arch.	2
Package Engineering	5
Packaging	1
Packaging News	1
Packaging Review	2
Physica	1
Phys. Rev.	1
J. Polymer Sci.	2
Revs. Modern Phys.	1
J. Roy. Aeronaut. Soc.	1
J. Sound Vibr.	1
J. Sci. Instr.	1
Shock and Vibration Bulletins	31
Soc. Exp. Stress Anal. Proc.	1
Trans. Am. Soc. Mech. Engrs.	11
Verpackungs Rundschau	3
Z. Ver. Deuts. Ing.	1

Appendix II

NOTATION

A	Constant, usually denoting amplitude of a time varying disturbance
A_a	Area under an acceleration-time curve
A_c	Area of a cushion exposed to static stress
A_i	Initial area of a variable orifice
A_m	Amplification factor
A_n	Arbitrary constant of the nth order
A_0	Area of a variable orifice at any instant; also, first term in a polynomial
A_p	Projected area of a cushion
A^*	Complex amplitude of a sinusoidal motion
$A_m{}^*$	Complex amplitude of the mth component wave
A'_m	Complex conjugate of $A_m{}^*$
a_i	Variable distance from the end of a container
a_n	Constants of order n, defined in the equations in which used
a_o	Initial slope of a stress-strain curve; also, when clear from context, the first of n constants of order n
a_p	Peak acceleration
a_T	Temperature shift factor
a'	Motion in a direction defined in an associated figure
$\dot{a}'$	Velocity of the motion a'
a'_o	Optimum value of a_o
$a'(\omega)$, $a''(\omega)$	Unspecified functions of frequency
a_1, a_2 ...	Directions of motion defined in pertinent figures
B	Bandwidth
B_i	Cushion mass factor
B_m	Arbitrary constant of the mth order

B'	ω_n/B
b_n	Constant of the nth order, defined in the equation in which used
b'	Motion in a direction defined in an associated figure
$b'(\omega)$, $b''(\omega)$	Unspecified functions of frequency
C_1, C_2 ..	Arbitrary constants defined in the equations in which used
C_m	Fourier coefficients
C_x	Sum of the coefficients of damping acting in the x-direction
C_y	Sum of the coefficients of damping acting in the y-direction
C_θ	The rotational damping coefficient; sum of the damping coefficient in each isolator times the square of its distance from the center of rotation
$C(t)$	Creep function
$C(\omega)$	Fourier transform of the creep function
$C'(t)$	Generalized creep spectrum
c	Damping coefficient
c_c	Critical damping coefficient
c_e	Damping coefficient of an element of the cushioned object
c_f	Coefficient of friction
c'_f	Air friction coefficient, or drag
c_i	Damping coefficient in the ith element
c_j	Damping coefficient of the jth element
c'_j	Damping coefficient of the jth element in a Maxwell model
c_n	Nonlinear damping coefficient
c_0	First term in a polynomial expansion of c_n
c_p	Specific heat per unit volume
c_r	Coefficient of restitution
c_T	Coefficient of thermal expansion
D	Depth of a cushioned object; when immediately followed by a variable symbol, an operator notation denoting differentiation.
D_m	Fourier coefficients
D_ϵ	Operator notation denoting partial derivative with respect to ϵ
D_1	Cross-sectional dimension of a thread of foam material
D^{-1}	Operator notation denoting integration of the variable immediately following

d	Deflection due to translational motion
d_c	Average foam cell diameter
d_T	Total deflection
d_θ	Deflection due to rotation
d_1, d_2 ..	Distances defined in the pertinent figure
E	Modulus of elasticity; usually taken herein to mean in compression; when tension, shear, rigidity or bulk moduli are meant, they are so specified
E_c	Young's modulus for the corrugating medium in corrugated fiberboard
E_f	Tensile modulus for a foamed sample; also, in Ch. 6, the effective modulus in compression
E_j	Elasticity modulus for the jth element
E_l	Loss modulus; imaginary part of the complex modulus of elasticity
E_m	Tensile modulus for an unfoamed material
E_n	Nonlinear modulus of elasticity
E_0	First term in a polynomial expansion of E_n
E_r	Storage modulus; real part of a complex modulus
E_{rn}	Value of E_r at the natural frequency of the cushion
E_{l1}	First-order nonlinear contribution to the nonlinear loss modulus
E_{r1}	First-order nonlinear contribution to the nonlinear storage modulus
$E(t,T)$	Modulus of elasticity as a function of time and temperature
$E_T(t)$	Modulus of elasticity at a given temperature as a function of time
$E_T(\omega)$	Modulus of elasticity at a given temperature as a function of frequency
E_{T_0}	Modulus of elasticity at a specified reference temperature T_0
E^*	Complex modulus of elasticity
E_1^*	First-order nonlinear contribution to a nonlinear complex modulus of elasticity
E'	Modulus of elasticity of a nonlinear material measured at a specified strain ϵ
E'_r	Storage modulus of a nonlinear material measured at a specified strain ϵ
e	Base of natural logarithms, $e = 2.71828$ ...
erf	Error function

$erfc$	Complimentary error function
e_1	Internal energy density per unit mass
e_2	Entropy per unit mass
F	Force
F^*	Complex force
$F_i(t)$	Time-varying input force
$F_i(x_i)$	Force in the ith mount due to displacement x_i
$F_i(y_i)$	Force in the ith mount due to displacement y_i
$F'_i(x_i)$	Force in the ith mount resisting rotation by displacement x_i
$F'_i(y_i)$	Force in the ith mount resisting rotation by displacement y_i
$F_i(\omega)$	Fourier integral transform of $f_i(t)$
$F_0(\omega)$	Fourier integral transform of $x_0(t)$
f	Frequency (cps)
$f(\ ), f[\ ]$	Denotes a function of the terms contained in the parentheses or brackets
$f(T_a)$	Temperature shift function
f_e	Natural frequency of an element (cps)
f_{it}	Impulsive disturbing excitation
$\bar{f}_i$	Root mean square value of $f_i(t)$
$f_i(t)$	Generalized time-dependent excitation function
$f_i(\bar{t})$	Artificial $f_i(t)$ in which a transient is converted to a steady-state excitation
f_n	Natural frequency (cps)
G_e	Equivalent static acceleration ratio
G_i	Peak input acceleration ratio
G_{im}	Peak acceleration ratio corresponding to frequency ω_i
G_m	Peak acceleration ratio
G_o	Minimum value of G_m corresponding to J_o
G_s	Maximum safe static acceleration ratio
G_1	Peak acceleration ratio from a hypothetical linear cushion
g	Acceleration of gravity
H	Magnification factor; absolute value of $H(\omega)$
$H(t)$	Unit step function

$H(\log \tau)$	Distribution function of relaxation times
$H(\omega)$	Complex magnification factor
$H_m(\omega)$	Complex magnification factor for the mth component wave
H_1, H_2	Magnification factors for subsystems 1 and 2
h	Height of drop
$h(t)$	Response to a unit impulse function
h_1, h_2	Heights defined in pertinent figures
I_a	Area moment of inertia
I_0	Moment of inertia of a complete system about a point O
I_1	Moment of inertia of m_1 about its center of gravity (c.g.)
I_2	Moment of inertia of m_2 about its c.g.
I_3	Moment of inertia of complete system about its c.g.
i	$\sqrt{-1}$, except when used as a subscript where it denotes the ith element in an assembly of many elements
J	Ratio of peak stress developed by a cushion to the energy absorbed per unit volume by the cushion at that stress
J_o	Minimum value of J
J_l	Minimum value of J for a hypothetical linear cushion
j	Subscript denoting the jth element in an assembly of many elements
K	Bulk modulus
K_c	One-fifth the compression modulus for an open celled foam
$K(T)$	Characteristic relaxation time of a polymer at temperature T_a
$K(T_g)$	Characteristic relaxation time of a polymer at T_g
K_x	Total spring rate acting in the x-direction
K_y	Total spring rate acting in the y-direction
K_θ	Rotational spring rate
k	Spring rate
k_e	Spring rate of an element of a cushioned object
L	Length of a cushioned object
L_1	Overall length of a container
l	Length of a capillary; also, length of a cantilever beam
l_c	Characteristic length of a cushion

ℓ_0 Unstrained length of an individual thread in a foam material

M Ratio of total deflection to translation deflection

m Mass of a cushioned object; when used as a subscript denotes the mth element in an assembly of many elements

m_c Mass of a cushion

m_e Mass of an element of the cushioned object

m_1 Sprung mass

m_2 Container mass

m_3 Mass of complete system

N^* Complex quantity defined in Eq. (6.33)

n A number; when used as a subscript denotes the nth element in an assembly of many elements

n_a Ratio of specific heats of air at constant volume and constant pressure

n_0 Number of zero crossings of a random variable

n_y Number of times $y(t)$ passes through y with positive slope

n_{yp} Number of peaks of $y(t)$ per unit time

O Point in space

P Proximity, the distance at any instant between two moving masses

$P(\ )$ Probability of the variable contained in the parentheses; where only a single variable is given it is to be understood that the probability meant is the probability that the value of the variable is equal to or less than some value of that variable

p Pressure

p_a Ambient pressure

p_i Internal pressure

p_n Structural response parameter, identified in the equation in which used

$p(\ )$ Statistical distribution function of the variable indicated in parentheses

p_1 Real part of N^*, Eq. (6.35)

Q Quality factor, numerically equal to $1/2\beta$

Q_f Heat flux in a thermodynamic system

Q_1 D_1^2/ℓ_0

q_1 Imaginary part of N, see Eq. (6.35)

R_n Structural response parameter defined in the equation in which used

R_x	Spring coupling constant denoting coupling from x-coordinate into y-coordinate
R_y	Spring coupling constant denoting coupling from y-coordinate into x-coordinate
R'_x	Damping coupling constant equivalent to R_x
R'_y	Damping coupling constant equivalent to R_y
$R_a(\omega)$	Any acceleration response spectrum
$R_{an}(\omega)$	Normalized (dimensionless) acceleration response spectrum
$R_d(\omega)$	Displacement response spectrum
$R_{dn}(\omega)$	Normalized displacement response spectrum
$R_v(\omega)$	Velocity response spectrum
$R_{vn}(\omega)$	Normalized velocity response spectrum
R_1	Radius of gyration of sprung mass
R_2	Radius of gyration of container
R_3	Radius of gyration of complete system about point O
R_4	Distance from point O to system c.g.
r	Radius of a capillary
$r(t)$	Relaxation function
$r'(t)$	Continuous relaxation spectrum
$r(\omega)$	Fourier transform of $r(t)$
S	Shape of a pulse (dimensionless)
$S_a(\omega)$	Standard acceleration shock response spectrum
$S_{an}(\omega)$	Normalized acceleration shock response spectrum
$S_d(\omega)$	Standard displacement shock response spectrum
$S_{dn}(\omega)$	Normalized displacement shock response spectrum
$S_v(\omega)$	Standard velocity shock response spectrum
$S_{vn}(\omega)$	Normalized velocity shock response spectrum
s_{tc}	Standard deviation of the mean time to first exceedance t_c
s_y	Standard deviation of the random variable y
s^2	Variance of a normal (Gaussian) variate
$s_1, s_2, \ldots$	Distances defined in the pertinent figures
T	Transmissibility; absolute value of $T(\omega)$
T_a	Absolute temperature

T_c	Cushion thickness
T_{ca}	Average thickness of the air in a foam cushion
T_g	Glass temperature of a polymer
T_m	Transmissibility corresponding to H_m
T_{max}	Maximum value of T
T_0	Reference temperature
$T(\omega)$	Complex transmissibility
$T(z_2)$	Return period for z_2
t	Time
t'	Time interval, very short compared to t
t_e	Mean time to exceedance of a stipulated value
t_m	Rise time; time at which maximum acceleration occurs
t_n	Natural period of a motion
t_0	Starting time
$t_1, t_2, \ldots$	Specific times identified in the equations in which used
U	Energy stored in a spring system at any instant
u	Change in the magnitude of a vector in the x-direction
V	Velocity
V^*	Complex velocity
V_f	Total volume of a foam material
V_m	Volume of solid material in a foam
V_R	Volume ratio, V_m/V_f
V_r	Rebound velocity
V_{ri}	Instantaneous value of V_r
V_1	Velocity of the dilatational wave
V_2	Velocity of the distortional wave
V_3	Velocity of a plane wave
v	Deflection in the y-direction
W	Weight
W_1	Weight of sprung mass
W_2	Weight of container
W_3	Weight of complete system
$W(\omega)$	Power spectral density

$W(\omega_n)$	Power spectral density in the neighborhood of ω_n
$W_{ia}(c)$	Input power spectral acceleration density for white noise
$W_{ia}(f)$	Input power spectral acceleration density (g^2/cps)
$W_{ia}(\omega)$	Input power spectral density
$W_{ia}(\omega B)$	Input acceleration spectral density in bandwidth B
$W_{ix}(\omega)$	Input motion power spectral density
$W_{oa}(\omega)$	Output acceleration power spectral density
$W_{ox}(\omega)$	Absolute output motion power spectral density
$W_{rx}(\omega)$	Relative motion power spectral density
w	Deflection in the z-direction
x	Cartesian coordinate
x_i	Input or excitation motion
x_i^*	Complex input motion
$x_i(t)$	Time varying input motion
x_{im}	Maximum value of an input motion
x_0	Absolute output motion
x_0^*	Complex output motion
x_{om}^*	$x_{om}e^{i\phi}$
$x_0(t)$	Time-varying absolute output motion
x_{om}	Maximum value of x_0
x_r	$x_0 - x_i$; relative motion
$x_r(t)$	Time-varying relative motion
x_{rm}	Maximum value of x_r
x_{st}	Maximum equivalent static motion
x_1, x_2, x_3	Dimensions
$\dot{x}_i$	Input velocity
$\dot{x}_0$	Output velocity
$\dot{x}_r$	Relative velocity
$\ddot{x}_a$	Average height of input acceleration pulse
$\ddot{x}_i$	Input acceleration
$\ddot{x}_0$	Output acceleration
Y	Compliance, $1/E$
Y^*	Complex compliance

Y_j Compliance in the jth element

Y_l Loss compliance; imaginary part of Y

Y_{l1} First-order nonlinear contribution to polynomial expansion of a nonlinear compliance

Y_0^* First term in polynomial expansion of a nonlinear complex compliance

Y_r Storage compliance; real part of Y

Y_{r1} First-order nonlinear contribution to polynomial expansion of the real part of a nonlinear complex compliance

Y_s Shear compliance

Y_1 First-order nonlinear contribution to the polynomial expansion of a nonlinear complex compliance

y Direction in Cartesian coordinates; also used as the designator of a variable quantity

Z Specific air resistance (Rayleighs/cm)

z Direction in Cartesian coordinates

z_1 Standardized, or normalized, statistical variate; the actual value of the variable divided by its standard deviation, otherwise known as the root mean square value

z_2 Particular value of z_1

z_c Characteristic largest value of z_1

z_p Peak value of z_1

z_m Most probable, or modal, largest value of z_1

α_n Phase angles corresponding to certain Fourier coefficients, defined in the equations in which used

α_1 Angle of departure of a dilatational wave reflected from a surface

α_2 Elastic constant depending on Poisson's ratio, Eq. (3.13)

α_3 Angle between corrugating medium and facing

β Ratio of damping coefficient to critical damping coefficient

β_e Damping ratio of an element of a cushioned object

β_1 Angle of departure of a distortional wave reflected from a surface

β_2 Linear component of a nonlinear damping component

γ_c Dimensionless damping parameters in a polynomial expansion of a nonlinear viscoelastic equation

γ_E Dimensionless elasticity parameter

Δ Dilatation, the change in volume of a unit cube; when followed immediately by a single variable, denotes a small, but finite, change in that variable

Δ_c Proximity criterion

∇ Laplacian operator, $\frac{\partial^2}{\partial x^2} + \frac{\partial^2}{\partial y^2} + \frac{\partial^2}{\partial z^2}$

δ Angle, usually a phase angle; loss angle in complex modulus terminology

$\delta(t)$ Dirac-delta function

δ_0 Peak loss angle for a standard linear solid

δ_p Permanent deformation

δ_y Deflection at the yield point

ϵ Strain

ϵ' Strain of individual threads in a foam material

ϵ^* Complex strain

$\epsilon(t)$ Time-dependent strain function

$\epsilon(t)_i$ Strain in the ith time-dependent strain variable

$\epsilon(t)_j$ Strain in the jth time-dependent strain variable

ϵ_b Bottoming strain

ϵ_c Strain on the viscous element of a nonlinear cushion

ϵ_E Strain on the elastic element of a nonlinear cushion

ϵ_f Forcing strain, *i.e.*, ratio between peak input motion and cushion thickness

ϵ_m Maximum value of strain

ϵ_0 Strain producing J_0

ϵ_x Strain in the x-direction

ϵ'_x Strain in the x-direction behind a wave front

ϵ_y Strain in the y-direction

ϵ'_y Strain in the y-direction behind a wave front

ϵ_z Strain in the z-direction

ϵ_1 Strain for a hypothetical linear cushion with slope equal to the initial slope of a nonlinear cushion

$\dot{\epsilon}$ Strain rate; $T_c\dot{\epsilon}$ = velocity

$\dot{\epsilon}_c$ Strain rate on the viscous element of a nonlinear cushion

$\dot{\epsilon}_E$ Strain rate on the elastic element of a nonlinear cushion

$\ddot{\epsilon}$ Rate of change of strain rate; $T_c\ddot{\epsilon}$ = acceleration

ζ Substituted variable; defined in equation in which used

$\theta_1, \theta_2, \ldots$	Angles, defined in the pertinent figures
$\dot{\theta}$	Angular velocity
$\ddot{\theta}$	Angular acceleration
κ	Velocity of a Rayleigh wave as a fraction of the velocity of a distortional wave
λ	Lamé coefficient
λ_1	Time parameter defined in the equation in which used
μ	Lamé coefficient; also rigidity or shear modulus
μ^*	Complex shear modulus
μ_i	Shear loss modulus; imaginary part of complex shear modulus
μ_r	Shear storage modulus; real part of complex shear modulus
ν	Poisson's ratio
π	3.14159 ...
ρ	Density of a material
ρ_0	Density of a material at reference temperature T_0
σ	Stress
σ^*	Complex stress
σ'	Reduced stress; $\sigma' = \sigma/a_0\epsilon_b$
$\sigma(t)$	Time-dependent stress function
$\sigma(t)_i$	Stress in the ith time-dependent stress variable
$\sigma(t)_j$	Stress in the jth time-dependent stress variable
σ_a	Average stress at 70 percent strain for honeycomb material
σ_l	Stress produced by a hypothetical linear cushion
σ_m	Peak value of stress
σ_0	Stress producing J_0
σ_s	Static stress on a cushion
σ'_s	Optimum static stress
σ_x	Stress in the x-direction
σ'_x	Stress in the x-direction behind a wave front
σ_y	Stress in the y-direction
σ'_y	Stress in the y-direction behind a wave front
σ_z	Stress in the z-direction

$\sigma_{xx}, \sigma_{xy}, \ldots$	Stress acting in a particular direction and in a particular plane; the first subscript denotes the direction and the second denotes the plane in which acting
$\dot{\sigma}$	Rate of change of stress
τ	Time, necessarily different from t; sometimes used to designate pulse length
τ_i	ith value of τ in an assembly of many values of τ
τ'	Relaxation or retardation time; in a standard linear solid $\tau = c/E_1$
τ'_j	Relaxation or retardation time of the jth element
ϕ	Phase angle
χ	Generalized response parameter
χ_1	Complementary solution of the differential equation of motion involving χ
χ_2	Particular solution of the differential equation of motion involving χ
ψ	Parameter reflecting the velocity of plane waves
$\psi(t)$	Arbitrary function of time
ψ_n	Phase angle difference
ω	Angular frequency (radians/sec)
ω_b	Fundamental frequency in a complicated wave
ω_c	Natural frequency of a cushion
ω_e	Natural frequency of an element of a cushioned object
ω_i	ith frequency in a cushion with distributed mass
ω_m	Frequency of the mth component of a complicated wave
ω_n	Natural frequency
ω_0	Frequency at which loss angle peaks; also used to denote frequency at which real and imaginary portions of complex impedance are equal
ω_p	Natural frequency of a pulse
$\overline{\omega}$	Median frequency in a frequency band
ω_1	Linear component of frequency in a nonlinear system

REFERENCES

1. C. T. Morrow, *J. Acoust. Soc. Am.*, **29** (5), 596 (1957)
   Defines shock spectrum, discusses second-order effects, which are readily inferred. Defines shock as a special case of vibration.
2. Y. C. Fung, Paper on Shock Loading and Response Spectra, in *Shock and Structural Response* (M. V. Barton, ed.) ASME, New York, 1960
   Basic discussion, with examples and bibliography, on uses of response spectra and how to derive them.
3. C. E. Crede, *Vibration and Shock Isolation*, Wiley, New York, 1951
   Introductory, lucid, text on shock and vibration-isolation principles.
4. J. P. Walsh, *Shock and Vibration Bull. No. 15*, 56 (March 1950)
   Early discussion of shock spectrum concept as applicable to packaging.
5. J. P. Walsh and R. E. Blake, *Proc. Soc. Exp. Stress Anal.*, **6** (2), 150 (1949)
   Generalizes Ref. 4. Discussed reed gage use. Shows that shock spectrum provides design conditions in the form of equivalent static stress and provides rational method for comparing severity of different shock motions.
6. A. E. H. Love, *A Treatise on the Mathematical Theory of Elasticity*, Dover Publications, New York, 1944
   Valuable historical background and rigorous derivations of many elasticity functions.
7. S. P. Timoshenko, *History of the Strength of Materials*, McGraw-Hill, New York, 1953
   Relatively short and reasonably readable account of the development of the field of strength of materials.
8. I. Todhunter and K. Pearson, *A History of the Theory of Elasticity and of the Strength of Materials from Galileo to Lord Kelvin*, Dover Publications, New York 1960
   Monumental three-volume text summarizing the work of all principal investigators.
9. H. M. Westergaard, *Theory of Elasticity and Plasticity*, Harvard Univ. Press, Cambridge, Mass., 1952
   Introductory chapter brings history up to date through 1940.
10. M. A. Biot, *Mechanics of Incremental Deformations*, Wiley, New York, 1965
    Contains very valuable hints on solving viscoelastic problems.
11. Y. C. Fung, *Foundations of Solid Mechanics*, Prentice-Hall, Englewood Cliffs, N.J., 1956
    Excellent text on theoretical solid mechanics. Primarily classical theory but includes thermodynamic problems and emphasizes use of calculus of variations.

12. L. D. Landau and E. M. Lifshitz, *Theory of Elasticity*, Addison Wesley, Reading, Mass., 1959
Advanced text using vector and tensor notation.

13. I. S. Sokolnikoff, *Mathematical Theory of Elasticity*, McGraw-Hill, New York, 1956
Advanced text using complex-variable techniques and variational analysis.

14. R. V. Southwell, *Theory of Elasticity*, Oxford Univ. Press, 1941
Statics primarily, but has an elegant derivation of the elastic constants.

15. T. Alfrey, *Mechanical Behavior of High Polymers*, Interscience. New York, 1948
One of the best texts on viscoelasticity found.

16. D. R. Bland, *The Theory of Linear Viscoelasticity*, Pergamon Press, New York, 1960
Axiomatic derivation of the theory of linear one- and three-dimensional elasticity. Also has many valuable simple hints and constants for a material from the empirical data.

17. J. L. Davis, "The Fundamentals of Materials Research, Part I—Viscoelasticity," Feltman Res. Labs, Picatinny Arsenal Tech. Rept. 3202, April, 1965
Excellent treatment of viscoelasticity. Starts with simple cases and concludes with own mathematical theories of nonlinear viscoelasticity.

18. F. R. Eirich, ed., *Rheology, Theory and Applications*, Academic Press, New York, 1958
Definitive three-volume work on flow of materials, of which plasticity and viscoelasticity are specialized subfields.

19. A. C. Eringen, *Non-Linear Theory of Continuous Media*, McGraw-Hill, New York, 1962
Comprehensive review of linear and nonlinear viscoelasticity through 1961.

20. J. D. Ferry, *Viscoelastic Properties of Polymers*, Wiley, New York, 1961
Excellent treatise from the standpoint of the polymer.

21. A. Brodeau, *Vibrations of Isotropic, Anisotropic, Homogeneous and Heterogeneous Solids*, Publications Scientifiques et Techniques du Ministre de l'Air, Paris, 1951
Discusses vibrations in isotropic, anisotropic, homogeneous and heterogeneous solids in terms of simple elastic theory. Excellent on plane waves.

22. H. Kolsky, *Stress Waves in Solids*, Dover, New York, 1963
Excellent review of classical theory of elastic waves in solids. Some discussion of anelasticity, and plastic and shock waves.

23. R. Houwink, *Elasticity, Plasticity and Structure of Matter*, Dover, New York
Standard treatise on rheological aspects of solids.

24. S. H. Crandall, ed., *Random Vibration*, MIT Technology Press, Cambridge, Mass., 1958
Introduction to concepts of random vibration, Fourier transforms, impedance, and mobility.

25. J. P. Den Hartog, *Mechanical Vibrations*, 4th ed., McGraw-Hill, New York, 1956
Standard text on vibrations.
26. C. M. Harris and C. E. Crede, ed., *Shock and Vibration Handbook*, McGraw-Hill, New York, 1961
Standard reference work on shock and vibration.
27. N. W. McLachlan, *Theory of Vibrations*, Dover, New York, 1951
Short, highly condensed treatment of most linear-vibration problems. A refresher. Not introductory.
28. C. T. Morrow, *Shock and Vibration Engineering*, Vol. 1, Wiley, New York, 1963
Excellent, partly philosophical treatise on shock and vibration technology. Much basic, practical information.
29. S. Timoshenko, *Vibration Problems in Engineering*, 3rd ed., Van Nostrand, New York, 1955
Standard text.
30. R. J. Roark, *Formulas for Stress and Strain*, 2nd ed., McGraw-Hill, New York, 1943
The stress analyst's *vade mecum*.
31. O. S. Kerstner, "General Principles of Package Design, Part I—Cushioning," Northrop Aircraft, Rept. NAI-57-187, Feb. 1957
Practical dissertation on principles of cushion design. Many examples.
32. D. Bancroft, *Phys. Rev.*, **59** (7), 588 (1941)
Extensive computations of wave velocity in cylindrical bars.
33. W. G. Soper and R. C. Dove, "Data Presentation for Cushioning Materials," 17th Annual Tech. Conf., Soc. of Plastics Engs., Paper 27-4, Jan. 1961
Basic derivation of J-energy curves. Many examples.
34. F. D. Murnaghan, *Am. J. Math.*, **59**, 235 (1937)
Discusses finite deformation of isotropic elastic solids.
35. A. E. Green and J. E. Adkins, *Large Elastic Deformations*, Oxford Univ. Press, 1960
Summarizes state of the art. Notes enormous strides since Murnaghan's pioneering work.
36. V. N. Smiley, "Investigation of Shock Waves Developed During Dynamic Tests of Cushioning Materials," WADC, Tech. Rept. 56-547, Aug. 1957
Shows good correlation between elementary wave theory and actual irregularities in the accelerometer record.
37. A. Tobolsky, R. E. Powell, and H. Eyring, *The Chemistry of Large Molecules*, Interscience, New York, 1943
Contains a highly theoretical explanation of possible causes for internal friction in elastomeric solids.
38. C. Zener, *Elasticity and Anelasticity*, Univ. of Chicago Press, Chicago, 1948
Extensive, lucid discussion of damping in metals.
39. B. J. Lazan and L. E. Goodman, "Material and Interface Damping," Ch. 36 in *Shock and Vibration Handbook*, McGraw-Hill, New York, 1961
Basic discussion of damping, with emphasis on structural damping.

40. A. C. Eringen and R. A. Grot, "Continuum Theory of Non-Linear Viscoelasticity," Purdue Univ., School of Aeronautics, Astronautics and Engineering Sciences, Tech. Rept. 32, Oct 1965
Assessment of recent developments in nonlinear continuum mechanics. Contains several useful engineering approximations.

41. A. J. M. Spencer, "A Review of Some Recent Developments in Continuum Mechanics," Royal Armament Research and Development Establishment, Memo (B) 7/63, April 1963
Covers significant developments in theoretical mechanics of nonlinear continua.

42. A. C. Eringen, "A Unified Theory of Thermomechanical Materials," Purdue Univ., School of Aeronautics, Astronautics and Engineering Sciences, Tech. Rept. 30, Sept. 1965
A unified theory of generalized three-dimensional viscoelasticity, taking into account thermal effects. Also reviews some recent history and shows that linear viscoelasticity is a special case of the general.

43. A. C. Pipkin, *Rev. Mod. Phys.*, 36 (4), 1034 (1964)
Stress relaxation integral of infinitesimal theory can be extended to cover small strains by adding terms of second and higher order. These terms enter in the form of multiple integrals.

44. B. D. Coleman, *Arch. Ratl. Mech. Anal.*, 9, 172 (1962)
Discusses specific restrictions on the forms of the stress-strain relationships in three-dimensional solids.

45. G. Lianis, "Constitutive Equations of Viscoelastic Solids Under Finite Deformation," Purdue Univ., School of Aeronautics, Astronautics and Engineering Sciences, Tech. Rept. 63-11, Dec. 1963
Broad forms of the constitutive relations are derived.

46. V. Volterra, *Theory of Functionals and of Integral and Integro-Differential Equations*, Blackie, London, 1930
Basic work upon which most modern viscoelastic material description depends.

47. H. K. P. Neubert, *Aeronaut. Quart.*, 14, 2 (1963)
Finds complex moduli for the "standard linear" solid and shows how the concept can be extended to multiple-spring models with steady-state and transient excitation.

48. E. Skudrzyk, *Ost. Ing.-Arch.*, 3, 356 (1949)
Develops general theory of stress-strain on basis of local-time derivatives and a power-series expansion. For simple harmonic motion, power series reduces to a power series in the frequency.

49. E. Skudrzyk, *Ost. Ing.-Arch.*, 6, 156 (1952)
Shows equivalence of power series to complex-modulus problem and then covers simple and complex relaxation, damping, hysteresis, and plastic flow. Theory checked against experimental results.

50. B. Gross, *Mathematical Structure of the Theories of Viscoelasticity*, Hermann *et Cie.*, Paris, 1953
Among other contributions, develops classification of equivalent viscoelastic moduli.

51. W. Goldberg and N. W. Dean, "Determination of Viscoelastic Model Constants from Dynamic Mechanical Properties of Linear Viscoelastic

Materials," Aberdeen Proving Ground, Ballistic Res. Lab., Rept. 1180, Nov. 1962
Contains a semi-graphical method for computing spring and damping constants.

52. A. S. Elder, "Analytical Relations Between Constants for Generalized Voigt and Maxwell Models," Aberdeen Proving Ground, Ballistic Research Lab. Memo Rept. 1460, Feb. 1963
Using Gross' equivalence diagrams, shows how to compute constants for a Voigt solid from a Maxwell solid's constants, and *vice versa*.

53. J. C. Snowdon, *J. Acoust. Soc. Am.*, **33** (10), 1295 (1961)
Derives response curves for tangent and arctangent elasticity to transient foundation displacements.

54. J. C. Snowdon, *J. Acoust. Soc. Am.*, **35** (3), 389 (1963)
Tangent and arctangent elasticity with linear damping exposed to rounded-step pulses.

55. C. W. Kosten and C. Zwikker, *Physica*, **4** (9), 843 (1937)
One of earliest papers on viscoelastic behavior of foam rubbers. Provides for damping by air in foam.

56. N. O. Myklestad, *J. Appl. Mech.*, **74**, 284 (Sept. 1952)
Discusses use of complex-modulus concept in solution of simple-vibration problems.

57. J. C. Snowdon, *J. Acoust. Soc. Am.*, **35** (6), 821 (1956)
Develops complex modulus concept. Has a solution for a damped rod. Some shear modulus data on a number of materials.

58. J. C. Snowdon, *Br. J. Appl. Phys.*, **9** (12), 461 (1958)
Develops transmissibility equation in terms of complex modulus. Transmissibility data for various common mount materials.

59. J. C. Snowdon, *Noise Control*, **6** (2), 18 (March, April 1960)
About the same as the previous reference.

60. J. C. Snowdon, *J. Sound and Vibr.*, **2** (2), 175 (1965)
Excellent review of own and others prior work in field of viscoelasticity. Uses time and temperature superposition to obtain complex moduli for a number of elastomeric materials. Discusses practical limitations.

61. J. C. Snowdon, *J. Acoust. Soc. Am.*, **37** (6), 1027 (1965)
Uses Love theory of a rod to develop viscoelastic wave effects where rod has mass.

62. J. C. Burgess, "Distributed Resilient Media for Shock and Vibration Isolation," WADD, Tech. Rept. 60-671, Oct. 1960
Uses mechanical impedance to determine complex moduli for a number of materials. Discusses possible materials to use and suggests that only foam materials offer significant promise.

63. W. P. Fletcher and J. R. Schofield, *J. Sci. Instr.*, **21** (11), 193 (Nov. 1944)
Covers variation between 0 and 40°C of dynamic moduli of a number of elastomers.

64. E. J. Cook, J. A. Lee, and E. R. Fitzgerald, "Dynamic Mechanical Properties of Materials for Noise and Vibration Control," Chesapeake Instruments Corp, Rept. 187, July 1962

Complex shear compliances of a number of materials from 5 to 5000 cps. Materials primarily usable for structural damping.

65. G. W. Painter, "Dynamic Properties of BTR Elastomer," SAE Nat'l Aeronautic Meeting, Los Angeles, Paper 83B, Oct. 1958
    Dynamic shear moduli for BTR elastomer at large and small strains.
66. G. W. Painter, *Trans. Am. Soc. Mech. Engrs.*, **76** (7), 1131 (1954)
    Shear moduli for a silicone rubber determined and compared with a conventional rubber formulation typically used in vibration-isolation mounts.
67. W. G. Soper and R. C. Dove, *J. Appl. Mech.*, **262** (June 1963)
    Uses principle of similitude to arrive at functional equations for the behavior of cushions. General theory for any arbitrary cushion and a simplified theory applicable to many practical problems. A basic contribution to cushion design. See also Ref. 33.
68. H. N. Abramson, "Non-Linear Vibration," Ch. 4 in *Shock and Vibration Handbook* (C. M. Harris and C. E. Crede, eds.) McGraw-Hill, New York, 1961
    Covers in brief form the problem of oscillations of nonlinear systems.
69. J. J. Stoker, *Non-Linear Vibrations in Mechanical and Electrical Systems*, Interscience, New York, 1950
    Text covering basic theory with many examples.
70. N. Minorsky, *Introduction to Non-Linear Mechanics*, Edwards Brothers, Ann Arbor, 1947
    An excellent basic text.
71. N. W. McLachlan, *Ordinary Non-Linear Differential Equations*, Oxford Univ. Press, 1956
    Most of the more frequently encountered nonlinear differential equations are discussed and solved here.
72. A. Levy and E. A. Baggott, *Numerical Solutions of Differential Equations*, Dover, New York, 1950
    How to go about solving difficult differential equations.
73. N. Kryloff and N. Bogoliuboff, *Introduction to Non-Linear Mechanics*, Princeton Univ. Press, Princeton, 1943
    Contains one of the classical methods for attacking nonlinear differential equations.
74. A. A. Andronow and C. E. Chaikin, *Theory of Oscillations*, Princeton Univ. Press, Princeton, 1949
    A good reference work on nonlinear oscillations.
75. Y. H. Ku, *Analysis and Control of Non-Linear Systems*, Ronald Press, New York, 1958
    Uses phase-plane-integration procedures to analyze control systems.
76. A. W. Nolle, *J. Polymer Sci.*, **5** (1), 1 (1950)
    The classic paper on the temperature- and frequency-dependence of the dynamic moduli of rubberlike materials. Compounds investigated were natural rubber, Buna N, Butyl, Neoprene, and GR-S. Among the salient features are the use of a number of different test techniques to arrive at broad frequency and temperature coverage. So far as is known, the first to draw a three-dimensional map of elastomeric behavior.

77. A. V. Tobolsky, "Stress Relaxation Studies of the Viscoelastic Properties of Polymers," Ch. 5 in Vol. 2 of *Rheology, Theory and Applications* (F. R. Eirich, ed.) Academic Press, New York, 1958
Clear account of how stress-relaxation experimental results can be used to predict the dynamic behavior of polymers.

78. R. A. DiTaranto, "A Short Survey of Viscoelastic Theory," Marine Engineering Lab. Sponsored Rept. 37/66, Jan. 1966
An exposition of some fundamental concepts in viscoelasticity. Particularly clear on the principle of time and temperature superposition.

79. J. D. Ferry, L. D. Grandine, Jr., and E. R. Fitzgerald, *J. Appl. Phys.*, **24**, 911 (1953)
Uses time and temperature superposition to compute master curves for the shear compliance of NBS polyisobutylene. The results form a compelling argument for further use of the technique with cushions.

80. M. L. Williams, R. F. Landel, and J. D. Ferry, *J. Am. Chem. Soc.*, **77**, 3701 (1955)
Develops an empirical equation for the time- and temperature-superposition shift factor as a function of the test temperature and the glass temperature of the polymer; seems universally valid for rheologically simple polymers. Equation reported as valid from T_g to $T_g + 100°C$.

81. A. V. Tobolsky, "Viscoelasticity of Amorphous Solids and Polymers," Frick Chem. Lab., Princeton Univ., Rept. RLT-91, Nov 1965
A summary report of current research on the behavior of relaxation times of certain polymers. Defines characteristic relaxation time.

82. A. V. Tobolsky, *J. Am. Chem. Soc.*, **74**, 3786 (1952)
Presents an idealized distribution of relaxation times, $H(\log \tau)$, which permits exact mathematical expressions for computing relaxation and dynamic moduli.

83. J. D. Ferry, E. R. Fitzgerald, L. D. Grandine, Jr., and M. L. Williams, *Ind. Eng. Chem.*, **44**, 703 (1952)
Quite accurate methods of determining $H(\log \tau)$ from experimentally obtained values of the relaxation modulus, using first- and second-order approximations.

84. A. V. Tobolsky and E. Catsiff, *J. Polymer Sci.*, **19**, 111 (1956)
Contains tabulations of $H(\log \tau)$ at 298°K as a function of $\log \tau$. Also shows computational methods similar to those in Ref. 83.

85. A. V. Tobolsky and H. Eyring, *J. Chem. Phys.*, **11**, 125 (1943)
Formulas relating distribution of relaxation times to the complex moduli.

86. E. Catsiff and A. V. Tobolsky, *J. Colloid Sci.*, **10**, 375 (1955)
Computations and tabulations of complex moduli from stress relaxation data.

87. J. D. Ferry, "Experimental Techniques for Rheological Measurements on Viscoelastic Bodies," Ch. 11 in Vol. 2 of *Rheology, Theory, and Applications* (F. R. Eirich, ed.) Academic Press, New York, 1958
Gives plotting variables for use in constructing master curves of viscoelastic behavior.

88. W. A. Volz, "Analytical Considerations in the Design of a Polyurethane Foam Shock Mount for Polaris," *Shock and Vibration Bull. No. 31*, Pt. 2, 265 (1963)
Brief description of some of the considerations in engineering a high-performance, reliable foam-shock-isolation system.

89. W. A. Volz, "Application of Polyurethane Foam to the Shock Isolation of Large Silo Based Missiles," *Shock and Vibration Bull. No.36*, Pt. 2, (1967)
Detailed analytical end experimental results with a new model of the behavior of polyurethane foam. An excellent contribution.

90. A. N. Gent and A. G. Thomas, "Mechanics of Foamed Elastomeric Materials," Proc. of Conference on Foamed Plastics, Washington, D.C., April 22-23, 1963
Basic analysis of foam structural behavior in terms of the foam characteristics and polymer characteristics. Basic to understanding of cushion behavior.

91. B. H. Venning, "Analog Models of Viscoelastic Materials," Proc. of Conference on Standardization of Packaging Dynamics, Ministry of Aviation, London, Paper 6, May 21-22, 1964
Measures complex moduli and derives elastic constants for a polyurethane foam at small excursions. One of only three studies (Burgess and Volz being the others) wherein viscoelastic properties are used to analyze cushion behavior.

92. B. H. Venning and J. Guttridge, "A Theoretical Approach to the Analysis of Package Cushioning Problems," Proc. Symp. on Dynamics of Package Cushioning, Royal Radar Establishment, Malvern, England, April 27-28, 1960
Preliminary discussion of analog computer use in analyzing behavior of package cushions.

93. B. H. Venning and J. Guttridge, *Br. J. Appl. Phys.*, **12**, 621 (1961)
Description of analog computer with cushion providing appropriate force data for analysis and results of preliminary test runs.

94. W. W. Soroka, "Analog Methods of Analysis," Ch. 29 in *Shock and Vibration Handbook* (C. M. Harris and C. E. Crede, eds.) McGraw-Hill, New York, 1961
Specific methods for setting up analog circuits to analyze specific mechanical models.

95. D. B. Osborn, personal interview, April 22, 1966
Overall discussion, includes development of new package-testing devices and British practice as it is influenced by materials availability and production quantity.

96. R. S. Jacobsen, "Shock Pulse Computer," Sandia Corp., Rept. SCL-DC-66-2, April 1966
Contains a very handy slide rule for computing parameters of various kinds of shock pulses.

97. R. D. Mindlin, *Bell Sys. Tech. J.*, **24**, 353 (July-October 1945) (also Bell System Monograph B-1369)
The classic example of the scientific approach to isolation of shock and vibration under velocity-change conditions. One of the basic references in shock and vibration theory.

98. F. Postlethwaite, "The Design of Spring Suspension Instrument Packing Cases," M.O.S., R.A.E. Tech. Note No. Inst 904, 1945
Early use of tension spring design for shock and vibration isolation in packaging. Mainly of historical interest.

99. F. Postlethwaite, *Engineering*, **158**, 321 (Oct. 1944)
Essentially same ideas as in previous reference.

100. H. E. Malmstrom and J. T. Gresham, "Dynamic Measurements of Cushioning," Kimberly Clark Corp., Neenah, Wis., Rept., Dec. 1945
Early efforts at determining properties of cushioning materials.

101. L. Lassen, K. Q. Kellicutt and W. J. Sanderson, "Properties of Cushioning Materials," Forest Products Lab., Rept. R-1489, June 1945
Primarily static data on a number of materials, but states dynamic data about to be collected. Static curves clearly show hysteresis effects.

102. H. H. Berk, *Modern Packaging*, **20** (2 and 3) (Oct.-Nov. 1946)
Two-part article on practical factors affecting cushion material selection. Few numerical data.

103. R. A. L. Cole, *Elec. Comm.*, **23** (3), 320 (Sept. 1946)
Early paper, with practical examples, on tension-spring crates for large transmitting tubes.

104. R. F. Ettinger, "Wool Felt Used as a Cushioning Material in Packaging," Wayne Univ., Detroit, Joint Ind. Conf. on Cushioning in Packing, Dec. 7-8, 1953
General properties of wool felts for packing. No design data.

105. D. J. Gasch, "Cushioning Properties of Wood Excelsior," Wayne Univ., Detroit, Joint Ind. Conf. on Cushioning in Packing, Dec. 7-8, 1953
Static stress-strain curves on wood excelsior, and an improved version called Curlex.

106. R. E. Jones, "Demonstration of Principles of Package Cushioning," Wayne Univ., Detroit, Joint Ind. Conf. on Cushioning in Packing, Dec. 7-8, 1953
Tutorial paper on basic principles of package cushioning. Elementary but very clear and covers essential points of shock isolation.

107. R. E. Jones and D. L. Hunzicker, "Calculating Cushion Thickness by Analysis of Stress Strain Curves," WADC, Tech. Rept. 53-334, Jan. 1954
Static stress-strain curves and energy-per-unit-volume curves for some 53 different materials. Also shows curves obtained with 10th loading compared with first loading. For this latter, it is still an excellent reference; at the time of publication, a very valuable contribution.

108. K. Q. Kellicutt, "Application of the Properties of Cushioning Materials in the Design of Cushioning," Forest Products Lab., Rept. R1627, Sept. 1946
Uses data from Ref. 101 to plot curves of constant energy level on coordinates of dynamic stress *vs* thickness for specific materials (isoenergy curves). Postulates a design technique based on these curves.

109. E. O. Lieberg, "Tufflex-Cellulose Fiber Felt," Wayne Univ., Detroit, Joint Ind. Conf. on Cushioning in Packing, Dec. 7-8, 1953

General properties plus static stress-strain curves for several material densities.

110. E. O. Lieberg, "Wood Fiber Felts for Protective Packaging," Forest Products Research Soc., Memphis, Tenn., 7th National Meeting, June 1953
Static stress-strain data, curve of apparent density of material *vs* recovery after 2/3 compression, and recovery after repeated impact loads.

111. M. Masel, *Modern Packaging*, **26** (9), 133 (May 1953)
Derives simple mathematics of behavior of cushioning materials. Has some data on effects of precompression and of cushion on top of object as well as on its bottom.

112. I. McNamee, "Space and Natural Frequency Requirements of Some Shock and Vibration Isolators," NBS Corona, Rept. 1243, Jan. 1954
Extends Mindlin by including effects of acceleration of gravity.

113. G. S. Mustin, "Use of the Energy Method in the Design of Package Cushions," Wayne Univ., Detroit, Joint Ind. Conf. on Cushioning in Packing, Dec. 7-8, 1953
Early attempt to use cushion-energy methods in the case of the rotational drop test. In the light of present knowledge, the attempt failed.

114. G. S. Mustin, "An Introduction to Shock and Vibration for Package Designers," Wayne Univ., Detroit, Joint Ind. Conf. on Cushioning in Packing, Dec. 7-8, 1953
A completely tutorial lecture on fundamentals of shock and vibration isolation. Stresses item response.

115. S. J. Ruffini, "Packing Design Parameters for Fragile Items Using Nonlinear Cushioning Materials," Picatinny Arsenal, Feltman Res. and Eng. Labs., Tech. Note, June 31, 1959
Uses tangent-elasticity function as a basis for design. Several practical design examples. Static curves for several materials, identified by code.

116. F. Stowell, H. C. Pusey, and K. N. Carr, *Flow*, p. 136 (Oct. 1954)
A tutorial-type paper emphasizing some of the basic engineering principles of package cushioning.

117. A. M. Underhill, *Modern Packaging*, **19** (12), 141 (Aug. 1946)
Short basic discussion of some of the general principles of package cushioning.

118. A. M. Underhill, *Basic Principles of Package Cushioning, Packaging Series No. 33*, American Management Assoc., New York, 1950
Ref. 117 expanded and brought up to date.

119. J. L. Gretz, *Modern Packaging*, **25** (8), 129 (April 1952)
Introduces concept of cushion efficiency as a means of optimizing a design.

120. J. L. Gretz, *Flow*, **7** (7), 100 (April 1952)
Essentially same information as in Ref. 119.

121. J. L. Gretz, *Principles of Cushioning*, Proc. of Short Course, Soc. Ind. Packaging and Mat. Hand. Engs., Boston, Oct. 1953
Essentially same information as in Ref. 119.

122. R. R. Janssen, "A Method for the Proper Selection of a Package Cushion Material and Its Dimensions," North American Aviation Rept. NA-51-1004, 1952
First development of concept of optimum cushion factors. A basic and fundamental idea unfortunately marred by the very elementary derivations used. However, still a basic reference.

123. R. R. Janssen, *SIPMHE Short Course*, Chicago, Oct. 1952
First exposure of Ref. 122 to the general public. Same contents.

124. R. R. Janssen, *Packaging Review*, **73** (79), 38 (March 1953)
Same information as in Ref. 122.

125. H. Himelblau, "A Comparison of Methods for Determining Dynamic Optimum Cushion Factors of Distributed Cushioning Materials," North American Aviation, Rept. NA-54-740, Dec. 1954
A discussion of various possible test procedures for obtaining dynamic properties of cushions.

126. J. A. Hoffman, *Package Eng.*, **4** (3), 27 (March 1959) and (4) 48 (April 1959)
Quasi-technical discussion of various curves used in package design. Includes an elementary method of estimating fragility from the existing package.

127. R. E. Jones and W. L. James, "Simplified Methods of Selecting and Designing Package Cushioning Materials," Forest Products Lab., Rept. 2031, April 1955
Uses curves derived from static stress-strain curves to arrive at design recommendations with various cushioning materials.

128. R. E. Jones and W. L. James, *Modern Packaging*, **29** (6), 137 (Feb. 1956)
Same information as in Ref. 127.

129. R. E. Jones and W. L. James, Ch. 9, Sections I, IIa and IIb in *Fundamentals of Guided Missile Packaging* (E. Klein, ed.), RD219/3, Office of the Assistant Secretary of Defense, Research and Development, Washington, July 1955
Same information as in Ref. 127.

130. R. B. Orensteen, "The Selection of Cushion Area in the Design of Package Cushioning," WADC, Tech. Rept. 53-43, March 1953
Uses static data and Janssen's procedure to discuss thickness determination and techniques of area selection for minimum container cubage.

131. R. B. Orensteen, "Techniques for the Design of Glass Fiber Cushioning," WADC, Tech. Rept. 53-68, Oct. 1953
Static data on several densities of glass fiber cushioning. Uses Janssen's procedure.

132. R. B. Orensteen, "The Design of Reclaimed Latex Foam Cushioning," WADC, Tech. Rept. 53-132, Jan. 1954
Static data on a number of different densities of reclaimed latex foam. Offers a tentative method for selecting not only thickness and area but also density, for use. Basically, Janssen's procedure.

133. R. E. Slaughter, *Comparison of Cushioning Materials*, The Stearns and Foster Co., Cincinnatti, undated

Discusses in elementary terms efficiency and cushion factor. His cushion factor is inverse of Janssen's but has same ingredients.

134. J. C. Snowdon, *Noise Control*, 5 (5), 32 (Sept. 1959)
General discussion of Mindlin, Janssen, and Hardigg. Has a number of static J-stress curves for polystyrene and polyurethane foams.

135. G. S. Mustin, *Shock and Vibration Bull. No. 28*, Pt. 4, 79 (Aug. 1960)
Discusses a simplified approach to designing shock-isolation systems for the rotational drop test. Discusses thickness determination for tangent elasticity.

136. S. Yurenka and C. R. Giacobine, "The Selection of Package Cushion Dimensions Based on Optimum Cushion Factors," Douglas Aircraft Co. Testing Div., Rept. Dev-2128, July 1956
Applies Janssen's principles to tangent, algebraic, and logarithmic elasticities and shows connection with Mindlin's approach. Some discussion of precompression.

137. J. S. Hardigg, "The Development of a Cushioning Nomogram," Container Labs., Inc., Rept. NOrd 13882, Feb. 9, 1954
Using static data and plotting stress/optimum stress *vs* strain/optimum strain, finds a master curve for a number of classes of cushioning material characterized by smooth stiffening.

138. J. S. Hardigg, *Modern Packaging*, 27 (12), 124 (Aug. 1954)
Same information as in Ref. 137.

139. J. S. Hardigg, *Flow*, 9, 110 (Aug. 1954)
Same information as in Ref. 137.

140. T. P. Wharton, *Flow*, 12 (11), 106 (Aug. 1957), and 12 (12), 110 (Sept. 1957)
Part 1 is a popularized explanation of Hardigg's nomogram. Part 2 goes into secondary factors such as creep in popular terms.

141. D. D. Hermansen, R. E. Evans, and G. S. Mustin, "Preliminary Study of Shock and Vibration Isolation Characteristics of Some Rubberized Hairs," Douglas Aircraft Co. Testing Div., Rept. Dev-3125, Feb. 1960
Fourteen densities of molded rubberized hair from two different sources combined into a single design curve using Hardigg's technique and static data. Some correlation between density and "stiffness".

142. W. G. Humbert and R. G. Hanlon, Package Engineering (April 1962)
Acceleration *versus* static-stress curves for polyethylene foam.

143. C. H. Abner, "Determination of Static Creep and Dynamic Properties of Materials Used as Package Cushioning," Northrop Aircraft, Inc., Rept. NAI-58-70, Feb. 1, 1958
Discusses acceleration *versus* static stress for a number of materials. Only one creep curve.

144. H. C. Blake, III, "Acceleration-Stress Properties of Selected Cushioning Materials," Michigan State Univ., School of Packaging, Project I, Tech. Rept. 1, Jan. 1, 1962
Acceleration static-stress curves for some polyurethanes and rubberized hairs at 30-in. drop height.

145. H. C. Blake, III, "Acceleration-Stress Properties of Additional Selected Cushioning Materials," Michigan State Univ., School of Packaging, Project I, Supplement to Tech. Rept. 1, April 1, 1962
Bonded hair and reclaimed polyurethane foams at 30-in. drop height.

146. H. C. Blake, III, "Peak Deceleration-Static Stress Curves for Selected Cushioning Materials," Michigan State Univ., School of Packaging, Project I, Tech. Rept. 4, July 10, 1964
Covers some polyurethane foams, reclaimed foams, expanded polystyrenes and wood-wool felts with various backings at 30-in. drop height.

147. H. C. Blake, III, "24" Drop Height Peak Deceleration-Static Stress Curves for Selected Cushioning Materials," Michigan State Univ., School of Packaging, Project I, Tech. Rept. 5, Nov. 1, 1964
Twenty-four-inch drop-height data for materials covered in Refs. 144, 145, 146, plus a neoprene foam.

148. MIL-HDBK-304, *Package Cushioning Design Handbook,* Defense Supply Agency, Washington, Nov. 25, 1964
A comprehensive review of various methods of designing package cushions with strong preference for acceleration-static stress approach. Data covering some 16 different materials typical of those available in U.S. A valuable first step but now needs revision.

149. E. A. Falkner, *Packaging Review,* **82** (4), 46 (April 1962)
Thorough coverage of packaging uses of rubberized hair. Develops a nomogram for this material.

150. General Electric Co., Light Military Electronics Dept., Cushioning Material Study Program, Report to Feltman Research and Engineering Labs., 1959
Static and dynamic test results on rubberized hairs, rubberized cocoa fiber, polyurethane foams, Tufflex, Fiberglas, Kimpak, and Sponge Rubber. Dynamic data presented as peak acceleration *versus* drop height.

151. M. E. Gigliotti, *Modern Packaging,* **34** (1), 148 (Sept. 1960)
A descriptive paper discussing work at Picatinny Arsenal in package cushioning. Advances argument for testing cushions in a confined state.

152. M. E. Gigliotti, "Design Criteria for Plastic Package-Cushioning Materials," PLASTEC, Picatinny Arsenal, Plastics Tech. Evaluation Center, Dover, N.J., Rept. 4, Dec. 4, 1961
Dynamic data on a number of plastic foams including polyurethanes, polystyrenes, polyethylenes, and some vinyls. Some discussion of uses of rigid and semi-rigid foams in packaging. Reviews testing programs and procedures. Excellent bibliography.

153. T. J. Grabowski, *Modern Packaging,* **33** (12), 119 (Aug. 1960)
Discussion of packaging uses of resilient foamed polystyrene. Some low temperature static data.

154. T. J. Grabowski, *Shock and Vibration Bull. No. 30,* Pt. 3, 76 (Feb. 1962)
Acceleration-static stress data on resilient polystyrene foam plus extensive tests in various containers to compare effects.

155. G. A. Gordon, "Evaluation of Cushioning Properties," Paper No. 2, Proc. of Symposium on Dynamics of Package Cushioning, Royal Radar Establishment, Malvern, England, April 27-28, 1960

Dynamic tests on latex foam, open-celled rubber, cellular neoprene, polyester urethane, closed-cell rubbers, molded wood wool, and rubberized hair. Some dynamic drift data and qualitative observations on creep.

156. G. A. Gordon and E. E. Wheeler, "Evaluation of Cushioning Material Properties, Part I," Preliminary Report, Printing, Packaging and Allied Trades Research Assoc. (PATRA), Rept. 21, Aug. 1961

Complete data upon which Ref. 155 was based.

157. R. G. Hanlon, *Modern Packaging*, **35** (10), 158 (June 1962)

Review of G *versus* static-stress argument. Some data on polyethylene foam, polystyrene foam, and Pelaspan 8.

158. J. S. Hardigg and G. C. Thomas, Modern Materials Handling (April 1959)

Popular-type article reducing some of the complexities of shock isolation theory to everyday, practical terms.

159. J. S. Hardigg, Industrial Packaging (December 1960, January-June 1961)

Five-part article dealing with some of the fundamentals of package cushioning. Uses approach: J *versus* energy per unit volume. Some data on air, rubberized hair, polyurethane foam, polyethylene foam, polystyrene foam, the Hardi-Pad, and the Hardigg Air Cushion.

160. M. T. Hatae and P. E. Franklin, "Optimum Cushioning Properties of Packaging Cushioning Materials," North American Aviation Missile Div., Rept. AL-2478, May 15, 1957

Describes NAA tester. Static data on 17 materials. Dynamic data on 9 materials. Many of these latter data are repeated in Ref. 161.

161. P. E. Franklin and M. T. Hatae, "Packaging Design," Ch. 41 in *Shock and Vibration Handbook* (C. M. Harris and C. E. Crede, eds.) McGraw-Hill, New York, 1961

Excellent review, as of 1961, of the state of the art in package cushioning.

162. P. E. Jockle, Jr., and L. T. Wilson, Materials Handling Engineering, 8 (1), 92 (Oct. 1958) and 8 (2), 96 (Nov. 1958)

Materials covered are modified and regular PVC, natural rubber, latex foam, vinyl, polyurethane, cellulose, glass fiber, felt and bound hair. Evaluations included static compression and shear, creep, and a limited number of dynamic tests at vibration and natural frequency, and some physical and chemical properties. A very thorough two-part paper.

163. S. M. Krakover and A. Olevitch, "Investigation of Design Criteria for Cushioning Materials," WADC, Tech. Rept. WADC-TR-58-639, Nov. 1958

Discusses with examples how to design with cushioning materials. Opts for acceleration-static stress. Also discusses static data and creep plus economic factors.

164. North American Aviation, Design Specifications Group, "Properties of Latex Hair Package Cushioning Material for Shock and Vibration Protection," Rept. AL-2609, Sept. 9, 1957
Acceleration static stress. Transmissibility from 2 cps to 200 cps. Some creep data and some testing at -50°F.

165. R. K. Stern, "The Cushion Factor Stress Curve and its Value for Classifying and Selecting Package Cushioning Materials," WADC, Tech. Rept. 58-233, Nov. 1958
Shows that single curve for cushion factor *versus* stress cannot be drawn for most materials.

166. R. K. Stern, *Modern Packaging*, **33** (4), 138 (Dec. 1959)
Much the same information as in Ref. 165.

167. R. K. Stern, "Recent American Developments in Package Cushioning," Paper No. 10, Proc. of Symposium on Package Cushioning Dynamics, Royal Radar Establishment, Malvern, England, April 27-28, 1960
Discussion of the development of dynamic testing procedures for cushioning. Some comparative dynamic data on unidentified materials.

168. R. K. Stern, *Shock and Vibration Bull. No. 30*, Pt. 3, 57 (Feb. 1962)
Tutorial lecture on trends in package-cushioning studies and design techniques. Contains an argument for acceleration/static-stress curves and some illustrative dynamic data, including effects of containers.

169. L. T. Wilson, *Shock and Vibration Bull. No. 25*, Pt. 2, 324 (Dec. 1957)
Static stress-strain curves for various materials, some transmissibility data. Drop-test data presented as energy per unit volume *versus* acceleration and strain.

170. L. T. Wilson, "Resilient Cushioning Materials," Sandia Corp. Tech. Memo 35-59(12), Feb. 1959
Properties of some 27 different materials. See Ref. 162.

171. G. S. Mustin, *Shock and Vibration Bull. No. 35*, Pt. 5, 193 (Feb. 1966)
Takes 16 materials from Ref. 48 and other sources. Finds, for the optimum points, a linear relation between peak acceleration, drop height, and thickness. For optimum static stress, a logarithmic relation between optimum static stress and acceleration, drop height, and thickness was discovered. Paper also discusses some of the limitations on the validity of the design technique suggested.

172. L. J. Van Der Toorn, Bibliography, "Shock and Vibration Absorption in Packaging (Cushioning)," Technisch Documentie En Informatie Centrum, The Hague, Nov. 1961
A very complete, thoroughly annotated bibliography of the package-cushioning literature through 1961. Abstracts are usually in the language of the country of origin. A very useful document.

173. J. W. Pendered, "An Historical Survey of the Literature Relating to Theoretical Aspects of Packaging Dynamics," Univ. College, London, Dept. of Mech. Engineering, Rept. 65/1, April 1965
A recent review of what is considered significant progress in the field since Mindlin's original paper. Implies, guardedly, that progress could have been greater.

174. E. N. Sabbagh, "Performance Characteristic of Cushioning Materials Impacted Under a Heavy Weight High Impact Shock Machine," WADC, Tech. Rept. 55-229, Feb. 1956

Proves that many conventional package-cushioning materials are not suitable for high-energy absorption problems. At the strain rates investigated, did not find that the materials investigated were strain-rate-sensitive. In the light of present knowledge, results not surprising.

175. S. M. Birnbaum, *Shock and Vibration Bull. No. 16,* 100 (Oct. 1950)

Notes an apparent set of exponential relationships for thickness, stress, and drop conditions. Ingredients of significant variable unfortunately not pursued. Compare with Ref. 171.

176. "Code of Practice for the Cushioning of Fragile Supplies, BD/45/09," Ministry of Aviation, Central Packaging Section, Cambridge Terrace, London, Sept. 1965

A simplified approach to package-cushioning design selection. Much of the more difficult mathematics has been reduced to reasonably simple graphs.

177. H. C. Blake, III, "A Cushion Design Method and Static Stress-Peak Deceleration Curves for Selected Cushioning Materials," Michigan State Univ., School of Packaging, Proj. I, Tech Rept. 2, Mar. 25, 1963

A design procedure, starting with projected area of object to be cushioned. Takes materials discussed in Refs. 144 and 145, and develops sets of design curves.

178. "Package Cushioning Materials," ASTM Specification D1372-55T, Am. Soc. for Testing and Materials, 1955

The procedural specification for determining significant dynamic properties of cushioning material.

179. G. Zell, "Vibration Testing of Resilient Package Cushioning Materials," Picatinny Arsenal, Tech. Rept. 3160, Aug. 1964

Thorough report on vibration behavior of three densities of polystyrene foam and polyether urethane. Test syllabus severe. Optimum shock static stress for some materials sometime produces poor vibration performance.

180. A. B. Burns, "Guide for the Selection and Application of Shock Mounts for Shipboard Equipment," American Machine and Foundry Co., Greenwich Engineering Div., Rept. to Bureau of Ships, Sept. 1, 1961

Excellent design engineer's *vade mecum* for shock mounts. Couched in simple language but contains many elegant solutions to common problems. An excellent work.

181. A. R. Payne and A. B. Davey, "Rubber in Engineering Practice," Maclarens and Palmerton, London, 1965

A basic text on rubber in shock and vibration isolation. Contains a chapter on the general problems of packaging.

182. H. C. Blake, III, "Some Package Drop Tests Utilizing the Package Cushion Design Method," Michigan State Univ., School of Packaging, Proj. I, Tech. Rept. No. 8, Feb. 15, 1965

Shows increase over predicted values resulting from cushion pad tightly fitting outer container. Direct comparison is made to packs with a loose-fitting cushion.

183. S. C. Schuler, *J. Roy. Aeronaut. Soc.*, 55 (7), 335 (May 1957)
General discussion of packaging problems. Contains a set of dynamic stress-strain curves for 5.75-pcf rubberized hair.

184. D. N. Keast and J. J. Baruch, "Effects of Simulated Space Environments of Cushioning Materials," WADC, Tech. Rept. 58-667, June 1959
Materials: glass fiber, rubberized hair, polyurethane foam, silicone rubber foam, and paper honeycomb. Static and dynamic stress-strain curves and transmissibilities at 75°F, −65°F and −200°F at ambient pressures and at 10^{-4} mm Hg. Definitely shows effects of air in some of the materials.

185. S. M. Goldberg, "Development of Configurations and Combinations of Polyurethane Foam to Produce Maximum Efficiency in Package Cushioning Materials," First Quarterly Progress Rept. to BuWeps, April 28, 1965
Improvement in dynamic performance through hole-cutting, laminating, egg-crating and preworking. An interesting approach to improving and standardizing the behavior of the material.

186. S. M. Goldberg, "Development of Configurations and Combinations of Polyurethane Foam to Produce Maximum Efficiency in Package Cushioning Materials," Second Quarterly Progress Rept. to BuWeps, August 4, 1965
Continues work of Ref. 185.

187. G. J. Mouri, "Development of Configurations and Combinations of Polyurethane Foam to Produce Maximum Efficiency in Package Cushioning Materials," Third Quarterly Progress Rept. to BuWeps
Continues Goldberg's work with different hole configurations, special shapes and some low temperature considerations.

188. W. Schmidt and J. Hoffmann, *Verpackungs Rundschau, Technical and Scientific Suppl.*, 16 (2), 9 (Feb. 1965)
Masterful exposition of packaging properties of a large number of resilient, semi-rigid and rigid polyurethane foams. Contains dynamic stress data, dynamic drift for semi-rigid and rigid foams, and recommendations on static loading for acceptable creep performance.

189. H. J. Hohmann, J. Penzkofer and R. Heiss, *Verpackungs Rundschau, Technical and Scientific Suppl.*, 16 (4), 25 (April 1965)
Evaluates shock-absorbing characteristics of materials as actually used in packages, compared with flat-pad design data. Shows definite change resulting from presence of side pads. Has a persuasive argument for shock-spectrum approach to cushion design.

190. D. C. Allen, *Packaging News*, 9 (4), 34 (April 1962)
Looks at effects of side friction on performance of cushioned packs. Side pads increase peak acceleration seen by contents.

191. K. S. Pearsons and E. E. Ungar, "Development of Packaging Material with Constant Restoring Force," WADD, Tech. Rept. 60-573, Dec. 1960
Develops a mount with collapsing foam columns and buckled linkages. Mount can be fabricated on a "do-it-yourself" basis.

192. R. H. Jacobsen, "New Medium for the Protection of Electronic Equipment Against Shock and Vibration," WADC, Tech. Rept. 57-530, April 1958

A silicone rubber matrix filled with alternating layers of Teflon rods.

193. A. R. Payne, "Design of Shock Absorption Mat of Solid Rubber," Paper No. 9, Proc. of Symposium on Dynamics of Package Cushioning, Royal Radar Establishment, Malvern, England, April 26-27, 1960

A corrugated mat of rubber with a collapsing-column effect. Excellent performance predicted on the basis of static data.

194. J. K. Bache, "The Development of a Torsion Bar Cushion Unit," Paper 11, Proc. of Symposium on Package Cushioning Dynamics, Royal Radar Establishment, Malvern, England, April 26-27, 1960

A device, useful for heavy loads, using torsion springs and friction. Popular in U.K. where cushioning materials and rubber mounts can be expensive.

195. L. W. Gammell and J. L. Gretz, "Effect of Drop Test Orientation on Impact Accelerations," Physical Test Lab., Texfoam Div., B. F. Goodrich Sponge Products Div., Shelton, Conn., 1955

Evaluation of the effects of the angle of impact on measured peak accelerations in packages.

196. D. M. Chase and I. Vigness, "Dynamics of Package Cushioning Involving Combined Rotations and Translations," Naval Research Lab., Rept. 4719, March 1956

Describes the behavior of a rigid article flexibly mounted in a rigid container. Equations apply for any type of elastic system, but no damping has been assumed. Useful solutions can be obtained by means of specific elasticity functions, or with a computer.

197. R. S. Ayre and J. I. Abrams, "Linear Theory of Vibration of an Elastically Supported Rigid Body Within a Container," Ch. 11 in *Fundamentals of Guided Missile Packaging* (E. Klein, ed.), RD219/3, Office of the Assistant Secretary of Defense, Research and Development, Washington, July 1955

A complete set of equations, with varying degrees of mounting symmetry, and solutions for linear springs in containers undergoing translational and rotational motions.

198. R. E. Blake, "Basic Vibration Theory," Ch. 2 in *Shock and Vibration Handbook* (C. M. Harris and C. E. Crede, eds.), McGraw-Hill, New York, 1961

Complete set of equations of motion, and some solutions for vibration problems involving rigid bodies. An excellent refresher.

199. J. J. Goodill, "Flexible Suspension Systems for Equipment in Transit," SAE Golden Anniversary Aeronautic Meeting, New York, April 18-21, 1955

A review of successful designs with mounts and a detailed design procedure. Some of this procedure is reproduced in Chapter 8 of RD219/3 (see Ref. 129)

200. R. S. Ayre and J. I. Abrams, *Shock and Vibration Bull. No. 23*, 35 (July 1956)

Extends the analysis of Ref. 197 to cubic elasticity, thus making

allowance for nonlinear mountings. Absence of damping forces assumed.

201. E. Y. W. Tsui and P. Stern, *Shock and Vibration Bull. No. 30*, Pt. 3, 194 (April 1962)
An excellent approach to the problem of rotational drop using nonlinear mounts with damping. Requires knowledge of energy absorption characteristics of the isolator.

202. J. N. Thompson and E. A. Ripperger, *Shock and Vibration Bull. No. 30*, Pt. 3, 261 (Feb. 1962)
A review to date of the work being done at the University of Texas on problems of cushioning for aerial delivery.

203. A. C. Browning, "A Theoretical Approach to Air Bag Shock Absorbers," R.A.E., Tech. Note Mech. Eng. 369, Feb. 1963
A complete theoretical review of the design procedures for air bag shock absorbers.

204. H. Matlock and J. N. Thompson, "Preliminary Tests on a Nonpressurized Air Bag, Cushioning for Aerial Delivery, Part III," Texas Univ., Structural Mechanics Research Lab. (SMRL), Austin, Texas, Oct. 15, 1957
Preliminary tests on Hardigg's paper air bag with variable orifice which is opened by a light spring.

205. J. P. Den Hartog, D. E. Newland, and J. F. Flory, "Feasibility Study of Shock Isolating a Very Large Structure," Tech. Doc. Rept. AFWL TDR-64-20, Sept. 1964
Discusses pros and cons of springs and metal bellows for bottom support of very heavy missiles in silos. Gives design suggestions for bellows.

206. R. K. Stern, "An Evaluation of Popcorn as a Cushioning Material," WADC, Tech. Rept. WADC-TR-56-600, May 1957
Drop and other tests on packages with popcorn as a cushioning material. Has marginal utility, only, and some severe drawbacks.

207. Y. Dagel, *Verpackungs Rundschau, Technical and Scientific Supplement*, **13** (11), 85 (1962)
Derives a general expression for the stress-strain behavior of cushioning materials in the form of a polynomial of arbitrary order and with damping as a binomial. Particularly interesting for his derivation of the stress-strain law for corrugated fiberboard.

208. D. L. Anderson, "Buckling of Shallow Viscoelastic Arches," Stanford Univ., Div. of Mech. Engr., Tech. Rept. 155, Aug. 1955
An interesting approach but more concerned with "snap through" buckling than with the type encountered with corrugated fiberboard.

209. J. W. Goff, "The Damping Capacity of Corrugated Paperboard as a Function of Stress and Frequency," Michigan State Univ., Dept. of Forest Products, Doctoral Dissertation, 1957
Measures damping capacity of A-Flute semichemical medium with 42-42-lb kraft liners. Also reviews other work on damping capacity of wood and paper.

210. A. Ali, "Dynamic Stress Strain Characteristics of Various Materials, Cushioning for Air Drop, Part VII," Texas Univ., Structural Mechanics Research Lab. (SMRL), June 3, 1957

Dynamic stress-strain curves, at air-drop velocities, for a number of resilient and quasi-resilient materials.

211. K. R. Marvin and G. S. Page, Jr., *Package Engineering*, 8 (3), 48 (Feb. 1963)
Preliminary studies (using a rather crude test rig) of the cushioning properties of some flat pads of corrugated fiberboard.

212. J. H. Toulouse and P. J. Berens, ASTM Bull. No. 152, 77 (May 1948)
Uses technique of foot-falls to failure to evaluate probability of bottle breakage in cases with corrugated fiberboard partitions. Failure is penetration through half-board thickness.

213. A. C. Beardsell and J. J. Kipnees, *Package Engineering*, 3 (10), 34 (Oct. 1956), 3 (11), 38 (Nov. 1956), and 3 (12), 49 (Dec. 1956)
Uses foot-falls to breakage or to 500g to evaluate various container combinations for whiskey bottles. Final recommendations based on cost effectiveness grounds.

214. H. C. Blake, III, "Response of Some Shock Measuring Devices to Package Drop Test Shocks," Michigan State Univ., School of Packaging, Proj. I, Tech. Rept. 3, June 15, 1964
Evaluation of several commercially available peak-shock indicators. Also extensive data on multiple drops onto two layers of corrugated fiberboard.

215. H. C. Blake, III, "The Degradation of Corrugated Board Utilized in Package Drop Tests," Michigan State Univ., School of Packaging, Project I, Tech. Rept. 10, Sept. 1, 1965
Evaluation of gradual breakdown of protection afforded by multiple layers of corrugated fiberboard.

216. H. C. Blake, III, "The Energy Absorbing Properties of Selected Creased Corrugated Pads," Michigan State Univ., School of Packaging, Project I, Tech. Rept. 11, April 30, 1966
Two rat traps and one spring pad made of 200-lb A-Flute and 275-lb A-Flute subjected to repeated drops. Initial protection very good but failure rapid.

217. J. Drysdale, G. A. Gordon, E. E. Wheeler, and P. D. Marsden, *Packaging*, 34 (396, 399, and 400), (March, June, and July, 1963) (Memoir No. 6, Packaging Div., PATRA)
Extensive tests and evaluations of packaging uses of expanded polystyrene foams.

218. K. Mahler and D. Stockburger, *Neue Verpackung*, 16 (4) 372 (April 1963) and 16 (5), 576 (May 1963)
Part II has some specific data on polystyrene foams with a nomogram. Also constructs an equation for heat transfer through a cushion in storage.

219. Sinclair-Koppers Co., "Dylite Expandable Polystyrene—Principles of Packaging Design"
Dynamic data for three common densities of expanded polystyrene foam plus deflection and permanent-set data. Practical design hints for ribs and efficient molding.

220. A. Ali and L. R. Benson, "Bibliography of Literature Pertaining to the Absorption of Impact Energy, Cushioning for Air Drop, Part IX,"

Texas Univ., Structural Mechanics Research Lab. (SMRL), June 9, 1957

Annotated bibliography, with over 90 entries, pertaining to title subject and divided into theory, available materials, test facilities and test results.

221. J. N. Brennan, ed., "Bibliography on Shock and Shock Excited Vibrations, Vol. 1," College of Engineering and Architecture, University Park, Pa., *Engineering Research Bull. No. 68* (Aug. 15, 1957), and Vol. 2 Tech. Rept. No. 6, Jan. 15, 1958

Monumental annotated bibliography, with over 800 entries, covering the open literature in the subject field.

222. G. W. H. Stevens, *Shock and Vibration Bull. No. 30,* Pt. 3, 290 (Feb. 1962)

A general discussion of the U.K. approach to aerial delivery problems including discussion of design requirements and techniques.

223. G. E. Murray, "Basic Concepts on the Energy Dissipation of Cushioning Materials," Quartermaster Research and Engineering Center, Natick, Mass., April 1958

Discussion of the goals to be sought in a material development program for air-drop cushioning. Energy dissipated per unit volume, dynamic stress-strain, and resilience are defined as the most important material properties.

224. C. H. Karnes, J. W. Turnbow, E. A. Ripperger and J. N. Thompson, "High Velocity Impact Cushioning, Part V—Energy Absorption Capacity of Paper Honeycomb," Texas Univ., Structural Mechanics Research Lab., May 25, 1959

Extensive discussion of the behavior of several paper honeycombs.

225. H. Matlock, E. A. Ripperger, J. W. Turnbow and J. N. Thompson, *Shock and Vibration Bull. No. 25,* Pt. 2, 305 (Dec. 1957)

A condensation of Ref. 226.

226. H. Matlock, E. A. Ripperger, J. W. Turnbow and J. N. Thompson, "High Velocity Impact Cushioning, Part II—Energy Absorbing Materials and Systems," Texas Univ., Structural Mechanics Research Lab., Aug. 26, 1957

A complete review of the major energy-absorbing systems and materials tested to date.

227. E. F. Williams, *Package Engineering,* 1 (6), 7 (June 1956)

Semi-technical exposition of Quartermaster Corps experience in air drop to date. For honeycombs, the article states that initial dynamic spring rate is about double static. Curves show typical initial-pulse "spike."

228. E. A. Ripperger, "Impact Determinations," Texas Univ., Structural Mechanics Research Lab., Oct 26, 1962

Final summary report covering materials studies, models of response, vehicle behavior, and a design guide.

229. B. C. Ellis, E. A. Ripperger and J. N. Thompson, "Design of Cushioning Systems for Aerial Delivery," Texas Univ., Structural Mechanics Research Lab., Aug. 1961

Practical design guide to cushioning vehicles for aerial delivery. Contains some suggestions for control of vehicle design details to minimize damage.

230. M. P. Gionfriddo, *Shock and Vibration Bull. No. 30*, Pt. 3, 276 (Feb. 1962)
Much the same information as in Ref. 229.

231. C. V. David, *Shock and Vibration Bull. No. 35*, Pt. 5, 169 (Feb. 1966)
Behavior of an aluminum honeycomb at impact velocities of 600 to 900 fps. Shows smashing in addition to column collapse.

232. J. W. Turnbow and C. C. Steyer, "Cushioning for Air Drop, Part II, Air Drop Cost Analysis," Texas Univ., Structural Mechanics Research Lab., 1955
Development of a cost-analysis technique applicable to the complete system used in air drops.

233. J. W. Turnbow, "Cushioning for Air Drop, Part VII, Characteristics of Foamed Plastics Under Dynamic Loading," Texas Univ., Structural Mechanics Research Lab., 1957
Dynamic stress-strain data on a number of polystyrene plastic materials.

234. R. I. Carr, E. S. Perry, E. A. Ripperger and J. N. Thompson, "The Effects of Shape of Load Pulse on Shock Mitigating Characteristics of a Styrofoam Plastic," Texas Univ., Structural Mechanics Research Lab., July 1965
Both the pulse shape and the peak value of the acceleration pulse affect the shape of the response pulse.

235. R. Shield and C. Covington, "High Velocity Impact Cushioning Part VI, 108C and 100C Foamed Plastics," Texas Univ., Structural Mechanics Research Lab., Sept. 1960
Impact tests on some specially formulated polyurethane foams.

236. D. L. Daigle and J. O. Lonborg, "Evaluation of Certain Crushable Materials, Calif. Inst. of Technology, Jet Propulsion Lab., Tech. Rept. 32-120, Jan 13, 1961
High-velocity impacts on polyurethane, polystyrene, epoxy and balsa wood.

237. A. Ali and H. Matlock, "Cushioning for Aerial Delivery Part VI, Preliminary Investigation of the Absorption of Shock Energy by Wood in Lateral Compression," Texas Univ., Structural Mechanics Research Lab., March 18, 1957
Good results achieved by jamming a Douglas-fir board through a tight fitting mandrel.

238. C. W. Morgan and W. L. Moore, "Cushioning for Air Drop Part V, Theoretical and Experimental Investigations of Fluid Filled Metal Cylinders for Use as Energy Absorbers," Texas Univ., Structural Mechanics Research Lab., 1956
Cylinders, including beer cans, containing liquid and with drilled orifices, offer some promise.

239. C. W. Kroell, *Shock and Vibration Bull. No. 30*, Pt. 3, 331 (Feb. 1962)
One-shot shock absorbers consisting of aluminum tubing rolled at one end. Available stroke is about twice length of tubing used.

240. J. W. Pendered, "The Shock Spectrum," Univ. College, London, Dept. of Mechanical Engineering, Rept. 65/10, Dec. 1965
Excellent short review of shock-spectra concepts and damage susceptibility criteria.

241. M. A. Biot, *Bull. Seismological Soc. Am.*, **31** (2), 151 (April 1941)
Introduction of the concept of shock spectra, originally proposed for analysis of earthquake motions.

242. R. S. Ayre, "Transient Response to Step and Pulse Functions," Ch. 8 in *Shock and Vibration Handbook* (C. M. Harris and E. E. Crede, eds.) McGraw-Hill, New York, 1961
Comprehensive set of response spectra to a wide variety of input motions.

243. S. Rubin, "Concepts in Shock Data Analysis," Ch. 23 in *Shock and Vibration Handbook* (C. M. Harris and C. E. Crede, eds.) McGraw-Hill, New York, 1961
Various methods of computing response spectra from input pulse records.

244. C. T. Morrow and D. E. Riesen, *J. Acoust. Soc. Am.*, **28** (1), 93 (1956)
An automated analog computer for determining shock spectra up to 2000 cps.

245. G. W. Painter and H. J. Parry, *Shock and Vibration Bull. No. 35*, Pt. 4, 129 (Feb. 1966)
New and improved automatic analog shock spectrum computer.

246. G. J. O'Hara, "A Numerical Procedure for Shock and Fourier Analysis," Naval Research Lab., Rept. 5772, June 1962
Establishes a set of recursion equations, for use in a digital computer to compute shock and Fourier spectra.

247. R. B. McCalley, Jr., *Supplement to Shock and Vibration Bull. No. 23*, 1 (June 1956)
Shows that transmissibility is greatly reduced when mass of element is considered.

248. M. Kornhauser, *J. Appl. Mech.*, **21** (4), 371 (1954)
Discusses methods of predicting sensitivity of equipment to damage. Develops damage-sensitivity curves.

249. C. E. Crede, *Trans. Am. Soc. Mech. Engrs.*, **77**, 957 (1955)
Suggests plotting shock spectra in terms of the area under the shock pulse.

250. G. G. Parfitt and J. C. Snowdon, *J. Acoust. Soc. Am.*, **34** (4), 462 (April 1962)
Develops a figure of merit for shock isolators. Suggests plotting acceleration ratio against displacement ratio, since most designs are displacement-limited for one practical reason or another.

251. E. A. Ripperger and W. T. Fowler, *Shock and Vibration Bull. No. 30*, Pt. 3, 302 (Feb. 1962)
A review of all the Texas University work to date on determining the response of structures to impact loading.

252. J. D. Huckaby, "A Study of the Plastic Deformation of a Single-Degree-of-Freedom System Subjected to Impulsive Loading," Texas Univ., Structural Mechanics Research Lab., Sept. 1960

Graphical results, based on experiment, of shock pulses producing permanent deformation. Effect of peak acceleration are isolated, but the effects of time ratio and impulse could not be separated from one another.

253. R. L. Luke, "The Impact Response of a Single-Degree-of-Freedom System with Viscous Damping," Texas Univ., Structural Mechanics Research Lab., June 16, 1960
Response spectra for six differently shaped pulses with some variation in damping.

254. W. T. Fowler, "An Analytical Study of an Undamped Nonlinear Single-Degree-of-Freedom System Subjected to Impulsive Loading," Texas Univ., Structural Mechanics Research Lab., Jan. 1962
Cantilever beams exposed to shock pulses of varying shape and duration. No correlation found between shock spectrum and amount of permanent deformation.

255. M. D. Reifel, "The Effects of Acceleration Pulse Parameters on Permanent Deformation of a Damped Single-Degree-of-Freedom System," Texas Univ., Structural Mechanics Research Lab., Aug. 3, 1961
Other factors being constant, damping reduces the amount of permanent deformation.

256. A. P. Richter, Jr., "The Response of a Two-Degree-of-Freedom System Subjected to Impulsive Loading," Texas Univ., Structural Mechanics Research Lab., Aug. 1960
Second-order shock spectra for a number of input pulse shapes.

257. E. H. Schell, *Shock and Vibration Bull. No. 35,* Pt. 6, 229 (April 1966)
Preliminary exposure of the complete data in Ref. 258.

258. E. H. Schell, "Applications of the Proximity Spectrum Including Spectra of Some Simple Shock Design and Test Motions," Flight Dynamics Laboratory, WPAFB, Tech. Rept. AFFDL-TR-66-4, May 1966
Complete derivation of the proximity-spectrum concept and over 150 sample proximity spectra.

259. R. E. Blake, *Shock and Vibration Bull. 35,* Pt. 5, 133 (Feb. 1966)
A progress report on efforts to define a near-optimum shock mount for single pulses.

260. T. Liber and E. Sevin, *Shock and Vibration Bull. No. 35,* Pt. 5, 203 (Feb. 1966)
Progress reports on efforts to define an optimum-shock isolator for shock motions having pulses in opposite directions. Uses linear programming techniques in arriving at expressions for optimum.

261. S. C. Schuler, *Shock and Vibration Bull. No. 30,* Pt. 3, 87 (Feb. 1962)
Same information as in Ref. 262.

262. S. C. Schuler, "Recent British Developments in Package Cushioning, Dynamic Testing and Instrumentation," Royal Radar Establishment Memorandum 1876, Oct. 1961
A review of then-current efforts in package-cushioning field in U.K. Stresses use of a lead-block decelerator to measure fragility of small stores.

263. J. W. Pendered, A Note on Fragility, Univ. College, London, Dept. of Mech. Engr., Rept. 65/9, Nov. 1965

A short, lucid review of the problems of determining equipment fragility; this cannot be separated from cushion performance.

264. G. J. O'Hara, *J. Acoust. Soc. Am.*, **31** (10), 1300 (1959)
Points out that envelope shock spectra are very dangerous as design limits, particularly for large equipment. The envelope concept assumes foundation impedance to be very large compared to item impedance; this is not true with heavy loads. Several examples illustrate the point.

265. M. Gertel and R. Holland, *Shock and Vibration Bull. No. 35*, Pt. 6, 249 (April 1966)
Excellent short review of the use of shock and Fourier spectra in the analysis of transient disturbances. Several examples plus an estimate of the very small error in O'Hara's recursion method for computing Duhamel's integral.

266. S. O. Rice, *Bell Sys. Tech. J.*, **23**, 282 (1944) and **24**, 46 (1945)
The basic, and still classic paper establishing the foundations of random-vibration theory.

267. J. D. Robson, *An Introduction to Random Vibration*, Edinburgh Univ. Press, 1964
An excellent treatise on the foundations of random-vibration theory and practice.

268. J. W. Miles and W. T. Thompson, "Statistical Concepts in Vibration," Ch. 11 in *Shock and Vibration Handbook* (C. M. Harris and C. E. Crede, eds.) McGraw-Hill, New York, 1961
Short review of the fundamentals of random-vibration theory. Introduces fatigue concepts.

269. G. S. Mustin and E. D. Hoyt, "Practical and Theoretical Bases for a Transportation Vibration Test," Reed Research Rept. 1175-36, Feb. 25, 1960
Derives response to a narrow-banded random-input function. Equates "sinusoidal" to "random" through fatigue methods. Proposes a single test on admittedly arbitrary grounds.

270. G. S. Mustin and E. D. Hoyt, *Shock and Vibration Bull. No. 30*, Pt. 3, 122, (Feb. 1962)
A condensation of the essential points from Ref. 269.

271. E. J. Gumbel, *Statistics of Extremes*, Columbia Univ. Press, New York, 1958
A complete, though difficult, treatise on the statistics of extreme values where the variable may follow one of many distribution functions, or even where the initial-distribution function is unknown.

272. C. L. Gray, *Shock and Vibration Bull. No. 35*, Pt. 4, 99 (Feb. 1966)
Considers the probability of the first occurrence of extreme amplitude of a Gaussian random variable.

273. J. A. Skoog and G. G. Setterlund, *Shock and Vibration Bull. No. 26*, Pt. 2, 315 (Dec. 1958)
Analyzes space requirements for equipment mounted in a structural space.

274. H. Himelblau and L. M. Keer, *J. Acoust. Soc. Am.*, **32** (1), 76 (1960)

Derives probability of collision of a mounted item with its own base and with an adjacent oscillator excited by the equipment base

275. E. L. Hixson, Mechanical Impedance and Mobility, Ch. 10 in *Shock and Vibration Handbook* (C. M. Harris and C. E. Crede, eds.) McGraw-Hill, New York, 1961

Concise introduction to the concepts of mechanical impedance and mobility. Contains many simple models and shows how to construct more elaborate ones.

276. Specification MIL-C-172, Cases; Bases, Mounting; and Mounts, Vibration (For Use with Electronic Equipment in Aircraft)

A general specification, with test methods, covering the area implied in the title.

277. A. A. Cohen, "Final Report on Phase A and Phase B, Development of a Multifunctional Isolating Barrier for Shock and Vibration," Naval Air Development Center, Rept. NADC-EL-6159, Oct. 17, 1961

A summary report of the extensive development and testing conducted on polyurethane-foam shock mounts. Many transmissibility curves.

278. P. C. Calcaterra, "Design Guide for Polyurethane Foam Isolation Systems," Naval Air Development Center, Rept. NADC-AE-6522, Dec. 2, 1965

Compares behavior of foam mounts to buckling isolators, gives some hints on designing foam mounts. Several questions admittedly unanswered.

279. P. C. Calcaterra, "In-Flight Evaluation of Conventional and Foam Shock and Vibration Isolation Systems," Naval Air Development Center, Rept. NADC-AE-6506, L5, Sept. 1965

Compares performance of certain foam isolators installed at various locations in an A-3D aircraft with the performance of conventional isolators.

280. Y. Hiroshige and S. Taylor, "Secondary Isolation System For the High Speed Track Research Testing," Air Force Flight Test Center, Edwards Air Force Base, Rept. AFFTC-TN-57-12, April 1957

Describes development and performance of polyurethane-foam cushioning system for the telemetering equipment used on high-speed track sleds.

281. J. C. Burgess, *Shock and Vibration Bull. No. 27*, Pt. 3, 1 (June 1959)

Describes the random-vibration acceleration spectral densities measured on a number of high-speed tracks.

282. J. C. Burgess, "Resilient Slippers for High Speed Track Sleds," Edwards Air Force Base, Interim Tech. Rept. PTFST-TOR-61-1, April 1961

Describes a woven stainless-steel mesh resilient liner for track slippers and compares performance.

283. J. C. Burgess, "Development of Resilient Slippers for High Speed Track Sleds," Edwards Air Force Base, Rept. FTC-TDR-62-19, May 1962

Final report on project discussed in Ref. 282.

284. Military Standard, MIL-STD-810,

A series of environmental test procedures.

285. C. Henny and F. Leslie, *Shock and Vibration Bull. No. 30,* Pt. 3, 66, Feb. 1962
Shows performance of a polyurethane foam under vibratory stress at varying stresses and temperatures.

286. W. H. Lehmberg, *Mech. Engineering,* **67** (2), 93 (Feb. 1945)
Contains the mechanical properties of the six SAE standard grades of felts.

287. F. G. Tyzzer and H. C. Hardy, *J. Acoust. Soc. Am.,* **19**, 5 (Sept. 1947)
Develops data on natural frequency and damping characteristics of felts at three different densities: 10, 22, and 39 pcf.

288. A. Ezzat, *Exp. Mechanics,* **2** (9), 274 (1962)
Results of an investigation into the vibration-isolation characteristics of dry Oregon pine sawdust.

289. M. T. Hatae, *Material Handling Engineering,* **17** (11), 78 (Nov. 1962)
Popularized review of elementary fundamentals for package designers.

290. C. T. Morrow, *Shock and Vibration Bull. No. 25,* Pt. 2, 332 (Dec. 1957)
A proposal to design packages to isolate maximum equipment resonances. Points out that tests on container survivability and equipment are not necessarily related.

291. C. T. Mcrrow, *Noise Control,* **5** (6), 32 (Nov. 1959)
Essentially same information as in Ref. 290.

292. R. M. Mains, *Shock and Vibration Bull. No. 23, Supplement* (Feb. 1956)
Discusses probable responses of multidegree-of-freedom systems to random shock and vibration.

293. M. A. Miner, *J. Appl. Mech.,* **12**, A159 (1945)
Develops the concept of linear accumulation of fatigue stresses up to a failure point.

294. A. Palmgren, *Z. Verein. Deuts. Ing.,* **68**, 339 (1924)
Develops the concept of cumulative damage determining the life of ball bearings.

295. J. A. Kasuba, *Shock and Vibration Bull. No. 35,* Pt. 5, 37 (Feb. 1966)
Uses Miner-Palmgren to arrive at an equivalence ratio for sinusoidal-vibration tests designed to simulate the rough-road truck environment.

296. M. Gertel, "Specification of Laboratory Tests," Ch. 24 in *Shock and Vibration Handbook* (C. M. Harris and C. E. Crede, eds.) McGraw-Hill, New York, 1961
Fundamental concepts of vibration testing. Contains much practical information on limitations of various testing methods.

297. N. W. Lee, "The Response of Packaged Military Stores to Cargo Truck Transportation, Real and Simulated," Proc. Soc. of Environmental Engineers Symposium, Volume 4, London, April 19-21, 1966
Develops an equivalence between tests of a package on an LAB tester and the same package in the bed of a cargo truck on a rough road. Data show that test is a repetitive shock test.

298. C. A. Jordan and R. H. Witting, "Properties of Various Cushioning Materials at −70°C.," Forest Products Lab., Rept. 207-21, 1951
A number of conventional package cushioning materials at the indicated temperature. Static data.

299. M. T. Hatae, "Determination of Extreme Temperature Properties of Polyurethane Cushioning Material for Use in Gyro Shipping Container," North American Aviation Memo MRR 57-9, Jan. 1, 1957
Static stress-strain curves at a number of temperatures down to −40°F. Uses Janssen theory to develop performance curves.

300. S. A. Eller, "Investigation of the Physical Properties of Resilient Polyurethane Foam Materials," New York Naval Shipyard, Materials Laboratory, Project 4981-23, Final Report, Jan. 26, 1959
Static properties of a large number of samples of polyurethane foam from commercial sources.

301. G. A. Gordon and E. E. Wheeler, "Evaluation of Cushioning Material Properties, Part II, Effect of Temperature," PATRA Packaging Laboratory Rept. 24, Oct. 1962
Determination of the lowest "safe" temperature for a number of cushioning materials commonly available in the U.K.

302. A. Letchford, "The Dynamic Performance of Certain Cushioning Materials at Temperatures Down to −50°C," Paper 13, Proc. Symposium on Package Cushioning Dynamics, Royal Radar Establishment, Malvern, England, April 27-28, 1960
Same approach as in Ref. 301.

303. J. H. Mazzei, "An Environmental Study: The Dynamic Properties of Confined Cushions of Rubberized Curled Hair in the Dry, Dry-Frozen, Wet, Wet-Frozen States," Picatinny Arsenal Tech. Rept. FRL-TR-58, May 1962
Effects of water on performance of rubberized hair. Presence of ice increases load-bearing capacity of the material.

304. W. B. Tolley, *Shock and Vibration Bull. No. 30,* Pt. 3, 100 (Feb. 1962)
Finds definite correlation between static and dynamic behavior at different temperatures for a polyurethane foam.

305. H. C. Blake, III, "Creep Properties of Selected Cushioning Materials," Michigan State Univ., School of Packaging, Project I, Suppl. to Tech. Rept. 2, June 20, 1963
As indicated in the title. One-month duration.

306. H. C. Blake, III, "Creep Properties of Selected Cushioning Materials," Michigan State Univ., School of Packaging Project I, Tech. Rept. 6, Nov. 15, 1964
More materials. One-month duration.

307. H. C. Blake, III, "Creep Properties of Selected Cushioning Materials," Michigan State Univ., School of Packaging, Project I, Tech. Rept. 9, Aug. 15, 1965
More materials, one-month duration. In all three references, static stress is set at optimum shock static stress for the material and thickness.

308. S. A. Eller, A. A. Stein, and C. K. Chatten, "Foamed Resilient Materials and Rubberized Hair for Package Cushioning Applications," Proc. 6th Joint Army, Navy, Air Force Conference on Elastomer Res. and Dev., Oct. 1960
Drift under stresses producing 20 to 25 percent strain.

309. F. Strachwitz, "Cushioning Materials for Packaging," Sandia Corp. Bibliography SCR-81, May 1959
Papers on packaging through 1959.

310. "Cushioning, A Bibliography and List of References," Ministry of Aviation, Central Packaging Section, April 1960
Bib. through 1960. Also contains some European leads not listed in American bibs.

311. M. T. Curtis, "Bibliography on Shock Absorption Studies (4th rev.)," Prepared for ASTM Committee D-10, U.S. Naval Ordnance Testing Station, China Lake, Cal., March 1957
Packaging papers through 1957

SUBJECT AND AUTHOR INDEX

Please note that the author entries appear in italics. The first number (in brackets) following the entry is the reference number. The second number is the page on which the reference was first cited.

* U. S. GOVERNMENT PRINTING OFFICE : 1968 O - 313-944